Fine-tuning stellar population models

by

L. Gustav Strömbäck

THE THESIS IS SUBMITTED IN PARTIAL FULFILMENT OF THE REQUIREMENTS FOR
THE AWARD OF THE DEGREE OF
DOCTOR OF PHILOSOPHY
OF THE
UNIVERSITY OF PORTSMOUTH

January, 2012

Copyright

This work is dedicated to my family and to my little one for all the support and love over the years.

Abstract

In this work we present new, high-to-intermediate spectral resolution evolutionary population synthesis models, complementing and extending the widely used Maraston models. The new models are based on four popular libraries of empirical stellar spectra, which has necessitated some modifications to the original code, while keeping much of the original ingredients – such as stellar energetics, treatment of the thermally pulsating asymptotic giant branch, and mass loss recipe – intact. In addition, we have computed models at very high resolution (R$= 20000$) based on the theoretical MARCS library, that extends far into the infrared region of the electromagnetic spectrum. A library-dependent, but model-independent comparison is made, where both photometric and spectroscopic similarities and discrepancies are highlighted. We find that stellar population models employing empirical stellar spectra exhibit considerably bluer (*B*-*V*) colours compared to models adopting theoretical spectra synthesised from the Kurucz model atmospheres (such as the BaSeL library), but that some differences arise between the empirical libraries due to, in particular, the adopted temperature scale. Furthermore, the results obtained with the theoretical MARCS library are fully consistent with the empirical libraries in this respect. The same effect can be found also in other EPS models that are based on empirical stars. We show that this discovery, whose origin can be traced mainly to cool stars ($T_{eff} < 5000$ K), leads to improved photometric agreement with both galaxy and Milky Way globular cluster data. Spectral energy distributions of the latter are also used for testing the models concerning their ability to reproduce, through full SED-fitting, the cluster ages and metallicities as derived through independent fitting in colour-magnitude diagrams. In general, the agreement is very promising, although the higher resolution of the new models cannot alleviate the age-metallicity degeneracy in the optical in any significant way. A comparison with models of absorption line indices with variable abundance ratios is also made, both for the full SED-fitting procedure and when measuring indices directly on the SED. We obtain satisfying agreement in the first case, but in the second case only when a subsample of indices are used, the combination of which is little sensitive to abundance ratio effects. As a side track we exploit for the first time for population synthesis purposes the vast stellar database of the *Sloan Digital Sky Survey*, but

find that the metallicity and age range of the stars is currently too narrow for computing sensible population models. Finally, we re-invigorate the Ca K line for the purpose of absorption feature diagnostics, presenting a new version of the index which will help in separating solutions for a key case of the age-metallicity degeneracy.

Preface

Whilst registered as a candidate for the above degree, I have not been registered for any other research award. The results and conclusions embodied in this thesis are the work of the named candidate and have not been submitted for any other academic award.

The work of this thesis was carried out at the Institute of Cosmology and Gravitation University of Portsmouth, United Kingdom.

Acknowledgements

First and foremost I thank my supervisor Claudia Maraston, for giving me this opportunity, and assisting me with valuable advice and insights over three enlightening years. I'm grateful for your patience with me, and for your understanding of my innumerable trips to Sweden. Jonas, my flatmate, deskmate, Wiimate, alemate, younameitmate, but most of all just friend, deserves recognition in the highest regard. Thank you to my viva examiners Prof. Brad Gibson and Prof. Will Percival for agreeing to read this thesis, and for the many comments which have greatly improved this work (I'm sure you had better things to do). Thank you also to Prof. Sofia Feltzing and the hospitality of the University of Lund. The following people have all contributed directly or through discussions in the development of our stellar population models: Daniel Thomas, Jonas Johansson, Janine Pforr, Chiara Tonini, Issi Doyle, Alessandra Beifiori, Harald Kuntschner, and Andrew Pickles. Thanks to Bengt Edvardsson and the MARCS group for aiding us with their model database and for providing additional computations and explanations. Acknowledgments also to Ricardo Schiavon for letting us use their composite spectrum of M67. All friends, co-workers, colleagues and staff at the ICG – thumbs up for you guys. A high five also goes out to the following Portsmouthian establishments for nourishing me and entertaining me in life outside of work: Tang's, Hole in the Wall, Coop at Castle Road, Vue Cinemas, Deli Too, Perfect Pizza, that place in Fareham where we rehearsed, Deco, Landlady Sue, and the Commons. Finally, all friends and family back home deserves a big slice of the gratitude cake as well, you know who you are.

Declaration of original publications and distribution of workload

Many of the chapters constituting this thesis contain material that has previously been published elsewhere. The original work was printed in the following publications:

CHAPTERS 3, 4, and 5
”Stellar population models at high spectral resolution”,
Maraston, C., & Strömbäck, G., 2011, MNRAS, 418, 2785

CHAPTER 5, Section 4
”Modelling the colour evolution of luminous red galaxies - improvements with empirical stellar spectra”,
Maraston, C., Strömbäck, G., Thomas, D., Wake, D. A., & Nichol, R. C., 2009, MNRAS, 394, L107

CHAPTER 7, Section 1
”Commissioning the Spectrographs for the Baryon Oscillation Spectroscopic Survey (BOSS)”,
Bhardwaj, V., Dawson, K., Anderson, L., et al., 2010, Bulletin of the American Astronomical Society, 42, #471.02

All the work on the stellar libraries, modifying the M05 code, and ultimately producing the MaStro models was done by the author of this thesis. Remaining parts of Maraston et al. (2011), interpretation of the results, and writing of the paper was done in unison with the co-author. In Maraston et al. (2009b) the author of this thesis contributed mainly with the models, and to some extent also to the writing and interpretation of the results. Finally, the author of this thesis participated in the Bhardwaj et al. (2010) paper by providing models with corresponding comments.

Acronyms

The following acronyms are frequently found throughout the pages of this thesis:

AGB	–	Asymptotic Giant Branch
BAO	–	Baryon Acoustic Oscillation
BS	–	Blue Straggler
CMD	–	Colour-Magnitude Diagram
CSP	–	Composite Stellar Population (alt. Complex Stellar Population)
E-AGB	–	Early Asymptotic Giant Branch
EPS	–	Evolutionary Population Synthesis
FCT	–	Fuel Consumption Theorem
HB	–	Horizontal Branch
IMF	–	Initial Mass Function
IUE	–	International Ultraviolet Explorer
LMC	–	Large Magellanic Cloud
LMS	–	Lower Main Sequence
LRG	–	Luminous Red Galaxy
MC	–	Magellanic Clouds
MS	–	Main Sequence
MW	–	Milky Way
OPS	–	Optimised Population Synthesis
PMS	–	Post-Main Sequence
RGB	–	Red Giant Branch
SDSS	–	Sloan Digital Sky Survey
SED	–	Spectral Energy Distribution
SGB	–	Sub-Giant Branch
SSP	–	Single Stellar Population (alt. Simple Stellar Population)
TP-AGB	–	Thermally Pulsating Asymptotic Giant Branch
T-RGB	–	Tip of the Red Giant Branch

In the beginning there was a bang, and it was big. Possibly it was not the beginning, but it was a beginning. We don't know what caused the birth of our Universe, but we live and breath the byproducts of it. In the great cosmic circle of life, stars are continuously being born. Like almost any other species in Nature they evolve and age, and then they die – thereby providing the soil in which new stars can spring to life and prosper.

Out of the billions and billions of stars in the Universe, only a very small fraction can actually be studied individually. Instead, we know that they exist only because of their tendency to cluster in the large congregations we call galaxies, for which the collective light of all the stellar constituents is bright enough to reach us even from times and places when the Universe was very young.

In order to learn more about the wealthy galaxy fauna, we must therefore first gather what we have learned by studying nearby stars, and then apply it to these more distant stellar systems, in the hope that the laws of star formation and stellar evolution rule also other galaxies, like they rule our own. Enter evolutionary population synthesis.

Table of Contents

List of Tables

List of Figures

Chapter 1

Introduction

On the need for evolutionary population synthesis models, a brief look back on the history in this particular field of research, and why another attempt has been made here.

1.1 Why physical properties of galaxies are important

Ever since the Great Debate, which took place in the 1920s' between Shapley and Curtis, ended with all the evidence supporting the claim that the Andromeda nebula and many other of its kind, were indeed distant, extragalactic "island universes", astronomers have set out to classify and explore the behaviour and characteristics of millions of galaxies and stellar populations. Their location in time and space as a function of their properties – how much mass each galaxy contains; which chemical elements can be found and in what proportions; and perhaps most importantly, how old each galaxy is, and what the fractions of old and young stars are – has given us and continues to give us critical information about the birth, expansion and structure of the Universe itself.

The very foundation of cosmology – the study of the structure of and changes in the present Universe – is directly dependent on the distribution and properties of galaxies for constraints. Mapping, for example, galaxy ages as a function of their redshift (Jimenez et al., 2007; Carson & Nichol, 2010; Moresco et al., 2010, to mention a few) constrains the expansion history of the Universe, and the ages of the oldest galaxies set a lower limit to its age. In addition, some branches of cosmology, such as studies of the baryon acoustic oscillation (BAO, see Percival et al., 2010), can benefit from careful mass determinations. Other areas are more indirectly linked, for example the ties that can be made between the temperature fluctuations in the cosmic microwave background (CMB) and the large-scale structure of dark matter haloes and galaxies (e.g. Lahav et al., 2002). Regardless of which area of research one finds the most interesting, it is clear that in order to

obtain a complete picture of the Universe from the perspectives of cosmology, one must first understand the galaxies that inhabit its vast realms.

A crucial step towards the goal of understanding galaxy formation and evolution, and in the end the very Universe, therefore lies in obtaining accurate measurements of the physical properties of galaxies and stellar populations. These properties cannot, however, be measured directly on photometric or spectroscopic data, but must be deduced indirectly by filtering observations through so-called *evolutionary population synthesis* models (hereafter EPS models – the subject around which this doctoral thesis will revolve). EPS models are theoretical predictions of the spectral energy distribution (SED) of an ensemble of stars – be it an entire galaxy or a smaller, intragalactic cluster of stars – as a function of key parameters such as the initial mass function (IMF), age, mass, metallicity, element abundance ratios, star formation history, etc. Comparing the models to actual observations allow us to extract these crucial pieces of information, which then constitute the conditions for galaxy evolution studies.

Clues to the large-scale picture can even be found within our own galaxy, which was illustrated, for example, by the discovery of e.g. Chaboyer (1995) that the mean age of the oldest Galactic globular clusters (GCs), once all known uncertainties were accounted for, lay between 11 and 21 Gyr (a more realistic assessment, however, deeming it unlikely that all the nonstandard assumptions occur at the same time, was 13-17 Gyr). This result – the lower limit being of particular interest – required a value of the Hubble constant that was at odds with measurements obtained using other methods and the standard model of inflation. With new constraints that could not be ignored, revisions of the cosmological models were necessary. We learn from this that any model trying to reproduce the history of the Universe and its galaxies must be able to explain the observed data, and the interpretation of this data relies heavily on EPS models, which stresses the need for them to be well calibrated and rigorously tested.

1.2 Evolutionary Population Synthesis – An overview

The finite speed of light and the sheer vastness of the Universe combine to offer us the possibility of studying galaxies at different epochs in their lives, simply by pushing observations to higher and higher redshifts. It has, for example, been revealed that galaxies at higher redshifts may exhibit distinctly different morphologies compared to the local

varieties, and that the fraction of peculiar galaxies and multi-component merging galaxies increase with look-back time (e.g. van den Bergh et al. 2000 to mention a classical reference; newer ones include for example Ravindranath et al. 2006), thereby showcasing some of the various stages that a galaxy may undergo during its lifetime. The problem, of course, lies in the fact that each individual galaxy can only be studied at a single given point in time. Clues to its origin and evolution up to that point must be sought for in the stellar content of the galaxy, where the star formation and chemical enrichment histories are imprinted. To connect to the previous section: in order to understand the Universe, one must first understand the galaxies, but in order to understand the galaxies it is imperative that one understands the intricacies of individual stars and their evolution.

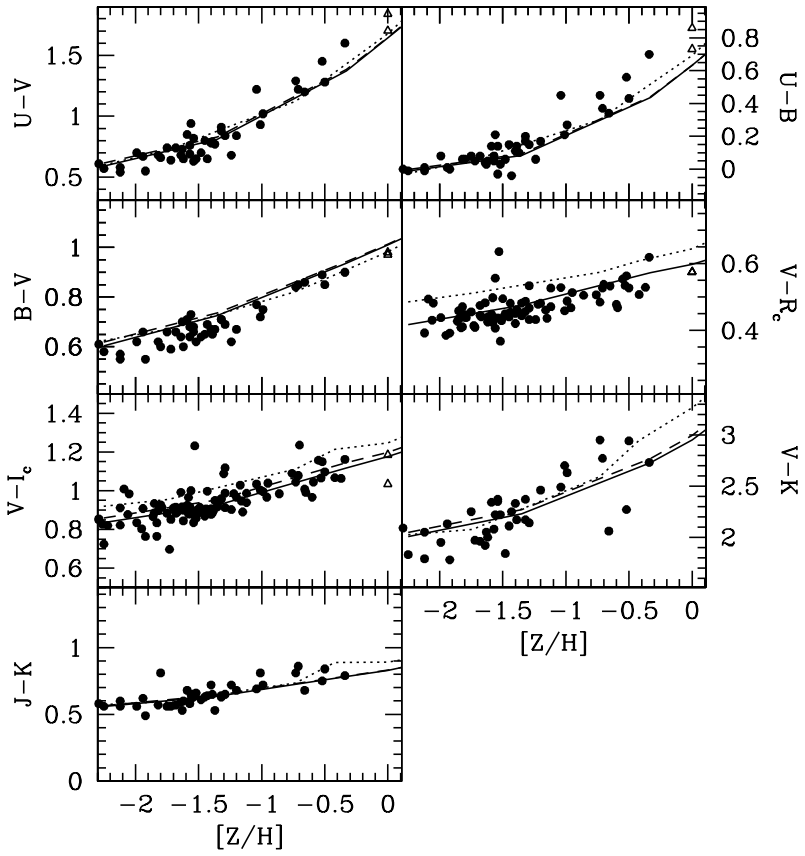

Figure 1.1: Reprint of Fig.21 in Maraston (2005). The broadband colours of Milky Way globular clusters are plotted as a function of metallicity and compared to the 13 Gyr EPS models of Maraston (2005, solid and dashed lines for Kroupa and Salpeter IMF, respectively) and Bruzual & Charlot (2003, dotted line, Kroupa IMF).

Evolutionary population synthesis is a method to model the photometric and spectroscopic properties of stellar populations, meaning broadband and narrowband colours

as well as more or less complete spectral energy distributions, or even just the strengths of individual absorption lines. Fitting the produced models to observed data is an absolutely essential tool for determining parameters such as masses, ages, metallicities, star-formation histories, chemical abundance ratios, chemical enrichment histories, velocity dispersions, and mass-to-light ratios of *unresolved* stellar systems. Fig.1.1 shows an example of such a procedure, comparing the broadband colours of Milky Way (MW) globular clusters to two different EPS models (acknowledging that, technically, MW GCs are not unresolvable).

It may already here be mentioned that the particular parameter for age is not unambiguous; is it the age of the oldest star in a population that determines the overall age, or do we require a certain fraction of all the stars to be of that age? What if that subcomponent of stars appear to be an accreted satellite galaxy, which is much older than the main population? To further complicate matters a majority of all the observable galaxies in the Universe still harbour stellar nurseries, and a newly born population of stars may be luminous enough to drown the signal from an older, less luminous population (the outshining effect, see Maraston et al. 2010). To sum up, it is necessary to make the distinction between mass-weighted ages and light-weighted ages (see e.g. Trager & Somerville, 2009), of which the former are usually more difficult to acquire.

The EPS technique rests firmly upon stellar evolution theory, developed during the twentieth century, and surely one of its great achievements. It tells us how stars of different initial masses evolve with time in terms of mass, temperature, radius etc., from the time of their births to the final, violent stages of their lives. With the exception of a few inconsistencies in the description of the very early and the very late phases – due to a lack of observations as much as shortcomings in the theoretical formulation – it has proven to be a solid theory, indeed. The review by Haxton (2008) regarding the problem of the solar neutrino flux as predicted by the standard solar model is one such example. This was not resolved until technology allowed for a more sensitive measurement of neutrino flavour – thus it was found that the discrepancy was not due to an incorrect estimate of the solar neutrino count from the equations of stellar nuclear burning, but rather to the ignored fact that a large fraction of the neutrinos convert to other flavours during their transit to Earth.

1.2.1 Simple and Complex Stellar Populations, and their relation to Globular Clusters and Galaxies

The simplest form of an EPS model is termed *simple* or *single stellar population* (SSP from here on out), in which it is assumed that all the stars were born out of the same molecular cloud without any extended star formation, i.e. they are all of the same age, and share the same chemical composition. In the observable Universe, the closest approximation to such systems would be the globular clusters, which are compact, dynamically stable clusters of $\sim 10^6$ assumingly homogeneous stars. The proximity of the Milky Way, and not to forget also the Magellanic Clouds (MC), globular clusters present an excellent opportunity to calibrate the EPS models. Because they can be resolved into individual stars, their age and metallicity can be determined independently from each other, and from the EPS models, using the techniques of colour-magnitude diagram (CMD) fitting and single star spectroscopy. This step is crucial when later applying the models to more distant, unresolvable stellar populations in order to obtain reliable parameter values (Maraston, 1998, 2005). Due to the fact that practically all known Milky Way GCs are old (> 10 Gyr, although there are a few clusters associated with the accreted Sagittarius and Canis Major dwarf galaxies that exhibit ages younger than 6 Gyr at intermediate metallicity, see Forbes & Bridges 2010), it is necessary to use clusters in the Large Magellanic Cloud (LMC) in order to calibrate models of younger SSPs. It may be mentioned that the calibration at this point is essentially restricted to broadband photometry and general SED behaviour, rather than looking at individual absorption features, for reasons that shall become apparent in later sections. Thus, if the MC clusters would happen to have somewhat different element abundance ratios compared to their MW brethren it has relatively little impact on the calibration of the SSP models, especially considering that abundance ratio effects on the continuum shape are visible mainly in old populations.

Fig.1.2 shows the observed CMD of metal-poor Milky Way globular cluster NGC 1851 (reprinted from Maraston, 2005), with the main stellar evolutionary phases indicated. The core hydrogen burning phase is called the main sequence (MS) due to the fact that in a stellar population around 90 % of the observed stars above 0.5 $M_\odot$ can be found in this relatively quiet state (Arnett, 1996). Individual stars spend between 75 and 90 % of their lifetime on the MS, depending primarily on their initial mass, metallicity and whether or not convective core overshooting is adopted in the calculations (see e.g. Schaller et al., 1992). When the hydrogen fuel becomes depleted in the core the star swells (due to core contraction and corresponding envelope expansion), passing through the sub-giant branch (SGB) phase before reaching the red giant branch (RGB) stage, in which hydrogen is burnt in a shell around a helium core that has not yet reached the temperature

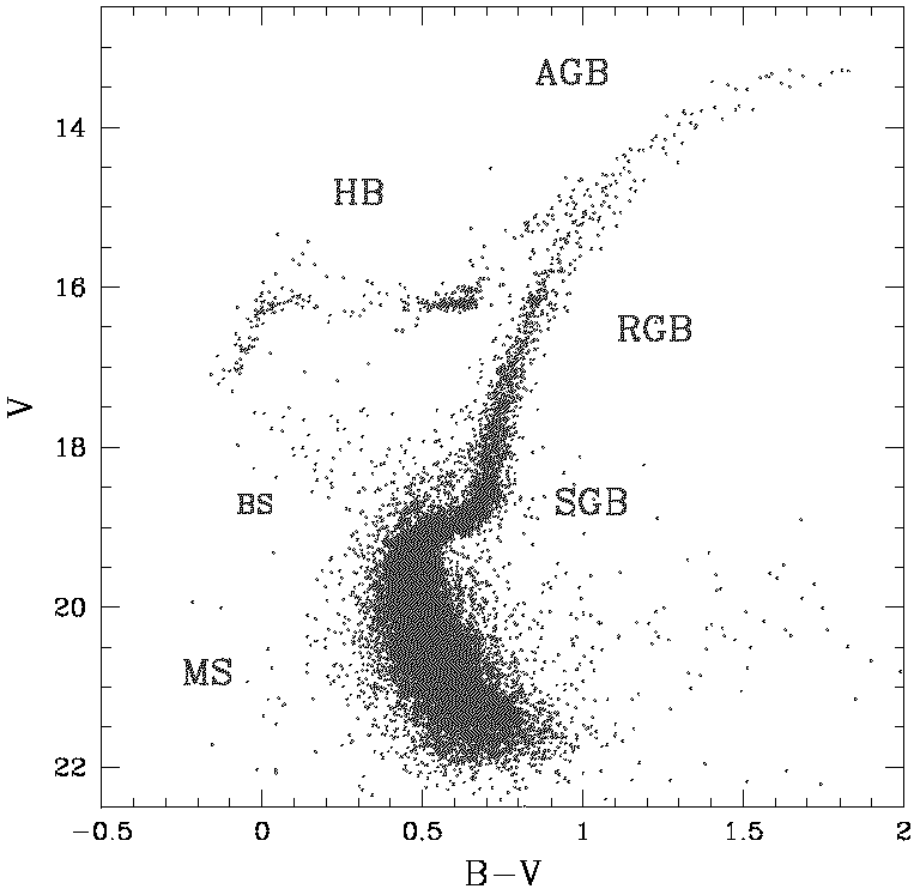

Figure 1.2: Observed colour-magnitude diagram of Milky Way globular cluster NGC 1851. The main stellar evolutionary phases are indicated as main sequence (MS), sub-giant branch (SGB), red giant branch (RGB), horizontal branch (HB) and asymptotic giant branch (AGB). See text for a description of the phases. Blue stragglers (BS) is class of stars thought to be the result from dynamical interaction between MS stars, rather than being a consequence of their internal evolution. Figure is a reprint from Maraston (2005).

required for helium fusion to commence. When it does, however, the star rapidly transfers to the horizontal branch or helium burning (HB) phase, marked by a relatively large increase in temperature. Finally, when the core helium is exhausted, helium burning will continue in a shell around a core now consisting mainly of carbon, which is called the asymptotic giant branch (AGB) phase. For a sun-like star this is the final thermo-nuclear active stage of its life. Slightly heavier stars (2-5 $M_{\odot}$) experience two stages of the AGB; the early asymptotic giant branch (E-AGB), and the thermally pulsating asymptotic giant branch (TP-AGB), in which an inner helium shell and an outer hydrogen shell alternately take turns in burning fuel, making the light of the star pulsate. If a star is massive enough, eventually carbon burning will ignite in the core, and later also even heavier elements, depending on the mass of the star. This may proceed all the way up to iron, after which fusion is no longer an effective means of producing energy. Such a star will have an

”onion-like” structure with an Fe core followed by shells of increasingly lighter elements as one reaches the stellar surface. Due to the short lifetime of these final stages, observations of the most massive stars is quite a rare event. Therefore, despite their high luminosity, they seldom contribute to the integrated light of a stellar population.

More complex stellar systems, in which star formation has occurred over an extended period of time, alternatively in discrete bursts, are modelled using SSPs as building blocks, convolving them with a given star formation history. These models are called *complex* or *composite stellar populations* (CSPs), and are used when SSPs are deemed inadequate, which is the case for most galaxies in the Universe. In a colour-magnitude diagram more complex populations would not have such well-defined evolutionary sequences as can be seen for example in Fig.1.2

However, lately the general consensus that globular clusters are analogous, or at least very nearly analogous, to SSPs has been challenged. More and more observations have found multiple evolutionary sequences and large star-to-star abundance variations for several GCs, spanning a wide range of global parameters (such as metallicity, HB morphology etc.). The bimodal heavy-element distribution of ω Centauri has been known for some time (e.g. Norris et al., 1996), and with technological advancements allowing for high quality colour-magnitude diagrams a splitting of the RGB (Pancino et al., 2000), as well as the MS and SGB (Bedin et al., 2004) has been observed. In fact, ω Cen is no longer believed to be a globular cluster at all, but rather a relic of a larger system, such as a dwarf galaxy. But bi- or multimodal sequences have been found also for other, lower-mass clusters (e.g. Piotto et al., 2007; Milone et al., 2008), and in a sample of unprecedented statistical quality, Carretta et al. (2009) find evidence for at least two generations of stars in all of the 19 Milky Way clusters studied. The populations differ in abundances of light elements (C,N,O,Na,Mg,Al,Si,F) only, whereas the intrinsic scatter in Fe abundance among all the clusters appear very small. As far as iron abundances are considered, globular clusters can therefore still be regarded as an example of simple stellar populations.

To conclude: even though globular clusters show evidence of not being unanimously equivalent to SSPs, they are still – by far – simpler systems than galaxies. One need only to take a look at the *Hubble Space Telescope* (HST) photometry of 74 Galactic GCs from Piotto et al. (2002) in order to confirm this. From an EPS modelling point of view they are therefore still also the best way of calibrating the SSP models.

1.2.2 Main ingredients of Evolutionary Population Synthesis models

For stellar population modellers, stellar evolution theory comes in the form of isochrones and/or stellar evolutionary tracks. Isochrones display in a *Hertzsprung-Russell* (H-R) diagram, where absolute magnitude or luminosity is given as a function of surface temperature, T_{eff}, or alternatively colour or spectral type (which in principal is just a measurement of the temperature), the theoretical loci of stars from a single-burst, single-metallicity population with some given mass distribution, and given a certain time since the birth of the population (i.e. its age). An isochrone is thus a snapshot of a simple stellar system, which means that stars whose fuel has already been exhausted are not included in the picture. Stellar tracks, on the other hand, follow the entire evolution (also in an H-R diagram), from ignition to extinction, of a single theoretical star of a given mass, see Fig.1.3.

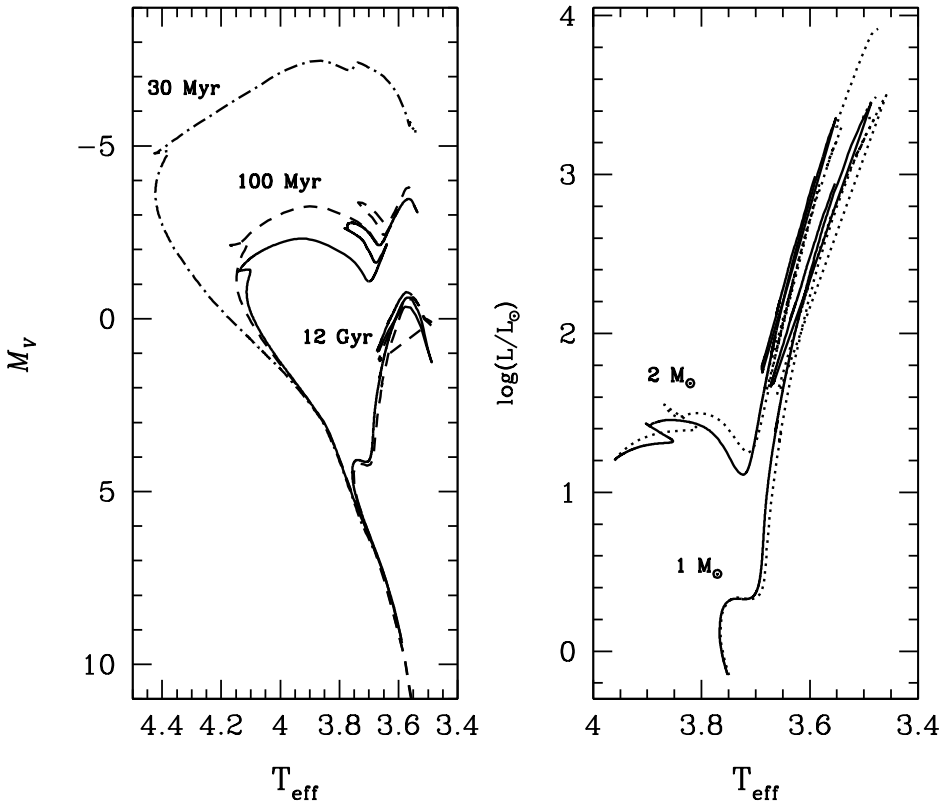

Figure 1.3: Isochrones (*left*) and evolutionary tracks (*right*) from a few of the most widely used stellar evolution models in the literature; the Geneva database of very massive stars (Lejeune & Schaerer, 2001, *dash-dot line)*, the BASTI database (Cassisi et al., 2006, *solid line)*, and the Padova database (Girardi et al., 2000; Bertelli et al., 2008, *dashed* and *dotted lines*, respectively). The reader is urged to compare the shape of these theoretical predictions to the distribution of stars in the observational HR-diagram in Fig.1.2.

Both isochrones and stellar evolutionary tracks are in turn available in many a variety in the literature (Bertelli et al., 1994; Girardi et al., 2000; Salasnich et al., 2000; Lejeune & Schaerer, 2001; Demarque et al., 2004; Cassisi et al., 2006; Dotter et al., 2007a; Bertelli et al., 2008, 2009; Pietrinferni et al., 2009, to mention just a few), differing from each other in the exact theoretical description of stellar evolution. Over the last decade it has also been customary to provide the evolutionary paths of stars with alternative chemical abundance ratios. Some tracks are even limited to certain phases of stellar evolution, like the core and shell helium burning tracks of Dotter et al. (2007b).

Accompanying isochrones and stellar tracks must be a way to transform theoretical predictions into observable quantities. This is usually obtained by means of relations between stars of different atmospheric parameters (temperature, surface gravity, metallicity, abundance ratios etc.) and their broadband colours, their line strengths for a select number of individual absorption features (i.e. fitting functions), or even their full spectral energy distributions. These relations can be either purely theoretical, or purely empirical, or a mixture thereof. With the emergence of more or less complete libraries of stellar spectra, most emphasis has over the last couple of decades been put on modelling the evolution of the stellar population SED (see Section 1.3).

Finally, a third crucial ingredient in EPS is a formula giving the relative abundances of stars of different initial masses, which is called the initial mass function. The first IMF was empirically constructed as early as the 1950's by E.Salpeter (Salpeter, 1955), by studying the stellar content in the solar vicinity. This resulted in a simple power law relation, which is very much still in use today. However, due to observational limitations of the contemporary instruments, the abundance of the lowest-mass stars could not be measured. Instead these faint stars were incorporated into the relation by means of extrapolation, resulting perhaps in a slight overestimation of their numbers. Therefore other, more intricate, multiple-component IMFs have followed since, of which perhaps Kroupa (2001) and Chabrier (2003) are the most widely used. Even though these are still based on observations, much theoretical work on the IMF has been published since. The large-scale, high-resolution, hydrodynamical simulations of molecular cloud fragmentation and star formation in Bate et al. (2003) produced an IMF consistent with observations. This was compared in Bate (2009) to a newer simulation with different initial conditions, but the results were indistinguishable from each other, suggesting the IMF to be relatively insensitive to environment – again consistent with observations within the Milky Way.

Alternatively to using the IMF over all evolutionary phases, the relative luminosity contributions from each evolutionary subphase to the total integrated light of a stellar population, can be computed using what is known as the fuel consumption theorem (FCT Renzini & Buzzoni, 1986), upon which the M05 models, and therefore the models in this work, are based. It should be noted that this method still requires an IMF in order to calculate the rate of stars evolving from one evolutionary phase to another, but much more on this later.

The procedure to construct an EPS model *requires* the three steps described above – a stellar evolution recipe, a way to transform this into observables, and an IMF to give weights to each type of star – but is not limited to them. Obviously, the integration procedure (i.e. *how* all these steps are merged into one code) and the numerical stability thereof, also matters for the end result. This can be seen for example in Fig.27 of Maraston (2005), where quite a large scatter in broadband colours are obtained with different EPS models, many of which adopts the same isochrones and spectral library. The method of applying the models to observed data, and the method for interpreting the results, are the last final steps in the creation and use of stellar population models. A detailed description of the EPS code employed in this work will be given in Chapter 2.

1.2.3 Theoretical uncertainties in Stellar Evolution

Apart from these three main constituents of evolutionary population synthesis (isochrones and/or stellar tracks, relations for transformation into observables, and IMF/fuels), there are additional aspects to consider, the inclusion and proper treatment of which might decide the reliability of a stellar population model. One such example is the *thermally pulsating asymptotic giant branch* – a late evolutionary phase for stars of intermediate initial mass (2-3 $M_{\odot}$), where a hydrogen and a helium shell around a degenerate carbon/oxygen core take turns (thus creating the pulsations) in burning their fuels. It was shown in Bruzual & Charlot (1993), and in Maraston (1998, hereafter M98) where the TP-AGB treatment was further refined, that when a stellar population has reached the critical age range 0.2 to 2.0 Gyr (i.e. when stars of initial masses 2-3 $M_{\odot}$ has evolved far enough to reach the TP-AGB stage), up to 40 % of the bolometric luminosity of the stellar population originates from the TP-AGB stars. In the *K*-band this figure can go up to an impressive 80 % (Maraston, 1998). Needless to say, this has huge consequences at high redshift, where the use of EPS models that do not take the TP-AGB properly into account leads to a derivation of systematically older ages for these galaxies, simply because the high near-IR flux of the TP-AGB stars must be compensated for by using models of older populations instead (see Maraston et al., 2006).

The theoretical modelling of such late, energetic evolutionary phases as the TP-AGB is still rather uncertain, and in any case very time consuming due to numerical difficulties in the stellar evolution calculations. Only recently have full AGB models for a comprehensive parameter grid (mass, metallicity, and abundance ratios) started to emerge (e.g. Weiss & Ferguson, 2009). As most incarnations of isochrones and stellar tracks terminate at the end of the *early* asymptotic giant branch and the onset of thermal pulses, including later phases in EPS modelling often requires the use of individual prescriptions. Another example is the mass loss that stars experience towards the end of the red giant branch, which is a deciding factor for the subsequent horizontal branch morphology of a stellar population. Because there is no firm theoretical foundation for mass loss, it has been necessary to use empirical relations to include mass loss in the stellar population models, usually by means of the Reimers formula (Reimers, 1977). Synthetic HB models have also been created using a randomised mass loss parametrisation (Dotter, 2008).

Yet another uncertainty concerns the theory for energy transport via convection in stars. The mixing length α, for example, is a parametrisation of the efficiency of convective energy transfer, and affects the surface temperature and the radius of the star. This parameter cannot be determined through direct methods, however, but must be calibrated using observational data, preferably for a wider selection of stars than just the Sun (which due to its proximity is by far the best candidate), so as to avoid making assumptions about the mixing length at non-solar metallicities (Salaris & Cassisi, 1996).

Since the borders between convective regions are not sharp and well-defined there is also an ongoing debate of how large impact this may have on the stellar core. Some evolutionary models (e.g. Girardi et al., 2000) adopt what is known as *overshooting* – a phenomenon in which the core, due to convective erosion of its surrounding regions, increases in size, thereby prolonging the MS lifetime of the star and consequently delaying the onset of the RGB. It is not difficult then to realise that models including overshooting will predict somewhat different stellar population ages compared to models without overshooting when applied to data. In the age range important to the RGB phase transition (500-1500 Myr), canonical models are able to produce more near-IR light at an earlier stage thanks to the availability of bright RGB stars – thus predicted ages should generally become slightly younger (how much younger depends on the amount of overshooting considered). The observational evidence so far points in the direction of convective core overshooting having a smaller impact than what was initially thought, although the phenomenon cannot be ruled out entirely, and the matter cannot be decided through first principles. Ferraro et al. (2004) showed using the number and luminosity ratio between bright RGB and He-clump stars in six LMC clusters that the amount of overshooting

included in the Girardi et al. (2000) tracks was overestimated, while canonical tracks could reproduce the data very satisfyingly. Then again, Sandberg Lacy et al. (2010) find their observations of eclipsing stars to be completely inconsistent with other models that neglect overshooting. The discussion is still ongoing, but in the end the amount of overshooting needed probably depends on the evolutionary tracks adopted, since they differ in many aspects of the input physics, not just the treatment of the convective core.

1.3 A brief history of EPS modelling

Considering all of the above described ingredients, not to mention all the various flavours each of them come in, it is not difficult to imagine a scenario in which any potential user of stellar population models is overwhelmed by a virtual landslide of different versions. Fortunately, this has not been the case – currently only models from a few EPS codes are widely in use among the members of the astronomical community.

All EPS models in the literature adopt one of two techniques (both of which will be thoroughly described in Chapter 2) – the isochrone synthesis technique, and the fuel consumption theorem. The former method makes full use of the isochrone; assuming an IMF, the flux contributions from each of the mass bins along the isochrone are integrated to yield the total light of the stellar population. Evolutionary phases for which the isochrones usually are not complete (late phases like the TP-AGB for example) must be included following separate prescriptions, whereas short-lived, luminous phases, during which the mass remains more or less constant (such as the RGB bump associated with the first dredge-up, wherein the hydrogen-burning shell is served a fresh plate of nuclear fuel), may also suffer from the resolution of the mass bins not being fine enough. The FCT approach on the other hand, adopts isochrone synthesis only up to the end of the MS, after which the fuel, i.e. the amount of hydrogen and/or helium available for nuclear fusion at each given *post-main sequence* (PMS) phase, is used as the integration variable. The fuel is directly proportional to the luminosity, and may in addition be calibrated with observations, meaning that stellar phases that are theoretically difficult to model can be included relatively straightforward. So far, only the EPS models of Buzzoni (1989), Maraston (1998), and Maraston (2005) have employed the FCT concept.

1.3.1 Traditional EPS models

The first signs of evolutionary population synthesis in the form we know it today saw daylight back in the 1970s', in a series of papers by B.Tinsley (Tinsley, 1972; Tinsley & Gunn, 1976; Tinsley, 1978). These early models utilised stellar evolutionary tracks and focused on the evolution of broadband colours and a few infrared features, but terminated the integration at the end of the RGB, thus neglecting important later phases such as the HB and AGB. Using a combination of theoretical and empirical stellar spectra, Bruzual (1983) modelled the full spectral energy distribution from the far ultraviolet into the infrared ($>$10000 Å), but also in these models the adopted evolutionary tracks did not continue beyond the ignition of helium burning. More comprehensive EPS models were the ones of Guiderdoni & Rocca-Volmerange (1987), in which the HB and AGB were accounted for to some extent, as well as nowadays ubiquitous components like reddening and nebular emission, but the stellar evolution calculations were compiled from several different sources, each with their own input physics, and this inhomogeneity among the stellar tracks naturally had an impact on the stellar population models as a whole. The models represented a range of ages for each of the standard Hubble sequence galaxy types, differing by the applied law of star formation per unit mass. Additionally, with a stellar library comprised of only 30 spectra the models were restricted to solar metallicity only. For an example plot of one of the models, see Fig.1.4. In another work also worthy of recognition, Olofsson (1989) present EPS models of metal-poor star-forming regions at a fairly high resolution (5 Å), obtained by the exclusive use of theoretical stellar spectra (except for last stages of massive stars, where empirical data had to be included). The integration technique resembles in many aspects that of Bruzual (1983), adding also components such as nebular emission and pre-main sequence stars.

A critical contribution to our understanding and modelling of the UV region of the electromagnetic spectrum at this time was made by the spectrograph on board the *International Ultraviolet Explorer* (*IUE*) satellite. The entire body of work connected to the data obtained with this instrument is too vast to recapture in any detail, but it may be worth mentioning here the library of mean, high-dispersion stellar spectra that was assembled for most spectral classes in a series of papers by Fanelli et al. (1987, 1988, 1990, 1992).

Another step forward was taken by Buzzoni (1989), who produced EPS models for a range of metallicities and even various HB morphologies, including in the synthesis all relevant stellar evolutionary phases. However, only models of relatively old stellar populations (4-18 Gyr) were produced. Additionally, these models were the first to

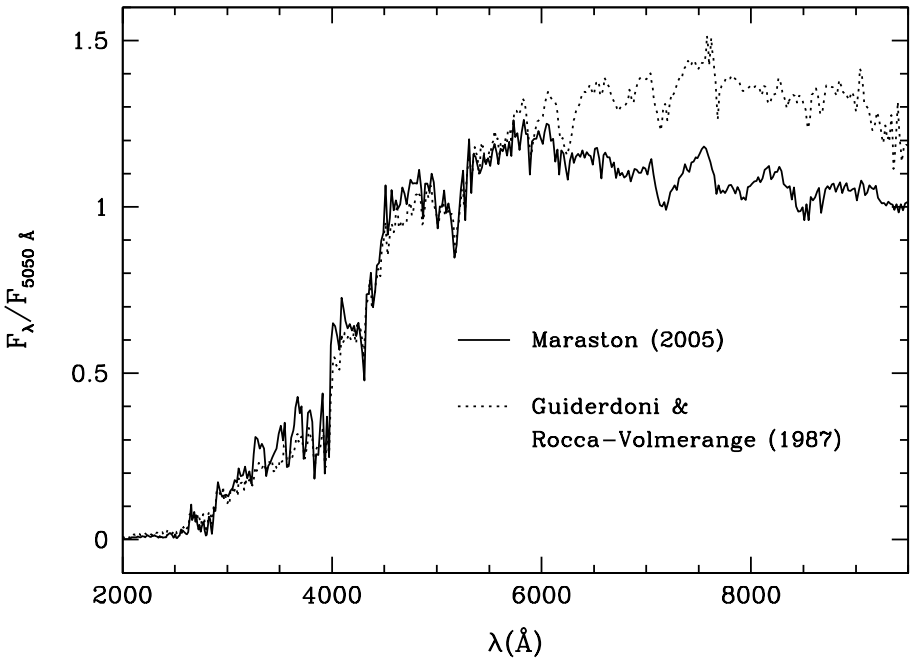

Figure 1.4: The 12 Gyr burst model of Guiderdoni & Rocca-Volmerange (1987) compared to a reference 12 Gyr CSP model from Maraston (2005). Both models assume a star formation history with an e-folding time of 1 Gyr (remember that the birth of an SSP is instantaneous). The large separation between the models is difficult to pinpoint exactly, but is most likely a combination of both a very limited spectral library and outdated evolutionary tracks in the Guiderdoni & Rocca-Volmerange (1987) models.

be built upon the foundation of the fuel consumption approach. The isochrone synthesis technique, on the other hand, was introduced by Chiosi et al. (1988), and followed by Charlot & Bruzual (1991) for photometry only. With advances in stellar evolution theory and computational power, the authors needed less sources to assemble their library of stellar tracks, out of which the isochrones could be built; but due to a lack of photometric calibrations the authors refrained from computing EPS models at non-solar metallicities. These models were updated and extended with spectroscopic information in Bruzual & Charlot (1993), using stellar spectra from a wide selection of observations, complemented with the theoretical atmospheres of Kurucz (1979) for filling in the gaps in stellar parameter space, in order to obtain spectral coverage from the far-UV to the far-IR. The same approach of combining empirical and theoretical stellar spectra was used in Bruzual & Charlot (2003, hereafter BC03)[1], with the optical wavelengths now being covered almost entirely by a single library of high-resolution observed spectra. Both the

[1]Seemingly following a 10-year-interval release plan, can we expect new models from Prof. Bruzual in 2013?

BC03 models and STELIB (Le Borgne et al., 2003), as the library is called, will be discussed more extensively in subsequent chapters (see e.g. Chap.3 for a description of the latter).

The isochrone synthesis technique had by the mid-90s' become the standard in stellar population modelling, much of which can be credited to the availability of comprehensive grids of isochrones and complete libraries of theoretical stellar spectra, combined with the fact that this is a very straightforward (albeit not entirely reliable) approach to evolutionary population synthesis. Worth mentioning here are the models of Bressan et al. (1994) and Bressan et al. (1998), as well as the PEGASE code (Fioc & Rocca-Volmerange, 1997), that relied on a mixture of observed and theoretical stellar spectra. The updated version of this code, PEGASE.2, adopted a fully theoretical scheme with the BaSeL library as a solid ground (Lejeune et al., 1997, 1998). A high-resolution version of the second installment of this code, based on the purely empirical library ELODIE (Prugniel & Soubiran, 2001, see Chap.3), was published in Le Borgne et al. (2004). The Starburst99 models (Leitherer et al., 1999), which expand upon the models of Leitherer & Heckman (1995) in order to, among other things, synthesise the full SED using the theoretical spectra of Lejeune et al. (1997), focus (as revealed by the name of the code) on the hot and massive stars of very young populations, putting little or no emphasis on later evolutionary stages like the AGB.

The two grids of high-resolution models in Vazdekis (1999) and Vazdekis et al. (2003), both of which are based on empirical spectral libraries, and both of which only cover rather narrow wavelength regions (the latter is devoted solely to the region around the near-IR Ca II triplet absorption feature) has recently been expanded upon in Vazdekis et al. (2010). The latter models will be further explored in subsequent chapters of this work as they are built around the MILES library (Sánchez-Blázquez et al., 2006), which is the most comprehensive compilation of empirical stellar spectra to date (and as such will also be thoroughly explored in this thesis from an SED point of view). Coelho et al. (2007) produced α-enhanced SSP models using high-resolution, theoretical libraries, but only for old ages and only for metallicities around solar. And finally, there are the Conroy et al. (2009); Conroy & Gunn (2010) models, which explore the propagation of uncertainties in evolutionary population synthesis – for example by varying the luminosity and temperature of stars in uncertain stellar phases like the TP-AGB and the HB, and in the blue straggler region – using a standard isochrone synthesis approach. Apart from the integration technique and the investigation into uncertainties, the actual EPS recipe share several solutions with those adopted in the M05 models, adding little new except using the latest set of isochrones which include the evolution of intermediate mass stars also

through the TP-AGB phase, and adopting a different calibration for the young GCs in the Magellanic Clouds. The implications of using a shifted age scale is discussed more extensively in Sec.4.8.

1.3.2 The Maraston EPS models

The M05 models (Maraston, 2005) were the first to extend the fuel consumption approach – which allows for a proper treatment of the contribution from TP-AGB stars to the total luminosity – to intermediate-age populations, thereby providing a satisfying reproduction of the spectral evolution also in this critical age range. M05 updated and extended the M98 models (Maraston, 1998) to non-solar metallicities, and added full SED synthesis in addition to the broadband colours already present. Since the work in this thesis is the result from a restructured version of the M05 models, they will be more carefully explained in Chap.2.

1.3.3 Optimised Population Synthesis

In parallel to the development of evolutionary population synthesis existed also another method for reproducing observed composite spectral energy distributions, called *optimised population synthesis* (OPS). Opposed to the evolutionary technique that involves a stellar evolution prescription and a parametrised star formation history, OPS is a direct, automatic optimisation method, that employs a set of stellar SEDs representing the most common spectral types, from which the optimal fit to a galaxy or cluster spectrum is built. The choice of using this technique over EPS is motivated by the fact that it in a straightforward way is able to disregard incomplete stellar evolution calculations, and include more exotic physical conditions not found in stellar populations in the solar neighbourhood. Like in O'Connell (1976, 1980), emphasis is often put on finding an astrophysically plausible solution, i.e. a mixture of spectral types that fulfil any number of preset constraints, such as continuity of evolutionary flow in the C-M diagram, restrictions of the mass-to-light (M/L) ratio in the composite model, or the contribution of a specific stellar component. However, even an unconstrained optimisation run may reveal interesting information – failure to acquire a good fit in this way implies that some component not present in the reference library is an important contributor to the integrated galaxy SED, or possibly that reddening has been insufficiently evaluated.

The literature on optimised population synthesis have declined with the progress of more sophisticated stellar evolution recipes. O'Connell (1976, 1980) has already been mentioned, where an attempt was made to recover the stellar populations in the nuclei of giant ellipticals and the peculiar M32, by fitting narrow-band spectrophotometry between 3300 and 10800 Å, using a library of 37 common stellar types. Other important work include Pickles (1985a,b), Pickles & Visvanathan (1985) on 17 Fornax galaxies, and the substantial contribution in Bica & Alloin (1986, 1987), where the approach for analysing galaxy nuclei was refined by using star clusters instead of a stellar library.

OPS could in many ways be an important complement to modern day EPS modelling. However, used on its own it lacks some of the strengths of the evolutionary approach. Unconstrained OPS for example, even though saying something about missing components in the stellar population, says little about the formation history and actual stellar content in a physically motivated way. In addition, with a comprehensive reference library, there may be an abundance of degenerative solutions to the optimisation problem in question. Constraining the fit on the other hand necessitates well motivated restrictions and requirements – often taken from stellar evolution theory – which may be better integrated in EPS modelling. The spectral fitting methods described in Sec.1.3.5, are essentially a combination of EPS and OPS.

1.3.4 Detailed modelling of individual absorption lines

A powerful new stellar population diagnostic that may be used as an alternative to, or in conjunction with, full SED modelling was presented in Worthey et al. (1994) and first implemented into EPS models by Worthey (1994). It concerns the behaviour of individual absorption lines in stellar populations, which are analysed through so-called indices – well-defined regions in wavelength space covering the absorption lines in question. Each such region is accompanied by two adjacent regions where no prominent features are found, and by connecting the midpoints of these regions at their mean flux a 'pseudo-continuum' is created. The strength of the index is then determined by measuring the flux within the line region relative to the continuum line (see Fig.1.5 for an example plot of the Hβ index). The reason for using this method over SED modelling lies mainly on the observational side – absorption line indices are in practice insensitive to interstellar reddening from dust, and a majority of the most widely used indices lie within a rather narrow, easily observable, wavelength range – and in the fact that each index may be independently calibrated. With full SED modelling on the other hand, a pixel-by-pixel comparison to the observations is possible, thus making use of all the information and not

just the regions around strong absorption features. However, from a theoretical perspective, the modelling of the full continuum is a very complicated procedure, with certain features either missing, or being predicted but not observed, which is another reason for modelling only a specific number of lines.

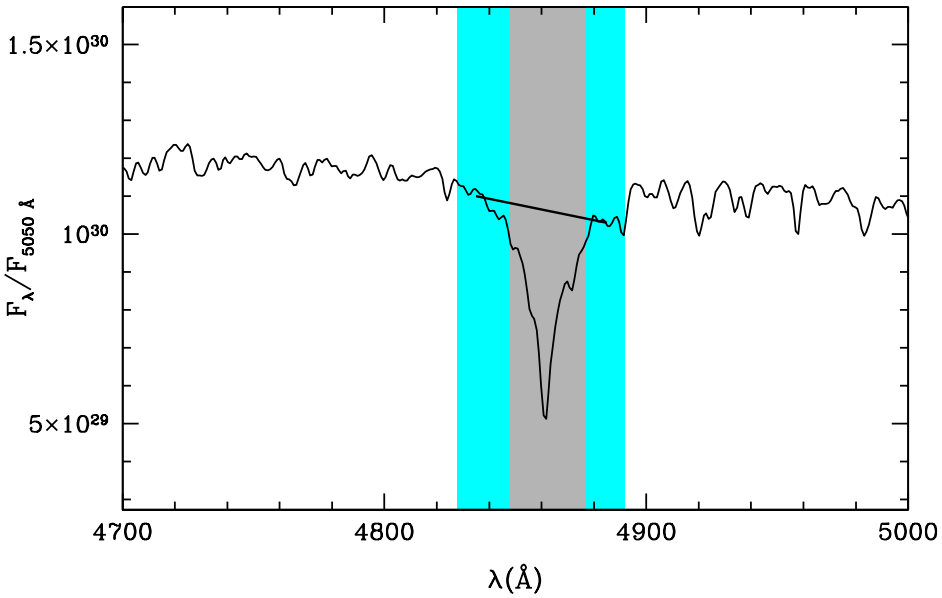

Figure 1.5: The absorption line and pseudo-continua bandpasses (*grey* and *cyan* shaded areas, respectively) of the Hβ index as defined in Trager et al. (1998). The strength of an index is computed by integrating the difference between the pseudo-continuum line and the observed spectrum within the absorption feature bandpass.

Having defined 21 absorption line indices with corresponding blue and red pseudo-continua, Worthey et al. (1994) measured these indices on the 460 empirical stellar spectra that constitute the so-called 'LICK/IDS' library. In this way they obtained empirical relations between absorption line strengths and the stellar parameters temperature, surface gravity and metallicity. These relations, which are called *fitting functions*, are then integrated in a normal isochrone synthesis procedure to yield – along with the more standard broadband colours and SEDs – a grid of absorption line strengths as function of SSP age and metallicity. In theory, this is a tool with great potential. For example, by using an index predominantly sensitive to age (such as Hβ) together with one mainly sensitive to metallicity, the notorious age-metallicity degeneracy can be alleviated (although not

entirely broken since Hβ through the temperature effects associated with different metallicities also indirectly becomes sensitive to metallicity, see Maraston & Thomas 2000). Updated definitions of indices and their pseudo-continua can be found in Trager et al. (1998).

The problem with these models, however, was the flux calibration of the stellar spectra, or rather, the lack of a proper one. This necessitated that a correction must be applied to all data to transfer it onto the LICK/IDS system, before an evaluation can take place (see e.g. Worthey & Ottaviani 1997, who also proposed four new indices). Another issue, that could not be addressed due to an incomplete stellar library, was that of varying element abundance ratios. Stellar populations exhibiting an enhancement of the α-elements (N,O,Ne, Na,Mg,Si,S,Ca,Ti) with regard to the so-called Fe-peak elements (Cr,Mn,Fe,Co,Ni, Cu,Zn) at high metallicity suggest a shorter star formation timescale, since the enrichment of the latter elements in the intracluster medium is generally considered to come primarily from SNe type Ia, which compared to core-collapse supernovae (type Ib, Ic, and II) are delayed by $\sim 10^9$ years. Gibson et al. (1997) showed for example that the Fe yield – on a per SN basis – is at least a factor 5 larger in SNe type 1a compared to type II using a Salpeter IMF. It should be noted, however, that this factor may be lower (even close to 1) for other Fe-peak elements, and depending on environment the SNe Ia:II-ratio could vary from 3:1 in early-type cluster galaxies to 1:5 in late-type field galaxies (see Mannucci et al., 2008). Thus, SNe type II may in certain systems contribute as much as type Ia to the enrichment of Fe-peak elements in the interstellar medium, but the α-enhancement may then generally still be seen at low metallicities (e.g. Feltzing et al., 2003). This naturally has an impact on the theory of galaxy formation, and with several observations confirming α-enhancement in early-type galaxies (e.g. Worthey et al., 1992), corresponding stellar population models are required in order to constrain their star formation history.

It should also be mentioned here, however, that even though a shorter and more effective period of star formation is the most probable explanation for the α-enhancement, there are alternative theories as well. For example, if the initial mass function is allowed to vary over cosmic time, a top-heavy IMF (compared to Salpeter-like IMFs) could produce similar effects even with prolonged star formation timescales. Another option is selective mass loss mechanisms, both for individual stars and for star clusters as a whole. Babel (1995) showed that, on the surface of stars where the magnetic pressure dominates (A and B type stars), radiative winds are able to selectively eject metals from the star, but not hydrogen, thus creating chemically differentiated stars. In addition, the stellar mass function of a cluster, and therefore also its spectrophotometry, can be altered by the

fact that low-mass stars preferentially occupy the cluster outskirts, where they are more easily stripped off (see e.g. Anders et al., 2008). This phenomenon should however affect galaxies to a much lower extent than smaller star clusters.

Utilising the so-called response functions of Tripicco & Bell (1995), which give the variations of line strengths with different abundance ratios, both Trager et al. (2000) and Thomas et al. (2003b) provided such models (based on the underlying SSP models of Worthey 1994 and M05, respectively). The response functions were computed with the help of theoretical stellar spectra on a 5 Gyr, $Z_{\odot}$ isochrone only, and the variations thus found were assumed to be applicable for any stellar population, regardless of age and total metallicity. SSP models with new response functions – this time calculated for stellar populations spanning a range of ages and metallicities – was given in Thomas et al. (2004). Very recently, these models have been extended (Thomas et al., 2011) by implementing new fitting functions based on the MILES library (Johansson et al., 2010, see Sec.4.9 for a comparison between indices predicted by these models and measured directly on SED models).

1.3.5 Full spectral fitting methods

Even though not the focus of this work, we mention here also the technique of full spectral fitting, i.e. using automated, pixel-by-pixel, spectral analysis algorithms such as MOPED (Heavens et al., 2000), VESPA (Tojeiro et al., 2007), STECKMAP (Ocvirk et al., 2006) or GANDALF (Sarzi et al. 2006, based on the PPXF routine by Cappellari & Emsellem 2004). These are useful in order to try to recover – often without a priori assumptions – galaxy parameters (star formation histories, masses, ages, chemical enrichment histories, velocity dispersions, mass-to-light ratios etc.) from the huge data sets nowadays associated with largest surveys (e.g. Reichardt et al., 2001; Tojeiro et al., 2009). Full spectral fitting methods all rely on one or more set of reference EPS models, and benefit from high-resolution, high signal-to-noise spectra. In principle, the method has a lot in common with OPS (see Sec.1.3.3).

1.4 Justification for this work

With the advancement in observational technology has come also the undertaking of state-of-the-art surveys of almost overwhelming proportions. For example, the *Sloan*

Digital Sky Survey (SDSS York et al., 2000) alone has gathered photometric and high-resolution spectroscopic data for more than a million galaxies, stars and quasars. Many other ambitious projects have followed in its wake, such as the GAlaxy Mass Assembly (GAMA) survey (Driver et al., 2009) and the long series of papers connected to the SAURON project that started with Bacon et al. (2001) and continues even to this day. In order to extract as much information as possible from these and future surveys, reliable stellar population models of correspondingly high resolution, for a large grid of population parameters, and with a broad wavelength coverage, are required. It is thus the aim of this thesis to take as large a step as possible in the direction of providing just that.

We do this by implementing several high-resolution *empirical* libraries of stellar spectra into the code of M05. As indicated in previous sections of this introductory chapter, the number of varieties of the different ingredients in evolutionary population synthesis, and therefore the many ways in which they can be combined, poses a serious challenge of fine-tuning to the stellar population modeller. Covering them all within the scope of this thesis would not be feasible, and we focus therefore exclusively on the stellar library part of the modelling, which is the second aim of this thesis.

Apart from gaining a higher spectral resolution with the substitution to the latest empirical libraries, we will also be able to make a comprehensive comparative analysis of the libraries themselves. The comparison is extended to include a few theoretical libraries as well, both of high and low resolution. True enough, there are other EPS models in the publication jungle that adopt empirical libraries in their synthesis, and some even use the same libraries that are examined in this work, but then only one library at a time is considered; also, a comparison of these different models would not just yield the impact of using empirical stellar spectra, but would also be affected by all the differences in input physics. As far as we know, this is the first time that the same EPS code has been used to produce SSP models based on all of the widely used libraries, both theoretical and empirical, which allows for an evaluation of stellar spectra as an isolated input parameter.

By providing the astronomical community with EPS models based on various stellar libraries, and the differences that come with each (in wavelength coverage, resolution, etc.) we give any potential users the option of choosing the version that best suits their needs. Notably, these are also the only high-resolution EPS models in the literature that rely on the fuel consumption theorem, as well as a proper treatment of the TP-AGB evolutionary phase.

1.4.1 Outline of the thesis

In Chapter 1 the basics of evolutionary population synthesis is laid out. This includes a brief description of the main ingredients, and some of the theoretical uncertainties that should be considered. A rather extensive literature review is also given, including both ”traditional” SED-based stellar population models, on which the focus of this thesis lies, as well as the approach using fitting functions and absorption line indices. The chapter is concluded with the justification for writing this work.

A more detailed and technical description of the M05 models and the modifications we made with regards to the new models, entitled MaStro, is given in Chapter 2. The stellar library as an ingredient in EPS will be highlighted, with the benefits and drawbacks of using empirical or theoretical stellar spectra, of either low or high spectral resolution, as the centre around which the discussion will revolve.

The four libraries of empirical stellar spectra that are adopted in the MaStro models will be described in Chapter 3, along with a few theoretical counterparts. How the empirical stellar spectra were implemented in the M05 code is outlined in Chapter 4, where also the resulting coverage in age-metallicity space of the new SSP models is given as a function of the library used. Any modifications or additions made to the models are also mentioned here.

Chapters 5,6, and 7 deal with various astrophysical applications of the MaStro models, such as comparing them with globular cluster and galaxy data (Chap.5; taking advantage of the high resolution of the new models to search for new insights into the age-metallicity degeneracy (Chap.6); and recapitulate how the models have been used in international collaborations on galaxy surveys (Chap.7). Finally, discussions and conclusions will be given in Chap.8, along with a look into what the future may bring for EPS modelling.

Chapter 2

Stellar Population Modelling

On the fundamental equations driving a fuel consumption-based EPS code, how we modified such a code to implement empirical stellar spectra, and why one should bother with empirical spectra in the first place.

2.1 Structure of the M05 code

Since the main objective of this thesis is to produce high-resolution versions of the M05 EPS models using libraries of empirical stellar spectra, it is of the utmost importance to understand how the fiducial code, upon which the MaStro models rest, is structured. The M05 code was thoroughly dissected in Maraston (2005), and so, only the key ingredients need to be recounted here. As previously mentioned, two different integration techniques are adopted in the fuel consumption theorem, depending on which evolutionary phase is currently being evaluated; fuel consumptions are applied only for PMS phases, whereas the MS luminosity is calculated using the traditional isochrone synthesis approach, which is a good approximation for such a well-understood and well-behaved phase (in the sense that during the MS the luminosity L of a star is effectively proportional to stellar mass M, which is no longer the case once the star evolves off the MS and into the PMS). This method of using two different integration schemes obviously assumes that the total bolometric luminosity (or the luminosity of any given photometric passband for that matter) of the entire stellar population is just the sum of the bolometric (or passband) luminosities of each constituent star, so that also

$$L_{tot}(t, C) = L_{MS}(t, C) + L_{PMS}(t, C) \tag{2.1}$$

for an SSP of age t and chemical composition C (Y, Z, and to a lesser extent, individual element abundance ratios). The two terms on the right hand side of the equation will now be treated separately.

2.1.1 The main sequence

All stars spend most of their lifetime in the core-hydrogen burning state, although the lifetime itself depends greatly on the mass of the star. A set of coeval stars with a given distribution of initial masses thus forms what is known as the main sequence – a nearly linear relation between mass and luminosity for stars who have yet to exhaust their central supply of hydrogen. With the exception of the very low-mass end of the MS (sometimes referred to as the *lower main sequence*, LMS) this relation is well reproduced by isochrones.

Evolution during the main sequence phase is very small. The exception is, of course, the turnoff region, where stars leave the relative safety of the first $\sim$90 % of their lifetime, to venture into the considerably more dramatic existence that is the post main sequence. The current mass at which this happens (known as the turnoff mass M_{TO}) in a simple stellar population is correlated with the time passed since the birth of the stars (in resolved stellar populations it is therefore a good estimator of the population age). By integrating the contributions from each mass bin along an isochrone up to the turnoff mass we obtain the MS luminosity L_{MS} at time t as:

$$L_{MS}(t, C) = \int_{M_{in}}^{M_{TO}(t,C)} L(M|t, C)\Psi(M)dM \tag{2.2}$$

where M_{in} is the minimum mass required to ignite nuclear fusion (around 0.1 $M_{\odot}$); $L(M|t, C)$ is the mass-luminosity relation from an isochrone of given t and C; and $\Psi(M)$ is the initial mass function.

2.1.2 The post main sequence

Unlike the main sequence, which spans a wide range of masses, the difference in evolutionary mass (i.e. not taking any mass loss effects into account) between a star in the turnoff region and a star at the end of its AGB phase is actually rather small. This implies that, at any given SSP age, all the PMS phases can be approximated by, and fuels can be computed from, the evolutionary track of a star with the current turnoff mass. It also means that the rate at which stars evolve off the main sequence is comparable to the rate

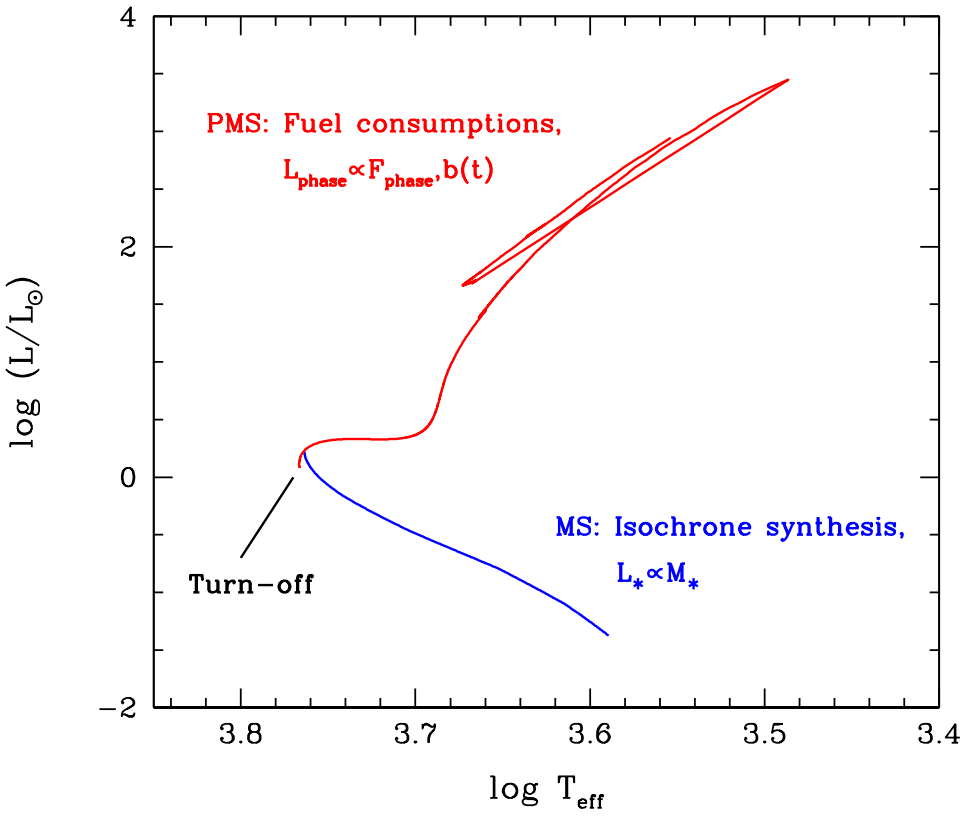

Figure 2.1: A schematic plot of the two methods of integration, separated by the turn-off. The MS (*blue*), in which the luminosity of a star is proportional to its mass, is integrated using the isochrone synthesis technique. The PMS (*red*) on the other hand is better handled using the fuel consumption theorem, where the luminosity of any given subphase depends on the amount of fuel that is spent there (computed from the evolutionary track of a turn-off star) and on the duration of the phase (determined by the in- and outflux of stars to that phase).

at which they evolve off any PMS phase (Renzini & Buzzoni, 1986). This is called the *evolutionary flux* $b(t)$, which in unit of stars per year is given as:

$$b(t) = \Psi(M_{TO})|\dot{M}_{TO}| \tag{2.3}$$

where $\dot{M}_{TO}$ is the time derivative of the relation $M_{TO}(t|C)$. The fuel consumption theorem states that "The contribution of stars in any given PMS stage to the integrated bolometric luminosity of an SSP is directly proportional to the amount of fuel burned during that phase" (Renzini & Buzzoni, 1986). If the fuel burned in PMS phase j is given by:

$$F_j(M_{TO}) = m_j^H + 0.1 m_j^{He} \tag{2.4}$$

with m_j^H and m_j^{He} being the mass (in solar units $M_\odot$) converted into light by hydrogen and helium, respectively, in that phase as computed by the stellar track of a turnoff star, and the factor 0.1 taking into account the fact that the energy obtained from fusing 1 gram of He into C and O is roughly 10 % of the energy released when fusing 1 gram of H into He, then the mathematical representation of the FCT becomes:

$$L_{PMS}(t, C) = 9.75 \cdot 10^{10} b(t) \sum_j F_j(M_{TO}) \tag{2.5}$$

where the emerging luminosity is given in solar units $L_\odot$. The factor $9.75 \cdot 10^{10}$ also incorporate the conversion of expressing the evolutionary flux in years, as well as the fuel in solar masses through the Einstein equation $E = \Delta Mc^2$, with $\Delta = 6.55 \cdot 10^{-3}$ (considering that the fusion of 1 g of H into He releases $\sim 5.9 \cdot 10^{18}$ ergs). For a schematic plot showing the separation between the two integration methods see Fig.2.1.

2.1.3 Transformation to observable quantities

With the energetics of the EPS models computed in the manner described above, a transformation of the obtained theoretical quantities into their observable counterparts is necessary if a comparison with actual observations is to be made. In the M05 models this transformation is performed by means of the fully theoretical library of stellar spectra presented in Lejeune et al. (1997, hereafter referred to as the BaSeL library) and Lejeune et al. (1998), which is based on the classical Kurucz model atmospheres (Kurucz, 1979). The BaSeL library is in principal complete with regards to the stellar parameter grid, encompassing spectra in the effective temperature range $2000 \leq T_{eff} \leq 50000$ K, and surface gravities between -1.0 and 5.5 dex., for metallicities [Z/H] [1] extending all the way from -5.0 to $+1.0$ dex. For extremely young populations, that require stars with temperatures above 50000 K, the M05 models adopt a strict blackbody curve (this is also a standard procedure for many other EPS codes in the literature). However, element abundance ratios are restricted to solar-scaled values only, and no specimens of more exotic stars, such as carbon or oxygen stars, are present (which is understandable considering the theoretical uncertainties and numerical difficulties involved in modelling such stars). Full SEDs are available for each individual star, stretching from the UV (91 Å) into the far-IR (160 μm), thus providing excellent wavelength coverage, but the

[1] The relative abundance [a/b] is from here on defined as

$$[a/b] = log_{10}(\frac{N_a}{N_b})_{star} - log_{10}(\frac{N_a}{N_b})_{sun} \tag{2.6}$$

where N_a and N_b is the number of atoms of elements *a* and *b* per unit volume, respectively.

resolution ($\sim$ 20 Å FWHM in the optical) is not adequate for applications to modern high-resolution observations.

In order to model the spectral energy distribution of a stellar population, stellar spectra must be assigned to each mass bin along the isochrone. Since the recipe adopted for the PMS in M05 involves stellar evolutionary tracks, not isochrones, it is also necessary to further divide the tracks into an appropriate number of subphases, so that changes in spectral type can be followed accordingly. It was found that a temperature difference of $\sim$ 100 K or less between subphases was enough for this purpose.

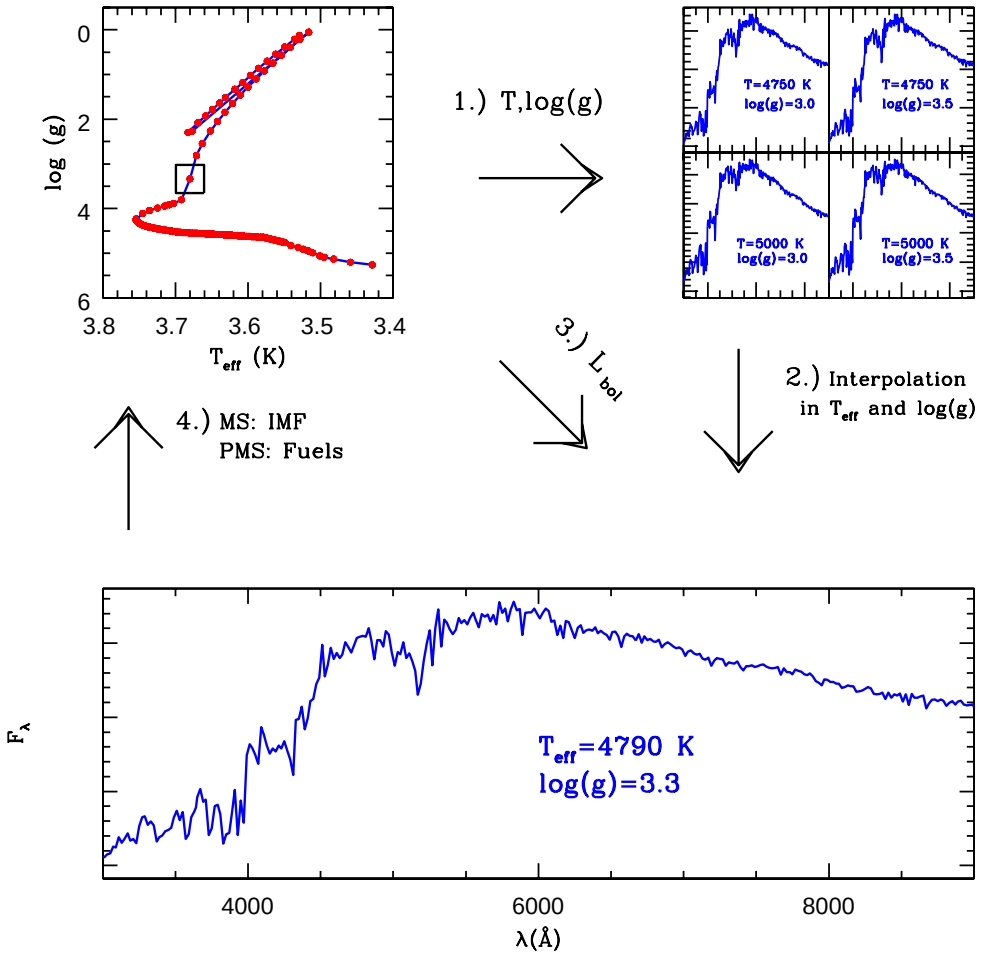

Figure 2.2: Schematic representation of how the energetics in the M05 code are transformed into observables for each individual mass bin, using the theoretical stellar spectra of Lejeune et al. (1997). A detailed description of all the steps is given in the text.

Fig.2.2 schematically describes how the theoretical stellar spectra enter into the M05 EPS code and how the representative spectra for each individual mass bin emerges. The

final integrated SED for the entire SSP is then produced by co-adding the representative spectra. Below follows a more detailed description of each step in this process.

1) Each mass bin of an isochrone and subphase of an evolutionary track is characterised by an effective temperature, T_{eff}, and a surface gravity, log(g). These parameters are passed on to a table of LCB97 stellar spectra corresponding to the metallicity of the SSP.

2) The code then finds the four spectra in this table that enclose the given stellar parameters, and performs a quadratic interpolation in T_{eff} and log(g) to obtain a spectrum that is representative of the mass bin or temperature bin (in shape, not yet in weight). Since the LCB97 library spectra are homogeneous, theoretical predictions computed from model atmospheres, they can be given in well-defined, absolute units of flux moment H_ν [$ergs\,s^{-1}\,cm^{-2}\,Hz^{-1}\,sr^{-1}$], which is converted into F_λ [$ergs\,s^{-1}\,cm^{-2}$ Å^{-1}] via the relation:

$$F_\lambda = \frac{0.4\pi c H_\nu}{\lambda^2} \tag{2.7}$$

where the factor 0.4π stems from converting flux moment into flux, and expressing the speed of light c in [$nm\,s^{-1}$] and the wavelength λ in [nm].

3) The fluxes of the representative spectrum calculated in the last step are still surface fluxes, however, and in order to convert them into luminosities [$ergs\,s^{-1}$ Å^{-1}], which is the preferred unit, additional information about the radii of the stars are required. Radii can be obtained using the Stefan-Boltzmann law, which state that the total power radiated per unit area from the surface of a blackbody is proportional to its temperature to the fourth power (assuming that stars behave as blackbody radiators, which is actually a fair approximation for all but the coolest most metal-rich stars). Thus,

$$R = \sqrt{\frac{L_{bol}}{4\pi\sigma T_{eff}^4}} \tag{2.8}$$

where the proportionality constant σ is called the Stefan-Boltzmann constant. For the MS, values of L_{bol} associated with each mass bin are provided by the isochrone. For the PMS, on the other hand, L_{bol} values are obtained from fuel consumption calculations.

4) The final step involves scaling the interpolated spectrum so that it is truly a representative spectrum for all the stars in the population that belong to the given mass or temperature bin. In the isochrone synthesis part of the integration, this is done by the IMF, whereas in the fuel consumption part, it is the fuels that determine the

contribution of the subphase to the total luminosity. Therefore, in the PMS this scaling effectively takes place during the third step described above, and the radius computed is not the radius of a typical star of that temperature bin, but rather the radius of a hypothetical star having the combined luminosity of all the member stars of the subphase.

The four steps are repeated for each isochrone mass bin and evolutionary track temperature bin, and the representative spectra are co-added to yield the spectral energy distribution for the entire SSP. Due to their peculiar nature, TP-AGB stars do not follow the recipe outlined above, and their treatment is instead described in the next section.

Stars as blackbody radiators

The effective temperature, T_{eff}, of a star is defined as the temperature an equally sized blackbody must have in order to yield the same total energy output per unit time (this also means the two bodies will have the same *bolometric* luminosity per unit surface area). For most stars, the SED continuum and corresponding blackbody curve coincide rather well, but the cooler, more metal-rich a star is, the worse the visual agreement becomes due to line blanketing effects from molecular absorption bands. In addition, a lower surface gravity also tends to increase the discrepancy. Concerns may therefore be raised about the validity of using the Stefan-Boltzmann law to obtain luminosities from surface fluxes under step 3 above. However, the radii in this step are obtained using bolometric luminosities and temperatures given by the stellar evolution computations (isochrones and stellar tracks). It is therefore not of the greatest importance that the stellar SED agree perfectly in shape with a blackbody curve, as long as the product of surface flux and radius becomes the desired value of bolometric luminosity, and by definition of the stellar effective temperature, they will. An example of this is given in Fig.2.3, where the bolometric surface luminosities are in excellent agreement, but more detailed photometry in the standard passbands reveals differences of up to about 1 mag.

Treatment of TP-AGB stars

As previously mentioned, carbon-rich and oxygen-rich stars, which are crucial in intermediate age populations, and for the near-IR light in particular, were not present in the LCB97 library (nor in any other theoretical library at the time for that matter). Instead, M05 utilised the empirical, time-averaged spectra of TP-AGB stars published by Lançon & Mouhcine (2002), which comprise of 5 and 9 mean spectra of carbon and oxygen stars,

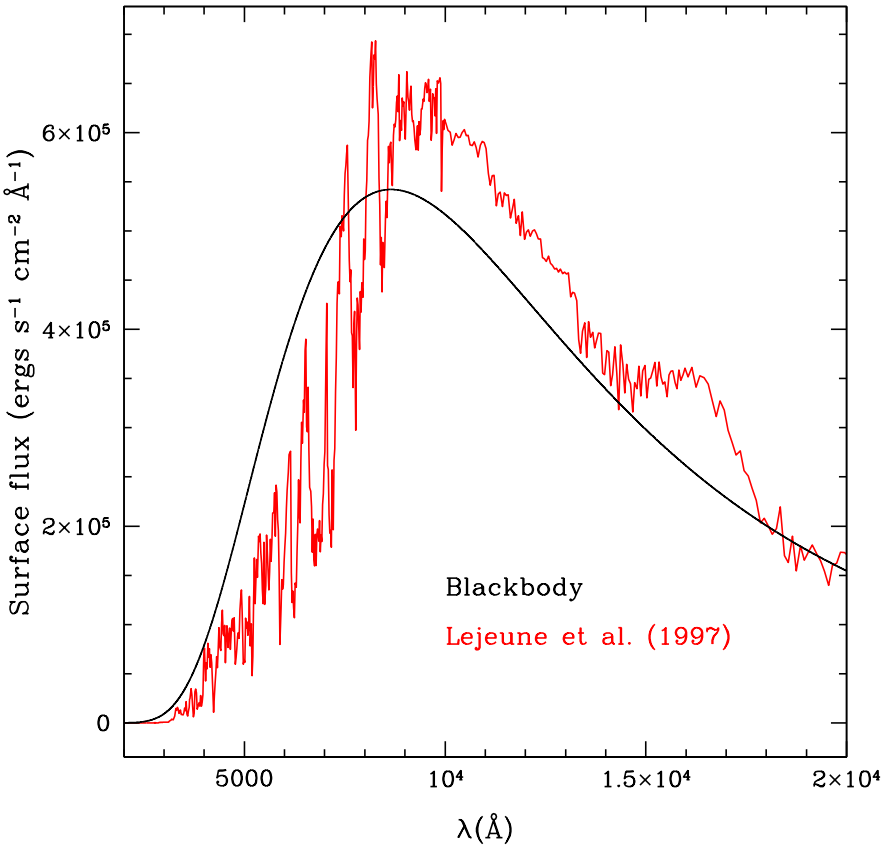

Figure 2.3: Comparison between a T_{eff}=3350 K, log(g)=4.50, $Z_{\odot}$ BaSeL spectra, and a blackbody curve of corresponding temperature. Bolometric surface luminosities are -24.634 and -24.636 mag., respectively.

respectively. In the context of evolutionary population synthesis it is especially important to use averaged spectra due to the pulsating nature of these types of stars, which may lead to large observational scatter, both between different stars, but also between several observations of the same star, and thus the introduction of stochastic effects in the synthesis.

The contribution of the TP-AGB phase to the bolometric luminosity was originally in M98 calibrated with measurements of LMC GCs (the metallicity of the LMC is roughly $0.5\ Z_{\odot}$). This calibration can be extended to other chemical compositions via an analytical recipe, after acknowledging that the total TP-AGB fuel does not depend significantly on metallicity. Unfortunately, the metallicities of the spectra in Lançon & Mouhcine (2002) are not determined, but since they are located in the solar neighbourhood one might expect them to also be representative of the chemical pattern of this region of the Galaxy. However, the authors also argue that metallicity effects should have little effect on the shape of the spectra.

What matters is instead the relative amount of TP-AGB fuel that is consumed by C-stars compared to that of O-stars. Generally, carbon and oxygen in the stellar envelope tend to bind into CO-molecules. A metal-rich star, displaying plenty of oxygen in the envelope, requires a lot of carbon to be dredged up during the thermal pulses in order for all the oxygen to be bound into CO. Higher metallicities therefore favour the production of O-stars. Equivalently, a metal-poor star requires much less dredged-up carbon, and the surplus atoms thus goes into making carbon stars. Fig.12 of M05, based on the calculations of Renzini & Voli (1981), shows the partition of the total TP-AGB fuel between C- and O-stars, as a function of age for the relevant metallicities. In addition, Brewer et al. (1995) found a fairly tight inverse correlation between metallicity and the C/M-ratio for carbon and oxygen stars in M31. It is interesting to compare their Fig.17 with the above mentioned figure in M05, although the different quantities on both the abscissa and the ordinate make an exact comparison rather difficult.

2.2 Empirical vs. Theoretical stellar spectra

One of the main motivations for this work is to produce high-resolution stellar population models based on the M05 EPS code. We opted to do so by using mainly compilations of empirical stellar spectra. However, with the rich fauna of high-resolution, theoretical libraries nowadays available in the literature (e.g. Bertone et al., 2004; Murphy & Meiksin, 2004; Brott & Hauschildt, 2005; Coelho et al., 2005; Martins et al., 2005; Munari et al., 2005; Rodríguez-Merino et al., 2005; Gustafsson et al., 2008), resolution can no longer be considered the only justification for employing empirical spectra, and a more expanded discussion about the reasons behind our choice is therefore in order.

It has been suggested that a few remaining problems with the broadband colours of stellar population models, such as the (*B*-*V*) colours of Milky Way GCs (e.g. Maraston, 2005), or the ($g' - r'$) and ($r' - i'$) colours of the SDSS *luminous red galaxies* (Maraston et al., 2009b, see also Sec.5.4), could be, at least in part, due to possible shortcomings of the theoretical stellar spectra used in the EPS models. Synthesising stellar spectra requires a careful balance between including extensive, but poorly calibrated, atomic and molecular line lists (all the so-called predicted lines), in order to try to simulate accurate line-blanketing and broadband colours, but perhaps with less precision in the high-resolution features; or, using instead an incomplete line list where special attention has been given to a smaller number of carefully calibrated lines, for which the outcome will then be the opposite. Therefore, by implementing empirical spectra into the EPS code, we hope to eradicate some of the discrepancies between models and observations.

Another advantage of using empirical spectra is that, quite often, galaxy data is procured with the same instruments that was used to build the stellar library. Using a stellar population model that is based on spectra obtained with the same spectrograph as the galaxy spectra ensures a certain degree of homogeneity and may reduce systematic errors. Thus, creating EPS models for several different empirical libraries, as proposed in this work, increases the opportunity for such a synergy.

However, empirical libraries are often restricted to a fairly narrow wavelength range, due to instrumental limitations as well as to physical limitations imposed by the atmosphere of the Earth, and in addition they require a careful flux calibration – a process that, as we shall see, is associated with great difficulties. Also, the grid of stellar atmospheric parameters, such as T_{eff}, log(g), and Z, is naturally limited to Milky Way stars and their complex chemical enrichment history. This means that solar metallicity stars, which are preferentially found in the Milky Way thin disc, will have solar composition ([α/Fe]=0), whereas the most metal-poor stars observed reside in the Galactic halo, where the α-enhancement will be appreciable ([α/Fe]$\sim +0.4$). The Galactic thin disc and halo are bridged by the thick disc, which also shows a rather large enhancement of the α-elements at [Fe/H]≤ -0.4 (Feltzing et al., 2003). Stellar population models reflecting the Milky Way trend of increasing α-enhancement with decreasing metallicity will not necessarily be a good representation of other galaxies, whose formation history and abundance patterns may differ greatly from that of our own. Massive early-type galaxies, for example, often display simultaneously high (even super-solar) metallicity and large α-enhancement, implying short, but effective, star-formation timescales (Thomas et al., 2005). There is no guarantee of finding a direct analogue for stars with this specific chemical composition in the Milky Way, but bulge stars are the most promising candidates. Maraston et al. (2003) showed that the two bulge clusters NGC 6528 and NGC 6553 in fact display relatively strong α-enhancement at high metallicity ($Z\sim Z_{\odot}$). Unfortunately, bulge stars are notoriously difficult to observe due to the vast amounts of dust in the Galactic plane, and are absent from the empirical libraries studied herein. Theoretical stars can instead be modelled for an arbitrarily well-sampled grid of stellar parameters at an arbitrarily high resolution, for an arbitrarily defined wavelength range. This flexibility is the greatest strength of using theoretical libraries.

2.2.1 The Milky Way bias

The fact that we are restricted to Milky Way stars will also be reflected in the age coverage at any given metallicity for the stellar population models that can be constructed from

each empirical library (see Chap.4). Since star formation is more or less restricted to the metal-rich thin disc, models at low metallicity will in turn be restricted to old ages. The issue of α-enhancement as a result of the specific star formation history and chemical enrichment history of the Milky Way has already been discussed. For now, a combination of empirical and theoretical stellar spectra and SSP models appears to be the best approach to tackle all the problems faced in the galaxy formation and evolution branch of astrophysics today.

Working around the bias introduced by the fact that we happen to live in a certain region of a certain galaxy, requires the use of theoretical stellar spectra, since they can be computed for any given set of parameters (T_{eff},log(g),[Z/H],[i/H]), where [i/H] is the abundance ratio of any chemical element *i*. The most common method is to simply fill in all the gaps in the empirical stellar parameter space with theoretical stars, thus ensuring a complete grid of stellar spectra in the synthesis. This does not, however, solve the problem of the abundance ratios. If one desires to remove the bias at non-solar metallicities, or adding an arbitrary amount of α-enhancement at any metallicity, but at the same time is interested in keeping an empirical foundation in the EPS models, a method similar to the one tested in Walcher et al. (2009) is necessary. Purely theoretical SSP models are here used to calculate so-called 'differentials', i.e. relative flux differences on a pixel-by-pixel basis between SSP models as a function of [Fe/H] and [α/H] for a given SSP age. These differentials are then applied to an empirical base model of solar metallicity and composition in order to obtain the desired combination of metallicity and α-enhancement.

In this work we will deal with the Milky Way bias simply by acknowledging the fact that we are restricted in terms of stellar parameter coverage, filling in important gaps in stellar parameter space using high-resolution theoretical spectra, but avoiding an extrapolation of the SSP models to younger ages since this requires an increasingly larger fraction of theoretical stars. All models will reflect the abundance ratio pattern of the Milky Way, leaving a correction of the chemical bias (for example using a method in the vein of Walcher et al. 2009) for a later time, as it is deemed out of the scope of this work.

2.3 Implementing empirical spectra into the M05 code

Inserting theoretical stellar spectra into an evolutionary population synthesis code is a relatively straightforward procedure, since they can be computed in absolute units, and for

any given choice of atmospherical parameters. The approach adopted in the M05 code, where a stellar spectrum is assigned to each [T_{eff}, log(g)]-bin by means of quadratic interpolation in T_{eff} and log(g) at fixed metallicity, is, however, generally not feasible when empirical libraries are used, due to their coarser sampling of the parameter space. Also, even though adopted by other EPS codes, such as the one of Vazdekis et al. (2010), this strict reliance in the stellar parameters for assigning stars to the [T_{eff}, log(g)]-bins introduce a risk of using stars that lie very close in parameter space but really belongs to a completely different evolutionary phase. For example it is possible for a T-RGB (tip of the red giant branch) star and a red supergiant to share a very similar set of parameter values, but when examining their spectral energy distributions a noticeable difference is revealed. Theoretical libraries do not make distinctions between separate evolutionary phases in this way.

Instead in this work, we take advantage of the fact that the M05 code synthesises each evolutionary phase separately, at least for populations that are old enough to have developed distinctly separate phases, which occurs after a few tens of millions of years. This feature was originally implemented in order to be able to calculate the contribution to the total light from each phase, but we will harness its power for additional purposes here.

For each empirical library we therefore created subsamples of stars, corresponding to the different evolutionary phases, i.e. main sequence, subgiant branch, red giant branch, horizontal branch, early asymptotic giant branch, and supergiants. The categorisation was performed mainly based on the surface gravities and luminosity classes of the spectra, but other discriminants, such as visual inspection of the spectra and comparisons to isochrones and theoretical spectra were also used; all taken together, this task of properly grouping the library spectra was a very time-consuming one given the number of stars involved.

More specifically, the cuts in surface gravity that were applied for each respective evolutionary phase are: MS (log(g)>4.0), SGB (3.5<log(g)<4.0), RGB, HB and E-AGB (1.0<log(g)<3.5), and supergiants (log(g)<1.0). These cuts are, of course, only approximate and depends somewhat on temperature and metallicity as well; it is not unusual for hot MS stars (spectral class A or B) or hot supergiants, to have surface gravities below 4.0 dex or above 1.0 dex, respectively. Spectra on the borderline between two evolutionary phases were therefore permitted to be present also in both subsamples – given of course that these two stages of evolution follow directly upon each other.

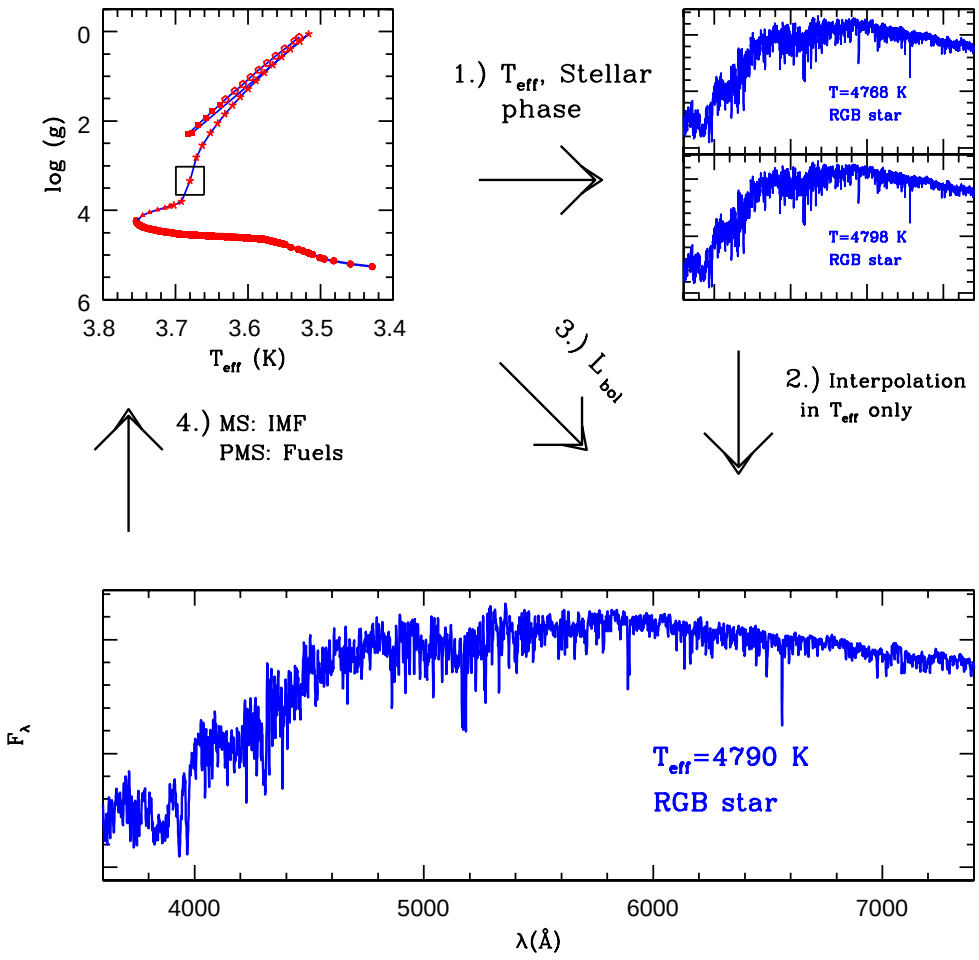

Figure 2.4: Same as Fig.2.2, but for empirical stellar spectra. The symbols in the upper left panel denotes respectively: *filled circles*=MS, *filled triangles*=SGB, *stars*=RGB, *filled squares*=HB, and *open pentagons*=E-AGB.

This new procedure, is outlined in Fig.2.4. Here, steps 3 and 4 are the same as in the case with theoretical stellar spectra (compare to Fig.2.2), whereas steps 1 and 2 have changed slightly. Where the M05 code integrates each evolutionary phase separately, but draws spectra from just one set of stars – which is the same for all phases – and then interpolates in temperature and surface gravity, the MaStro code by means of a newly written subroutine assigns to each evolutionary phase only stellar spectra that belongs to the subsample of stars corresponding to that specific phase, now interpolating solely in temperature (to be more precise, the representative spectrum is calculated by means of linear interpolation, in T_{eff}, of the logarithmic fluxes). In this way – contrary to a scheme where the stellar parameters temperature and gravity alone determine the interpolation procedure – the stars are used only in evolutionary phases where they belong, providing, of course, that the classifications of the stellar spectra are reliable. It is also

assumed that the difference in surface gravity between the isochrone or stellar track point and the two stars involved in the interpolation, is of the same order as the observational errors in surface gravity, or at least small enough to have a negligible impact on the spectral shape of the stars. Generally, the shape of stellar SEDs have a stronger temperature than gravity dependence.

In the next chapter we present a detailed description of all the libraries of empirical stellar spectra that are employed in this way to produce MaStro models.

Chapter 3

The Libraries of Empirical Stellar Spectra

On the different compilations of empirical stellar spectra adopted in the new models, how they must be scaled before use, and a little bit about that necessary evil known as flux calibration.

When modelling empirical spectral energy distributions in evolutionary population synthesis, there are in principal two requirements on the stellar library that need to be fulfilled. First of all, it should be complete, i.e. comprise stars of all relevant evolutionary stages, for at least one metallicity. The [T_{eff},log(g)] parameter space needs also to be relatively well-sampled, preferably all the way from the very cool stars of the lower main sequence, the tip of the red giant branch, and the red supergiant phase, to the hottest MS and blue supergiant stars. Second of all, it is imperative that the library is properly flux calibrated, since we strive to model both the general SED shape (broadband colours) of stellar populations, as well as the high-resolution spectral features; if no flux calibration has taken place, the continuum slope will be skewed and the broadband colours will become completely unreliable.

These prerequisites limited our choice of stellar libraries, but in the end the four most extensively used libraries in the community, each with their own strengths and weaknesses, all fulfilled the requirements and were therefore chosen. A brief summary of the Pickles (Pickles, 1998), STELIB (Le Borgne et al., 2003), MILES (Sánchez-Blázquez et al., 2006), and ELODIE (latest version Prugniel et al., 2007) libraries can be found in Table 3.1. Note that the values of [Fe/H] that are listed in the table are quoted values

Table 3.1: SUMMARY OF THE EMPIRICAL LIBRARIES USED IN THE MASTRO MODELS.

Library	No. of stars	Wavelength range (Å)	FWHM (at 5500 Å)	[Fe/H]
Pickles (1998)	131	1150-25000	11 Å	[−0.8, +0.6]
STELIB	249	3200-9300	3.0 Å	[−2.75, +0.6]
MILES	985	3500-7430	2.3 (2.54)* Å	[−2.9, +1.6]
ELODIE v3.1	1388	3900-6800	0.55 Å	[−3.0, +1.0]

* Beifiori et al. (2011)

from each library. In reality this means they are minimum and maximum values only, and therefore says nothing about the actual sampling of the parameter space, or the limits for EPS modelling. For example, in the MILES library only three stars have a metallicity higher than [Fe/H]$= +1.0$, which, even though it is impressive in itself to find such metal-rich stars, is certainly not adequate for EPS purposes. Surely, this was also not the intentions of the authors, as these stars are very rare.

Also the way in which the metallicity is determined may vary between libraries; thus the meaning of the [Fe/H] parameter (which is actually iron abundance) and its relation to [Z/H] (total metallicity) for each respective library is a bit unclear (see Thomas et al. 2003b for a discussion on the definitions of these parameters). Finally, the resolutions in Table.3.1 are also quoted values, and as we shall see later on some of them are in need of slight revisions.

A more fair view of the library contents is given in Fig.3.1, which display the metallicity distributions of the STELIB, MILES, and ELODIE library. The Pickles library was here omitted as it basically contains only solar metallicity stars. Due to a large library-to-library variation in the number of stars, the scale on the y-axis is logarithmic. It is clear from this figure that the MILES library offers the most complete sampling of metallicity space of the three. A more thorough review of the important features of each library, together with a description of any alterations we may have imposed upon the spectra, follow in the next few sections.

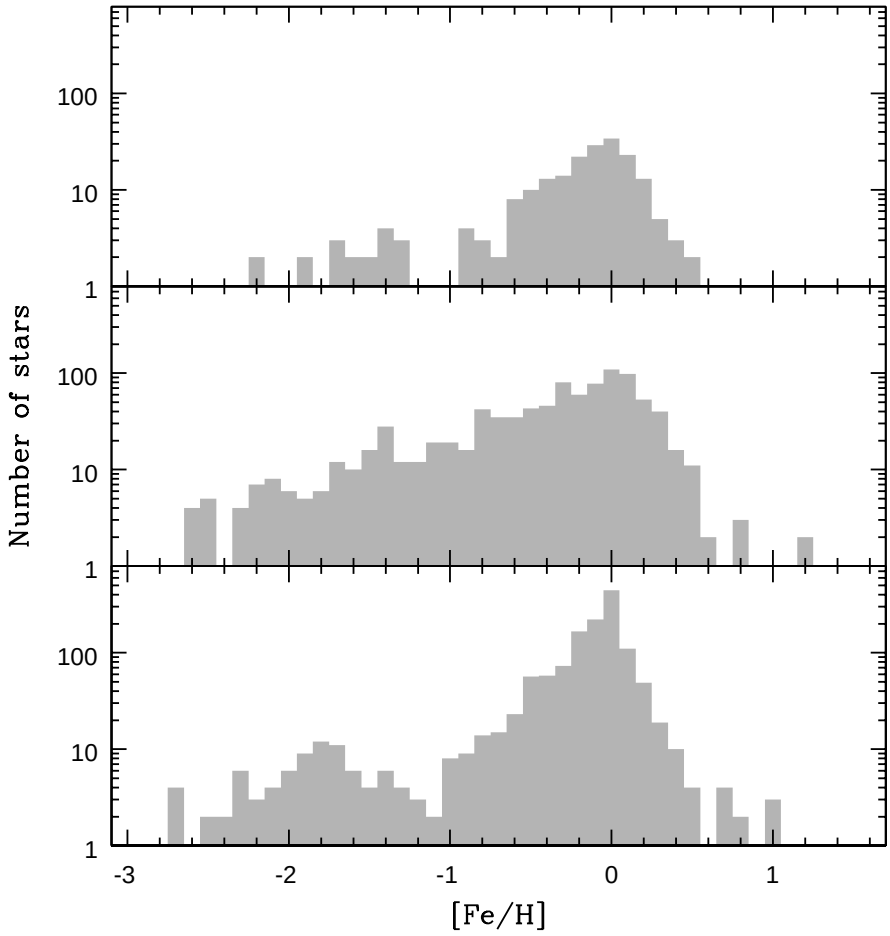

Figure 3.1: Metallicity distributions of the STELIB, MILES, and ELODIE libraries. The scale on the y-axis is logarithmic due to the large difference in number of stars between libraries.

3.1 The Pickles library

The Pickles library (Pickles, 1998) is the only one out of the four chosen that does not contain spectra of individual stars. Rather, the author has vacuumed the literature for a versatile collection of stellar libraries covering different regions of the electromagnetic spectrum, and combined the various observations, in order to provide standard spectra for all normal spectral types and luminosity classes. Because they are (for the most part) averages of spectra from several sources, the Pickles spectra should not be as affected by systematic and random observational errors, as a library containing single observations of each star using the same setup.

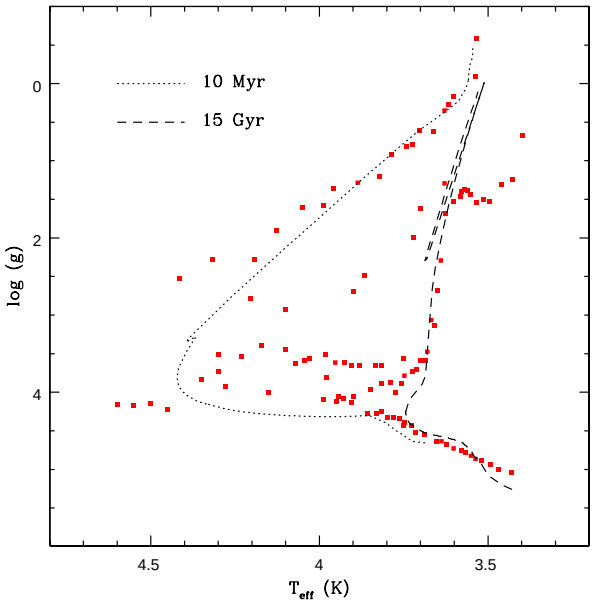

Figure 3.2: Evolutionary coverage at $Z_{\odot}$ for the Pickles library. Superimposed are the 10 Myr and 15 Gyr isochrones (MS) and stellar tracks (PMS) that are used in the synthesis (see M05 for a description of the isochrones and tracks).

The library has exemplary coverage of evolutionary phases, as can be seen from Fig.3.2, encompassing everything from the coolest M dwarfs and giants ($T_{eff} \approx 2500$ K) to hot O-type stars and supergiants (both blue and red). Rather unfortunately, only solar metallicity models can be computed from this library, since there are not enough spectra to cover all required evolutionary phases to a satisfactory degree at non-solar metallicities.

The fairly low resolution of the Pickles library (R$= 500$) is somewhat compensated for by very robust photometry, and the widest wavelength range of all empirical libraries described here, ranging all the way from the far-UV (1150 Å) into the short-wavelength IR including the K-band (2.5 μm). Above $\sim 1\,\mu$m, about half of the spectra lack spectroscopic observations, and the author constructed here instead a smooth energy distribution from broadband photometry of various sources. Also, at these wavelengths, the M giant spectra are purely synthetic. Finally, carbon- and oxygen-rich stars of the TP-AGB phase are not included in the Pickles library – something it has in common with all the other libraries considered in this work.

The effective temperatures of the Pickles spectra were assigned by the author by means of (*V*-I_C) and (*V*-*K*) colour-temperature relations taken mainly from Bessell (1979),

and from Fluks et al. (1994) for the M giants. No accurate metallicity calibration was performed, other than sorting the spectra into solar or non-solar metallicity based on a recipe described in Pickles & van der Kruit (1990), which should be sufficient since we only use the $Z_\odot$ stars anyway. Surface gravities are not given for any of the library stars, but we have obtained estimates by matching the stars in a M_V-(*B*-*V*) colour-magnitude diagram to the isochrones of Girardi et al. (2000). These estimates are for reference only and will not be used explicitly, but they serve as an internal check of the luminosity class designation of the Pickles spectra.

3.2 The STELIB library

Le Borgne et al. (2003) obtained roughly 250 stellar spectra of fairly high resolution (~ 3 Å FWHM) and with good wavelength coverage. Most spectral types and luminosity classes are included, with a fair coverage in metallicity. In particular though, there is a deficit of stars with [Fe/H]< -1.0. Several spectra lack atmospheric parameter determinations, and many do not have complete spectroscopic observations over the entire quoted wavelength range. Such stars were excluded from the synthesis. In addition to this, the spectra suffer from telluric contamination. We have circumvented this problem by simply interpolating over the most affected wavelength regions, more precisely 6850-6950 Å, 7580-7700 Å, and 8850-9050 Å. Granted, this might not be the most aesthetically pleasing solution, and it is by no means a complete eradication of all telluric absorption features, but it acts as a warning beacon to users and ensures that no science can be done within said regions. The STELIB library has previously been adopted for stellar population synthesis by Bruzual & Charlot (2003, hereafter BC03). These authors replaced the contaminated segments with theoretical spectra, computed using the (then) latest Kurucz model atmospheres, for stars cooler than 7000 K, or with Pickles (1998) spectra for hotter stars.

The evolutionary coverage for the STELIB library at solar, half solar, and twice solar metallicity can be seen in Fig.3.3. There appears to be a general lack of cool stars in the library; both dwarfs and giants are missing at non-solar metallicities, while at $Z_\odot$ it is mainly LMS stars. At metallicities lower than -1.0 $Z_\odot$ the sampling of stellar parameter space is deemed too sparse, and also 2 $Z_\odot$, where large gaps in the parameter grid can be found, may be considered a borderline case.

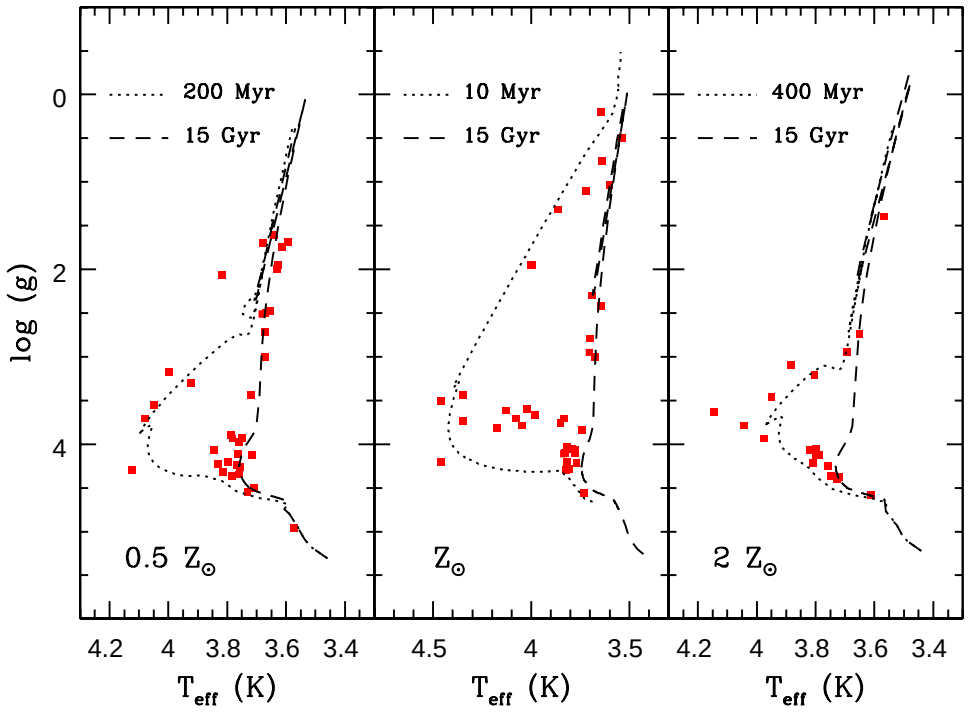

Figure 3.3: Evolutionary coverage for the STELIB library at solar, half solar, and twice solar metallicity. Isochrones (MS) and stellar tracks (PMS) that are used in the synthesis have been overplotted to indicate the approximate age range that can be modelled.

Upon inspection of the individual spectra of the STELIB library, MacArthur et al. (2009) found an rms spread of 1.09 Å in starting wavelength and 0.00033 Å in wavelength dispersion. If not corrected for, this will cause the co-addition of any spectra into the SED of a stellar population to have a degraded resolution compared to the resolution of the individual stellar spectra, acting effectively as a velocity broadening. In addition to this, they also found an rms error of 11.4 km s^{-1} for the radial velocities adopted by Le Borgne et al. (2003), which will further add to the downgrading of the stellar population model resolution.

In order to rectify these problems with the STELIB wavelengths, thus avoiding loosing valuable resolution, we have applied small, non-linear shifts to the wavelength scale, derived for each individual STELIB spectrum, by fixing the positions of eight strong absorption features, and using interpolation to obtain the wavelength shifts for all flux points in between. The spectra were then rebinned to our adopted scale of 3201-9296.5 Å in steps of 0.5 Å. The reason for straying from the 1 Å step-size is that we found that the rebinning was accompanied by a small, but non-negligible, smoothing of some absorption features, which could be made insignificant with a finer sampling.

The majority of atmospheric parameters in STELIB were taken by the authors from the Cayrel de Strobel et al. (1997) and Cayrel de Strobel et al. (2001) catalogues of [Fe/H] determinations, which are compiled from a vast number of different sources in the literature. These values were complemented with additional T_{eff} determinations from Alonso et al. (1996), Blackwell & Lynas-Gray (1998), di Benedetto (1998) and Alonso et al. (1999). Colour-temperature relations from the latter has also been used where available. Several stars that are also part of the ELODIE library (Prugniel & Soubiran, 2001) were given the atmospheric parameters listed therein if no other values could be found. If more than one determination of a parameter for the same star was available, these were averaged, with a larger weight given to the most recent determinations. Having been compiled from so many different sources, the atmospheric parameters of the STELIB stars are likely to be somewhat inhomogeneous.

3.3 The MILES library

The MILES library (Sánchez-Blázquez et al., 2006) provides spectra for almost 1000 stars, and covers most evolutionary stages – at least based upon what can be expected to exist in our Galaxy – at all metallicities down to [Fe/H]~ -2.0. Only stars at the extreme ends of the temperature scale are lacking, such as giants cooler than around 3400 K at 2 $Z_{\odot}$, and young stars hotter than $\sim$26000 K at Milky Way star-forming metallicities (i.e. around solar). Again, the number of cool LMS stars is very low at all metallicities. These points are illustrated in Fig.3.4, where the reader should also notice the extended HB morphology at 0.01 and 0.05 $Z_{\odot}$, caused by mass loss along the RGB, which requires hot stars at relatively low surface gravity in the library, and may impact the possibility of modelling very old stellar populations with blue HB.

The wavelength range is primarily confined to the optical (3500-7400 Å), and the resolution is high, although the quoted value of 2.3 Å FWHM is a bit underestimated (see Beifiori et al. 2011, and the discussion in Sec.4.5), and should instead be just over 2.5 Å. Values for all atmospheric parameters were taken from a large number of sources in the literature, but a careful attempt was made to homogenise the different scales. The reader is referred to Cenarro et al. (2007) for a detailed description of this procedure. When it comes to the effective temperatures, however, it should be noted that the reference system adopted for this calibration comprises only a very limited range of values, so that the temperatures of stars outside of the approximate interval 4000-6300 K, may not necessarily be of the same high homogeneity.

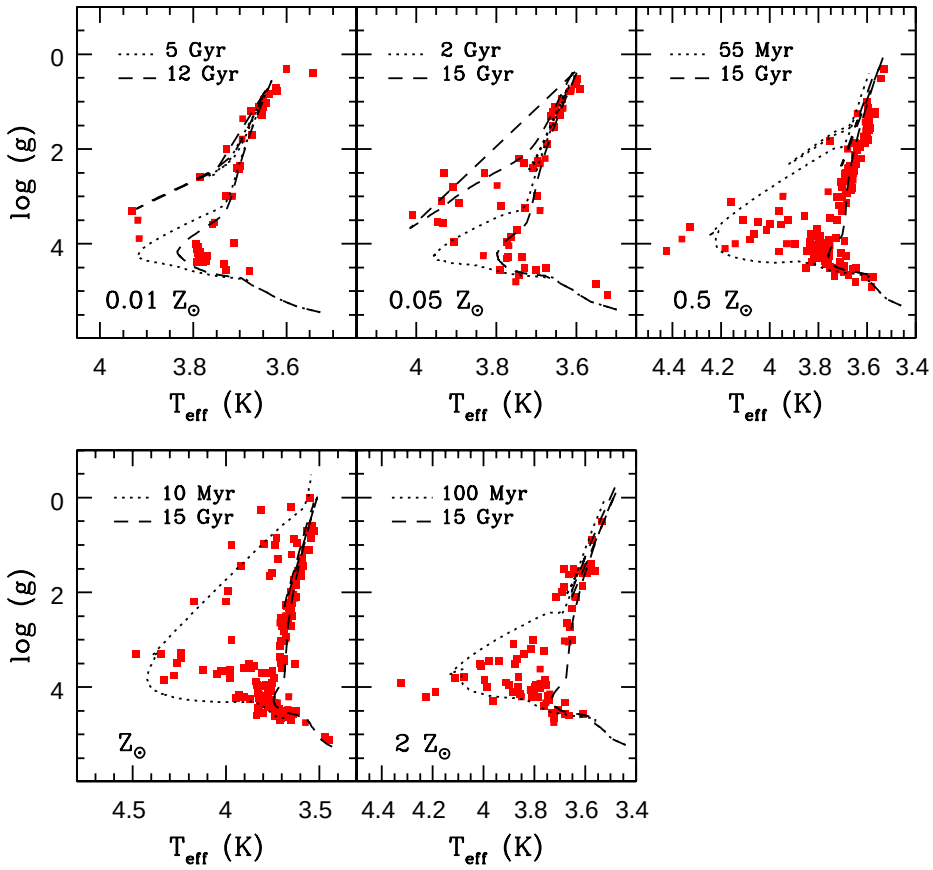

Figure 3.4: Evolutionary coverage of the MILES library at all metallicities for which MaStro models are available. The approximate age ranges that can be modelled are indicated by the isochrones and stellar tracks, in accordance with Fig.3.3. Notice the extended HB morphology due to mass loss at the two lowest metallicities.

In regards to the discussion in Sec.2.2 about the Milky Way bias, Milone et al. (2010) has recently published [Mg/Fe] abundance ratios for roughly 75 % of the stars in the MILES library. The characteristic 'knee', which signals the onset of enrichment from SN Ia, occurs at [Fe/H]~ -0.9, below which the [Mg/Fe]-enhancement lies fairly constant around $+0.4$, albeit with a large scatter (their Fig.1). Stellar population models incorporating MILES spectra must therefore be expected to follow the same abundance pattern, and in fact any model based on empirical Galactic stars should.

3.4 The ELODIE v.3.1 library

Compared to the original library of ELODIE echelle spectra (Prugniel & Soubiran, 2001), the latest version, ELODIE v3.1 (Prugniel et al., 2007), contains roughly twice as many stars (now almost 1400) and a slightly increased wavelength range. The latter is still rather narrow, spanning only around 3000 Å in the optical, which is not surprising considering the extremely high resolution (R≈10000). One may argue about the relevance of applying stellar population models of such high resolution to velocity-broadened galaxy spectra, and for this purpose alternative versions of the library with lower resolutions may be computed. There are, however, stellar populations in which velocity broadening is less prominent, such as dwarf galaxies and globular clusters, that might benefit from such a high-resolution model.

Most stars in the ELODIE library have solar or near-solar metallicity. Only 68 stars out of 1388 are listed as having [Fe/H]< -1.0, which limits our ability to produce ELODIE-based models at low metallicity. In conformity with the other libraries, the lack of cool LMS stars is present at all metallicities, see Fig.3.5. There is also a clear deficiency of giants at 2 $Z_\odot$, and it is debatable whether the large gaps in parameter space found at 0.01 $Z_\odot$ would permit any SSP models to be constructed at this metallicity. The amount of stars at 0.05 $Z_\odot$ is certainly not sufficient for such an undertaking, and this metallicity has therefore been left out.

In the original paper the atmospheric parameters were derived using the TGMET method (Katz et al., 1998), which is an automated classification procedure using a least-squares comparison with 211 reference spectra of well-determined parameters, or taken from the literature (Carney et al., 1994; Alonso et al., 1996, 1999; Cayrel de Strobel et al., 1997, 2001; Thevenin, 1998; Blackwell & Lynas-Gray, 1998). Colour-temperature relations from Alonso et al. (1996) and Alonso et al. (1999) were also used, and in all, the methods and sources resemble very much the ones later used in Le Borgne et al. (2003) for the STELIB library. Final parameter values were taken as averages of multiple determinations, giving lower weight to old references. In the latest version, Prugniel et al. (2007), these parameters have been updated using more recent publications.

The stellar parameter determinations and flux calibration of the stars in the ELODIE library have also been assigned quality flags by the authors. We take advantage of this to create as reliable SSP models as possible, by allowing only stars with the highest quality of flux calibration to contribute, and in cases where two or more stars occupy the same location in stellar parameter space, choosing the one with the most reliable parameter

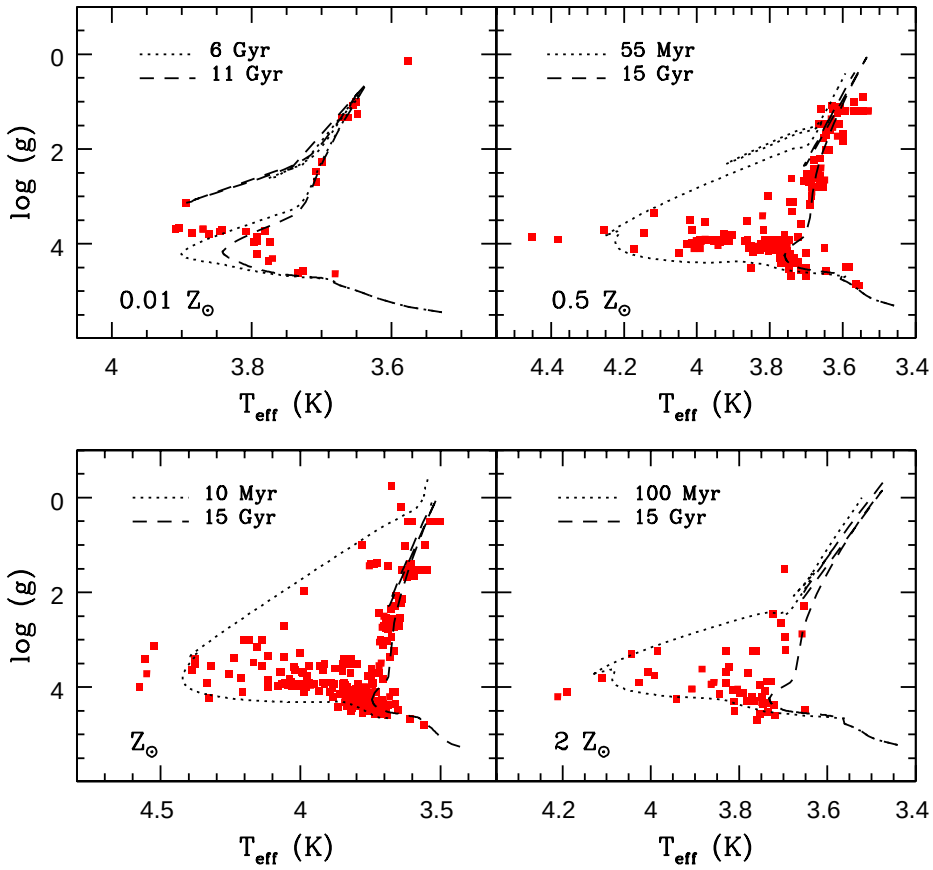

Figure 3.5: Evolutionary coverage of the ELODIE library at all metallicities for which MaStro models are available, except 0.05 $Z_{\odot}$. The approximate age ranges that can be modelled are indicated by the isochrones and stellar tracks, in accordance with Fig.3.3. Notice the extended HB morphology due to mass loss at 0.01 $Z_{\odot}$.

estimations. Some stars have also been observed multiple times. Again, in such cases we chose the spectrum with the highest values of the quality flags. If there are two or more spectra of the same star and with the same quality flags we compute an average spectrum for this star, taking also the average of the stellar parameters.

3.5 Flux calibration of the empirical spectra

The fact that the STELIB, MILES, and ELODIE libraries have a few stars in common with each other, gives us the possibility to obtain some indication of the quality of their

flux calibration. In Fig.3.6 we compare four stars of intermediate-to-hot temperatures that are present in all three libraries, and chosen to represent a large range in metallicity and gravity. The stars have been smoothed to a common, low resolution of R=500, and normalised to unity at 5050 Å, in order to make any differences in the continuum slope more clearly distinguishable. It can be mentioned that none of the stars are known to be a variable, which means that, ideally, the spectra of the same star in different library should look the same. However, as can be seen in the figure, for at least two of the stars there are surprisingly large discrepancies.

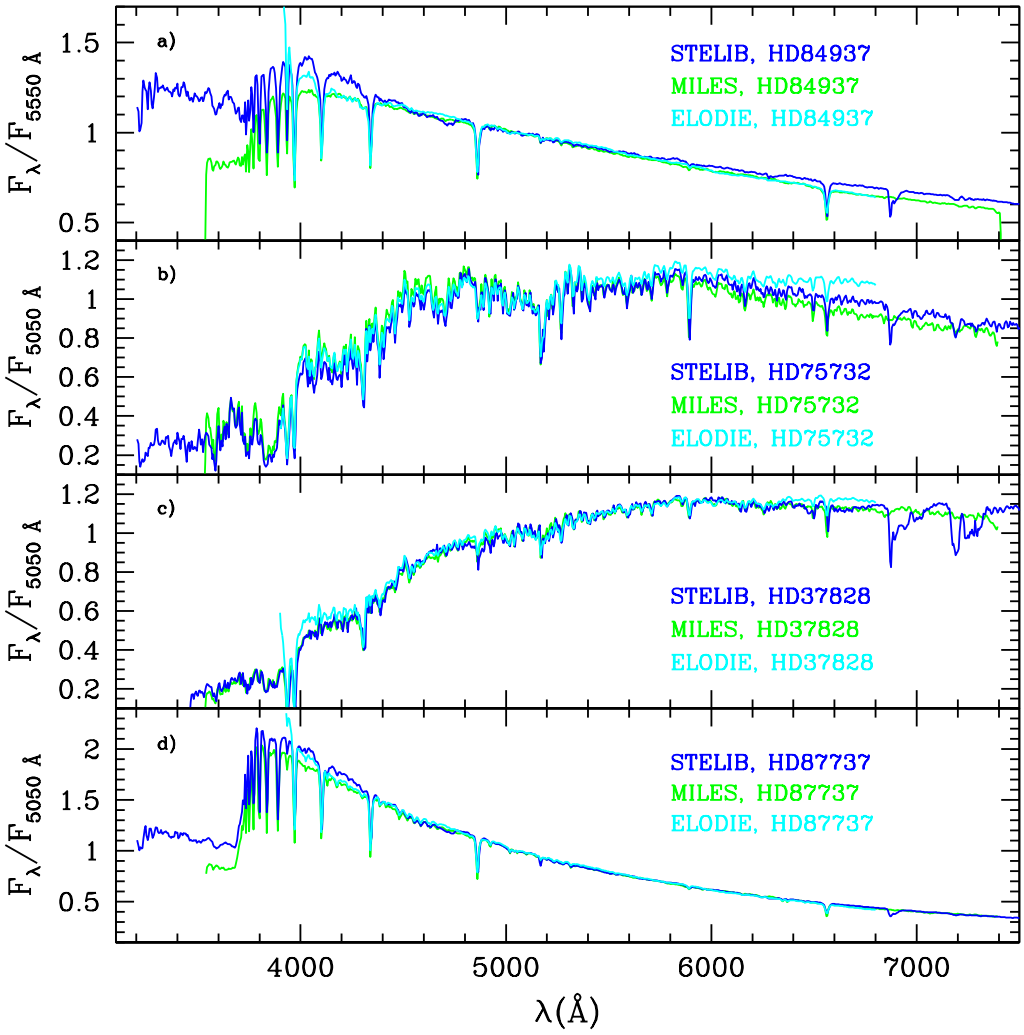

Figure 3.6: Comparison of the flux calibration in the STELIB, MILES, and ELODIE libraries. The three panels depict three different stars present in all libraries, smoothed to a common, low resolution of R=500, where *a)* is a metal-poor sub-dwarf; *b)* a super-solar metallicity MS star; *c)* a metal-poor giant; and *d)* a solar metallicity supergiant. See text for more details.

Shown in the top panel of Fig.3.6 is metal-poor ([Fe/H]< -2.0) star HD84937, classified as a sub-dwarf F5 star[1]. The spectra from MILES and ELODIE agree fairly well over their common wavelength range, except in the bluest ~ 200 Å, where the latter receives a boost of flux. It must be expected that flux calibration becomes increasingly difficult towards the spectrograph limits, where the S/N ratio steadily decreases. This behaviour on part of the ELODIE spectrum could therefore be attributable to detector sensitivity (it is present also in the bottom panel and several other stars that were examined). The STELIB spectrum on the other hand, differs rather dramatically from the other two, having more flux both redwards and bluewards of the normalisation wavelength. This gives it a different shape altogether, which must be due to the flux calibration of this spectrum.

The second panel displays the spectra of HD75732, an ordinary MS star (spectral class G8V) of super-solar metallicity (here the libraries disagree somewhat; while the MILES library assigns the star [Fe/H]$= +0.16$, both in ELODIE and STELIB it is given [Fe/H]$> +0.3$). The continuum shapes of the MILES and STELIB spectra appear tilted with respect to each other, in the sense that the MILES spectrum is bluer. The ELODIE spectrum does not show any anomalies in the blue part, but instead the red part has a slightly peculiar slope (a similar slope can also be seen in the lower panel).

In the third panel are given the spectra of metal-poor giant HD37828 ([Fe/H]$= -1.4$, luminosity class unknown). In this case the three libraries agree very well, giving very similar SED shapes, with the exception of the red and blue ends of the ELODIE spectrum, something that has already been mentioned. Clearly visible in all three panels, but most prominent in the bottom one, are also the telluric absorption features in the STELIB spectra around 6900 Å.

Finally, in the bottom panel is solar metallicity supergiant (HD87737, T_{eff} ∼10000 K). The overall agreement is rather good, except in the blue end, where the MILES and STELIB spectra, like in the top panel, deviate quite substantially from each other. There are indications that this behaviour appears to be systematic for hot stars, and will thus be reflected in the EPS models constructed thereof (see Sec.4.7.1). Unfortunately, hot stars (T_{eff} >10000 K) in common between all three libraries are extremely scarce.

To conclude, the three different examples presented in Fig.3.6 are hinting at the uncertainties involved in accurately flux calibrating a stellar spectrum. If the differences in flux calibration are due to systematics, these will also be transferred over to the SEDs of the

[1]SIMBAD: http://simbad.u-strasbg.fr/simbad/

stellar population models. However, if the temperature scale of the libraries are different as well, the two effects on the continuum slope behaviour (flux and temperature calibrations) are very difficult to disentangle, as they may both amplify and cancel each other depending on the homogeneity of these procedures in the library (see also Sec.4.7.3). We have decided to keep all original temperature calibrations, as a homogenisation of the stellar parameters is out of the scope for this work. Thus, we leave it up to the users to decide which library best matches their requirements.

3.5.1 Notes on the flux calibration in the reference papers

A careful description of the complex flux calibration process for the ELODIE echelle spectra is given by Prugniel & Soubiran (2001). Since this library is a compilation of archive spectra rather than being part of a specific observation programme, no standard stars have been observed. The instrumental response is therefore evaluated by comparisons to several other low- and high-resolution libraries, and the spectra are corrected thereafter. At 3900 Å – the blue limit of the ELODIE spectrograph – the global efficiency of the instrument drops by a factor of 50, which may compromise an accurate flux calibration in the blue end of the spectra (something we may have seen the result of in the previous exercise).

The flux calibration of the STELIB stars was tested in Le Borgne et al. (2003) by comparing synthetic photometry on the library spectra against published photometry in the Lausanne database (Mermilliod et al., 1997). The *(B-V)* colour is by far the one with the smallest rms dispersion, 0.083 mag, with no discernable offset. The *(U-B)* and *(R-I)* have the largest dispersions, which according to the authors are due to inhomogeneities in the photometric systems, and the fact that the STELIB stars do not quite have the required wavelength coverage for the *U*- and *I*-band filters. Again, there are no clear offsets for these colours either. There appears to be a slight trend in the *(V-R)* colour, such that the reddest (coolest) stars appear somewhat bluer in the STELIB library. It is argued by the authors, that this is most likely due to differences in the photometric systems. It should also be noted that these tests were performed on stars not corrected for interstellar reddening. All this taken together makes it difficult to assess the accuracy of the flux calibration in bands other than *B* and *V*.

The MILES stars have gone through a rigorous spectrophotometric quality control (Sánchez-Blázquez et al., 2006). An internal consistency check, comparing several observations of the same stars, revealed that the random rms error affecting the flux calibration is around 0.013 mag for the *(B-V)* colour. An external comparison with the Lausanne photometric database (Mermilliod et al., 1997), showed a mean offset of 0.015 mag for *(B-V)*, in the sense that the MILES spectra are bluer. The rms dispersion of 0.025 mag is considerably smaller than the one obtained in Le Borgne et al. (2003) for the STELIB stars. For stars in common with the STELIB library, the MILES *(B-V)* colours are, on average, 0.01 mag bluer, but with a trend that essentially all stars with T_{eff} <5600 K are bluer, whereas almost all stars hotter than ∼7200 K appear redder (see their Fig.11). The authors also defined seven box filters with effective wavelengths between 4000 and 6200 Å, in order to compare synthetic colours for stars in common with the STELIB and ELODIE libraries. For all possible combinations of filters allowed by the wavelength range in common between the libraries, any statistically significant offsets show the MILES stars to exhibit bluer colours. For colours involving the filters with the largest central wavelengths, there once again appears to be a trend of the coolest stars being significantly bluer in the MILES library (their Fig.9), whereas the situation is the opposite for the hottest stars. It's difficult to assess the flux calibration redwards of around 6500 Å, since this portion of the spectra is more or less left out of the quality check.

3.6 Scaling of the empirical spectra

Another difference between using theoretical and empirical stellar spectra in EPS modelling is the flux units. Whereas theoretical spectra preferentially are given in absolute units, such as luminosity (ergs s^{-1} $Å^{-1}$) – or any other unit that can easily be converted into luminosity; the main point being it makes the population synthesis very straightforward – things are more complicated with empirical spectra. Either fluxes are given as they were measured (ergs s^{-1} cm^{-1} $Å^{-1}$) and thus dependent on the distance to the stars, as is the case with STELIB and ELODIE spectra, or they have been normalised to unity at some wavelength, a method adopted in the Pickles and MILES libraries. In both cases, the true relative energy scale between the spectra is washed out.

Various schemes for how to bring the empirical spectra onto an absolute flux scale were discussed. In principle, all attempts to scale the spectra using an empirical approach inevitably relies on precise distance measurements to the stars. One could then use, for example, apparent magnitudes and count backwards. However, such accurate

distance determinations are not available for all library stars, and would in turn lead to inconsistent and unreliable determinations of the luminosities, especially considering that luminosity depends on the square of the distance.

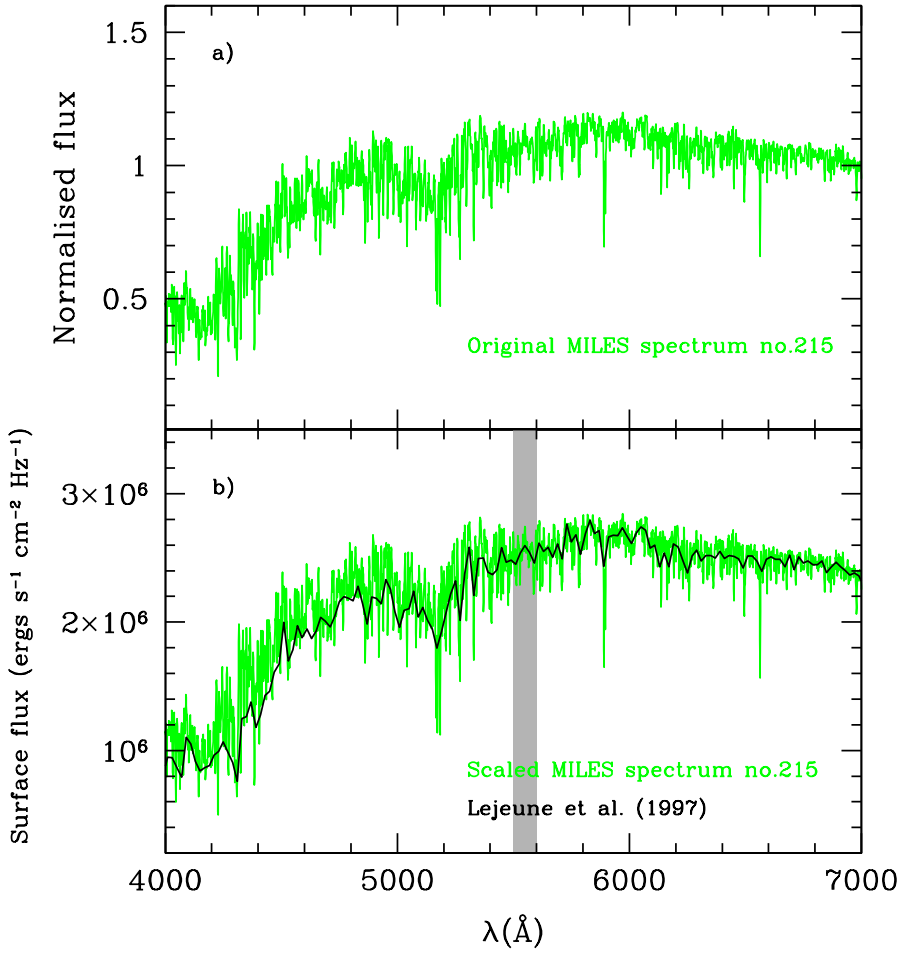

Figure 3.7: Summary of the scaling procedure of the empirical stellar spectra. Prior to entering the population synthesis, each individual spectra – in this case MILES star no.215 (a K2III red giant with surface parameters $T_{eff} = 4577$ K, log(g)$= 2.34$, and [Fe/H]$= 0.08$, *top*) – is scaled to the average flux within a 100 Å passband around 5550 Å (*grey* area) of a Lejeune et al. (1997) theoretical star with the same set of atmospheric parameters (obtained through interpolation if necessary, *bottom*).

Therefore, in order to be able to use a consistent approach for all the empirical libraries, the following prescription was adopted. i) We (re-)normalise all stellar spectra to the average flux within a 100 Å passband around 5550 Å. ii) The spectra are then scaled with the luminosities (again using the average flux in a 100 Å passband centered at 5550 Å) of theoretical spectra with the same stellar atmospheric parameters (interpolated as necessary) from the grid of Lejeune et al. (1997) (which were the input in the

M05 models). In short, the scaling of the empirical spectra will be based on theoretical spectra. The specific passband used in the scaling needs to be broad enough not to be dominated by individual absorption lines, but also narrow enough not to be affected by large-scale temperature effects, i.e. by the slope of the continuum. The procedure is schematically outlined in Fig.3.7.

It has previously been mentioned that the representative spectrum for each [T_{eff}, log(g)]-bin is obtained by means of linear interpolation in effective temperature. It is important to realise that any scaling to absolute fluxes of the spectra taking part in the interpolation, must occur *before* the interpolation is performed. Otherwise the shape of the interpolated SED may be compromised. This is particularly crucial when the spectra sample the stellar parameter space poorly.

3.6.1 Scaling methods in other models

The method of scaling the empirical stellar spectra varies between different EPS models, and will affect the absolute flux levels, i.e. the mass-to-light ratios, of the integrated SEDs. If done in an inconsistent way it may also affect the continuum shape. Chapter 4 will describe in more detail the procedures of assigning and scaling empirical spectra that are adopted in Bruzual & Charlot (2003) and Vazdekis et al. (2010), but it may be worth mentioning here that the models of Conroy & Gunn (2010, hereafter CG10), which are also based on the MILES library, utilise a method very similar to ours, even down to the same theoretical reference library (BaSeL), although using a much wider wavelength range for the scaling region (4000-7000 Å). We have verified that the effect on our models by using such a large scaling band is actually completely negligible, thus any difference between the MaStro models and the CG10 models is not due to the scaling of the empirical spectra.

Chapter 4

The MaStro Stellar Population Models

On the models constructed from each empirical library, what necessary improvements have been made to them, and how the new models fare against each other.

Adopting the evolutionary population synthesis approach outlined in Chap.2, and using the libraries of empirical stellar spectra described in Chap.3, we construct four different sets of SSP models, one for each library, the completeness of which determines the sampling of the SSP age-metallicity space. The new models will be known collectively as the MaStro models, and individually as MaStro-Pickles, MaStro-STELIB, MaStro-MILES, and MaStro-ELODIE. It is important to remember that the various sets of models are all built on the same stellar evolution foundation, and differ *only* in the input spectral library.

The simple stellar population models that can be calculated for each of the four different empirical libraries, in terms of age and metallicity, are shown schematically in Fig.4.1,4.2, 4.4 and 4.5. It is evident that empirical spectra alone cannot account for all desired combinations of these parameters. For example, no library contains the hot stars of low metallicity that are required to build metal-poor SSP models of young ages. Needless to say, this is because star formation in the Milky Way takes place in the metal-rich thin disc. We have here decided not to extrapolate the models down to younger ages by means of e.g. hotter stars of other metallicities or using theoretical stars, mostly because such young populations are completely dominated by the light from the hot turnoff stars. Instead we present only models that can, at least to a certain degree, be reliably constructed considering the age-metallicity coverage of the empirical libraries in question.

All MaStro models are, in accordance with the M05 models, provided for two different morphologies of the horizontal branch, namely intermediate-red and blue, following the standard M05 recipe for mass-loss that has been calibrated on Milky Way GCs. This is mostly important at low metallicity, hence only affects the models based on libraries that contain a reasonable amount of metal-poor stars. Finally, the figures does not account for varying element abundance ratios, other than the omnipresent Milky Way bias, which adds another dimension of complexity to the use of empirical libraries in EPS. In the following sections the different MaStro models will first be discussed separately, and then later compared to each other.

4.1 MaStro-Pickles

As previously mentioned, and as seen from Fig.4.1, the MaStro models based on the Pickles library are only available at solar metallicity. However, the author has done an excellent job in sampling the stellar parameter space, and the presence of O-type stars and a wide selection of supergiants in the library allows for very young ages to be modelled. The lower limit lies around 2 Myr, where the turn-off stars have a temperature of roughly 40000 K, but these spectra are also – not surprisingly, considering the dusty environment of star formation – significantly attenuated by dust absorption in the UV. As a side remark it may be noted that the extension into the UV in the Pickles spectra was accomplished by the low-dispersion *International Ultraviolet Explorer* (*IUE*) spectra (Heck et al., 1984). Since the integrated light of such young stellar populations is completely dominated by the light from the turn-off stars, the shape of the model SEDs will undoubtedly be affected by dust attenuation. Thus, keeping this in mind, the ultraviolet part of the Pickles-based SSP models with the youngest ages (below ~ 100 Myr) should be used somewhat more cautiously.

There are two versions of the MaStro-Pickles models, simply due to the fact that there are two versions of the library itself. In the first version, which has a wavelength coverage of 1150-10620 Å, all stellar spectra are purely empirical. In the second version, the wavelength range is extended up to 25000 Å, but as described in Sec.3.1 half of the stars lack spectrographic observations above 10000 Å, and the M giants are here purely synthetic (below 10000 Å the M giants are now semi-empirical in order to provide a smooth transition from observed to theoretical spectra). We will refer to this second version of the models simply as the *extended* MaStro-Pickles models.

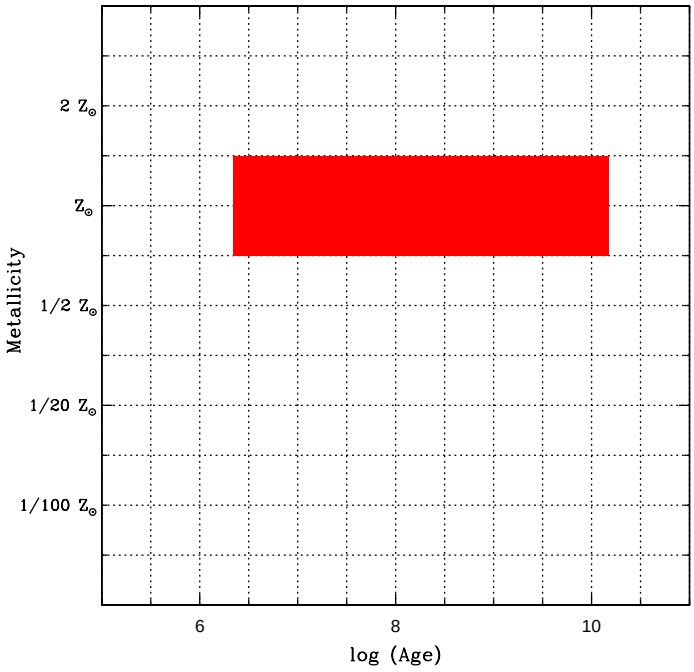

Figure 4.1: Schematic view of the available MASTRO-Pickles models, in terms of age and metallicity, Z.

4.2 MaStro-STELIB

The amount of spectra in the STELIB library with twice solar, solar, and half solar metallicities is adequate to produce SSP models down to relatively young ages, although the sampling is rather sparse in certain regions of stellar parameter space (see Fig.3.3). This holds especially true for the 0.5 and 2 $Z_{\odot}$ models, where also some of the stars important from the perspective of EPS do not have complete spectroscopic observations over the entire quoted STELIB wavelength range. Despite this drawback, we decided to keep them in the synthesis, lest no models at all could be made at these metallicities. The consequence of this being that the half and twice solar metallicity models have a shorter wavelength range (3200-7900 Å) compared to the solar metallicity ones (3200-9300 Å). In Fig.4.2, this is visualised by the striped areas. Flux values outside of the confined wavelength region have been put strictly to zero, as they are not a proper physical interpretation of the stellar population fluxes, considering that the contributing light from several important types of stars is missing.

In the STELIB library there are very few stars of metallicities lower than [Fe/H]$=-1.0$, which is why any undertaking to compose low-metallicity models based solely on

STELIB stars must be considered rather futile. Also, in common for all three metallicities where the amount of stars is deemed acceptable, there is a lack of cool MS stars and giants, even at $Z_{\odot}$. For the sake of completeness, complementary stars has therefore been taken from the MARCS library of high-resolution, theoretical stellar spectra (Gustafsson et al., 2008), smoothing them to the nominal resolution of the STELIB library before entering the synthesis (the specific choice of this particular library over other theoretical libraries will be discussed later).

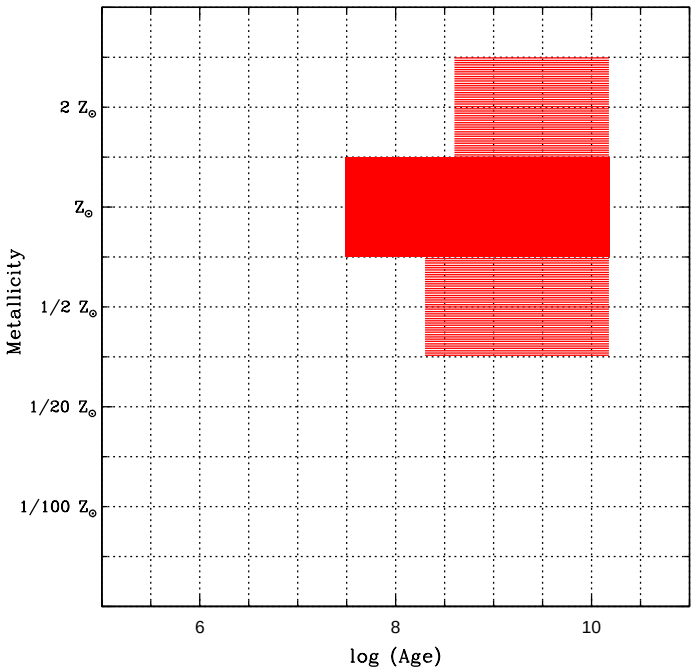

Figure 4.2: Same as Fig.4.1, but for MaStro-STELIB. Models in the striped areas have limited wavelength coverage (see text for more details).

An attempt was also made to keep the empirical approach to stellar spectra intact, by taking complementary stars from the Pickles library instead, which is the only one of the four empirical libraries that contain cool enough stars to cover the entire lower MS and the T-RGB. We found, however, that the number of the lower resolution Pickles stars needed to appropriately sample the atmospheric parameter space, were enough to affect the overall resolution of the integrated SEDs slightly. Interestingly, the lower limit of 30 Myr at solar metallicity was determined, not by a shortage of hot stars, but by a lack of red (cool) supergiants, which despite their rather few numbers make a significant contribution to the integrated light of stellar populations in their early years, thanks to their high luminosity.

4.2.1 Selection of STELIB stars in the BC03 models

We have previously mentioned in passing the BC03 models (Bruzual & Charlot, 2003), which is the one other EPS code in the literature that also employ the STELIB library. These models are available at a very wide range of metallicities ($-2.3 <$[Fe/H]$< +0.4$), which appears in rather stark contrast to the more conservative range adopted above for the MaStro-STELIB models. A comparison of the selection criteria therefore seems in order.

The lack of hot stars at non-solar metallicities and cool stars at all metallicities is acknowledged also in BC03. To circumvent the former problem the authors have included hot stars of solar metallicity at all other metallicities, since hot stars are not expected to depend strongly chemical content. It is a bit unclear which exact value of the temperature that is defined as 'hot', but both 7000 and 10000 K are mentioned. In the optical, 10000 K is probably an adequate number for this to work, whereas at the high resolution of the STELIB library a 7000 K, $Z_{\odot}$ star is certainly not indistinguishable from a 7000 K, [Fe/H]$= -1.3$ star. This is also illustrated in Fig.4.3 (using MILES stars, which are of only slightly higher resolution, but offer a better coverage of stellar parameter space).

Concerning the gaps in the cool regime of stellar parameter space, a number of K- and M-dwarfs from the SDSS Early Data Release have been added at all metallicities in a similar fashion as the hot stars, i.e. disregarding metallicity effects of the stellar spectra. This seems contrived as cool stars show very strong metallicity dependence, and even though the LMS contribution to the integrated light of a stellar population is not great, it cannot be neglected, especially for a Salpeter IMF or even more dwarf-dominated IMFs. Abundance ratio effects are in this way also not given any consideration.

As apparent from the numbers plotted in their Figure A1, at [Fe/H]$= -0.7, -1.7$ and -2.3 about half of the stars (from a total of ~ 45 chosen for each metallicity) are either hot solar-metallicity stars or cool SDSS-EDR stars. In addition to this, the models at the two lowest metallicities are constructed from more or less the same STELIB stars, which also comprise the entire [Fe/H] range from about -3.0 to -1.0. Considering the extent to which STELIB-based EPS models have been used in the literature for the purpose of absorption line studies at non-solar metallicities (e.g. Kauffmann et al., 2003)), it would be very interesting to see a comparison of those results with results obtained from newer models addressing all of the issues of the STELIB library highlighted above.

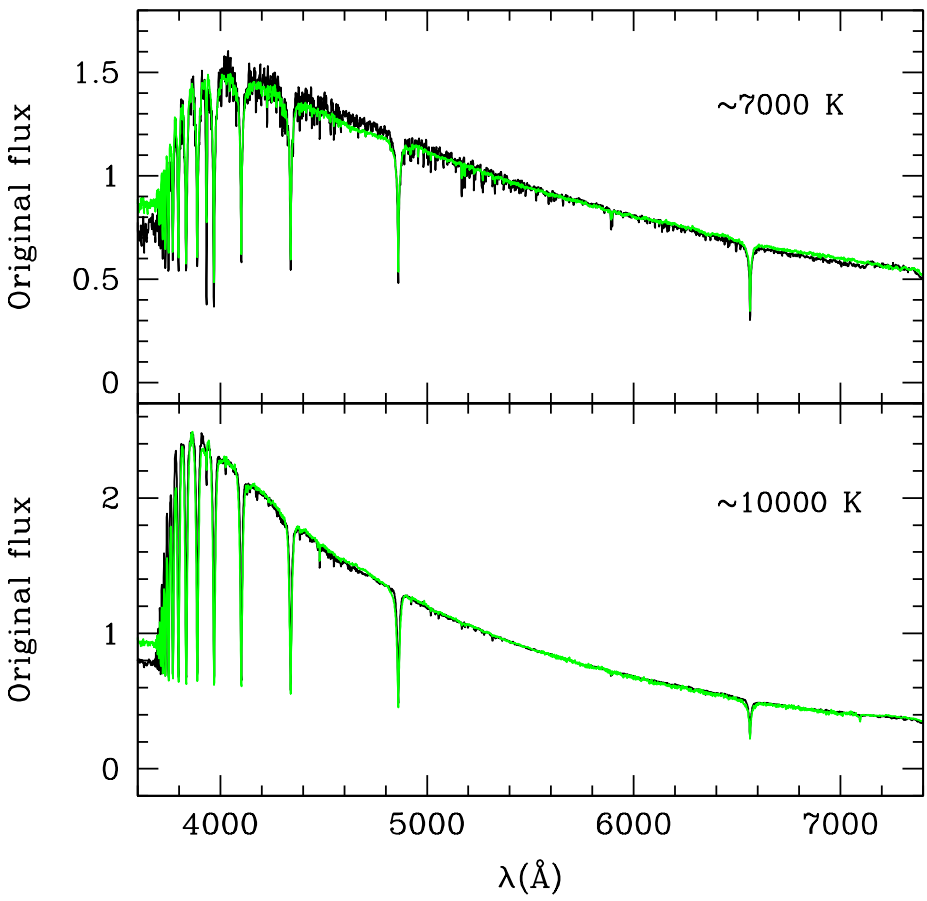

Figure 4.3: Comparison of similar stars at different metallicities. The spectra are from the MILES library which is of only slightly higher resolution than the STELIB library, but offer a larger selection of stars. *Top:* A 7000 K, log(*g*)$= 4.15$, [Fe/H]$= -0.25$ star (*black*) is compared to a 6910 K, log(it g)$= 4.00$, [Fe/H]$= -1.49$ star (*green*). At these temperatures the differences between the spectra are clearly visible. *Bottom:* The *black* line is now a 10282 K, log(*g*)$= 3.50$, [Fe/H]$= +0.20$ star, whereas the *green* line is a 10250 K, log(*g*)$= 3.40$, [Fe/H]$= -1.20$ star. Here the spectra are much more difficult to tell apart, indicating the approximate temperature required in order to use near-solar metallicity stars also at lower metallicities in EPS modelling. Interestingly, in both panels there is a large separation between the continuum levels of the two spectra bluewards of the Balmer break.

It is also interesting to note that BC03 rely on the colour-temperature scale of one of the (theoretical) BaSeL libraries when assigning STELIB spectra to the different isochrone bins. In effect, this means choosing the STELIB spectrum that best matches the BaSeL spectrum that was assigned to that same [T_{eff},log(g)]-bin, where the match is determined in terms of the shape of the continuum. By default, the colour-temperature scale of the STELIB stars used in the construction of the BC03 models will therefore

always be similar to that of the BaSeL library, which seems like a rather effective way of washing out any potential differences between theoretical and empirical stellar spectra. Translating this to broadband colours, the difference between the higher resolution, semi-empirical BC03-STELIB models, and the low-resolution, theoretical BC03-BaSeL 3.1 models, should not be very prominent, and may explain the difficulty experienced by Wake et al. (2006) in finding a good match between observed galaxy colours and the colours computed from these models (whereas we found that models based on empirical spectra could, in fact, solve the problem; more on this in Sec.5.4). It is not clear from the reference paper exactly how the STELIB spectra are scaled to absolute flux units, but considering the approach described above, it lies close to believe that the empirical stars are in some way given the fluxes of the best-matching theoretical stars. A comparison between MaStro-STELIB and BC03-STELIB model SEDs is performed in Sec.4.7.4.

4.3 MaStro-MILES

Given that the MILES library comprise the most well-balanced distribution of stars of all the four empirical libraries (Figures 3.1 and 3.4), it is only natural that the MaStro SSP models based on MILES also display the most comprehensive sampling of the age-metallicity grid, as evident from Fig.4.4. Reflecting the chemical evolution of the Milky Way, no particularly young ages can be modelled at the lowest metallicities, and when mass loss along the RGB is accounted for (blue HB morphology) also the oldest ages (> 12 Gyr) are ruled out due to a lack of hot HB stars. In general, the mapping of stellar atmospheric parameters is rather coarse at [Fe/H]$= -2.0$, hence these models should be treated with some reservation. As previously mentioned, the [Fe/H]$= -2.0$ models, together with the [Fe/H]$= -1.3$ models, are expected to be enhanced in [Mg/Fe] by around $+0.4$ dex on average (Milone et al., 2010). The effect of an Al-Mg anticorrelation as observed in both Galactic and extragalactic globular clusters (Colucci et al., 2009, see also discussion in Sec.5.1) should be small as only 10-15 % of the library spectra (and of those selected for the models) are cluster stars. A statistical significance of such an anticorrelation could also be difficult to detect due to the initially very large spread in [Mg/Fe] abundances (see Figure 1 in Milone et al. 2010).

Looking at Fig.3.4 it is also apparent that the LMS is rather sparsely sampled at most metallicities, and that a few T-RGB stars are missing at 2 $Z_{\odot}$. Again, even though these types of stars do not contribute significantly to the total light in the optical, we have for the sake of completeness added complementary, high-resolution, theoretical stars from Gustafsson et al. (2008). We have tested that this addition yields a small, but detectable

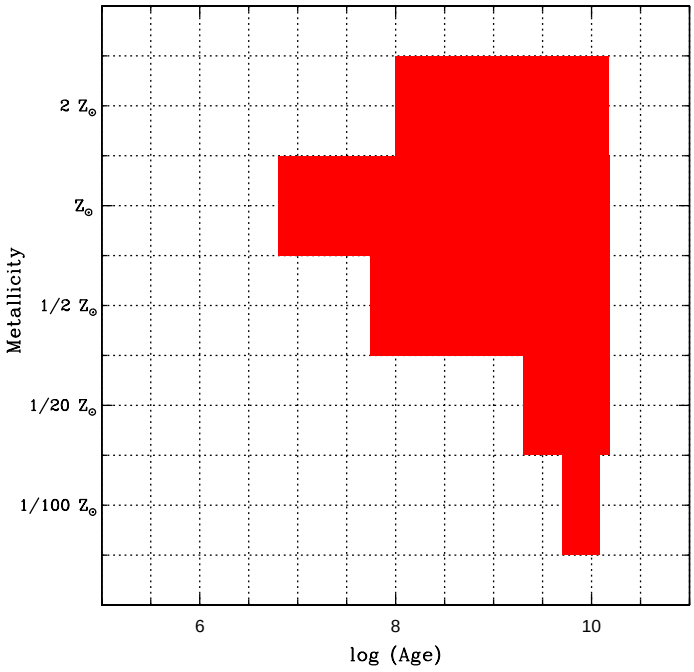

Figure 4.4: Same as Fig.4.1, but for the MaStro-MILES models.

addition to the flux in the reddest parts of the integrated spectra of the oldest populations. What the LMS stars lack in luminosity they make up for in numbers, and what the T-RGB lack in numbers they make up for in luminosity.

4.3.1 Selection of MILES stars in the V10 models

Very recently, Vazdekis et al. (2010, hereafter V10) published a set of EPS models based on the MILES library (using the same code as in Vazdekis et al. 2003). The authors introduce a quality parameter to measure the reliability of their SSP models from the perspective of appropriately sampling stars with the desired parameters, and in that determines what range of ages can safely be used at a given metallicity.

Unlike the comparison between MaStro-STELIB and BC03, MaStro-MILES and V10 agree upon what metallicity range is feasible for the model grid. There are instead minor differences in the lower limits for the ages. Generally the V10 allow for slightly younger ages at non-solar metallicities, which can probably be attributed to two things; 1) stars hotter than 9000 K are in the V10 models used at any SSP metallicity, irrespective of the metallicity of the star; 2) the selection of stars in the V10 code is based solely on the required stellar parameters, which means that the evolutionary stage of the stars is not

taken into account. The latter point is generally not a problem, but certain parts of the HR-diagram are more sensitive to this than others. For example, red supergiants, T-RGB stars, and carbon- and oxygen-rich AGB stars may all inhabit the same region of stellar parameter space, but they also exhibit very different spectra, so that a distinction must be made between these types of stars in the synthesis.

Despite using the same underlying technique for evolutionary population synthesis as BC03, i.e. isochrone synthesis, V10 opt for a slightly different approach regarding the scaling of the empirical spectra. First, each spectrum is normalised to the flux in the V-band. The theoretical parameters (T_{eff},log(g),Z) given by the isochrone are then transformed via metallicity-dependent *empirical* relations for colours and bolometric fluxes (mainly from Alonso et al. 1995, 1996, 1999) into a V-band flux that is then used for the scaling to absolute units, rather than relying on the flux of theoretical stars. As we shall later see, this method seems to be on par with the approach selected in the MaStro code for scaling empirical stellar spectra (Sec.4.7). However, several other differences between the codes ensure they will not perform equally when tested with observations; for example when compared to the SDSS broadband colours of globular clusters in M31, the MaStro-MILES models produce a better match to the data than the V10 models do (Peacock et al., 2011).

4.4 MaStro-ELODIE

The ELODIE library contains a number of very hot O-type stars, which in principle would allow us to produce models as young as 1 Myr. The spectra of these newborn stars are naturally severely reddened by close-in dust, and/or displaying various amounts of emission lines. It is true that observing O-type stars without these features is not very common, and in fact it might even be seen as something positive as they are an integral part of any star-forming stellar population, and should thus be included in the integrated spectrum. However, due to the scarcity of these stars in the libraries and the fact that they completely dominate the integrated light (making the EPS model dependent on just a few stars), as well as to the fact that there are large star-to-star variations regarding e.g. dust absorption, it is from a modeller's point of view preferable to add on such effects afterwards in a controlled, parametrised manner, just as it is desirable to separate the pure absorption and emission line spectra. Many of the hottest stars in the ELODIE library therefore had to be discarded before inclusion in the population synthesis, thereby setting the age limit at solar metallicity to $\sim$3 Myr (see Fig.4.5). It should be noted, though, that

despite the removal of the worst spectra, the youngest models are not completely unaffected by the dust reddening of their turnoff stars. A concern regarding the temperature calibration of the hottest stars might also be raised, seeing how the overall spectral slope of these stars are generally less steep than e.g. theoretical BaSeL spectra of the same temperatures. At half-solar metallicity it is instead a lack of hotter supergiants ($>$ 6000 K) that sets a limit to the age of the youngest model.

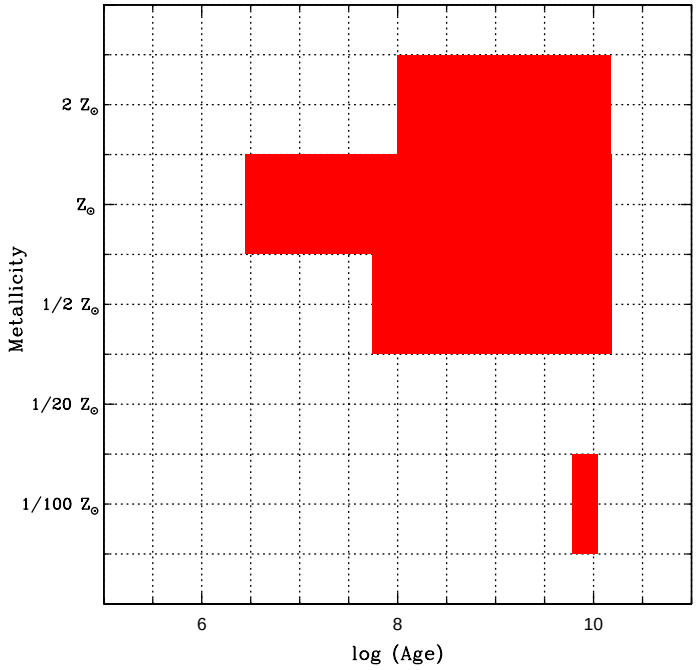

Figure 4.5: Same as Fig.4.1, but for the MaStro-ELODIE models.

At the lowest metallicity, 1/100 $Z_{\odot}$, the sampling of (T_{eff}, log(g))-space in the ELODIE library is fairly crude. A few ages can be modelled, but a complete evolutionary coverage is lacking, and they should thus be treated with some caution. If mass loss (blue HB) is included, there is also an upper limit to the SSP ages that can be modelled (in this case it is 11 Gyr), due to a deficit of hot HB stars in the library. There are not enough stars around [Fe/H]$= -1.30$ to warrant the production of any ELODIE-based models at that metallicity. Fig.3.5 reveals, in accordance with the other empirical libraries, a lack of cool stars – both dwarfs and giant – at all metallicities, but particularly at 2 $Z_{\odot}$. The same prescription is used to fill in these blanks as was used for the STELIB and MILES models, i.e. high-resolution, theoretical MARCS spectra (Gustafsson et al., 2008).

4.5 An interlude on the effective resolutions of the MaStro models

At this point a remark about the effective resolutions of the MaStro models must be made. Note that the quoted resolutions in Table 3.1 are the nominal ones cited in the reference papers for individual library stars. However, much evidence points in the direction that these values are not directly applicable to SSP models based on those same stars. We have already discussed the findings of MacArthur et al. (2009), where it was discovered that the resolution of the BC03 models is worse than the resolution of individual STELIB spectra by about 0.4 Å in FWHM (or really by ~ 0.3 Å, since it was also found that the resolution of individual STELIB is 3.08 Å, not 3.0 Å). This discrepancy was caused by errors in the radial velocities applied, and by slightly different values of the actual starting wavelength and wavelength dispersion (which according to the authors must have been overlooked in the construction of the BC03 models), so that the co-addition of the spectra acted effectively as a broadening of the absorption lines. We have tried to correct for this in the MaStro-STELIB models, but may not have succeeded entirely, and the effective resolution adopted for these models is therefore 3.3 Å FWHM.

Additionally, through stellar velocity dispersion tests on SDSS spectra using the GANDALF software we found that we could with an unaltered version of the MaStro-MILES models reproduce the exact values obtained from the SDSS pipeline (the GANDALF software was developed by Sarzi et al. 2006 and adopts the PPXF routine written by Cappellari & Emsellem 2004 for measuring gas and stellar kinematics; see also Chap.7 for further references to these papers). The latter adopts SDSS stellar spectra, that are supposedly of coarser resolution than MILES spectra, which suggested that the *actual* resolution of the SSP models based on the MILES library is slightly lower than the value cited in Sánchez-Blázquez et al. (2006), and resembles more the resolution of SDSS spectra.

This has also been confirmed just recently, when Beifiori et al. (2011) published their findings on the matter, determining the resolution of the stellar spectra in the MILES library to 2.54 ± 0.08 Å FWHM, which is in good agreement with the value of 2.5 Å determined independently and simultaneously by Falcón-Barroso et al. (2011). The reason for the difference between these values and the nominal 2.3 Å appears, according to the former, to be a previous overestimation of the spectral resolution for the INDO-US library (Valdes et al., 2004), which was used in Sánchez-Blázquez et al. (2006) to determine the MILES resolution. Interestingly, Beifiori et al. (2011) also derived the resolution of the

MaStro SSP models based on MILES, and found the same value as for the individual stellar spectra, suggesting a very accurate wavelength calibration in this library.

The spectra in the version of the ELODIE library that we adopt for the MaStro models have already been downgraded from the original resolution of R$= 42000$ by convolution with a 0.54 Å FWHM Gaussian function (Prugniel & Soubiran, 2001). Measurements in Beifiori et al. (2011) confirm that this seems to be a well-determined value for the resolution of ELODIE spectra, and we therefore consider it to be in no need of further revision. Detailed tests of the resolution of the MaStro-Pickles SSP models have not yet been performed. The resolution of the Pickles spectra was originally rather ill-determined (R≈ 500), but it is already low enough for this to matter little.

4.6 High-resolution theoretical SSP models

In addition to the empirical libraries to which this work is mainly dedicated, there is a need for complementary high-resolution stellar spectra – and even entire SSP models – based on theoretical stellar atmosphere calculations. We have already mentioned the MARCS library briefly, which was used to fill in the gaps in the cool regime of the HR-diagrams of the various empirical libraries. Another very useful resource will be the UVBLUE library (Rodríguez-Merino et al., 2005) that was employed by Maraston et al. (2009a) for constructing SSP models covering the ultraviolet part of the electromagnetic spectrum. Both of these libraries will be further described below.

4.6.1 The MARCS library and MaStro-MARCS models

The latest version of the MARCS code for model atmospheres (Gustafsson et al., 2008, the original code dates back to the early '70s) comprises a comprehensive grid of mainly cool stars (2500-8000 K at all metallicities) with a very high resolution ($R = 20000$) throughout over the impressive wavelength range 1300-200000 Å. Both plane parallel and spherically symmetric models are available, but neither cover the entire range of surface gravities (giants, $-0.5 \leq$log(g)≤ 3.5, are spherically symmetric, whereas dwarfs and subgiants, $3.0 \leq$log(g)≤ 5.5 are plane parallel). In addition, the standard chemical composition of these spectra follow the general Milky Way trend, i.e. displaying a moderate enhancement of α-elements ([α/Fe]=0.1-0.3) at [Fe/H] between -0.25 and -1.0, with more metal-poor objects having [α/Fe]$= +0.4$. Before entering the synthesis, the MARCS spectra were smoothed to the lower resolution of the corresponding empirical

library. The justification for choosing MARCS spectra over other theoretical spectra as complement to the empirical libraries shall become more apparent in Sections 4.7 and 4.8.

One of the most obvious limitations of empirical SSP models is the narrow wavelength range imposed by current spectrographs. Galaxy redshift surveys, for example, while becoming increasingly more sophisticated and covering an increasingly larger part of the electromagnetic spectrum, will benefit from having similarly extensive EPS models. Consequently, there appears to be a need for high-resolution models extending beyond the *I*-band and into the near-IR. For this purpose we have also created purely theoretical SSP models based on the MARCS library, that exhibit the same wavelength coverage and resolution as the individual MARCS stars. These models may, if desired, be concatenated with any empirical MaStro model of the same age and metallicity at an arbitrary wavelength, or they may be used on their own. Unfortunately, however, the maximum effective temperature of 8000 K in the library puts restrictions on what ages can be modelled. Naturally, the exact ages will be dependent on metallicity; at 2 $Z_{\odot}$ the minimum age is 0.8 Gyr, while at the lowest metallicity the minimum age is still as high as 6 Gyr. In the latter case a problem arises also for old populations (> 11 Gyr) when taking mass loss into account. If the shedding of mass towards the end of the RGB phase is severe enough, horizontal branch stars hotter than 8000 K will be produced (see Maraston 2005 for a more detailed description of the mass loss prescription adopted herein).

4.6.2 The UVBLUE library and MaStro-UVBLUE models

In the study of galaxy formation and evolution, an extension into the UV is generally even more crucial than covering the near-IR. As redshift gets progressively higher, more and more of the UV will be shifted into the optical, which is still the most common wavelength range for such surveys. However, of the four empirical libraries adopted in this work, only the Pickles spectra have a UV-extension, but the low resolution and restriction to solar metallicity only prevents this library from being used also for models based on the other libraries. The still most widely used source of empirical stellar UV-SEDs was compiled by Fanelli et al. (1992), which is based on *IUE* spectra, but several aspects of this library made it redundant for use in the MaStro models. With a spectral resolution of 6 Å, it is still inferior to three of our four libraries; also, the wavelength coverage of 1230-3200 Å would create a gap in the SEDs when merging the Fanelli et al. (1992) library with either MILES or ELODIE; and finally, at non-solar metallicities not all evolutionary stages are properly sampled.

It seems a theoretical approach is the best solution. The MaStro-MARCS models, used for the IR extension of old populations, are unfortunately not suitable for the task. Though they cover a significant portion of the ultraviolet (down to 1300 Å), the lack of hot stars prevents the construction of models with low ages, thereby counteracting one of the main purposes of UV-models: to study galaxies with a high amount of star formation (i.e. with very low light-averaged ages), for which the UV part of the SED contains a wealth of information that will help shed light on galaxy formation and evolution theory.

The choice therefore fell upon the UVBLUE library (Rodríguez-Merino et al., 2005), which is a set of very high resolution (R=50000) spectra synthesised from the 1993 version of the classical Kurucz (1979) model atmospheres. In addition to the high resolution, stellar parameter space is sufficiently sampled at all metallicities, and the wavelength coverage of 850-4700 Å accounts for near-UV as well as for both far- and mid-UV, so that a merging with the empirical libraries can take place without creating any gaps in the SEDs. Conveniently enough, a complete grid of EPS models based on UVBLUE spectra are already available (Maraston et al., 2009a). Reassuringly, the authors of this paper found that absorption indices measured directly on the SEDs of the theoretical models perform equally well (and equally bad for some indices) as indices derived from fitting functions based on the empirical *IUE* spectra of Fanelli et al. (1992).

Alternative versions of all MaStro models have been constructed, in which we have performed a concatenation with the UVBLUE-based SSP models of Maraston et al. (2009a), downgraded from their nominal resolution of R=10000 to the resolution of the corresponding empirical library; also, the starting wavelength is slightly higher – 1000 Å. After normalising the UVBLUE-models onto the M05 models (as M05 was also the standard onto which the empirical spectra were normalised), using a 100 Å wide passband centered at 3050 Å, the actual merging took place around 3750 Å. The exact wavelength varies a little bit from model to model for aesthetic purposes. Fig.4.6 shows an example of such a merging. The only exception is of course the ELODIE models, where the merging was performed around 3975 Å, since the starting wavelength of ELODIE spectra is 3900 Å.

When combining both theoretical and empirical models for different parts of the stellar population SED, it is interesting to compare the two in the overlapping region. This is done in Fig.4.7, where the UVBLUE-based models of Maraston et al. (2009a) are compared with the MaStro-MILES models in the region 3700-3900 Å (normalised at 3850 Å) for a wide range of ages at different, near-solar metallicities. In general, the agreement must be considered quite satisfactory, although for two features between ~ 3770 and

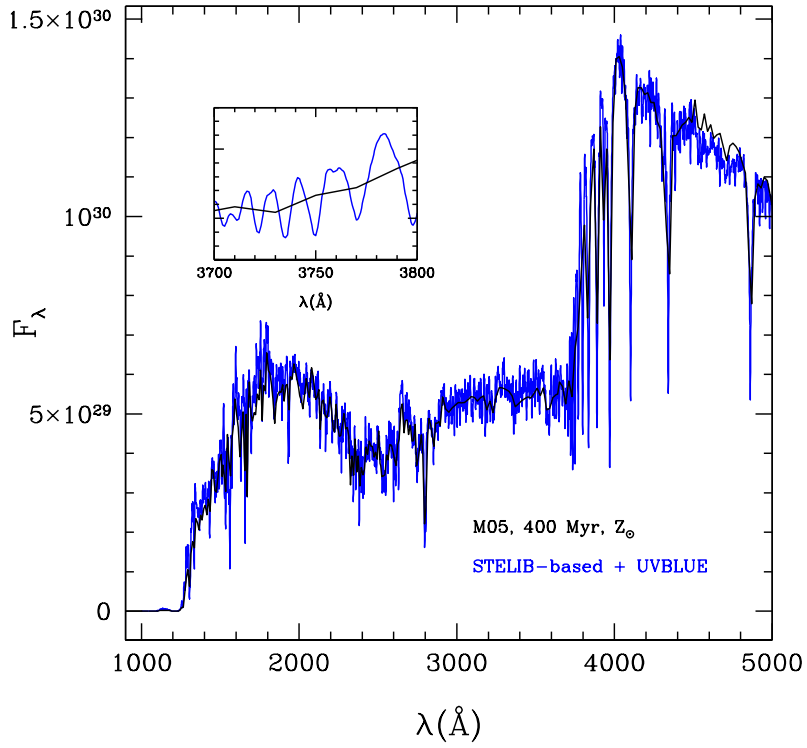

Figure 4.6: MaStro-STELIB 400 Myr, $Z_{\odot}$ template merged with the corresponding UVBLUE-based model (Maraston et al., 2009a). The zoomed-in region shows the area where the concatenation took place (in this specific case at 3752.5 Å).

$\sim$ 3815 Å the UVBLUE-based models display noticeably higher flux levels, a discrepancy that is enhanced at higher ages and metallicities. This suggests either a miscalibration of these lines in the theoretical stellar atmospheres, or a lack of (alternatively a too low weight of) a certain type of spectrum in the empirical library, but considering the excellent evolutionary coverage in MILES at these metallicities, it is more likely to be the former. It is difficult to pinpoint the exact origin of these lines, but Fe I is a probable candidate having a few strong absorption lines in the affected regions, most likely also in combination with the absence of line blanketing effects that causes the suppression of the continuum in the MILES-based models. At young ages (i.e. at hot temperatures, where metallicity effects are more subtle), the agreement is very convincing. This naturally holds also for lower metallicities, which is the reason why they are absent in the figure. Since the merging between MaStro and UVBLUE models takes place around 3750 Å, the highlighted region will follow the empirical, less pronounced behaviour. Once again, the exception is the MaStro-ELODIE models, where this part of the SED will be theoretical UVBLUE only.

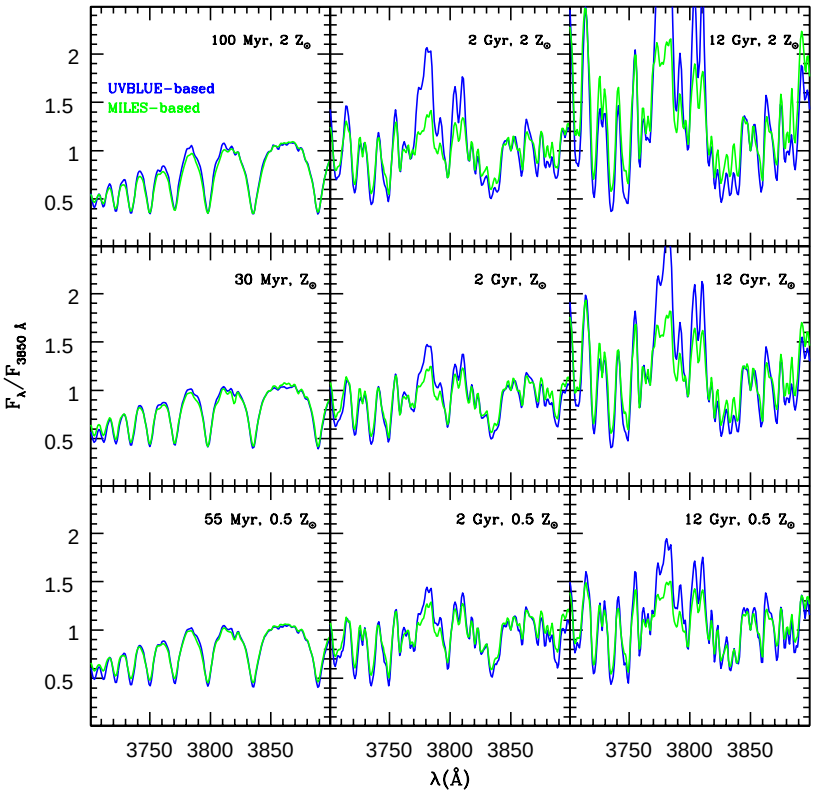

Figure 4.7: Comparison of the UVBLUE-based models of Maraston et al. (2009a) (*blue*) with the MaStro-MILES models (*green*) in the overlap region for a range of ages and metallicities. The merging between UVBLUE and MaStro models takes place around 3750 Å (except for MaStro-ELODIE), i.e. before the discrepancies in the region 3770-3815 Å.

4.7 Model SED Comparisons

This section will deal exclusively with the SED behaviour of the MaStro SSP models, i.e. how they compare to each other, and to other models in the literature that are based on the same empirical libraries. The reference point will always be the M05 models, but other models based on theoretical libraries, such as the aforementioned MARCS and UVBLUE, will also enter the analysis. Finally we will reflect upon how the differences in most cases can be traced to differences in the input stellar spectra. The broadband colours of the models will instead be treated in the following section.

4.7.1 MaStro models at different ages and metallicities

Naturally, comparing the SEDs of more than four different sets of SSP models at every age and metallicity requires more space than what is feasible in this work, and is often not very interesting. We will instead select a few often-used cases to highlight important differences among the libraries.

Young models at solar metallicity

Fig.4.8 displays the overall spectral behaviour of the various MaStro models for a 30 Myr young SSP of solar metallicity. For clarity, all SEDs have been smoothed to the resolution of the Pickles library (R$=500$), and the corresponding M05 model is shown for reference. All models have been normalised at 5050 Å.

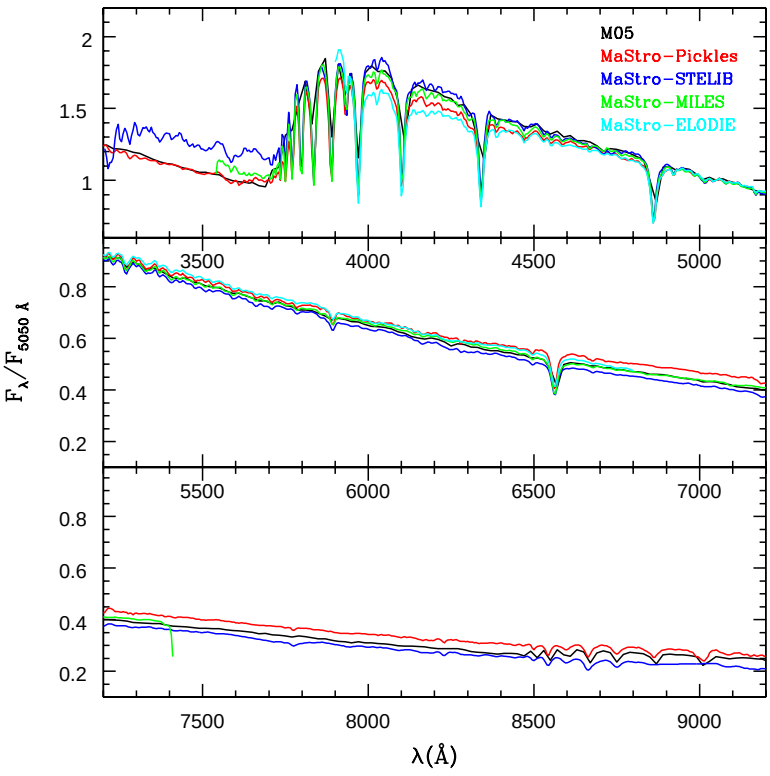

Figure 4.8: Comparison of the four sets of MaStro models for a 30 Myr, $Z_\odot$ SSP with Salpeter IMF. For clarity, all SEDs have been smoothed to the resolution of the Pickles library (R$=500$), and the corresponding M05 model is shown for reference. All models have been normalised at 5050 Å. The colour coding is given in the top right of the upper panel.

It is clear that the spectral shapes of all empirical models are very similar, but that the slopes are significantly tilted with respect to each other, thus impairing the agreement when measuring broadband colours. The STELIB-based model appear to be the bluest within the explored wavelength range, followed by the MILES-based (which is also the one running closest to the M05 model), and the Pickles-based. Regarding the ELODIE-based model, which is the reddest of the four, a concern was raised in Sec.4.4 about the temperature calibration of the hottest stars in this library, which could help explain the flatter behaviour of the integrated SED. Bluewards of ~ 3700 Å the STELIB-based model deviate considerably from the others, exhibiting much higher flux levels. It is difficult to assess exactly what is causing this discrepancy, but given that it occurs in a relatively confined region, whereas the remainder of the spectrum behaves more predictably, it is likely to be caused by the flux calibration of this part of the SED for hot stars in general and for hot supergiants in particular (see e.g. the bottom panel of Fig.3.6).

Old models at solar metallicity

A similar comparison, but for an old 12 Gyr population (still at solar metallicity) can be found in Fig.4.9. Colour coding and spectral resolutions are the same as in Fig.4.8. The normalisation at 5050 Å now reveals some very interesting differences between the models, which appears more complex than the situation at young ages, and does not just involve a pivoting around the normalisation point.

Bluewards of ~ 5300 Å all empirical models are in excellent agreement, and run very close also to the M05 model, although the latter exhibits a small surplus of flux around 4700 Å. In the range 5300-6300 Å the empirical models again behave in exactly the same manner, but this time very differently from the M05 model, which here displays a quite significant excess of flux. This trend was noticed in Maraston et al. (2009b) and will be further discussed in later sections. The only exception to the trend is the ELODIE-based model, which, even though it has a lower amount of flux than the M05 model, has noticeably higher flux levels than the other empirical models, thus landing it somewhere in between the two. At wavelengths $\lambda > 6300$ Å (middle panel) MaStro-ELODIE reconciles with M05. The reason for this deviation with respect to the other empirical-based MaStro models is as of yet unclear, but it could possibly be related to the flux calibration, which at the high resolution offered by the ELODIE spectrograph is a rather complicated process.

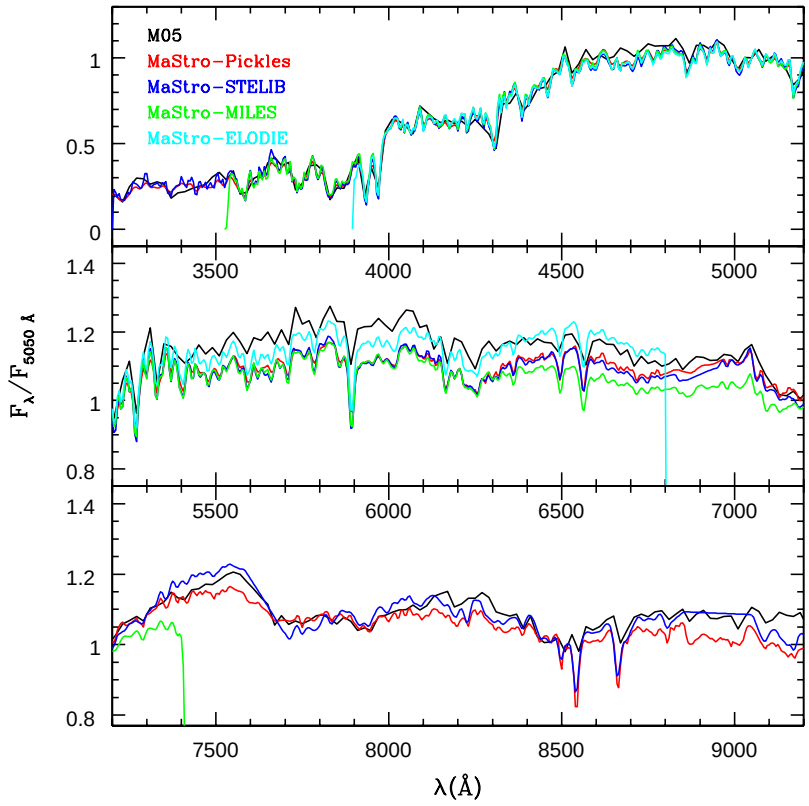

Figure 4.9: Same as Fig.4.8, but for a 12 Myr, $Z_{\odot}$ SSP with Salpeter IMF. Notice the considerable drop in flux between 5500 and 7000 Å for a majority of the models based on empirical libraries compared to the M05 model.

In addition, the MILES-based model display a lack of flux with respect to the Pickles- and STELIB-based models at wavelengths $\lambda > 6300$ Å. As we shall see later on, this deviation is most likely caused by the temperature calibration of the stellar spectra in the MILES library, but small effects from the flux calibration is impossible to rule out.

Finally, the MaStro-Pickles and MaStro-STELIB models coincide very well up to around 7300 Å, after which the Pickles-based model demonstrate overall lower fluxes, although this behaviour is more undulating than strictly systematic. Calibrating this part of the spectrum, however, currently poses a big challenge, since it would require high-quality near-IR spectra of old, metal-rich globular clusters, of which the Milky Way has a limited supply. A few can be found in the Galactic bulge, but these are quite strongly affected by dust reddening, and at the moment no such spectra exist.

The UV region of young models

The empirical exploration of the UV region has not rendered nearly as much data as the comprehensive studies of the optical region, one reason obviously being Earth's opacity to ultraviolet rays. Even in space a similar problem may arise as light from UV sources is easily scattered by intervening dust. The existence of good data is, however, crucial for stellar population modelling, in order to evaluate the spectra of star-forming galaxies, whose light-averaged ages can be very young, and also of high redshift galaxies, whose observed frame spectra often display the restframe ultraviolet. To this day, the stellar spectra of the *IUE* satellite (Heck et al. 1984 and Fanelli et al. 1992 for low- and high dispersion, respectively) is still the most valid source for this purpose.

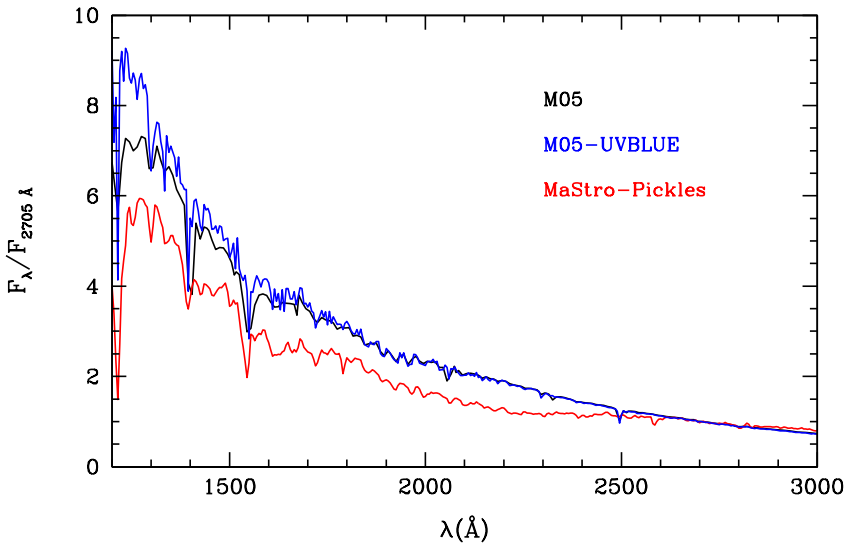

Figure 4.10: Comparison of the UV region for a 3.5 Myr, $Z_{\odot}$ model with Salpeter IMF, normalised at 2705 Å. The M05-UVBLUE model has been smoothed to the resolution and binning of the Pickles library. Dust attenuation is clearly present in the empirical-based MaStro-Pickles model.

Of the empirical libraries only Pickles contains a UV extension, consisting essentially of the Heck et al. (1984) spectra. Fig.4.10 shows the comparison of the UV region for a very young, 3.5 Myr old, stellar population at solar metallicity and Salpeter IMF, between the MaStro-Pickles, M05 and M05-UVBLUE models (where the latter has been smoothed to the resolution of Pickles). To be more precise, M05 (black line) and M05-UVBLUE (blue line) displays in a simple way the pure difference between the theoretical spectra of Lejeune et al. (1997) and Rodríguez-Merino et al. (2005), whom both adopt the Kurucz (1979) model atmospheres. Redwards of 1700 Å these models are in perfect

agreement, whereas at bluer wavelengths some differences arise, most notably a stronger continuum in the UVBLUE-based model. The Pickles-based model, on the other hand, show clear signs of dust attenuation. This is not surprising, considering that very hot O-type stars (> 30000 K) are entered into the synthesis at these ages, and the effect can with little effort be traced to the individual stars of the Pickles library (see Sec.4.7.2). This also highlights the danger on relying indiscriminately on empirical spectra for EPS – since they are already biased towards a specific dust attenuation law, getting an independent handle on this parameter will prove difficult.

The near-IR region of old models

Similarly to the UV, the near-IR region can be of great importance when analysing galaxy spectra. Maraston (2005) showed that this part of the electromagnetic spectrum provide a valuable tool for breaking the age-metallicity degeneracy between young, metal-rich and old, metal-poorer populations. As discussed before, this is due to a proper treatment of the TP-AGB phase, which in the K-band provide a considerable fraction of the total luminosity (up to 80 %). With new instrumentation available the near-IR is now becoming an increasingly promising area for galaxy and star cluster research (e.g. Lançon et al. 2008 and Riffel et al. 2009). However, obtaining empirical spectra or calibrating theoretical spectra for the entire near-IR region is an impossible task with ground-based instruments alone, due to complete opaqueness of the Earth's atmosphere to NIR radiation in various wavelength bands.

In Fig.4.11 we show the spectra of various models for a 12 Gyr, solar metallicity population up to the K-band, which is the limit of the Pickles spectra (although the theoretical libraries extend much further into the IR). The only difference between the M05 and M05-MARCS models (black and orange line, respectively) lie in the input theoretical library. It is important to remark here that the MARCS model atmospheres (Gustafsson et al., 2008) are completely independent from the Kurucz recipe; hence we also note more pronounced differences in the resulting SSPs. For the adopted normalisation, the M05 model displays significantly more flux than the MARCS-based model in the range 8000-13000 Å (including for e.g. the *J* band), but the two seem to coincide for the remainder of the explored region.

The MaStro-Pickles model is here semi-empirical, in the sense that all M-type stars are theoretical at these wavelengths. Additionally, absorption line analysis should be

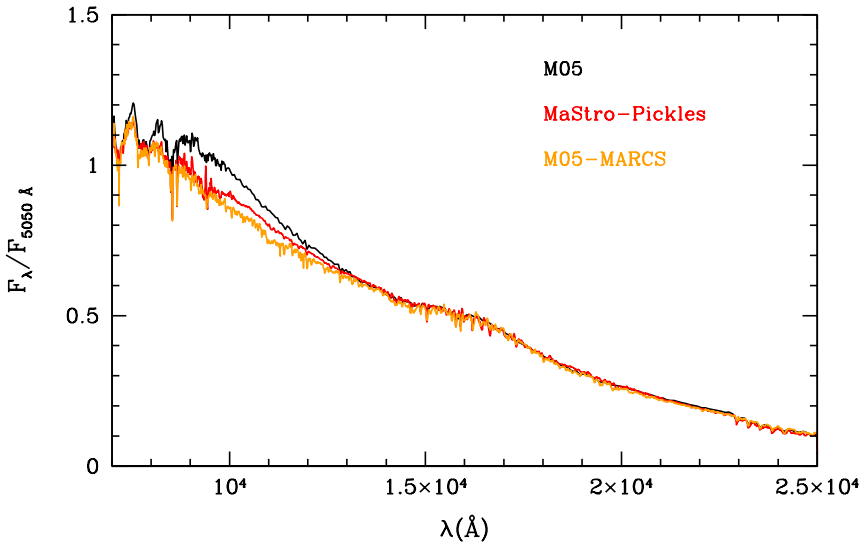

Figure 4.11: Comparison of the near-IR region for a 12 Gyr, $Z_\odot$ model with Salpeter IMF, normalised at 5050 Å. The M05-MARCS model has been smoothed to the resolution and binning of the Pickles library. The MaStro-Pickles model is here semi-empirical, whereas the other two models are built on purely theoretical spectra.

avoided, considering that about half of the spectra in the Pickles library lack proper spectrographic observations redwards of ~ 10000 Å. For these spectra, Pickles (1998) instead constructed smooth energy distributions from photometry alone. The integrated spectrum should therefore still be a valid representation of the continuum shape of a population with the given parameters. As can be seen from the figure, the Pickles-based model (red line) closely resembles the M05-MARCS model, apart from a non-negligible discrepancy between ~ 9500 and ~ 12500 Å, where the former display a minor excess of flux. It is clear, however, that it is the Kurucz-based M05 model that is the diverging one here.

Very metal-poor old models

A final comparison that might be of interest is for the old, very metal-poor population, which is found in e.g. the halo globular clusters. This can be found in Fig.4.12. The number of stars with [Fe/H]< -2 in the empirical libraries are easily counted, and only the MILES and ELODIE libraries were deemed complete enough to make any models at this metallicity, but even for these compilations we had to stretch the boundaries of the metallicity bin in order to include stars such that all important stellar phases could be covered. The result of this procedure is that, while the metallicity of the input isochrone and stellar tracks is [Z/H]$= -2.25$, the average metallicity of the stars lies closer to [Fe/H]~ -2.

However, we believe that this difference is of minor importance for the integrated SED, considering how few absorption lines are found in general in such metal-poor stars.

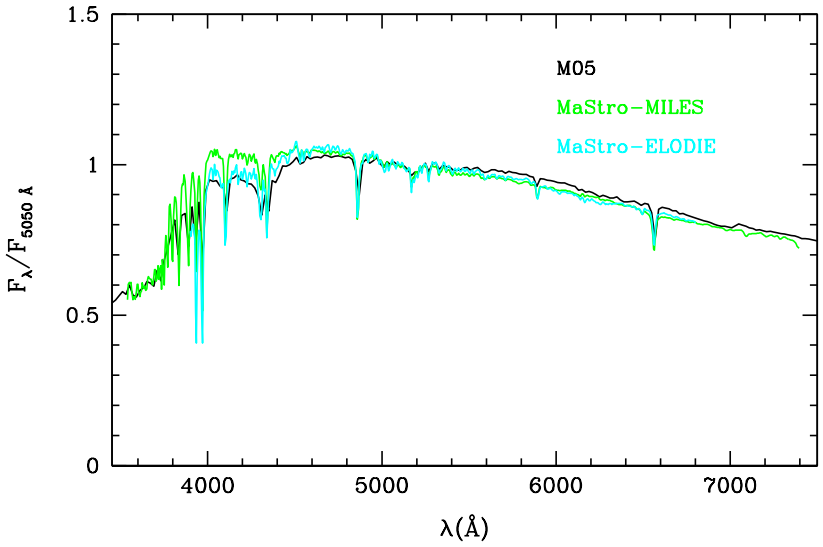

Figure 4.12: Comparison of a 10 Gyr, Z$= -2.25$ model with Salpeter IMF, normalised at 5050 Å. The resolution of the empirical models has been downgraded in order to enhance the clarity of the differences. The theoretical M05 model appears redder, despite the fact that the stars in the empirical models are of higher average metallicity.

The most striking feature of Fig.4.12 is that the M05 model appears redder than the models based on empirical stellar libraries, even though the theoretical stars have a lower average metallicity. This relationship between the models is just about visible for the ELODIE-based SED, while it is quite certainly so for the MaStro-MILES one. This may present a solution to the previous mismatch in (*B*-*V*) colour between Galactic globular clusters and EPS models, see Sec.5.3 for more details.

The flux excess around 6000 Å seen in the (BaSeL/Kurucz-based) M05 version of an old, solar-metallicity population is here only vaguely discernable, suggesting a decline with metallicity – a conclusion we reached already in Maraston et al. (2009b). This was based on the fact that the higher abundance of metals there are in a star, the more difficult it becomes to predict the number of and strengths of the absorption lines they give rise to (and even more so for cool and intermediate temperature stars that dominate old populations).

4.7.2 Tracing the SED behaviour in individual stellar spectra

The behaviour and SED shape of the integrated light of a stellar population model should always be traceable back to the corresponding shape and behaviour of its individual building blocks, i.e. the stars. This point is actually crucial in order to really understand how to interpret the result obtained when comparing models to models, or models to observations. With a procedure like the one we have adopted, where we construct SSP models based on several different libraries using the same EPS code while keeping the original stellar parameters as given by the respective reference papers, the global model behaviour depends on each library's flux and temperature calibration. Therefore, one should in principle be able to explain all the differences between models seen in the preceding section, by looking at the stellar spectra of the participating libraries. We will here give a few examples that this is also the case.

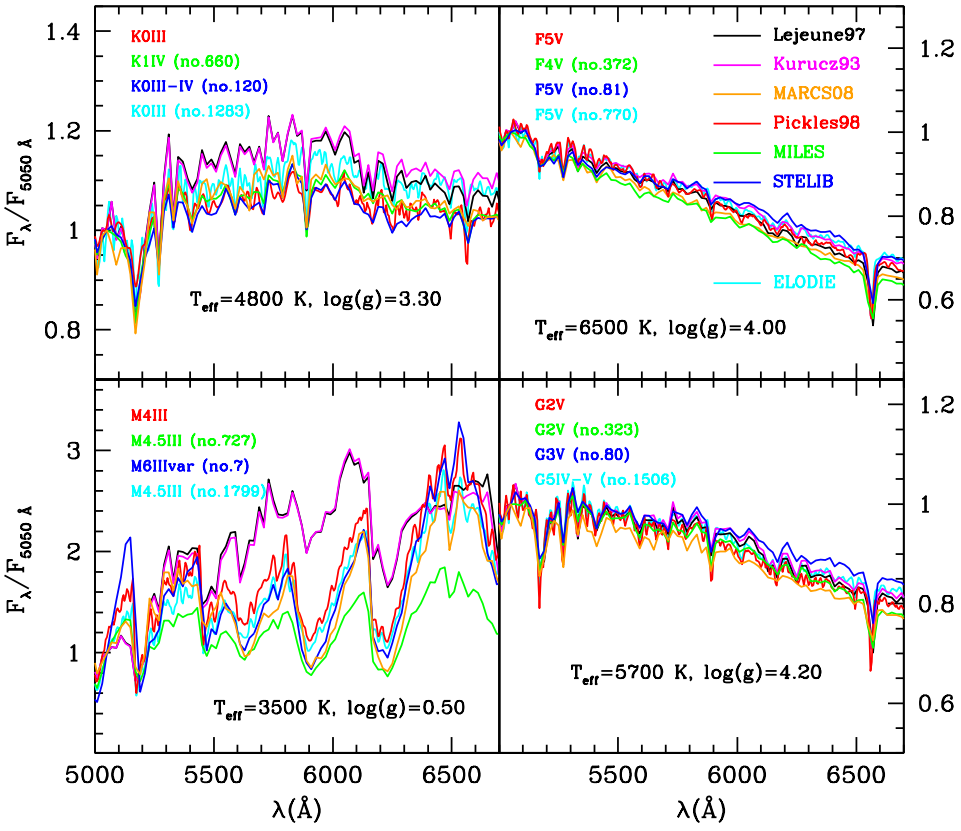

Figure 4.13: Comparison of individual stellar spectra from several libraries, both empirical and theoretical, for various sets of stellar parameters as indicated in each panel, in order to trace the flux drop seen in Fig.4.9.

Certainly one of the most important discoveries with the MaStro models so far (Maraston et al., 2009b) was seen in Fig.4.9. The clearly visible drop in flux around 6000 Å of most of the empirical-based MaStro models with respect to the theoretical-based M05 model (when normalised at 5050 Å) had significant consequences for the broadband colours of massive, passively evolving galaxies (see Chap.5). In Fig.4.13 we compare individual stellar spectra from the various libraries considered, both empirical and theoretical, focusing on the wavelength region around the flux dip and on stars of importance for an old, metal-rich population. Starting from the upper left and continuing clockwise, the panels show an RGB bump star, a turnoff star, a typical MS star, and a T-RGB star, respectively. The RGB bump is a stage of the RGB phase associated with the so-called *first dredge-up*, in which the H-burning shell due to convective processes receives a fresh boost of hydrogen. This means that the star stays in that region of the HR-diagram for a prolonged period of time before proceeding along the RGB track. A lot of fuel is burned in the RGB bump, contributing generously to the total luminosity of the population.

Evidently, the flux drop is more pronounced in cool stars (left panels), whereas it is not discernable at all for the hotter turnoff and MS stars. It may be noted that cooler MS stars also display the feature but these stars do not contribute significantly to the integrated flux, and has been left out here. Regarding the giants, T-RGB stars are indeed very luminous. However, their small number and the fact that most of their bolometric light is emitted at longer wavelengths means they are not the main contributor of the flux drop. This can also easily be deduced by looking at the shape of the integrated population spectrum, which contains none of the large molecular features of the T-RGB giant in this wavelength range. Instead it is the RGB bump that is likely to induce much of the difference. Empirical-based EPS models not properly accounting for the RGB bump (which is more difficult to do when using the isochrone synthesis technique, and depends on the specific choice of isochrones) may therefore not experience the same drastic drop in flux, even though it should still be present since all stars below ~ 5500 K contribute.

Bono et al. (2001) presented a new parameter, R_{bump}, for estimating the RGB bump lifetime in GCs, and showed that theoretical predictions from canonical evolutionary computations (as adopted by the M05 and MaStro models) are in fairly good agreement with observations. The R_{bump} parameter is defined as the ratio between the number of stars in the bump region and the number of RGB stars in a normalisation region by the base of the RGB. By using star counts and a cluster-specific normalisation instead of more conventional RGB luminosity functions, the authors avoid the crucial dependence on bin size and absolute photometry. We have verified that using the fuel consumption

theorem on our choice of evolutionary tracks produces RGB bump lifetimes in accordance with both the observed and the theoretical values of R_{bump} in Bono et al. (2001), although acknowledging that the scatter of the empirical values – and their corresponding errors – are fairly large.

Apart from the BaSeL library (*black*), which was the stellar library utilised by M05, we have also included in the figure spectra from the 1993 version of the Kurucz library (*magenta*), whose model atmospheres the BaSeL library relies on. This was done in order to confirm that no mistake was made on the part of Lejeune et al. (1997) when synthesising the stellar spectra. As can be seen, this does not appear to be the case, as the BaSeL and Kurucz spectra are very similar. Finally, also plotted in the figure are the spectra of the likewise theoretical MARCS library (Gustafsson et al., 2008, *orange)*, whose model atmospheres are completely independent from the Kurucz ones. Contrary to the latter, the MARCS spectra follow very well the behaviour of its empirical counterparts, which supports our claim that cool spectra synthesised from the Kurucz model atmospheres are to some extent miscalibrated in the optical. Note that this result is obtained by trusting the stellar parameters provided by the libraries. The good agreement with the purely theoretical MARCS-based models suggests that this strategy is not in need of revision. As a final remark, the flux dip in the ELODIE spectrum of the top left panel is not as pronounced as for the other empirical libraries, in accordance with Fig.4.9.

Another example of how the behaviour of an integrated SED is traced back to individual stellar spectra is given in Fig.4.14, where the UV part of the 3.5 Myr, $Z_{\odot}$ MaStro-Pickles SSP is analysed (see Fig.4.10). It is clear that the Pickles spectra of the hottest turnoff stars are suffering from dust attenuation (*left panel*), which is reflected also in the integrated spectrum of the SSP. The better agreement found at slightly lower temperatures (*right panel*) is of little importance, since the light of such a young population is completely dominated by the turnoff stars (up to 80 %).

4.7.3 Importance of the library temperature scales on the integrated SEDs

As mentioned in Sec.3.5 systematics in both the flux calibration and the adopted temperature scale of the stellar spectra contribute to the library-dependent differences in the integrated SEDs. While the former seems rather difficult to get a handle on, and most likely only contribute to more subtle differences, the temperature scale is a more drastic way of modifying the entire continuum shape. A small constant shift of $\sim$ 100 K

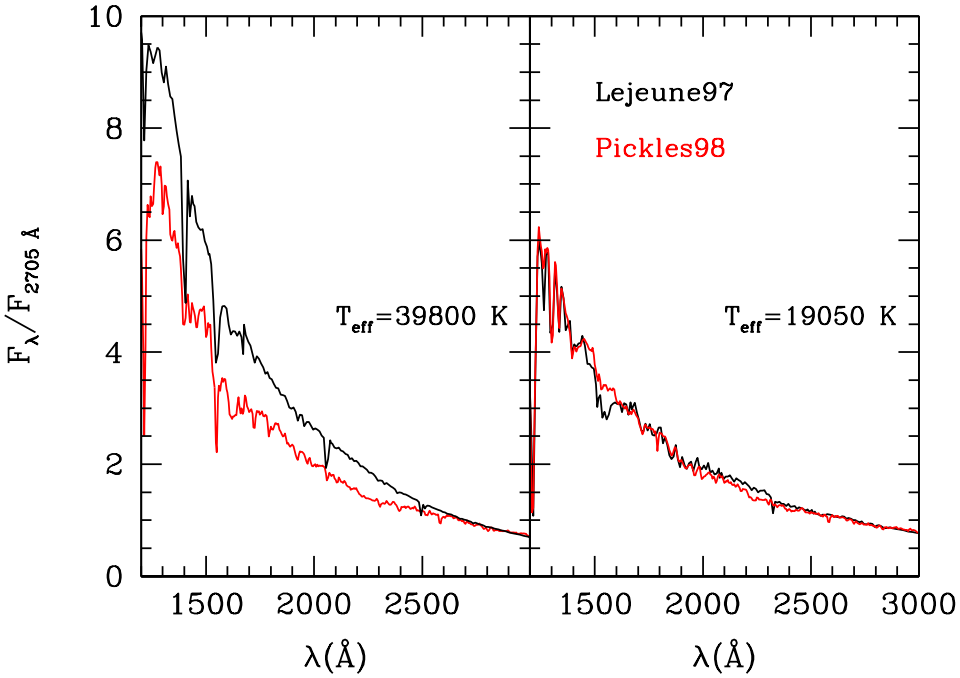

Figure 4.14: The continuum shape in UV of a very young population, see Fig.4.10, is traced to the extremely hot turnoff stars.

is enough to see a measurable effect in the broadband colours. Our strategy of keeping the original library parameters is mainly motivated by the vast amount of work required in order to properly homogenise (in the spirit of Cenarro et al. 2007) so many different libraries. In addition, star numbers vary considerably between the libraries, hence a common scale constructed avoiding extrapolation could involve only a subsample of stars, resulting in a reduced number of stars available for population synthesis. The decision was also partially motivated by the fact that the specific choice of reference scale would be extremely crucial for any future use of the models in interpreting data.

However, we could not refrain from carrying out one simple exercise in order to witness to what extent the temperature scale may matter for the shape of the integrated SED. Using the MILES library as a starting point, due to its satisfying coverage of stellar parameter space and the attention that was paid to homogenise said parameters, we construct a relation for the stellar temperatures as a function of (*B*-*V*) colour at given metallicity. Focus lies on the temperature range important for the turnoff and RGB bump

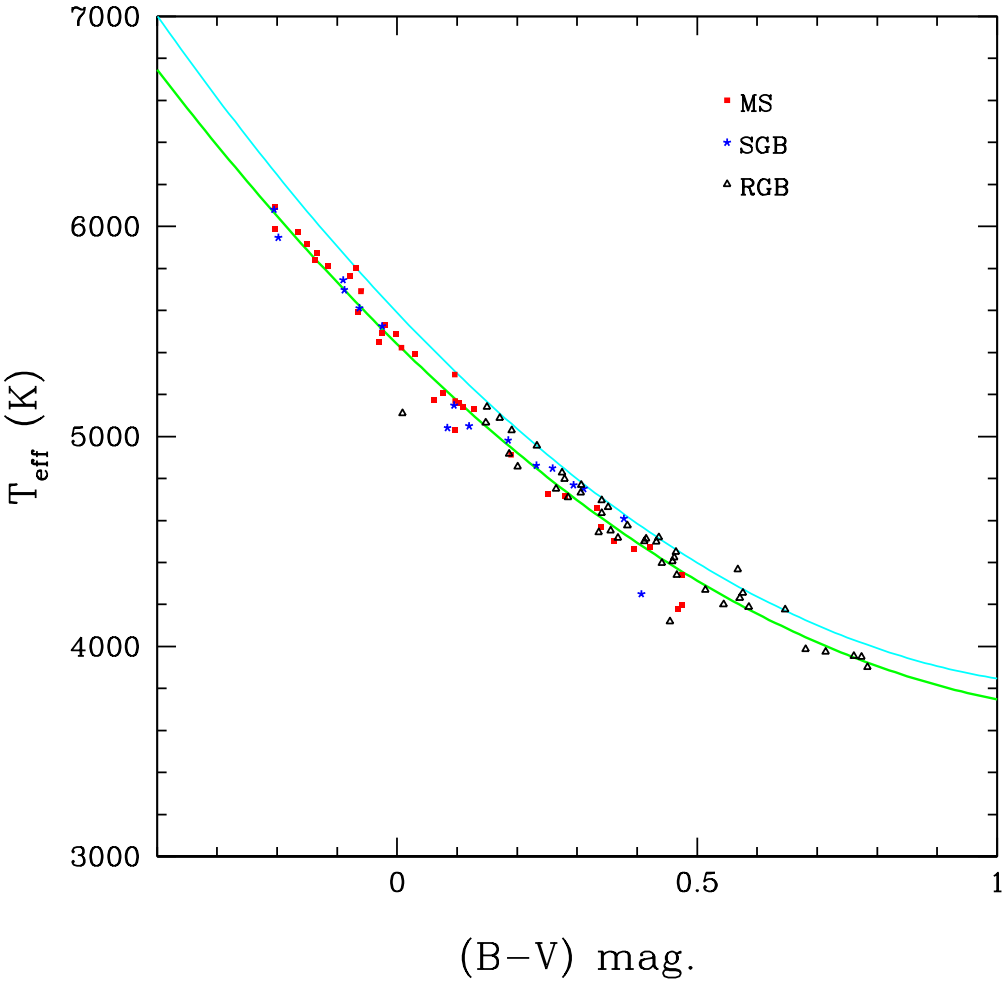

Figure 4.15: (*B*-*V*) colour-temperature relation for solar metallicity MILES stars (*green*) in the temperature range important for turnoff and RGB bump stars in old stellar populations. Overplotted is the same relation for STELIB stars (*cyan*). All data points are MILES stars.

stars in old, solar metallicity populations, which can be fitted with a second-degree polynomial. The result is shown in Fig.4.15, where the green line is a fit to the data points. Given in the plot is also the same relation for STELIB stars (cyan line).

An alternative version of the MaStro-STELIB models could then be computed, using the (*B*-*V*) colour of the STELIB spectra in order to assign a new MILES-based temperature scale to the stars participating in the synthesis of old, solar metallicity SSPs. The comparison in Fig.4.16 shows the illustrative case of a 12 Gyr, solar metallicity SSP. When tied to the MILES temperature scale – using the relation in Fig.4.15 – the MaStro-STELIB model displays a considerably lower amount of flux redwards of ~ 6000 Å, resulting in a much better agreement with the corresponding MaStro-MILES model. From

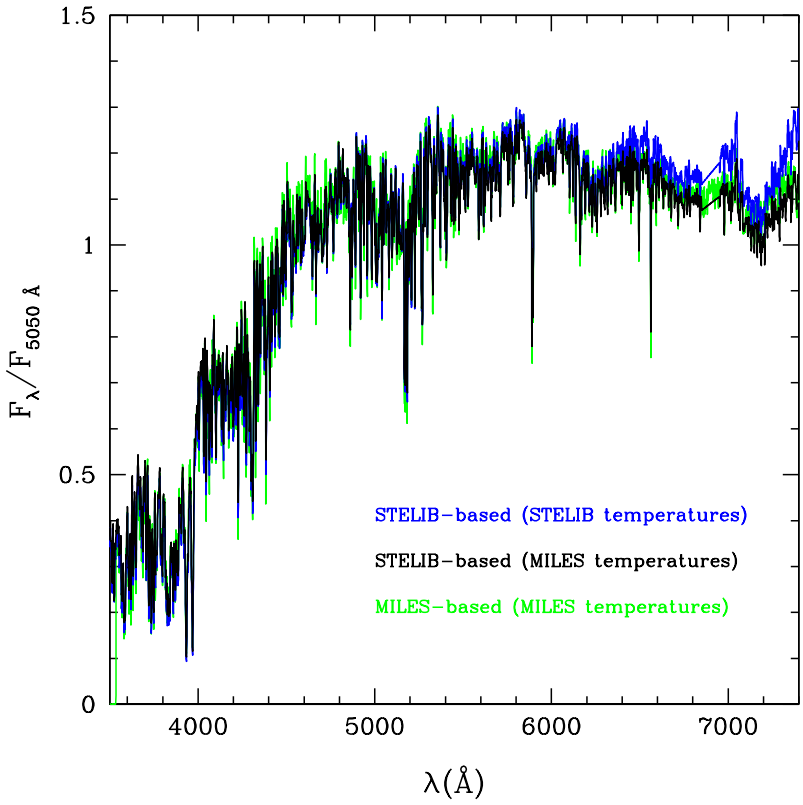

Figure 4.16: Effect of changing the temperature scale on the integrated SED of a stellar population model, for the specific example of a 12 Gyr, $Z_{\odot}$ SSP. The original MaStro-STELIB model (*blue*) displays a considerably lower amount of flux redwards of $\sim$ 6000 Å when tied to the MILES temperature scale (*black*), using the relation in Fig.4.15. For reference, the corresponding MaStro-MILES model is given as well (*green*).

this one may draw the conclusion that much (but not all) of the discrepancies in the near-IR between the MaStro-MILES and MaStro-STELIB models (see Figures 4.9 and 4.21) can be attributed to the calibration of the the respective temperature scales, which is also seen as a more or less constant offset between the MILES and STELIB relations in Fig.4.15.

4.7.4 Comparison to other models in the literature

The fact that some of the empirical libraries explored in this work have been used for EPS purposes in other publications begs the question of how these models fare against the corresponding MaStro ones. As a comparison between all models at every age and metallicity is a rather ambitious task we will here only outline the main similarities and differences.

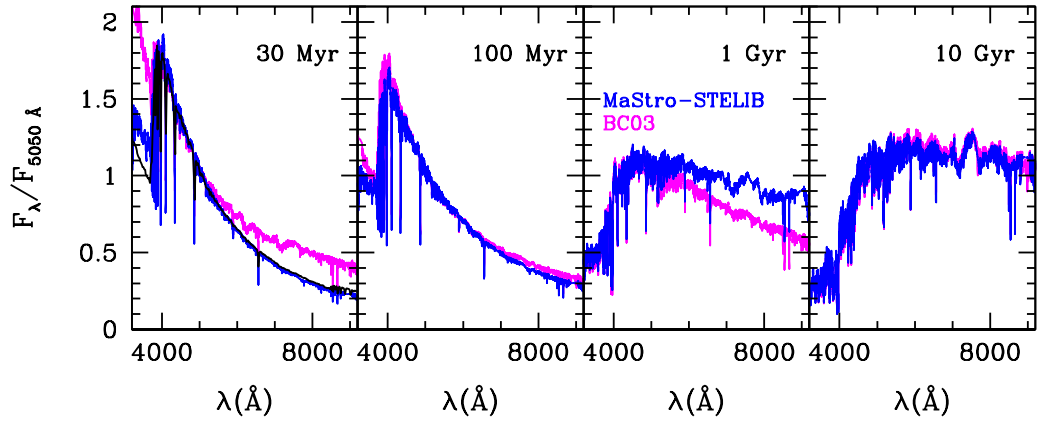

Figure 4.17: STELIB-based MaStro (*blue*) and BC03 (*magenta*) solar metallicity SSP models at various ages. At 30 Myr the corresponding M05 model has been superimposed for reference (*black*). The large discrepancy in the 1 Gyr model is due to the lack of contribution from the TP-AGB phase in the BC03 model.

One of the most widely used EPS model in the literature is the STELIB-based BC03, which has previously been discussed. In Fig.4.17 is a comparison at solar metallicity of the STELIB-based MaStro and BC03 SSP models for a number of various ages. Striking differences can be found in two of the panels. At 1 Gyr the MaStro models display a much higher flux longwards of ~ 5500 Å. This is not something unique to the MaStro models, but is due to the treatment and empirical spectra of the TP-AGB phase originally implemented in M05. At 30 Myr the BC03 model appears to be dominated by much hotter stars with respect to the MaStro model, resulting in a significantly steeper slope bluewards of a less pronounced Balmer break, and with a higher amount of flux also redwards of 5000 Å due to cool, but extremely luminous supergiants. The corresponding M05 model has been superimposed for reference, and shows a good agreement with the MaStro SED. This more or less rules out the possibility that the discrepancy arises from the way the empirical spectra are assigned to each isochrone bin in the BC03 code, since they are forced onto the theoretical BaSeL temperature scale, and that should be present also in the M05 model. Hence the different isochrones themselves are most likely the cause for the mismatch here.

The same can also be said for the more subtle differences in the other two panels where the overall agreement is still considerably better. It is for example known that the Padova evolutionary tracks (Bertelli et al., 1994) employed by BC03 has redder RGBs

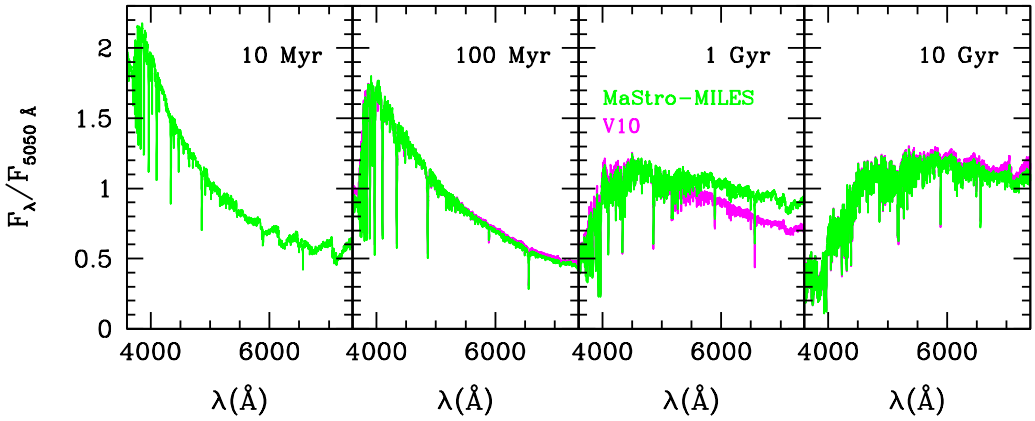

Figure 4.18: Similar to Fig.4.17, but comparing MILES-based MaStro (*green*) and V10 (*magenta*) SSPs, still fixed at $Z_\odot$. No V10 model exists at 10 Myr. The large discrepancy in the 1 Gyr model is due to a lack of proper TP-AGB treatment in the V10 model.

than the tracks adopted herein (see discussion in Maraston 2005). At 10 Gyr – an age where we have shown that discrepancies between empirical and theoretical spectra give rise to a separation in the integrated SEDs around 6000 Å (when normalised at 5050 Å) – it is likely that the BC03 method for assigning and scaling STELIB spectra to each isochrone bin also contributes to the higher fluxes in these models.

Fig.4.18 is similar to Fig.4.17, but compares instead the MILES-based MaStro and V10 SSP models, still at fixed solar metallicity. The latter have not published models of such young ages as 10 Myr, therefore the leftmost panel contains only the MaStro model. Again, the large separation between the models at 1 Gyr can be ascribed to a lack of proper TP-AGB treatment in the V10 version, while the minor differences at 100 Myr and 10 Gyr can be traced to the use of the redder Padova tracks (Girardi et al., 2000) in that code as well.

Finally, it is very interesting to note that the most debated result of the MaStro models so far, i.e. the flux drop around 6000 Å in the empirical-based models compared to theoretical Kurucz-based models at old ages (when normalised at 5050 Å), is visible also in the purely theoretical MaStro-MARCS model of the same age, and in the completely independent V10 model, see Fig.4.19. This lends strong support to our case, even though it has previously been rather heavily criticised from some directions (one direction in particular had strong objections, despite the fact that their own models actually display a similar result as ours, see Maraston et al. 2011 for a discussion on the matter). As can

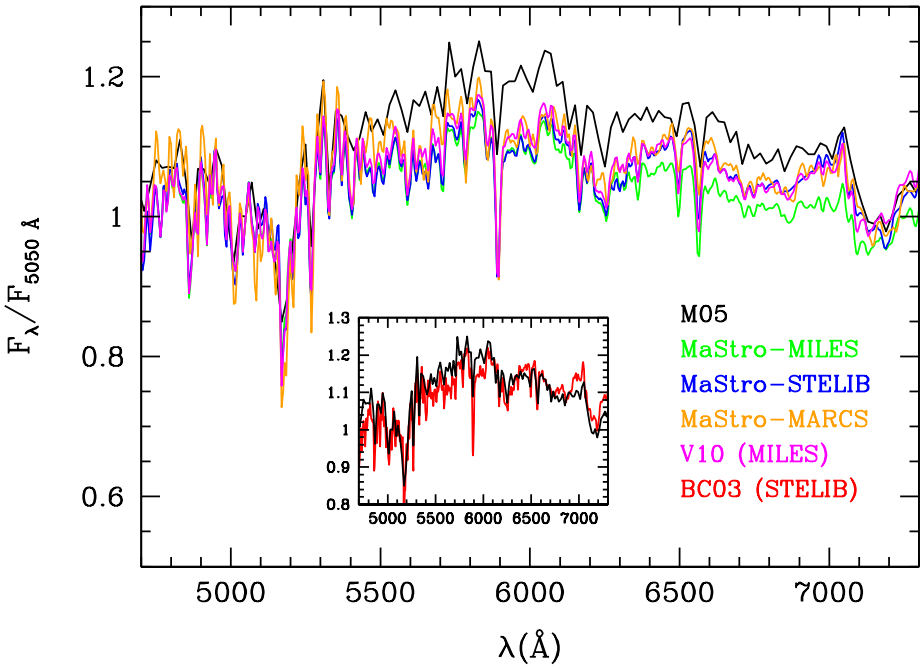

Figure 4.19: The spectral region around the *V*-band for various 10 Gyr, $Z_\odot$ SSP models with Salpeter IMF. All high-resolution models have been smoothed to the resolution of the Pickles library. Apart from the BC03-STELIB model (inset), all empirical MaStro models, as well as the theoretical MaStro-MARCS, and the completely independent V10 model, display the characteristic flux drop around 6000 Å.

also be seen in the figure, the BC03-STELIB model (inset) does not show the characteristic flux drop. This is due to the fact that the authors tied the temperature scale of the STELIB spectra to that of the theoretical BaSeL library.

4.8 Model Broadband Colour Comparisons

The transition to higher resolutions in stellar population modelling by means of empirical stellar spectra did not only affect the behaviour of individual absorption lines, but also, as we have amply shown in the preceding sections, the overall continuum shape of the population SED. It is important to note here that it is not the higher resolution itself that causes the discrepancies, since measuring broadband colours directly on SEDs is independent of spectral resolution (as long as the flux calibration has been properly performed and, of course, as long as the resolution is not ridiculously low). Regardless of resolution, it is obvious that a change in the synthetic broadband colours measured on model SSPs will also have consequences when photometrically deriving galaxy properties such

as ages, metallicities, masses, and star formation rates. Considering also how much science is still made with photometry (much thanks to low costs and large volumes of data) it is therefore necessary to more quantitatively get a handle on the effect on broadband colours introduced by the new stellar libraries in EPS modelling.

In Figures 4.20 and 4.21 we compare the integrated colours of the MaStro models to several other relevant EPS models, for all standard passbands in the Johnson-Cousins photometric filter system. Only the colours that could be computed given the intrinsic wavelength range of each library is displayed. For example, MILES only allow for the (*B*-*V*) colour to be measured, whereas STELIB, with its greater extension into the near-IR allows also for the (*V*-*R*) and (*V*-*I*) filter combinations. All UV colours, i.e. (*U*-*B*) and (*U*-*V*), are computed on the corresponding UVBLUE-extended versions (see Sec.4.6.2), and should thus run very similar between libraries, especially the former. All spectra in the Pickles library are intrinsically extended into the UV by means of empirical *IUE* low-dispersion spectra, but seeing that the colours of the original MaStro-Pickles models agree very well with the UVBLUE-extended version we only show the first in the figures.

Young ages, from the lower limit dictated by the stellar content of the library, up to about 1 Gyr, are displayed in Fig.4.20. Overall, the agreement is very good in most panels. For the colours involving the *U*-band this is largely because of the concatenation with the UVBLUE models, which are the same for all empirical MaStro models; at the same time this confirms that the merging procedure was done in a homogeneous way. Some discrepancies can be found for optical-to-near-IR colours in the age range where red supergiants thrive (around 10 Myr). This mismatch is however within the typical scatter associated with colour indices at these young ages (Marigo et al., 2008), which in turn is due to the shortness and luminosity of the red supergiant phase, causing large stochastic cluster-to-cluster variations. It may be noted that only the Pickles library provide spectral coverage of the *J*, *H* and *K* passbands.

A comparison between Fig.4.20 and Figure 2 in Conroy & Gunn (2010) is also worth commenting, as it has been discussed extensively as of late. The latter shows the M05 models (and therefore the MaStro models as well) to be significantly redder than the data consisting of MC GC broadband photometry, and exhibiting an age scale shifted towards younger ages, thus arguing that the M05 models are miscalibrated. However, since the age range in which TP-AGB stars are held to be relevant is calibrated with the ages of these MC GCs, it crucially depends on the choice of evolutionary tracks adopted to determine the cluster ages, as well as on the fitting method. In the M05 models the age range

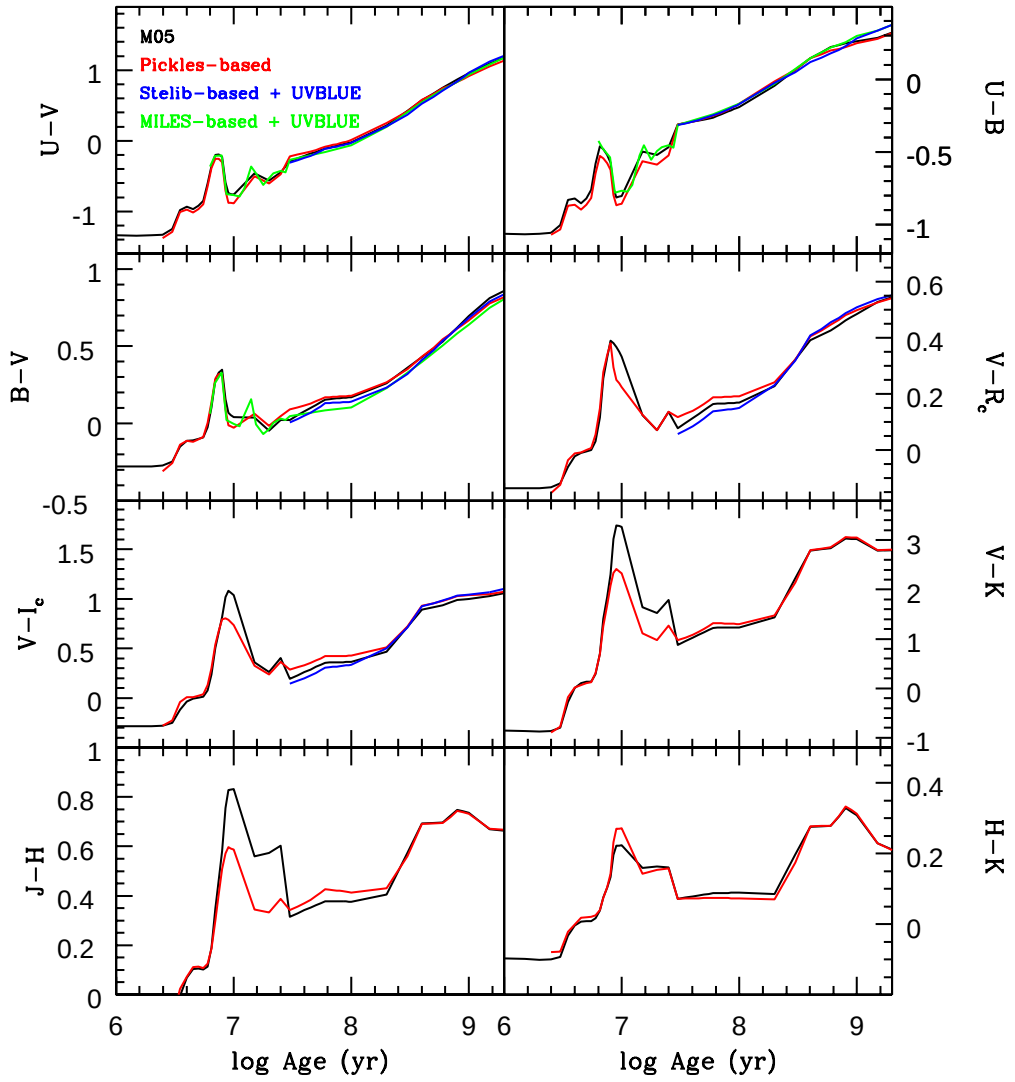

Figure 4.20: Integrated broadband colours of young SSP models for various spectral libraries. The wavelength range of each library determines which colours can be computed, while the stellar content sets the lower age limit. The UVBLUE-extended version of MaStro-Pickles behaves identical to the original and has therefore been omitted.

associated with the TP-AGB is between 0.2 and 2 Gyr, conveyed from turnoff ages derived using canonical (non-overshooting) tracks on the data of Persson et al. (1983). This age scale has since been confirmed by Mucciarelli et al. (2006). The CG10 models adopt instead the age scale of Pessev et al. (2008), where cluster ages has been determined from new observations using tracks with overshooting, and also including post-MS stars in addition to the turnoff when fitting the data. Both of these remarks shifts the peak ages to older values (Kerber et al., 2007; Marigo et al., 2008), which explains the different age scales exhibited by the M05 and CG10 models (the uncertainties regarding the amount of overshooting present in stars were discussed already in Sec.1.2.3). It also removes the discrepancy between the M05 models and the Persson et al. (1983) data seen in Figure 2

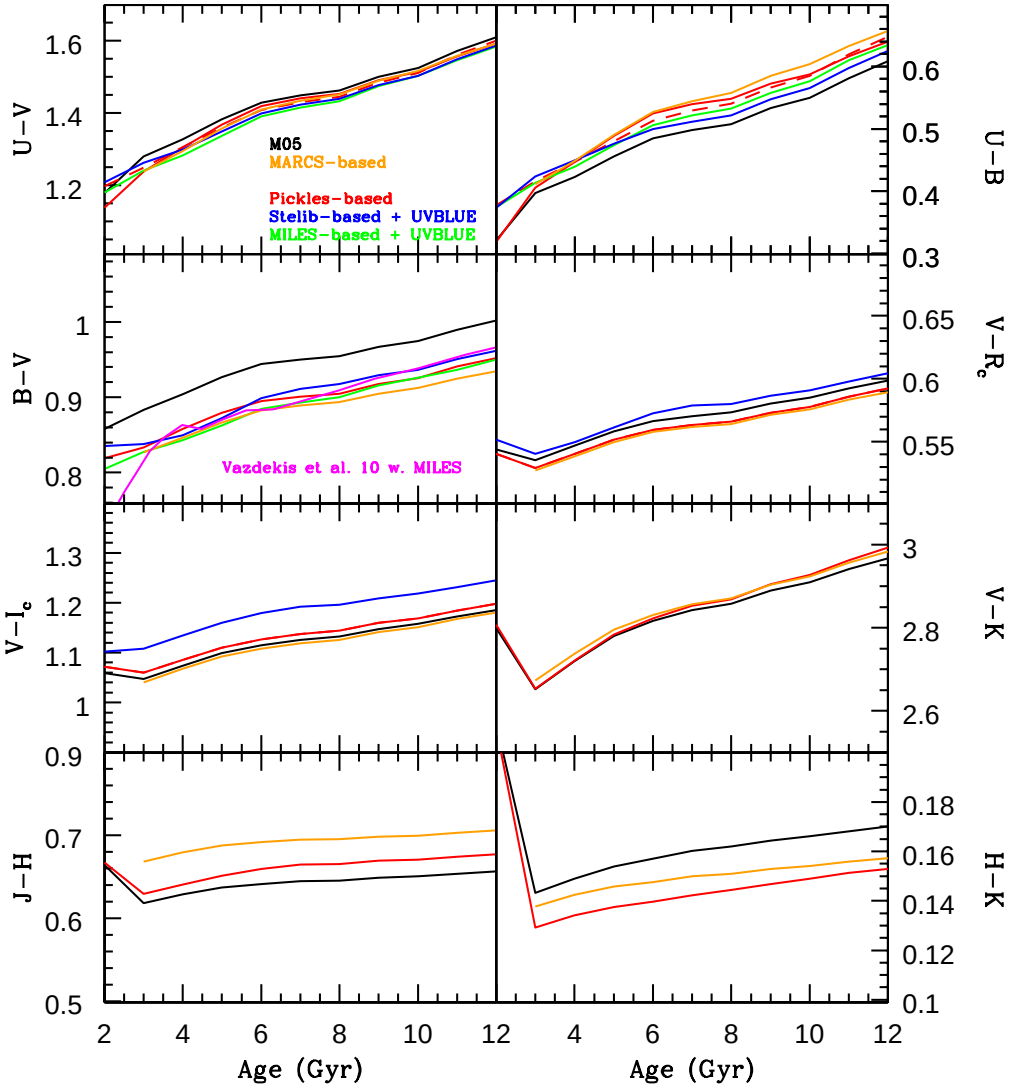

Figure 4.21: Same as Fig.4.20, but for old population models. The theoretical MaStro-MARCS, and the independent MILES-based V10 models have been added where possible. The UVBLUE-extended version of MaStro-Pickles is indicated by a red, dashed line.

of Conroy & Gunn (2010), since this data was re-evaluated and displayed using the scale of older ages from Pessev et al. (2008).

Integrated colours of old model ages (up to 15 Gyr) are instead given in Fig.4.21. Here we confirm the statements in the previous section about the (*B*-*V*) colour – i.e. the flux drop around 6000 Å when normalised at 5050 Å – which is present in all empirical-based MaStro models (MaStro-ELODIE is excluded here due its short wavelength range), as well as in the theoretical MaStro-MARCS and the completely independent MILES-based V10 models, resulting in a (*B*-*V*) colour that is consistently bluer by about 0.05 mag compared to the Kurucz-based M05 models. The complex behaviour of the crossing

models around the *H*-band spotted in Fig.4.11 can here be seen in the (*J*-*H*) and (*H*-*K*) panels. The agreement for the (*V*-*K*) colour is on the other hand excellent. Finally, an interesting point can be made about the (*V*-*I*) index, where the MaStro-STELIB model appears redder by about 0.05 mag. with respect to the other models. This is once again due to the flux drop in the *V*-band. The reason why the MaStro-Pickles and MaStro-MARCS models follow the M05 in this colour is that they display a lower amount of flux compared to the latter also in the *I*-band, whereas the STELIB-based model instead show similar flux levels here (compare to Fig.4.9, bottom panel).

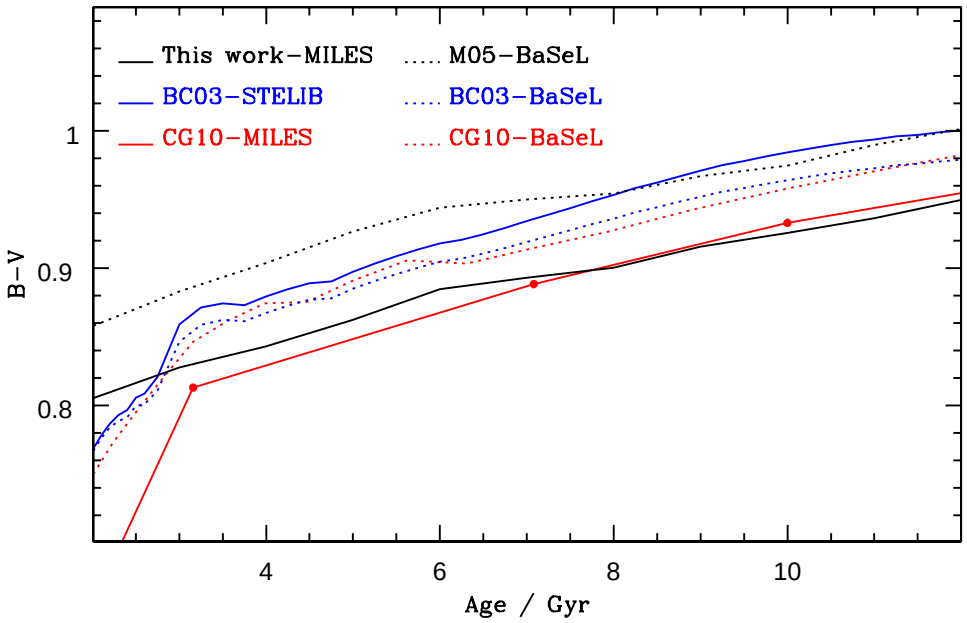

Figure 4.22: Integrated (*B*-*V*) colour as a function of age for the EPS codes that have produced models based on both the theoretical BaSeL library (dotted lines) and on an empirical library (solid lines). The CG10 models refer to a Chabrier IMF, but this has little impact on the integrated colour.

Two other EPS codes in the literature have so far produced SSP models based on both the BaSeL library (Lejeune et al., 1997, who used Kurucz model atmospheres) and on an empirical library. Given the results obtained with our models for the (*B*-*V*) colour, a similar comparison between those EPS models testing different spectral libraries within the same code is worthy of investigation. In Fig.4.22 the (*B*-*V*) as a function of old ages is given for the M05/MaStro models (BaSeL and MILES), the BC03 models (BaSeL and STELIB), and for the CG10 models (BaSeL and MILES). It is interesting to see that the latter models behave as ours – even though not acknowledged by the authors – in the sense that when based on an empirical library the (*B*-*V*) becomes bluer by about 0.05 mag. The BC03 models, as have already been pointed out, does not. In fact, the

STELIB-based BC03 models are *redder* than their corresponding theoretical version, a behaviour that we are unable to explain at this point. As a side remark, the delayed onset of the RGB due to overshooting evolutionary tracks is clearly visible in this figure as a rather sharp increase in colour around 3 Gyr for the BC03 and CG10 models.

4.8.1 Tracing the integrated colours in individual stellar spectra

Similarly to the integrated SED of a stellar population, it should always be possible to trace the behaviour of the integrated colours back to the individual stellar spectra. In order to avoid repeating ourselves, we will here only show one example that this is also the case. Fig.4.23 show the (*B*-*V*) colour as a function of temperature for a few stars in the BaSeL, MARCS and MILES libraries. In agreement with previous conclusions, the latter two display bluer (*B*-*V*) colours compared to Kurucz-based stars, given the intrinsic library temperatures. The discrepancy also appears to increase with decreasing temperature. At ~ 5700 K the values are in near-perfect agreement, which can probably be ascribed to the fact that this is the spot in stellar parameter space occupied by the Sun – an essential star for nearly any astronomical calibration.

4.9 Absorption line indices - the short story

Empirical EPS models can in principle be built from three different perspectives – broad-band colours, individual absorption line indices, and the SED approach. The latter has the advantage that, in principle, it could implement the first two as well, since colours and absorption line strengths are easily measured on the SED. In reality however, it is not so simple. Even though the synthetic colours of flux calibrated empirical spectra are well-behaved, the problem is that spectroscopic observations are usually restricted to a rather narrow wavelength range, thus setting a limit to which colours may be computed. This issue can be circumvented by using theoretical stars in the population synthesis, since these are calculated with an arbitrary wavelength coverage, but as we have shown in this chapter the colours of theoretical stars may be subject to miscalibration, even in the optical. Regarding atomic and molecular absorption line indices, these still have the benefit of being individually calibrated by means of their corresponding fitting functions (see Sec.1.3.4). But with a growing number of spectra in the empirical libraries, the possibilities of rejecting a seemingly fine spectrum due to a suspicious line index are also increasing (note that in order to reject a spectrum, fitting functions must still be constructed first). In this section we will therefore briefly summarise how the standard set

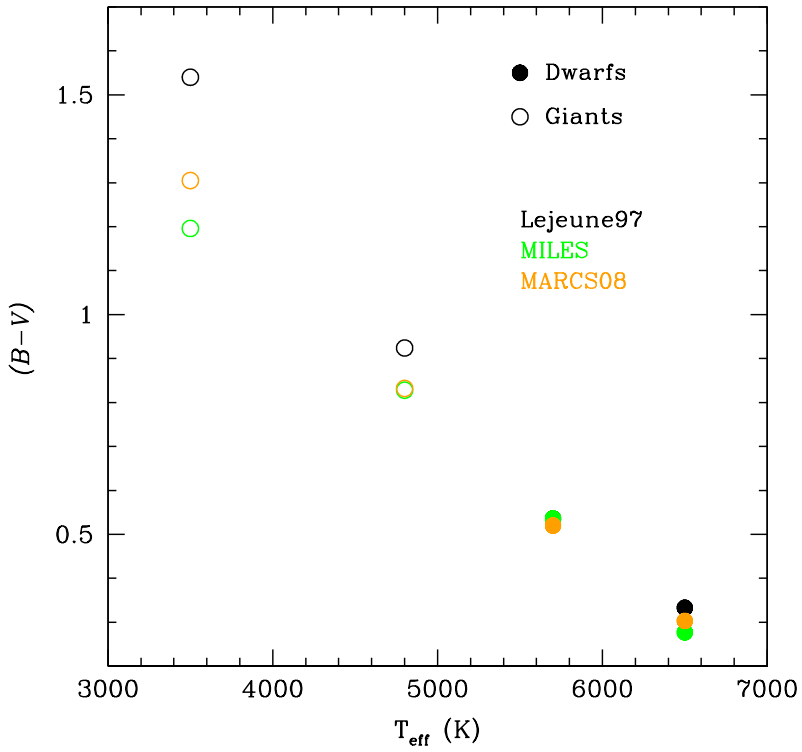

Figure 4.23: (*B*-*V*) colour as a function of temperature for a few individual stars of various libraries. The Kurucz-based Lejeune et al. (1997) stars display redder colours with respect to the others, increasing consistently with decreasing temperature.

of Lick indices measured on the MaStro-MILES SEDs compare to the index strengths predicted by the stellar population models of absorption line strengths by Thomas et al. (2011) (hereafter TMJ), who utilises fitting functions created from the MILES library (Johansson et al., 2010).

First of all it is important to remember that a proper analysis of Lick indices in the context of integrated stellar populations requires the element abundance ratios to be taken into account (see e.g. Thomas et al., 2005). This may be flexibly handled in the TMJ code by means of response functions, whereas the MaStro models instead reflect the global abundance pattern of the Milky Way given a certain metallicity. The exception is the stars in the Galactic bulge, who display significant [α/Fe]-enhancement also at metallicities around solar; such stars are not included in the empirical libraries. A similar chemical pattern to the Bulge can be found also in massive elliptical galaxies.

Fig.4.24 shows a comparison between different methods of obtaining Lick index values (at Lick resolution) for all 25 Lick indices, listed in order of increasing wavelength, except for the Balmer lines which are listed at the top. The indices calculated

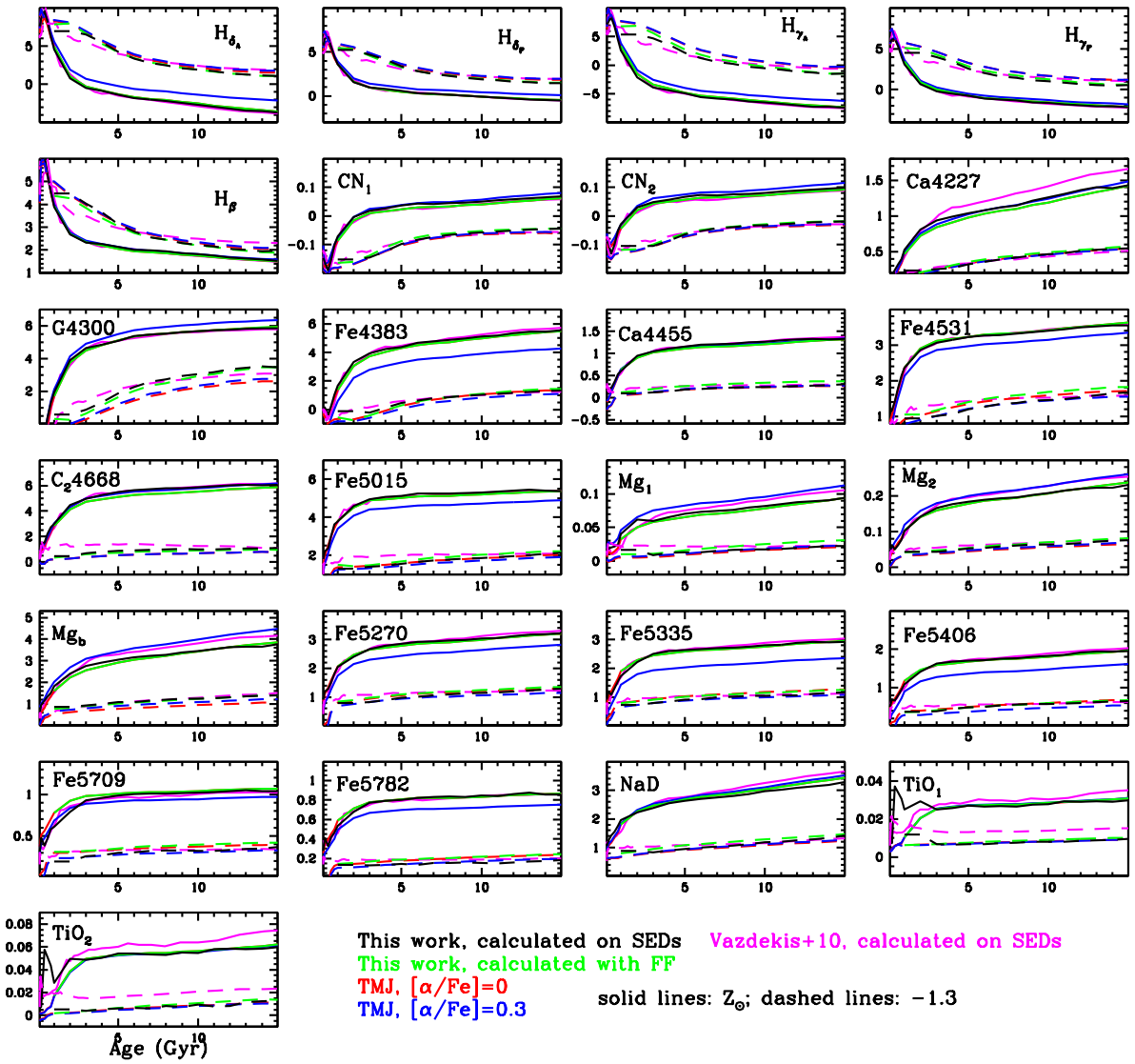

Figure 4.24: Comparison between Lick indices modelled with different techniques; calculated directly on the integrated MaStro-MILES SEDs (*black*); given by the TMJ models with variable abundance ratios (*red* for solar scaled [α/Fe]$=0.0$, and *blue* for alpha-enhanced [α/Fe]$=+0.3$); and finally, as an intermediate step, computed using the MILES-based fitting functions of Johansson et al. (2010) in the M05 code (*green*). The *magenta* lines show the values obtained from measuring directly on the MILES-based SEDs of the V10 models. Solid lines refer to solar metallicity, while dashed lines represent sub-solar, [Z/H]~ -1.3.

directly on the MaStro-MILES model SEDs are given as black lines, while the TMJ model predictions are given for two different abundance ratios – [α/Fe]$=0.0$ (red lines) and [α/Fe]$=+0.3$ (blue lines). Solid and dashed lines refer to solar and sub-solar ([Z/H]~ -1.3) metallicity, respectively. For reference, we have also included the Lick

indices obtained by integrating the MILES-based fitting functions of Johansson et al. (2010) in the M05 code with the usual energetics. This latter model will help discriminate how much of the difference is due to fitting functions and how much depends on the TMJ recipe. The index strengths measured directly on the model SEDs of Vazdekis et al. (2010) are also included as magenta lines.

Relating to the discussion above, the indices measured on the MaStro-MILES model SEDs (black lines) should in general coincide with the solar-scaled TMJ models at solar metallicity (red, solid lines), and with the alpha-enhanced models in the metal-poor regime (blue, dashed lines). For the majority of the cases this actually holds remarkably true. In the few cases where discrepancies are found, the integrated fitting functions (green lines) will help resolve wherein the differences lie. Neglecting minor differences, such as for the Ca4227 index, the SED and fitting function approach agree extremely well. The only panel in which a perceivable offset is seen between the two approaches is for the Fe4531 index at sub-solar metallicity. According to Johansson et al. (2010) the Fe4531 index of giant stars in this region of stellar parameter space are particularly sensitive to gravity effects, and we have verified that the discrepancy is indeed caused by a small deviation in the corresponding fitting function for these stars (Johansson, private communication). From both an SED and fitting function perspective, this index is therefore rather complicated to model, especially at metallicities below -1.0, where the number of MILES stars decreases rapidly. It should be noted that the Fe4531 index measured on the MaStro-MILES SEDs agree perfectly with the corresponding TMJ values, and the latter has been thoroughly calibrated against globular clusters (see Thomas et al., 2011).

While all the SED-based indices matches the solar-scaled TMJ values very well at solar metallicity (except for some minor differences in e.g. CN1, which is probably due to the fitting function technique giving slightly lower values), some indices do not follow the expected trend at [Z/H]$= -1.3$. Most noticeably the SED approach gives weaker Hγ and stronger G4300 with respect to the TMJ model, but as can be seen it is not the fitting functions that are responsible for the mismatch (except, perhaps, at the younger ages for Hγ). The explanation instead lies in the correction of the element ratio bias in the TMJ code, which assumes the input stellar library parameter [Fe/H] to reflect true iron abundance rather than total metallicity, and as a consequence, the metallicity scale gets slightly shifted, resulting in weaker metal indices and stronger Balmer indices at low metallicity. Again, it should be pointed out that these indices are very well calibrated with GC values (Thomas et al., 2011).

At ages around 1 Gyr the two TiO indices are significantly stronger in the SED approach. This is a pure effect from the contribution of TP-AGB stars and the empirical TP-AGB spectra that are included in the M05/MaStro integration (see Sec.2.1.3). Corresponding stars are absent in the MILES library, and thus missing also in the fitting function calibration. To a lesser extent, the same effect can be seen also in the Mg_1 index, which has been shown to be sensitive to carbon (Tripicco & Bell, 1995). Due to the wavelength restrictions of the MILES spectra, many interesting indices in the near-IR, such as the Ca II triplet (Cenarro et al., 2001) and the new Mg and TiO definitions of Cenarro et al. (2009), could not be computed for this comparison.

Finally, a comment about the indices measured on the V10 model SEDs. Discrepancies are found for the same indices which have already been discussed, but these are typically larger and display a somewhat different age dependence (see for example the G4300, $C_2$4668, and Fe5015 indices at low metallicity). In addition, other indices, such as Ca4227 and TiO, are significantly offset. The exact reason for this deviation is difficult to pinpoint, but it may be worth remembering that the V10 models adopt a different set of evolutionary tracks that include overshooting and redder RGBs.

Chapter 5

Astrophysical Applications of the MaStro Models

On replicating Nature's own simple stellar populations, and how the new models may have solved a long-standing problem in galaxy evolution.

Ultimately, EPS models are produced to be applicable to a wide range of astrophysical observations and measurements, and for the results to be reliable, they are thus required to be well-calibrated and rigorously tested. The input physics and the energetics of the EPS code adopted in this work were extensively discussed in M05, and will not be repeated here – they have not changed. Instead, three tests will be performed, that focus more on taking advantage of the new features introduced in the MaStro models, i.e. a higher resolution, and the implementation of empirical stellar spectra; 1) Comparison to high-resolution spectra of Milky Way open and globular clusters; 2) Comparison to high-resolution galaxy spectra; and 3) Comparison to the broadband colours of old, massive, passively evolving galaxies.

5.1 Globular Clusters spectra

One of the more critical tests for our new EPS models is the comparison to observed globular cluster SEDs. Calibrating SSP models with GCs is a technique adopted in both M98 and M05, since a globular cluster is in most cases almost a direct analogue to a simple stellar population, and in addition offer independently determined values for age and metallicity, from colour-magnitude diagrams and high-resolution spectra of member stars, respectively. However, integrated high-resolution, high signal-to-noise spectra of

Milky Way GCs are not particularly abundant in the literature; the works of Puzia et al. (2002) and Schiavon et al. (2005) that will be examined in this section are, as far as we are aware, the only ones available at the time this work was carried out (with the exception of the Gibson et al. 1999 spectra of 47 Tuc at 1 Å resolution). Main focus will lie on the Schiavon et al. (2005) compilation, which consists of 40 objects that represent in a good way the full range of MW GC parameters at high instrumental resolution and very high S/N ratio. Puzia et al. (2002), whose spectra are of slightly lower resolution (about half the resolution of Schiavon et al. 2005), have instead concentrated on the more metal-rich bulge clusters, but 11 out of their total number of 12 objects are in common with the Schiavon et al. (2005) compilation, thus enabling a comparison between different samples. Both sets of spectra have been flux calibrated, but neither have been corrected for reddening, since the primary objective of these investigations was the measurement of absorption line indices. Just recently (unfortunately too late for inclusion in this work), Colucci et al. (2009, 2011) presented very high-resolution spectra (R$\sim$25000) of around 20 globular clusters in total from several Local Group galaxies; these would indeed be very interesting to examine in future works.

We will in this section derive the GC parameters age and metallicity, for which we have written a standard, minimum χ^2 SED-fitting procedure, adopted over the wavelength range 3600-6200 Å, taking the HB morphology into account, and weighting pixels according to the S/N maps. Both Salpeter and Kroupa IMFs are considered, although the outcome is practically indifferent to the specific choice. Only the MaStro models based on the MILES library will be used, since they exhibit the best coverage of parameters relevant for GCs. As already discussed, the MaStro-MILES models, being based on empirical Milky Way field and GC stars, follow a rather well-defined pattern of chemical abundance ratios as a function of metallicity (Milone et al., 2010), especially considering no bulge stars are part of the sample. We therefore do not attempt a detailed comparison of individual absorption indices, since this has already been done in e.g. Thomas et al. (2011), but focus instead on the full SED fitting. The MaStro model grid have for this exercise been interpolated in age and metallicity in order to avoid a clustering of solutions around the grid points.

Our results will be compared to the CMD-derived ages of De Angeli et al. (2005) and the metallicities in the latest version of the Harris (1996) catalogue of Milky Way Globular Clusters, as well as to parameters obtained from the EPS models of the Lick/IDS system of absorption line indices (Thomas et al., 2011), which are based on new empirical fitting functions constructed from the MILES library (Johansson et al., 2010). Also the ages and metallicities from Marín-Franch et al. (2009) are examined, which take element

abundance effects explicitly into account. In addition, it is interesting to see how indices measured directly on the SED compare to the other methods when deriving cluster parameters. The GC spectra are de-reddened prior to the fitting, using a simplified version of the wavelength-dependent MW interstellar extinction law of Fitzpatrick (1999) with R=3.1. This parameter naturally depends strongly on the line-of-sight; however, since the purpose of this exercise is merely to show that, despite a rather simple approach, very reasonable estimates of globular cluster parameters can still be obtained in all but a few cases, such approximations may be forgiven. The *E(B-V)* values are taken from the Harris (1996) catalogue.

Abundance ratio considerations

Given the importance of globular clusters as SSP calibrators a few words regarding the effects of varying element abundance ratios are in order. The models are constructed from MW stars that follow a certain chemical abundance pattern, and at the time being specific abundance ratios is not a variable over which the user has any control. It was mentioned already in Sec.1.2.1 that the primary stage of calibration involves broadband colours and overall SED shape only, leaving individual absorption features for later consistency checks (like in Sec.4.9). Effects from different abundance ratios on the overall SED shape are generally quite small, and visible only in old populations (Salasnich et al., 2000). It is therefore relatively safe, for example, to use MC clusters for calibrating SSPs at young ages. However, even within the MW there are abundance ratio variations at the same metallicity, depending on which Galactic structure the stars belong to. Colucci et al. (2009, 2011) found, using high-resolution, integrated spectra of both Galactic and extragalactic GCs, abundance ratio anomalies relative to MW field stars, for example Mg-Al and O-Na anti-correlations. Such trends will *not* show up in the metal-poor MILES-based SSP models, consisting mainly of field stars, as only 10-15 % of the stars in the MILES library (and in the MaStro models constructed therefrom) are GC stars. This is an important fact to know when making detailed studies of individual absorption features in globular clusters, but in the SED-fitting exercises to come, this will matter little though, since the main driver in the fitting is the overall continuum shape. Interestingly, as will also become apparent, measuring absorption line indices directly on the SED can be potentially devastating if no consideration is given to the α-enhancement sensitivity of the indices.

5.1.1 The S05 sample

The Schiavon et al. (2005, hereafter S05) sample consists of 40 integrated spectra of Milky Way GCs, spanning a wide range of cluster parameters. An instrumental resolution of 3.1 Å FWHM, and S/N ratios between 100 and 400, ensures a very high quality of the spectra, and seems like an ideal test for the new MaStro models. Fig.5.1 shows 6 examples of SEDs from the S05 library (black), overplotted with their best-fitting (in terms of minimum χ^2) MaStro-MILES model template (green). The parameters of the best fits are indicated in each panel as well, and are in good agreement with the values derived in De Angeli et al. (2005) and Harris (1996). An indication of the goodness-of-fit is given by the residuals below each SED panel. The six clusters represent a fair sampling of the MW GC parameter space, and are also the six clusters with the least amount of reddening (E(B-V)≤ 0.06).

In general, the fits are excellent. As pointed out in Vazdekis et al. (2010) the CN feature around 3850 Å is weaker in the models, but only for cluster NGC0104 is it eye-catching (Thomas et al. 2003b showed that the corresponding CN Lick indices of these clusters can be matched well by enhancing the nitrogen abundance, without disturbing the good match of other indices). A recurring discrepancy may be spotted just redwards of the 4000 Å break, where the models appear to have lower fluxes compared to the observed spectra. The models also display somewhat lower flux levels bluewards of ~ 3750 Å, but here the S/N has decreased roughly a factor 3 compared to the values around 5000 Å. A similar plot is given also in V10 for the clusters NGC 104, 5904 and 7089 (their Figure 20), with derived cluster parameters in good agreement with ours (also for NGC 7089, which is not shown here). The fitted wavelength range in V10 is narrower by 800 Å, but for the region in common with our fits, the residual curves display a very similar behaviour.

The peak values in the marginalised age- and metallicity χ^2 distributions obtained from SED-fitting with the MaStro-MILES templates, are given in the left-hand panels of Figures 5.2 - 5.5 for the entire cross-sample between S05 and De Angeli et al. (2005), between S05 and Harris (1996), and between S05 and Marín-Franch et al. (2009), respectively. Also included are the values derived from Lick indices measured directly on those same SEDs (middle panels) using both all available indices (filled symbols) as well as a subset of indices that are known to be insensitive to abundance ratio effect (more precisely Hδ_A, Mg*b*, Fe4383, Fe5335, and Fe5406, see Thomas et al. 2011). In the right-hand panels are the values predicted by the TMJ Lick/IDS absorption line index models with variable abundance ratios, based on empirical MILES fitting functions (Johansson

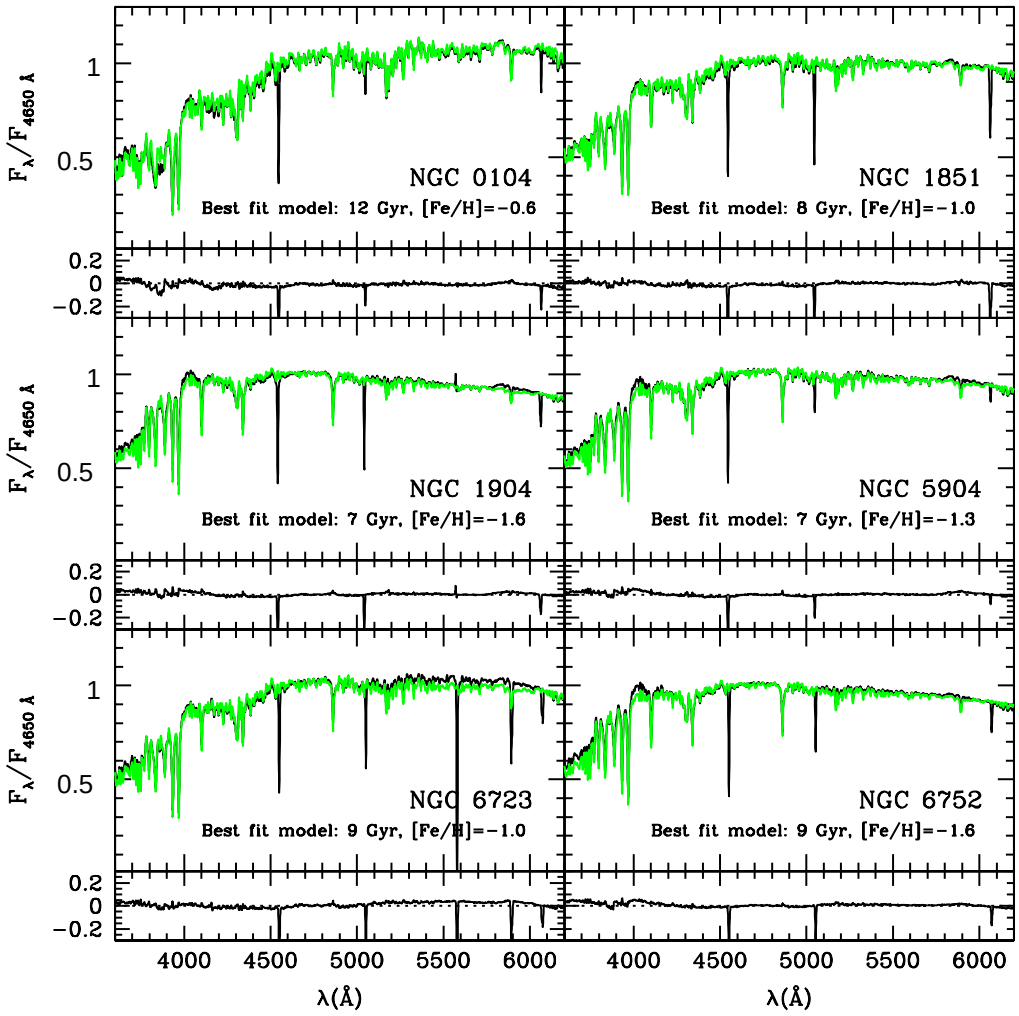

Figure 5.1: Globular cluster SEDs from Schiavon et al. (2005, *black)*, overplotted with their best-fitting (in terms of minimum χ^2) MaStro-MILES template (green), taking into account the HB morphology of each cluster. The residuals of the fits are given below each panel, and the age and metallicity parameters of the best fits are indicated as well.

et al., 2010), by using a combination of the best calibrated indices. It's worth noting that, unlike the SED-fitting, the latter methods allow for solutions older than 15 Gyr through extrapolation, which yields a few clusters with ages well above the estimated age of the Universe. However, these values are still consistent, within the errors, with the CMD-derived ages.

Concerning the ages, the same trend is displayed in all three panels in Fig.5.2; whereas the CMD-derived ages span a rather narrow range in age (3-4 Gyr centered around 10 Gyr), the other methods produce a larger spread, but are still consistent within the errors. Ages derived using full SED-fitting or with the TMJ models, which consider abundance ratio effects, are in much better agreement with the CMD ages compared to

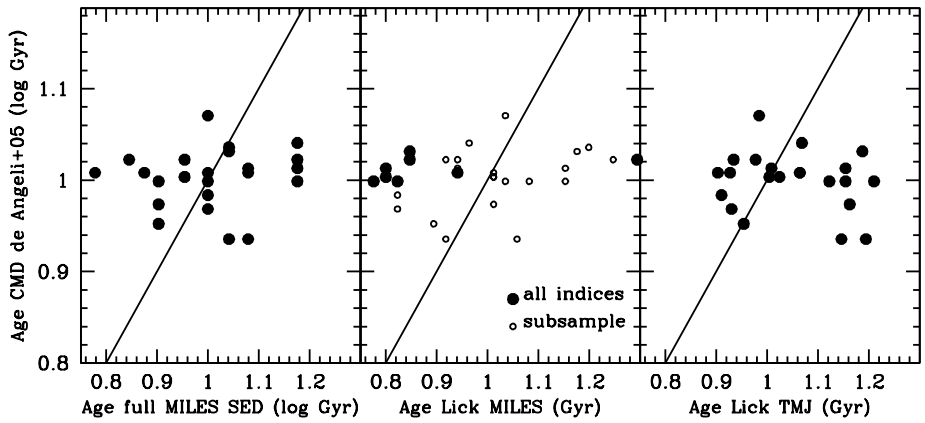

Figure 5.2: Comparison of ages for the cross-sample between Schiavon et al. (2005) and De Angeli et al. (2005) obtained through full SED-fitting using the MaStro-MILES models (*left panel*), Lick indices measured directly on the same SEDs (*middle panel*) using all available indices (filled symbols) and a subset of indices that are insensitive to element abundance ratios (open symbols), and finally the TMJ Lick index models with variable abundance ratios based on the MILES fitting functions.

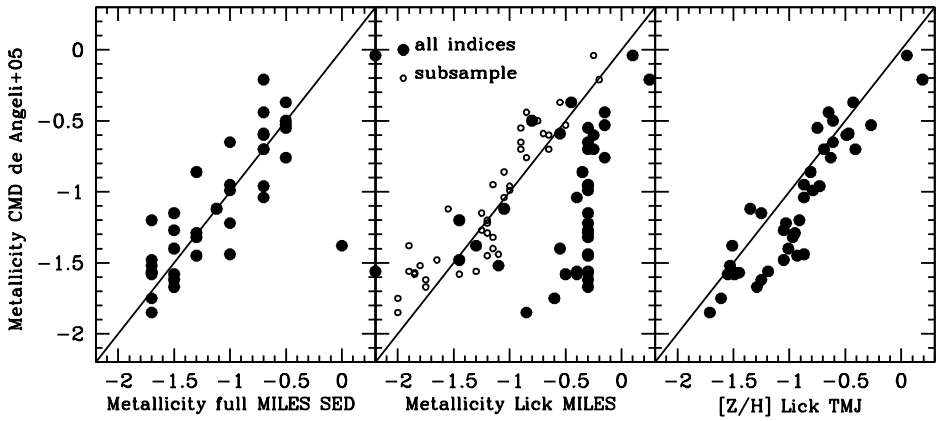

Figure 5.3: Comparison of metallicities for the cross-sample between Schiavon et al. (2005) and the latest version of the Harris (1996) catalogue. The values are obtained with the same methods and displayed in the same panels as in Fig.5.2.

the values obtained using indices measured directly on the SED, which naturally do not take abundance ratios into account. The latter are clearly underestimated when using all of the available indices (which in turn is linked with the metallicities being overestimated), but when adopting the [α/Fe]-insensitive combination of indices the situation is much improved. Here it can also be noted that the SED-fitting procedure gives a slightly smaller standard deviation when using a Kroupa IMF instead of a Salpeter IMF (2.51 Gyr compared to 2.66 Gyr).

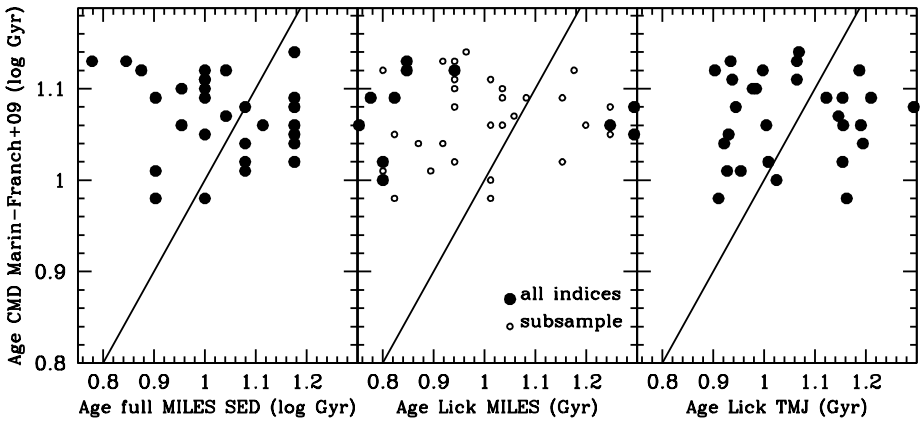

Figure 5.4: Same as in Fig.5.2, but for the CMD-derived ages of Marín-Franch et al. (2009) instead, where abundance ratio effects are explicitly taken into account.

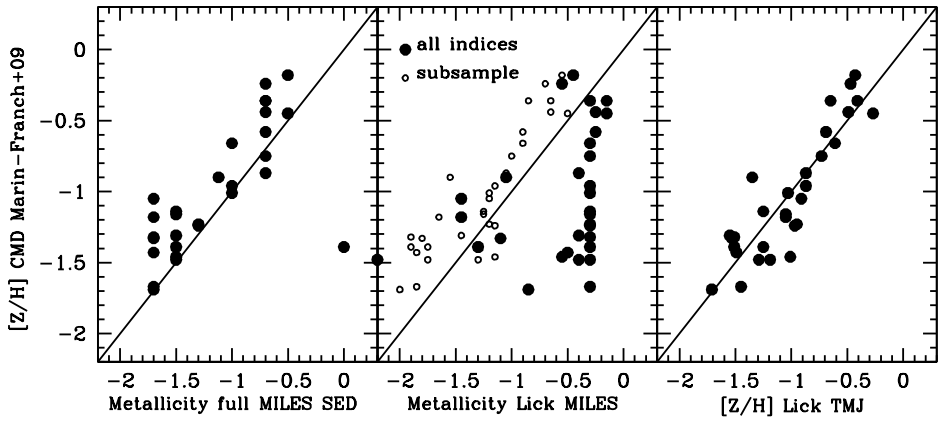

Figure 5.5: Same as in Fig.5.3, but for the CMD-derived metallicities of Marín-Franch et al. (2009) instead, which are corrected for abundance ratio effects and therefore considered to reflect total metallicity.

Relevant to this exercise is also to point out that the CMD-derived ages are not entirely bias-free, but carry their own problems related to which set of isochrones that was adopted for the fitting. The zero-point is for example dependent on whether element abundance ratios are taken into account or not. Thus, Fig.5.4 shows an age comparison similar to Fig.5.2, but using instead the CMD ages derived in Marín-Franch et al. (2009), where a correction for abundance ratio effects have been made. Though the overall trend remains unchanged, the CMD ages have shifted towards older values (now clustered around 11 Gyr rather than 10 Gyr). Concerning the ages obtained from the integrated light, there was better agreement with the De Angeli et al. (2005) values, where the median of the age differences (in the sense CMD−integrated light) was -0.03 ± 1.8 Gyr for the SED-fitting and -0.71 ± 2.83 Gyr for TMJ. For the Marín-Franch et al. (2009)

values these numbers become larger but more compatible with each other (1.5 ± 2.2 and 1.3 ± 2.76 Gyr, respectively).

Far more striking is the difference between the comparisons to the metallicities of Harris (1996) and Marín-Franch et al. (2009) in Figures 5.3 and 5.5, respectively. Whereas all three methods (neglecting the results from using *all* the indices measured on the SEDs) produce excellent agreement with the values listed in the Harris (1996) compilation, the metallicities derived with SED-fitting or SED-indices are systematically lower compared to the Marín-Franch et al. (2009) determinations, while the agreement for the TMJ method is actually slightly improved. Since both Marín-Franch et al. (2009) and TMJ aim to trace total metallicity [Z/H] this could point to the possibility that the MaStro models (regardless of fitting the full SED or measuring Lick indices) reflect instead mostly iron abundance [Fe/H]. The individual MILES stars are listed as [Fe/H], but given the large number of different sources used for the parameter determinations, it is difficult to assess whether this can be regarded as true iron abundances. It was in Thomas et al. (2003b) concluded that the Zinn & West (1984) scale, upon which the Harris (1996) values rest, refer to total metallicity, but in the subsequent Thomas et al. (2011) that conclusion rather points to the opposite – the scale reflecting iron abundance instead. This ambiguity of the metallicity scales was extensively discussed in both papers, and our contribution speaks in favour of the latter.

In Figures 5.3 and 5.5 a few data points are completely off the scale in the SED-fitting panel. These outliers are incidentally also the clusters with the highest amount of reddening. NGC 6544, the cluster with the second highest amount of reddening in the sample, has for example been given a considerably higher metallicity than the reference values. Since the shape of the continuum slope is the driving factor in the fitting procedure, it seems plausible that clusters with such a large amount of reddening as exhibited by NGC 6544 and 6553 (*E(B-V)*> 0.6) require a more sophisticated de-reddening method than the one adopted for this exercise.

It is important also to remember that the values from the SED-fitting are the peak values in the marginalised χ^2 distributions. Error bars have been omitted on purpose, since in almost all cases even a 95 % confidence interval would encompass ages practically from 1 to 15 Gyr – a perfect showcase for the age-metallicity degeneracy. On the other hand, in all but a few cases the peak values are actually in very good agreement with the literature values. Two such examples are given in Figures 5.6 and 5.7, where the normalised age- and metallicity χ^2 distributions are highlighted for one of the best (NGC 1851) and one of the worst (NGC 6544) fits.

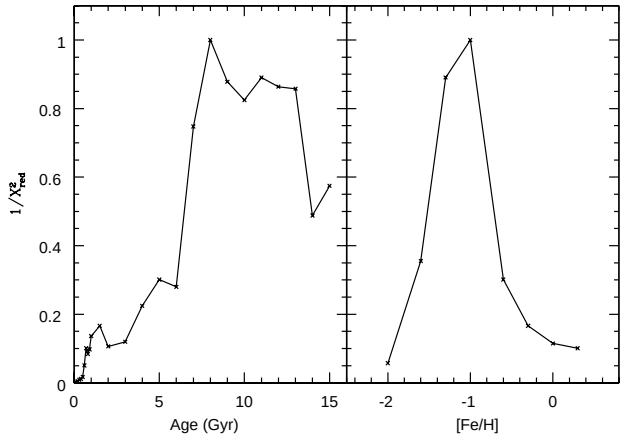

Figure 5.6: Marginalised age- and metallicity probability distributions for the Schiavon et al. (2005) globular cluster NGC 1851 from SED-fitting with MaStro-MILES models, normalised at the peak values. This cluster represents one of the better fits.

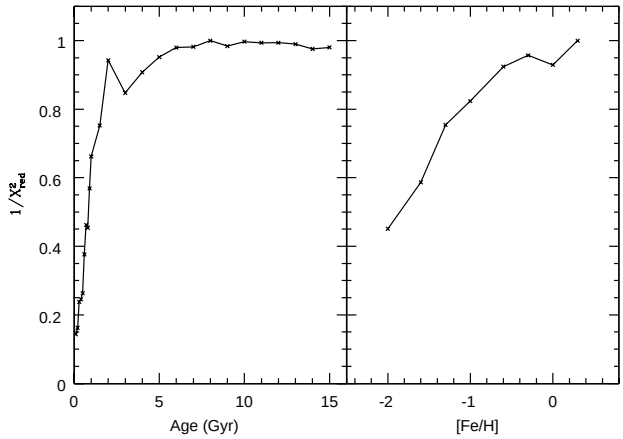

Figure 5.7: Same as Fig.5.6, but for NGC 6544. Notice the large age-metallicity degeneracies, making this clusters one of the most poorly constrained.

The findings from this simple test can be summarised as follows: when utilising globular clusters to test SSP models, the CMD-derived values (to which the models are compared) are not bias-free. Results obtained from absorption line diagnostics carried out with models that do not take element abundance ratios into account are misleading. This can be rectified by using a combination of indices that are known to be insensitive to abundance ratio effects. Also full SED fitting is a viable alternative, but neither of these two methods can rectify the abundance ratio parameter.

5.1.2 The P02 vs. S05 globular cluster samples

In Puzia et al. (2002) absorption line diagnostics was performed on the integrated spectra of the metal-rich bulge GCs, and of the bulge field itself. Out of the total sample of the 12 clusters studied, 11 are present also in the Schiavon et al. (2005) sample, which allows for a comparison between parameters derived from different observations, but using the same stellar population models. This test is important for determining the effect on best-fitting parameters of the observational obstacles involved in measuring the spectral energy distributions of extended objects within the Milky Way. It is especially crucial for clusters in such crowded regions as the Galactic bulge, where foreground contamination may be difficult to avoid, and reddening is severe.

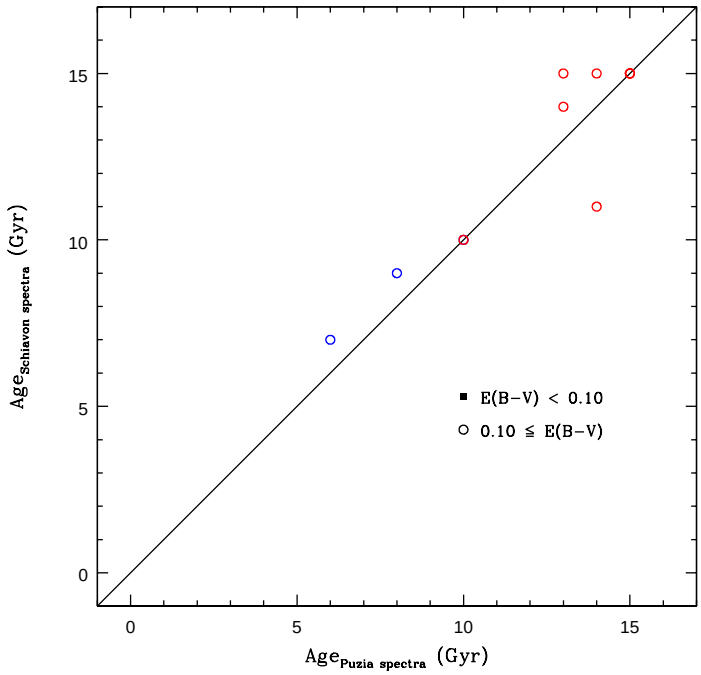

Figure 5.8: Comparison between the ages derived for the cross-sample of Puzia et al. (2002) and Schiavon et al. (2005) globular clusters, using SED-fitting with the MaStro-MILES models. The black line corresponds to the one-to-one relation.

The result of this comparison, using SED-fitting with the MaStro-MILES models as described in the previous section, can be viewed in Figures 5.8 and 5.9. In most cases the outcome is the same, or at least a very similar, set of parameters (the number of points in both plots seemingly disagree, both with each other and with the stated number of 11, but can be explained by the fact that 2 or more points occupy the same position). A few minor discrepancies can be seen, but considering that for these clusters there are noticeable differences in the shape of their spectra, and considering that even subtle differences can

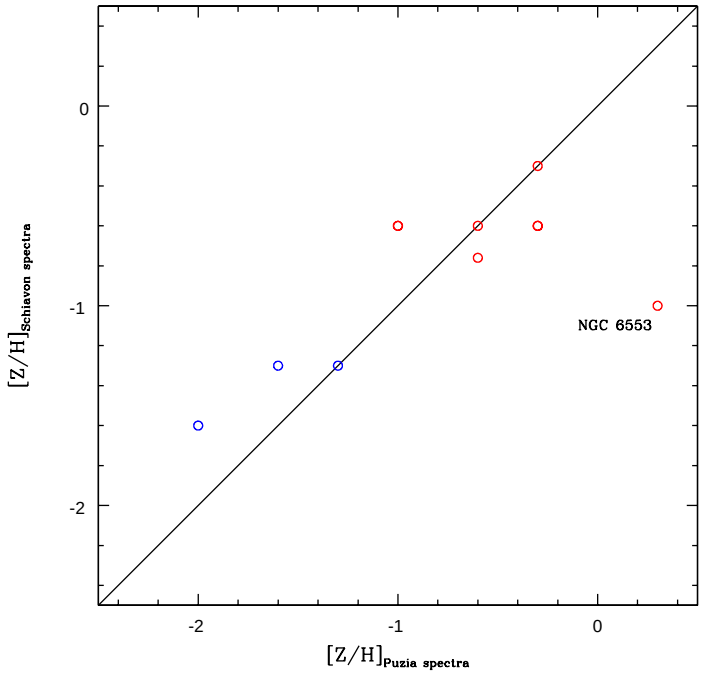

Figure 5.9: Same as Fig.5.8, but for metallicities.

have an effect on the fitting, since age-metallicity degeneracies are large and probability distributions poorly constrained, the agreement is surprisingly good. The only exception is the rebellious NGC 6553, for which the S05 version has been assigned a considerably lower metallicity, despite the fact that this is known to be one of the most metal-rich MW GCs (although not as metal-rich as predicted in the fitting of the P02 spectrum).

Still it is worth remembering that the outcome of SED-fitting depends on both observations and models alike. This is especially true for nearby, spatially extended objects like globular clusters, whose integrated spectra are not easily obtained.

5.2 The open cluster M67

The globular clusters in the previous section were all old and metal-poor, with the exception of the two metal-rich bulge clusters NGC 6528 and NGC 6553, that on the other hand display clear signs of enhancement in the alpha-elements. Since the empirical-based MaStro models are solar-scaled at high metallicity, something other than Milky Way GCs is required to check the models in this regime. The neighbouring Magellanic Clouds do contain young globular clusters, but the only high resolution, high S/N spectra of these that exist in the literature was not published until just recently by Colucci et al. (2011),

which however, was too late for inclusion in this work as previously mentioned. A comparison to their broadband colours was performed already in Maraston (2005) and will not be repeated here. Instead we will fit the high-resolution (2.7 Å FWHM) spectrum of the old, *open* cluster M67 from Schiavon et al. (2004) (meaning old with respect to other open clusters; compared to globular clusters it is still a toddler), which is believed to have a metallicity and abundance ratios close to solar values, and a CMD-fitted age between 3 and 5 Gyr (see Chaboyer et al. 1999 for a review of these determinations). Due to the dispersive nature of open clusters it was not possible to directly obtain an integrated spectrum of this object, so the authors co-added observations of individual cluster members in a fashion similar to EPS modelling. The high metallicity also allows us to test MaStro models other than just the MILES-based.

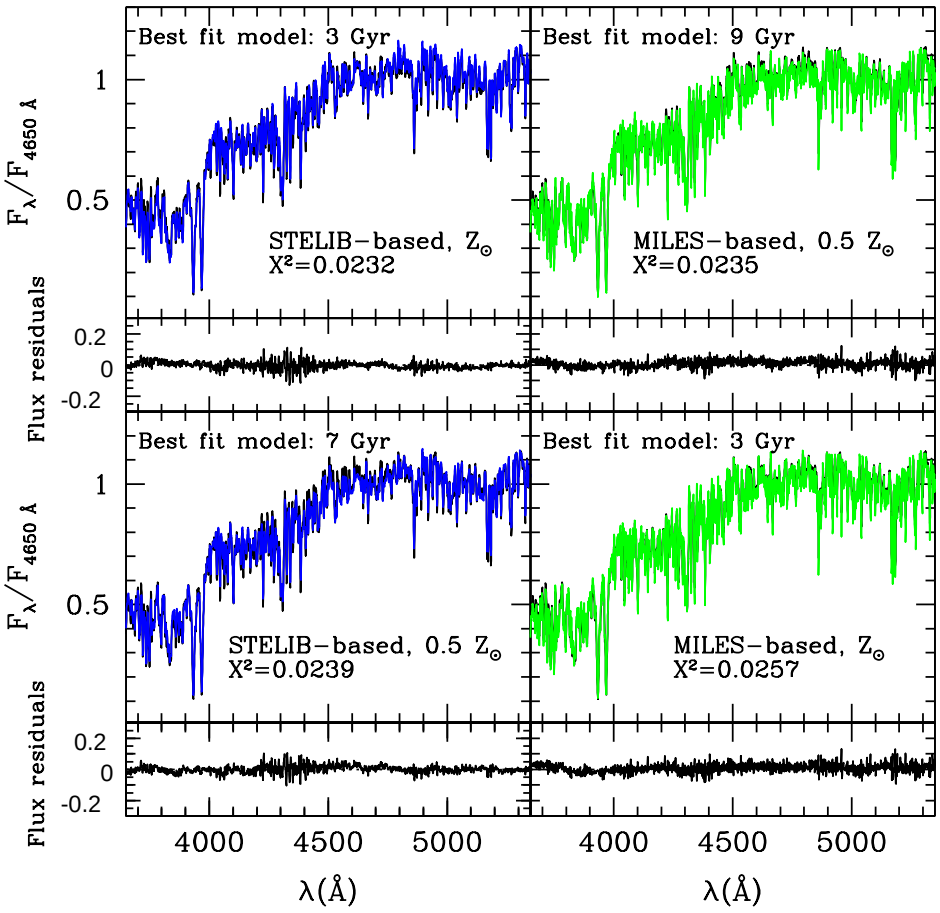

Figure 5.10: First ranked fits at $Z_\odot$ and 0.5 $Z_\odot$ of the MaStro-STELIB (*blue*) and MaStro-MILES (*green*) models to the composite spectrum of Galactic open cluster M67 (Schiavon et al., 2004, *black)*). The residuals to each fit is given below the respective panel.

In the upper panels of Fig.5.10 we show the best-fitting (in terms of minimum χ^2) MaStro-STELIB and MaStro-MILES models for the M67 composite spectrum. Given in each panel are the ages and metallicities of these best-fitting models, along with the goodness-of-fit indicated by the χ^2 value and the residuals just below. The first-ranked STELIB solution is more or less identical to the parameters obtained from CMD-fitting, while the MILES-based models – although the fit is equally superb – release an older and slightly more metal-poor solution. The lower panels show instead the third-ranked fits, which sees a shift between the solutions presented by the two models, with the MaStro-STELIB giving an older and more metal-poor solution, while MaStro-MILES reproduces the literature values. There is a minor rise in χ^2 in the latter, but it must be noted that, statistically, all these solutions are equally good. This highlights a danger of blindly trusting the χ^2 as a discriminator between fits. In Fig.5.11 we have combined the parameters in the two panels for each respective library in order to show that the implied age-metallicity degeneracy in Fig.5.10 is not just the result of a too narrow fitting range and/or the choice of the normalisation wavelength. As can be seen, the residuals in these fits are clearly worse.

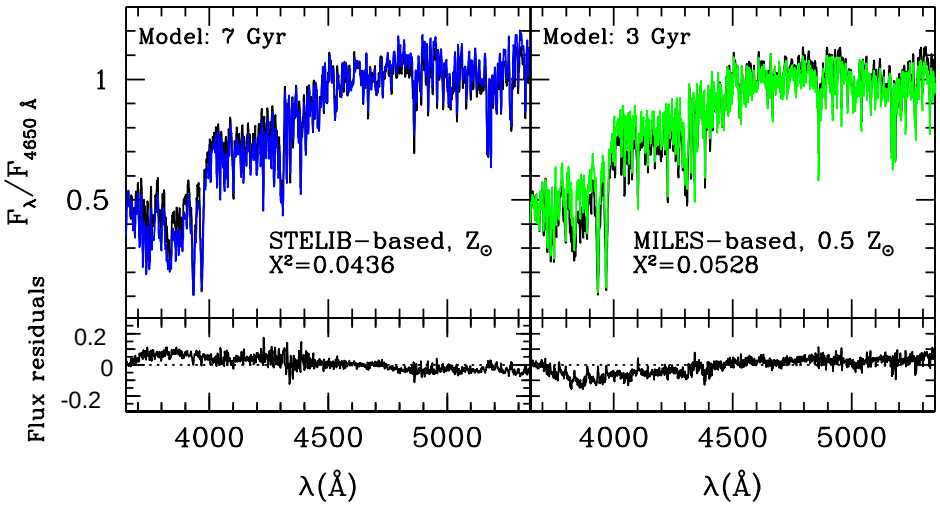

Figure 5.11: Similar to Fig.5.10, but combining the parameters in the two panels for each library, respectively. This example illustrates that the age-metallicity degeneracy is perfectly in place.

Looking closer at the marginalised χ^2 distributions for age and metallicity in Fig.5.12 the bimodal age distribution is clearly visible for both models, another strong evidence that the age-metallicity degeneracy is still in place, even at high resolution. We verify that

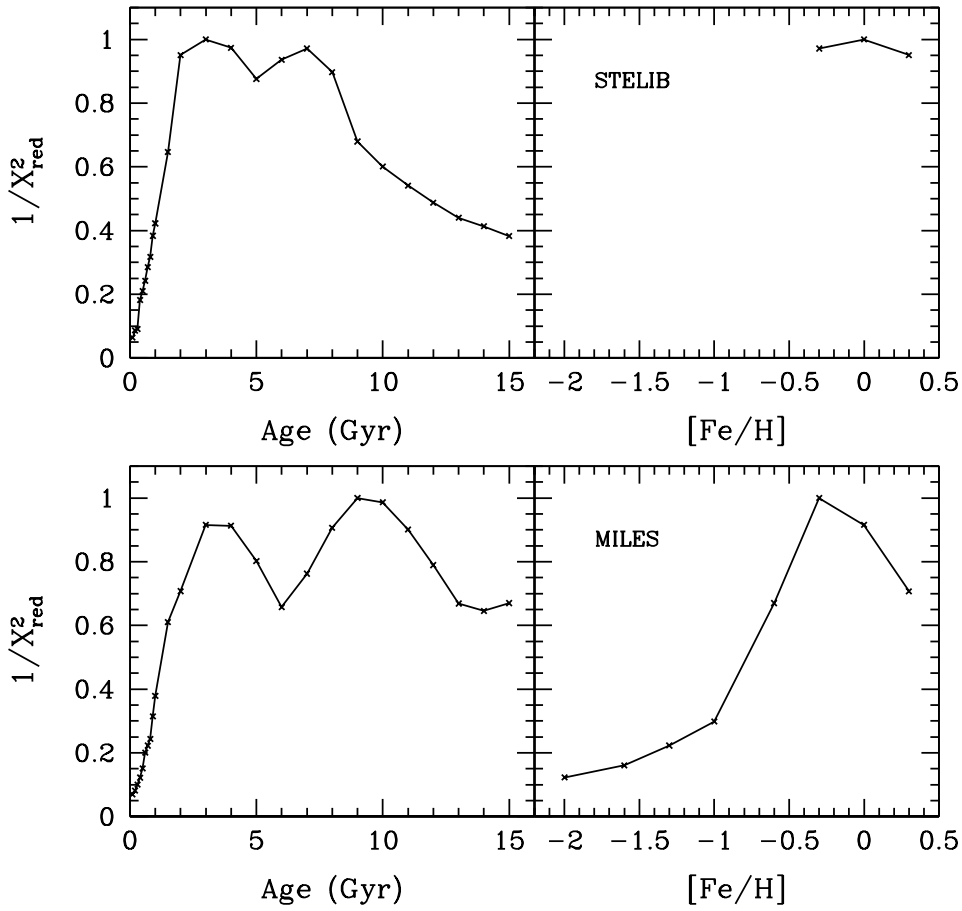

Figure 5.12: Marginalised age and metallicity χ^2 distributions from fitting the M67 spectrum with MaStro-STELIB (*upper* panels) and MaStro-MILES (*lower* panels). The bimodal age distribution is a result of the age-metallicity degeneracy.

taking into account a 68 % confidence interval would include the CMD-derived parameters for both the STELIB- and MILES-based models. In addition, when using only solar metallicity models, the 3-4 Gyr solution comes out directly also for the MaStro-MILES. An obvious explanation to the somewhat different output between the two models would lie in the fact that the MILES-based models exhibit slightly bluer broadband colours in the optical (see e.g. Fig.4.21), which would then require older ages to compensate for this effect. However, we have verified that using MaStro-STELIB models where the individual stellar spectra have been tied to the temperature scale of the MILES library (see Sec.4.7.3), still releases the CMD solution of 3 Gyr and $Z_{\odot}$. This suggests that the near-IR slope is not the driving factor in the SED-fitting procedure.

These findings may be commented in several ways. One could argue that the STELIB library better traces stars at solar metallicity, but on the other hand Vazdekis et al. (2010) claim to obtain the CMD-derived values as their best fit with MILES-based models. Remembering that the M67 spectrum is composed from individual stellar spectra through the population synthesis code of Schiavon et al. (2004), which in many respects is similar to the EPS code of Vazdekis et al. (2010) (i.e. isochrone synthesis on Padova evolutionary tracks), one should not rule out library-dependent effects between models, however unlikely. It might be worth mentioning here the results of Peacock et al. (2011), who showed that the MaStro models perform better than the V10 models in fitting SDSS-band colours of M31 GCs.

In the end, we refrain from drawing conclusions based on just one astronomical object, and focus instead on three things; 1) the fits for both models are excellent and, statistically, indistinguishable from each other; 2) the sole consideration of minimum χ^2 as discriminant may be misleading; 3) the age-metallicity degeneracy is perfectly in place and the higher resolution of the new models is not sufficient to eradicate it.

5.3 The *B*-*V* colour of Milky Way globular clusters

A well-known problem of stellar population models, dating back to Worthey (1994), regards the (*B*-*V*) colour of Milky Way GCs. Whereas the colour-metallicity relations for all other colours can be very well reproduced by the models, this particular one deviates noticeably (see Fig.1.1), the models being too red by about 0.05 mag. Maraston (2005) traced the problem to either a defect in the model atmospheres, a photometric filter mismatch, or a combination of both, but was not able to cure the problem. A constant *ad hoc* offset of 0.05 mag. has therefore been applied to achieve a better match up to this point.

In Fig.5.13 we plot a remake of the corresponding panel from Maraston (2005), this time adding the colour-metallicity relation of a 12 Gyr, Salpeter IMF, MaStro-MILES model (*green*). MILES is the only empirical library that allow for a continuous computation of (*B*-*V*) colour along the entire metallicity scale. Consistent with our discussion in previous chapters, the MILES-based model produce a (*B*-*V*) colour that is bluer by about 0.05 mag., resulting in a much improved agreement with observations. It is here interesting to note that Conroy & Gunn (2010) did *not* find a disagreement between MW GC (*B*-*V*) colours and models based on the theoretical BaSeL stellar spectra, neither for their own models, nor for the M05 or BC03 models (see their Figure 6b). This discrepancy

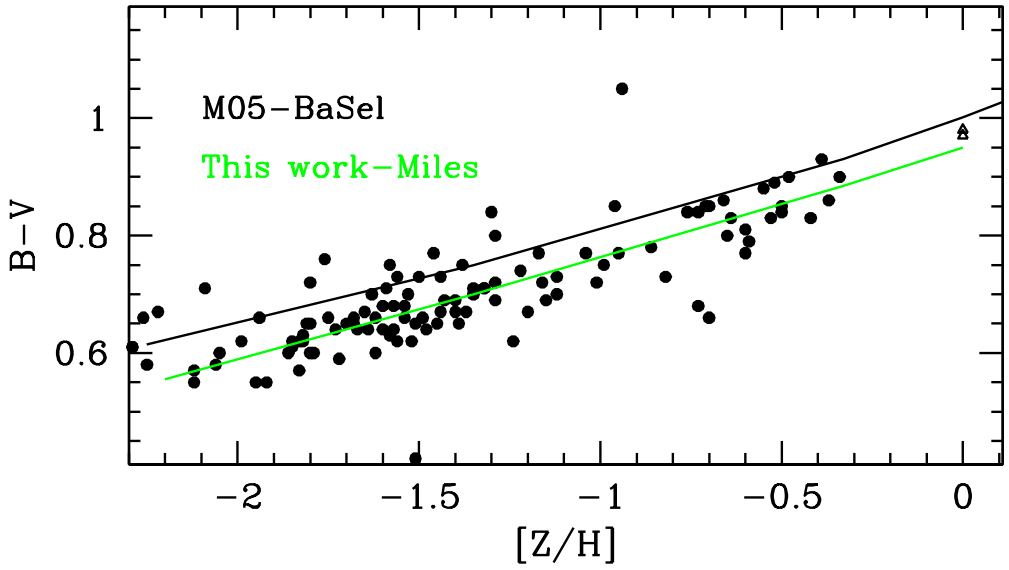

Figure 5.13: Remake of corresponding panel in Fig.21 of Maraston (2005). The (*B*-*V*) colour as a function of metallicity of Milky Way GCs (from the Harris 1996 catalogue) can be much better reproduced by the use of MaStro-MILES models over BaSeL-based ones. The models refer to a 12 Gyr SSP with Salpeter IMF.

could possibly be explained by the choice of reddening law, considering that Maraston (2005) found the BC03 models to behave like the M05 models, i.e. with a 0.05 mag. offset. However, Conroy & Gunn (2010) also found the (*B*-*V*) colours of their MILES- and BaSeL-based models to be practically identical – a result at odds with Fig.4.22 in this work. We are unable to explain the different findings at this point.

5.4 The redshift evolution of the SDSS LRG broadband colours

This section will summarise the findings of Maraston et al. (2009b), wherein it was shown for a specific application to the most massive, old, passively evolving elliptical galaxies how the MaStro models proved to be a significant improvement over previous stellar population models, whether they are based on theoretical stellar spectra or not. The issue in question is a long-standing one, and concerns a simultaneous and opposite mismatch in the redshift evolution of the $(g'-r')$ and $(r'-i')$ optical broadband colours of a sample of Luminous Red Galaxies (LRGs) from SDSS, as first reported in Eisenstein et al. (2001). It was noticed that solar-metallicity SSP models could not reproduce the observed frame $(g'-r')$ colour in the redshift range 0.1 to 0.4, regardless of EPS code. Models of other metallicities and with more complex star-formation histories were also tested in order to

remedy the discrepancy, but to no avail. In the end, an ad hoc shift of 0.08 mag to bluer colours was applied to the model predictions.

The LRG sample was extended in Wake et al. (2006) to include also the $(r' - i')$ colour, in addition to increasing the redshift range to $z \sim 0.7$. LRGs were selected under the assumption that they are old, passively evolving galaxies, thus ensuring that the same galaxy population was sampled at all redshifts (see the reference paper for details on this procedure as well as on the merging of the two data sets). Obviously, the selection criteria (colour cuts as a function of redshift) ultimately depends on the model adopted for identifying the LRGs. In Wake et al. (2006) this was originally done by using BC03 models, but the sample was reselected in Maraston et al. (2009b) using M05 models for self-consistency. Regardless of the choice of model employed for the colour cuts, the discrepancy between models and data remained the same.

Whereas the $(g' - r')$ colour was systematically too red in the models at lower redshift ($z < 0.4$), to further complicate the situation the $(r' - i')$ colour was instead predicted too blue at $z < 0.15$ and too red at higher redshifts. Above $z = 0.4$ the model $(g' - r')$ incidentally matched the data very well. The posed problem is illustrated in the left panels of Fig.5.14, to which it may be added that the $(g' - i')$ colour was actually well matched by the adopted models, suggesting a specific problem around the r'-band. Wake et al. (2006) could not remedy the problem with any type of stellar population models or star-formation history, and indeed, the light from young blue stars, while curing the $(g' - r')$ syndrome at the lowest redshift, would only worsen the discrepancy at high redshift for the same colour and at low redshift for the $(r' - i')$ colour, such that these models would then become too blue. All taken together, this presented a serious challenge and pointed to a potential fundamental flaw in the optical region of the contemporary stellar population models, which had consequences both for the interpretation of existing data, and for the planning of future surveys.

The green line in the left panels of Fig.5.14 represent the median of the LRG data points (taken from Wake et al., 2006). Also plotted in these panels is the colour evolution of a solar metallicity, single-burst (SSP) M05 model (i.e. Kurucz-based) that has an age of 12 Gyr at redshift zero. The simultaneous and opposite colour mismatch at low redshift is clearly visible. Typical observational errors as a function of redshift is indicated by the error bars in the same figure, while the corresponding residuals between the model and the data points are given in the left-hand panels of Fig.5.15.

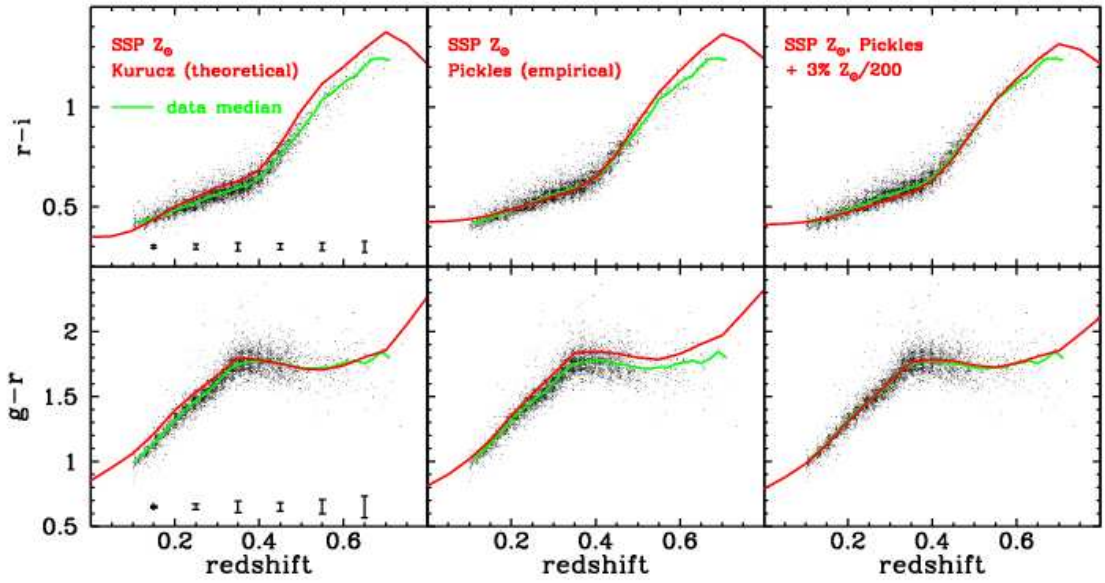

Figure 5.14: The $(g' - r')$ and $(r' - i')$ colours as a function of redshift (data from Wake et al. 2006), with the typical errors indicated by the error bars at corresponding redshift. The median of the data points is given as a green line, while the red line represents as follows: *Left panels* An M05 solar metallicity, passively evolving, single-burst model of age 12 Gyr at redshift zero. *Middle panels* A MaStro-Pickles SSP model with the same characteristics as in the left panels. *Right panels* A composite model, where 3 % by mass of metal-poor stars (M05 SSP, [Z/H]$= -2.25$, also 12 Gyr at redshift zero) has been added to the solar metallicity Pickles-based model in the middle panels.

Seeing how the inclusion of empirical spectra in EPS modelling affects precisely the optical colours at old ages (one of the main results from Chap.4) the next obvious step is to seek a solution using the MaStro models. Of the empirical libraries tested in this work only the Pickles spectra has the intrinsic wavelength coverage to support such an exercise for the entire redshift range, since at increasingly higher look-back time the observed frame g'-band will sample further and further into the rest frame UV. With the UVBLUE-extension to the other libraries, however, a similar comparison can now be made also with the MILES and STELIB libraries (the ELODIE spectra still lack coverage in the red end). The fact that MaStro-Pickles models are only available at solar metallicity is not an issue, since this is the most relevant metallicity for massive galaxies such as the LRGs. Note also that the resolution of the models is of little importance because we are here only interested in the broadband colours.

The result of using the empirical Pickles-based models to match the LRG colours instead of the theoretical-based M05 is displayed in the middle panel of Fig.5.14 (the

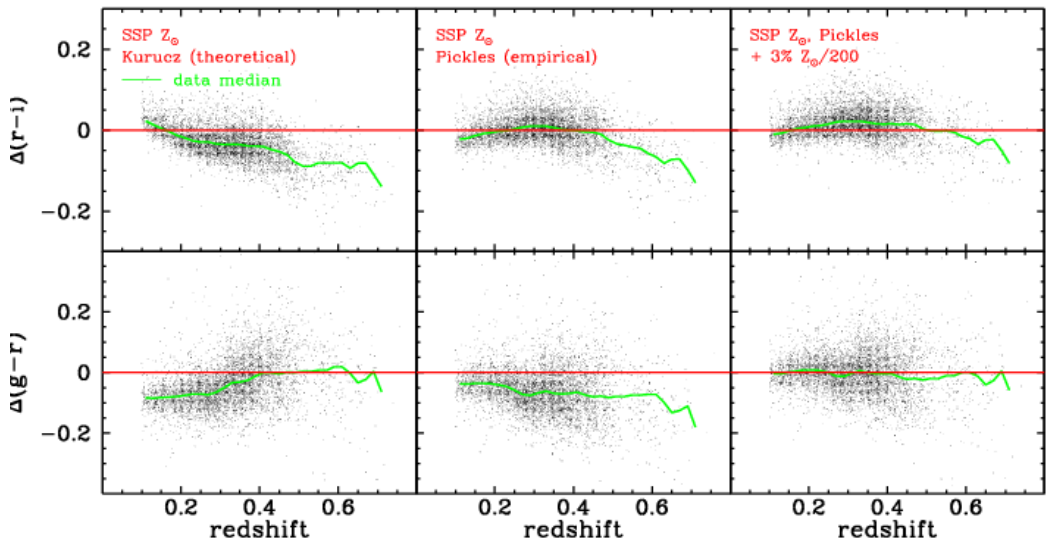

Figure 5.15: Residuals between the model and data points in Fig.5.14. The *green* line is now the median of the residuals.

residuals are shown in the corresponding panel of Fig.5.15). As can be seen the MaStro-Pickles models are able to rectify the situation at the lowest redshifts with respect to the data. Around $z = 0.1$ the predicted $(g' - r')$ colour becomes bluer and the $(r' - i')$ colour appears redder, while the effect is opposite at higher redshift. Thus, the model is still in need of further modifications in order to correctly track the colour evolution over the redshift range, but the important point is that the colours no longer require revisions in the opposite directions. Fig.5.16 shows the effect of the empirical spectra on the photometric passbands. Notice how the r'-band at low redshifts sample exactly the region where the empirical spectra give rise to lower flux levels compared to theoretical Kurucz spectra (when normalised at 5050 Å), which results in bluer $(g' - r')$ and redder $(r' - i')$ colours.

The flatness of the $(g' - r')$ beyond $z = 0.4$ suggests that any component introduced to make the colours bluer must be slowly evolving with look-back time. This does not favour the option of adding residual star-formation to the main component. In the right-hand panels of Fig.5.14 we present our final solution to the problem, which is instead based on introducing a small (3 % by mass), coeval, metal-poor population. Due to intrinsically high stellar temperatures such populations often develop blue HBs even without assuming a large amount of mass-loss during the RGB phase (Maraston, 2005). By contaminating the solar metallicity main component with a small fraction of metal-poor stars the composite SED receives a higher amount of flux predominantly in the UV and optical bands, while leaving the flux redwards of ~ 9000 Å unaltered. The $(g' - r')$ colour consequently becomes bluer at low redshift without perturbing the $(r' - i')$,

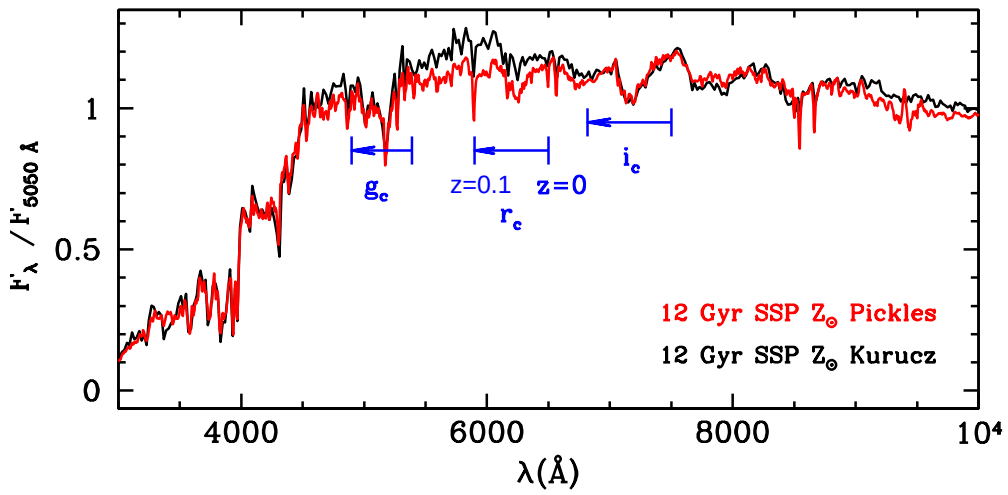

Figure 5.16: Effect on the SDSS photometric passbands at low redshift when using the empirical-based MaStro models over theoretical Kurucz-based models. The central wavelengths of the g', r' and i' bands at redshifts 0 and 0.1 are indicated by the short, vertical lines.

while at higher redshifts both colours are shifted in the blue direction, as required by the data. The residuals in the right-hand panels of Fig.5.15 verify the improvement with this model.

As previously mentioned the MaStro-Pickles models come in no other flavours than solar metallicity – the metal-poor subcomponent is therefore taken from the original M05 models. This may seem contradictory, since the very origin of the problem was inadequacies in the theoretical stellar atmospheres, but we can safely neglect this fact for two reasons: 1) The contamination of metal-poor stars constitutes only 3 % by mass of the composite population, and 2) Due to significantly lower abundances the discrepancies in the theoretical spectra should diminish with decreasing [Z/H]. Fig.4.12 also points in this direction.

5.4.1 Alternatives to the metal-poor component

The presence of a metal-deficient subcomponent in these passively evolving, metal-rich galaxies requires a comment. It may be that the 3 % by mass of very metal-poor stars is just a reflection of the metallicity gradient known to exist in massive galaxies, and LRGs are indeed among the most massive ones (for a more extensive discussion on the metallicity gradient, see Maraston & Thomas 2000 and Sec.6.3 in this work). A similar result

could, for example, be obtained using a larger trace population of a slightly higher metallicity. Another explanation could also be that the subpopulation is the result of accreted metal-poor dwarf satellites during the evolution of the galaxy, although as mergers tend to trigger additional star formation this is less likely. In the end the chosen solution is still the preferred one compared to the other options.

We have also examined the possibility of adding residual star formation since the birth of the galaxy to the present, in order to solve the colour mismatch, but can confirm that the observed frame $(g' - r')$ then becomes *too* blue at high redshifts. The only way to avoid this effect is to assume that the level of star formation in LRGs has been steadily increasing since at least redshift 0.7 – a solution that seems contrived. The inclusion of a BHB in a metal-rich population is also ruled out by the fact that a very large fraction (~ 50 %) would need to develop the BHB, which is also very unlikely. A final consideration is the effect from [α/Fe]-enhancement, which is known to be present in LRGs (Eisenstein et al., 2003). The iron deficiency associated with an enhancement in the α-elements leads to bluer stellar and composite SEDs, but this has a visible impact only in old populations. Thus, the models would predict bluer colours at low redshift, while remaining unchanged at $z > 0.4$.

5.4.2 An LRG-driven revision of the MaStro-MILES model

In the process of fitting the colour evolution of LRGs it was noticed that the MILES-based MaStro models – since brandishing a lower amount of flux longwards of ~ 6300 Å (when normalised at 5050 Å) with respect to the other empirical-based models as well as the theoretical MARCS-based models, resulting in somewhat bluer broadband colours – did not offer as good a match to the observations. Due to the reliable performance in obtaining Milky Way GC parameters, and due to other benefits of the MILES library, such as high resolution and excellent evolutionary coverage, it is important to understand why this is the case. We have traced the behaviour to have three origins:

i) *The temperature calibration.* In Sec.4.7.3 it was concluded that much of the discrepancies between MILES- and STELIB-based MaStro models could be attributed to the temperature scales, and it seems rational to believe that the situation is similar also for MILES- and Pickles-based models. In order to test this hypothesis, we obtained for each Pickles standard spectrum the best-fitting MILES spectrum (in terms of minimising the sum of squared residuals). In general, it appears that the

MILES temperatures are slightly underestimated in comparison to corresponding Pickles values. In particular this holds true for most of the RGB bump and tip stars, whose contribution to the near-IR of old populations is significant. A spectral library with, on average, cooler temperatures will also result in an integrated SED with bluer colours. Thus, by tying the MILES spectra to the Pickles temperature scale we are able to raise the near-IR flux of the MaStro-MILES models noticeably. With the Pickles library lacking spectra of both metal-rich and metal-poor stars this exercise was only performed at solar metallicity, which is anyway the most relevant for LRGs.

ii) *Small gaps in stellar parameter space.* By shifting the coolest MILES giants to slightly higher temperatures there are no longer any cool enough stars to cover the small gap opened up in stellar parameter space, which are required by the adopted stellar evolution prescription for the tip of the RGB as well as the E-AGB. By adding sufficiently cool spectra, for example from the Pickles library, the near-IR flux receives yet a small boost. Note that the lower resolution of the Pickles spectra will not impact the overall resolution of these MILES-based models, since only a few spectra are added and they contribute only slightly in the reddest part of the wavelength range, where absorption features are generally broader.

iii) *A short wavelength range systematic offset* Besides the overall bluer colours of the MaStro-MILES models, another small discrepancy emerged between 6500 and 7000 Å when comparing the MILES and Pickles stellar spectra. After smoothing the former to the appropriate resolution of R~ 500, even the best-matching spectra still display a separation in this wavelength range, in the sense that the MILES spectra exhibit a flux deficiency, or alternatively the Pickles spectra a flux excess. In Fig.5.17 is plotted four such examples, accompanied by their respective flux ratios as a function of wavelength. Such a discrepancy can certainly not be ascribed to any difference in stellar parameters such as temperature, surface gravity etc. A more likely explanation is instead that this is an artefact originating from the MILES instrumental setup (reminding the reader that the Pickles spectra are averages composed from several different observations, and as such, should be less prone to systematic deviations, while the MILES spectra were all obtained using the same observational tools). Another option is that the adopted procedure for telluric absorption removal is responsible, but this seems however more unlikely.

Note that this offset is discernable only when an otherwise identical spectrum at moderate resolution, such as provided by the Pickles library, exists. As such a close match is not available everywhere in the inter-library comparison, the artefact cannot be verified for all MILES spectra. However, seeing that it *is* present in the best fits, and noticing that after correcting for points i) and ii) above, there is still a disagreement between the integrated MaStro-MILES and MaStro-Pickles models exactly between 6500 and 7000 Å, we strongly believe the offset is a systematic associated with *all* MILES spectra. A makeshift procedure is therefore devised to counterbalance the effect. Choosing 12 of the best-fitting MILES spectra (6 dwarfs and 6 giants), second-order polynomials are then fitted to the flux ratios in the aforementioned spectral range of all twelve components. The straight average of these fitting curves (see Fig.5.18) is afterwards applied to all solar-metallicity MILES stars.

Based on the above three corrections, we provide two versions of the MaStro-MILES solar-metallicity models – original and LRG-revised, where the SED shapes of the latter are in near-perfect agreement with those of MaStro-Pickles, and thus constitutes a better fit to the colour evolution of SDSS LRGs compared to the original version (and at much higher resolution than the MaStro-Pickles models). A comparison of the original and revised versions, for the illustrative case of a 12 Gyr SSP, can be found in Fig.5.19. The flux residuals are generally very small over the wavelength range; only the near-IR portion of the spectrum is appreciably affected by the revision, which was also the intention. We recall that a similar exercise, being based on Pickles spectra, cannot be performed at non-solar metallicities.

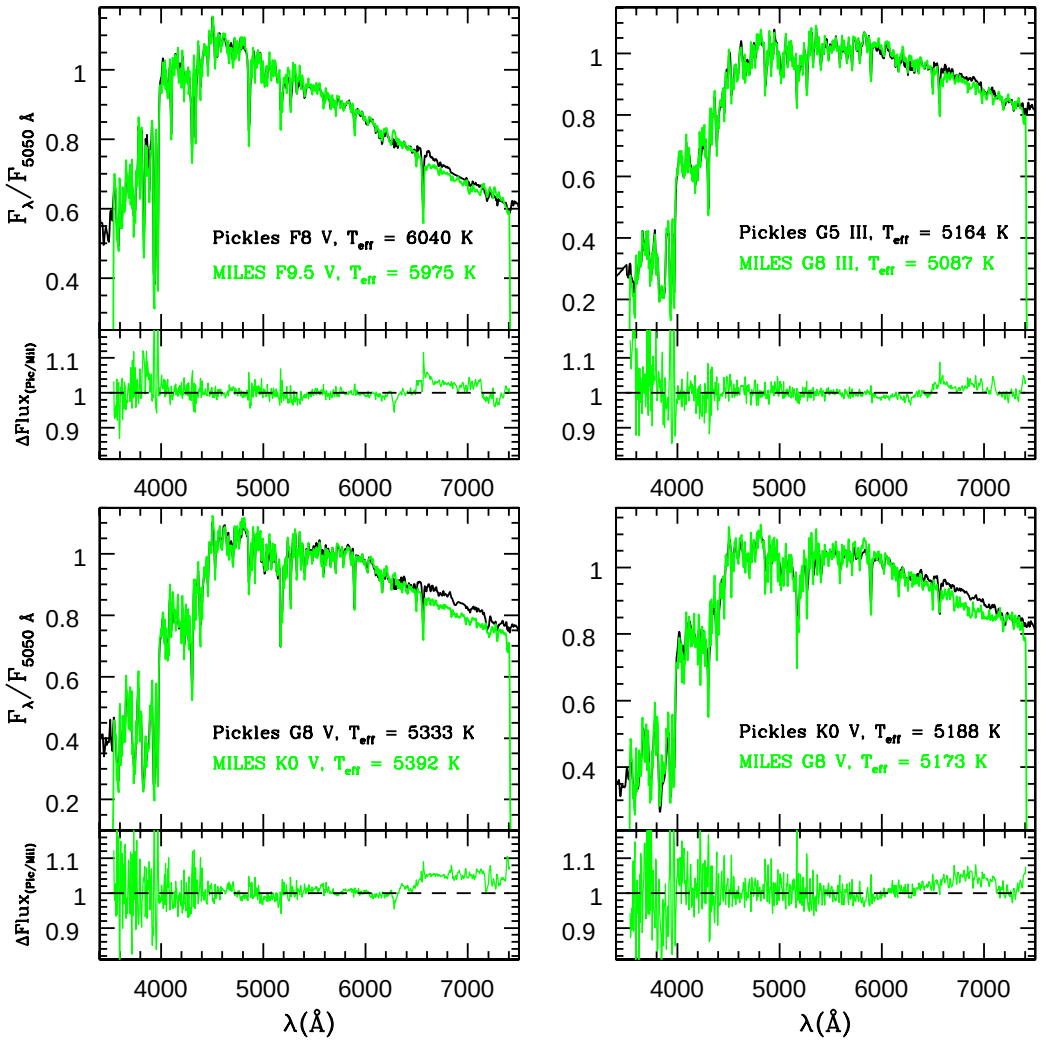

Figure 5.17: Best-fitting MILES spectra to four standard Pickles spectra, accompanied by their respective flux ratios as a function of wavelength, defined as $\Delta F_\lambda = F_{\lambda,Pickles}/F_{\lambda,MILES}$ (smaller panels). Flux ratios are scattered around 1, except between 6500 and 7000 Å, where a systematic flux deficiency in the MILES spectra can be observed. For this exercise the MILES spectra have been smoothed and rebinned to the Pickles resolution and sampling.

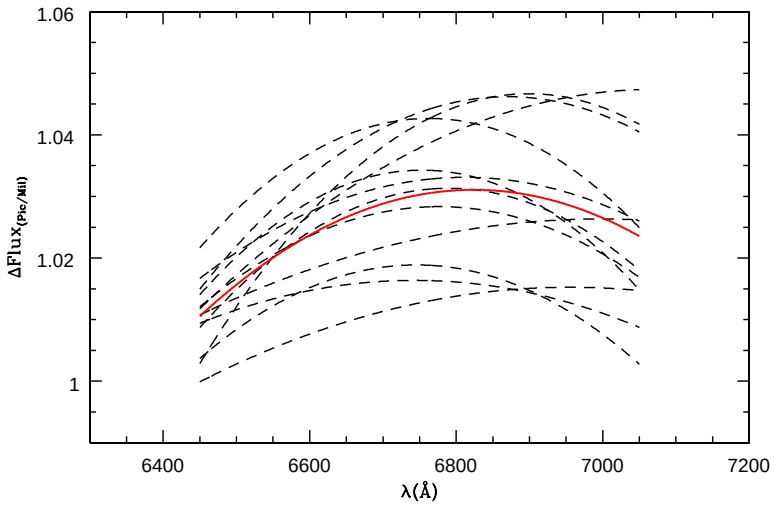

Figure 5.18: Second-order polynomial fits to the flux ratios of 12 best-fitting MILES spectra to Pickles standard spectra (six dwarfs and six giants), in the wavelength range 6450-7050 Å (*dashed black lines*). The straight average of these curves (*red solid line*) is applied to all MILES spectra in the LRG-revised version of the MaStro-MILES solar metallicity models.

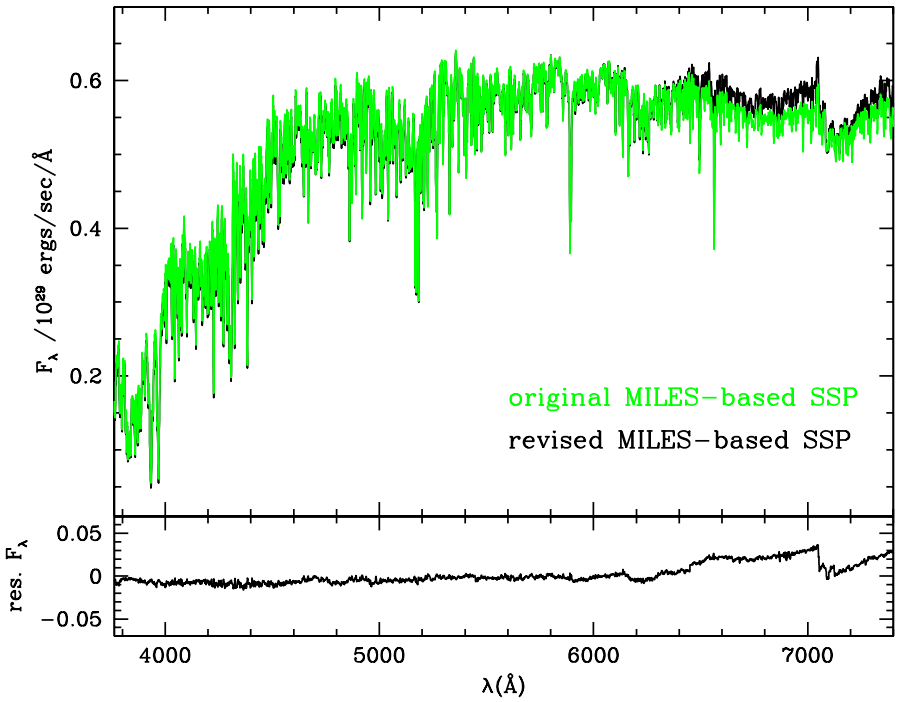

Figure 5.19: Comparison between the original and LRG-revised version of the 12 Gyr, $Z_{\odot}$ MaStro-MILES SSP. The flux residuals (shown in the lower panel as $F_{\lambda,revised} - F_{\lambda,original}$) induced by the revision are very mild over most of the spectrum and affect only the near-IR part.

Chapter 6

A note on the age-metallicity degeneracy - Revisiting the Ca K index

On disentangling age and metallicity effects at high resolution, and how a new version of an old index may provide valuable insights.

6.1 Background

The age-metallicity degeneracy – so named because of the notion that, in the optical wavelength region, old, metal-poor stellar populations, and young, metal-rich ones, are practically indistinguishable from each other – has tormented astrophysicists for years. Around 1980, the problem of the non-uniqueness of population synthesis models based on low-resolution spectrophotometry was noted, and in particular the difficulty of disentangling metallicity and temperature (in principal, age) effects. It has later been shown that this degeneracy can be broken once data is acquired also outside of the visual range, including UV and/or near-IR broadband colours in the fitting (e.g. Maraston et al., 2006; Kaviraj et al., 2007). However, since most galaxy data is limited to optical wavelengths, it would be desirable to have an equally good method also in this part of the electromagnetic spectrum. Following the discussion in Worthey (1994), the most promising approach for obtaining such a method, is probably using a combination of various age- and metallicity-sensitive absorption line indices.

Out of the original 21 Lick absorption indices, Worthey (1994) found that the four Fe indices Fe4668, Fe5015, Fe5709, 5787 are the ones most sensitive to metallicity, whereas Hβ is the most age-sensitive. Thus, by plotting Hβ versus any of the iron indices for GC and galaxy data, it is possible to get a handle on the age-metallicity degeneracy. This

method was further refined by the introduction of the [MgFe] and [MgFe]' indices (Gonzalez et al. 1993 and Thomas et al. 2003b, respectively), which, being virtually insensitive to abundance ratio effects, effectively trace the total metallicity. The Hβ index, on the other hand, probably deserves an entire chapter on its own, but suffice it to say that it has been notoriously difficult to reproduce the Hβ values of intermediate-resolution integrated Galactic GC spectra (Puzia et al., 2002; Schiavon et al., 2005) with current stellar population models – the observed values being systematically lower than those predicted by the models (see e.g. the discussion in Poole et al. 2010), although progress has recently been made in this matter (Thomas et al., 2011)). Whether the discrepancy is due to observational errors (for example, higher order Balmer lines, such as Hγ and Hδ, are perfectly reproduced by the models), or some physical phenomenon unaccounted for in the models (such as nebular emission fill-in), remains to be decided.

However, it is important to note that the method outlined above is only directly applicable for stellar populations that are very well approximated by an SSP, such as GCs (Maraston et al. 2009b showed that the addition of a subcomponent constituting only 3 % by mass may compromise the SSP behaviour, see Chap.5). As soon as composite stellar populations are considered, the complexity of the problem increases drastically. One such example is illustrated in Maraston & Thomas (2000), where the large scatter in measured Hβ values of elliptical galaxies is addressed. Traditionally, this has been interpreted by assuming a similarly large scatter in their light-averaged ages, thereby implying the occurrence of recent star formation and the presence of young, metal-rich subpopulations in many of these galaxies. The different solution proposed by Maraston & Thomas (2000) was to model the observed Hβ line strengths by including instead a subpopulation of *old, metal-poor* stars (up to 10 % in mass). Metal-poor SSPs naturally display strong Hβ lines since their horizontal branch morphologies are almost exclusively blue. With this approach there is no longer any need to invoke younger ages and star-formation for elliptical galaxies, which fits better with the anti-hierarchical picture of galaxy formation (e.g. Thomas et al., 2005)), since hierarchical scenarios always predict residual star-formation also in these types of galaxies. In addition, a hierarchical assembly process does not produce in a simple way the enhanced abundance ratios of α-elements that are seen in massive galaxies (Nagashima et al., 2005; Pipino et al., 2009). It should be noted that the introduction of this solution does not break the age-metallicity degeneracy – both alternatives can fit the data equally well – so that other indicators must be used in order to discriminate between the two options.

6.2 What can a higher spectral resolution reveal?

In principal, there should be an adequate amount of information encoded in the integrated light of a stellar population to break any degeneracies, as long as the resolution and signal-to-noise (S/N) ratio of the spectrum are high enough, although this has yet to be demonstrated. The widely used Lick/IDS system of absorption line indices, for example, was defined for the rather coarse resolution of 8-11 Å (FWHM), and the individual indices could therefore be affected by elements other than those they were designed to trace (such as Fe4668, which is a blend of mainly Fe, Mg, and C_2, see Worthey 1994). Even though this technique is still a very powerful galaxy diagnostic tool, much information may be lost in the transition from modern, high-resolution observations to the standards of the Lick/IDS system.

A few investigations have been aimed at finding new absorption indices, or re-defining old ones, at a higher resolution. In general, wider indices are more robust against measurement error (thus requiring lower S/N), and are applicable also to massive elliptical galaxies, which are intrinsically broadened by velocity dispersion effects, but may, as mentioned above, smooth out valuable information. The Hγ_{HR} index defined in Jones & Worthey (1995), for which also fitting functions were computed, is narrower by an order of magnitude compared to a regular Lick index ($\sim$3.5 Å and $\sim$40 Å respectively), and the red and blue pseudo-continuum passbands are reduced to single points on each side of the central line. This index proved very sensitive to age, but the index definition itself is highly sensitive to the resolution and velocity broadening, and requires a very high S/N ($>$100). In a first practical use of this index, Gibson et al. (1999) applied it to a high-resolution spectra of 47 Tuc, but due to the weak Balmer lines of this particular cluster the predicted age of more than 20 Gyr was well off the CMD-derived age of around 14 Gyr. Vazdekis & Arimoto (1999) tried to improve upon this situation and defined from measuring on the SEDs of the Vazdekis (1999) EPS models a set of indices Hγ_σ, which have different widths of the central line and pseudo-continua depending on the characteristics of the observed spectra, in order to compensate for the effects of resolution and velocity broadening. It can be noted that the trend of heightened age-sensitivity with smaller band-widths was found also by Worthey & Ottaviani (1997), who studied the Hγ and Hδ indices for two different line widths (working at the usual Lick/IDS resolution).

6.2.1 Intentions with this exercise

In this Chapter we will concentrate on the two-component problem, i.e. the degeneracy that arise when an old, metal-rich population is contaminated by trace amounts of either a young and metal-rich, or an old and metal-poor subpopulation. More specifically, we will investigate if the new high-resolution MaStro models presented in this work offer any additional insights on how to distinguish between the solutions for this particular case of the age-metallicity degeneracy. We will work exclusively with the MaStro models based on the MILES library, since this library provides the best model coverage in terms of SSP ages and metallicities. It is important to remember that this exercise is not intended to be an in-depth, analytic analysis of the age-metallicity degeneracy. Rather, it is meant to provide (or find a lack of) a few line indices that could be further developed in future studies to help alleviate the problem.

6.3 SED comparisons

For the major stellar population component we will use a 12 Gyr, $Z_{\odot}$, MILES-based SSP model with Salpeter IMF. This will be polluted with a subcomponent (3-10 % in mass) that is either a 1 Gyr, 2 $Z_{\odot}$ model, or a 12 Gyr, $1/100$ $Z_{\odot}$ model. From the aspect of galaxy evolution, these combinations represent in a simplified form an old, massive elliptical of solar metallicity, that either has experienced a burst of (chemically enriched) star-formation around 1 Gyr ago, or contains a remnant subgroup of low-metallicity stars from an earlier epoch of star-formation. For the sake of simplicity, we will for the remainder of the chapter adopt the following abbreviations:

Model Y: 12 Gyr, $Z_{\odot}$ (90-97 %) $+$ 1 Gyr, 2 $Z_{\odot}$ (3-10 %) *Old + Young*

Model O: 12 Gyr, $Z_{\odot}$ (90-97 %) $+$ 12 Gyr, $1/100$ $Z_{\odot}$ (3-10 %) *Old + Old*

Model C: 12 Gyr, $Z_{\odot}$ (100 %) *Clean, unpolluted*

The alternative with a trace population of very metal-poor stars (Model O) may at first seem physically contrived, especially when comprising 10 % of the total mass. However, as already explained, the intention with this exercise is merely to study the case of the age-metallicity degeneracy where a separation between an old, metal-poor or young,

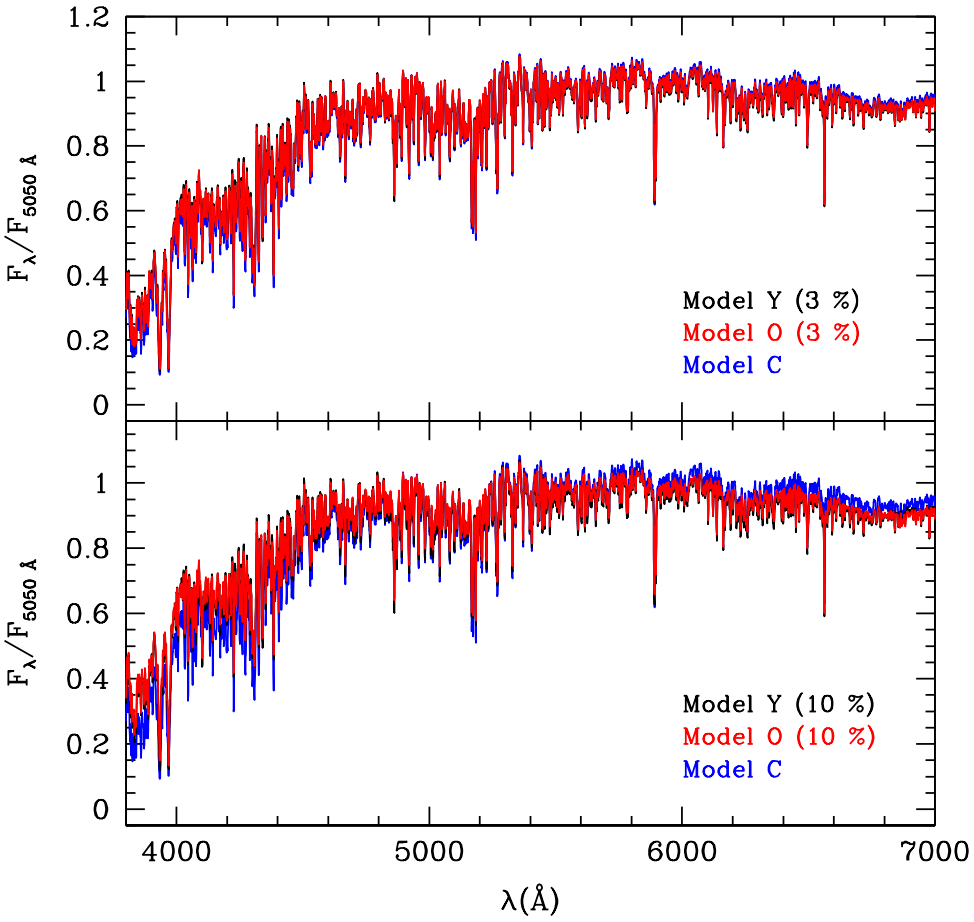

Figure 6.1: Comparison of the SEDs of Models Y, O, and C, normalised around 5050 Å, given a minor component fraction of 3 % (*upper panel*) and 10 % (*lower panel*).

metal-rich contaminant is of interest. The highest fractions act therefore more as means of excluding certain solutions. Nonetheless, this toy model could, for example, represent an average value of the metallicity gradient observed in many early-type galaxies (e.g. Davidge, 1992; Mehlert et al., 2003; Ogando et al., 2005). In addition, Lotz et al. (2000) noticed that several mid-UV indices could only be reproduced by the addition of an old, metal-poor component (constituting less than 10 % in mass) to an old, metal-rich population.

It is important to realise here that the results obtained using two discrete populations may be mimicked using a distribution of metallicities or a larger (by mass) population of a somewhat higher metallicity than adopted in Model O. Mehlert et al. (2003) found an average metallicity gradient of Δ[Z/H]$= -0.16$ at around $1\,r_e$ in their sample of 35 early-type galaxies, although with a fairly large spread. The steepest gradient was -0.34 dex.,

and there was also a general trend of finding steeper gradients in the most massive (highest velocity dispersion) galaxies. Interestingly, the authors did not find any correlation between [α/Fe] and galactocentric distance, suggesting that star formation timescales do not vary significantly inside a galaxy as a function of radius. Instead it is the fraction of gas lost in the galactic wind that depends on radius, where the higher potential in the central parts (compared to the outskirts) of these galaxies is able to retain and process a larger fraction of gas to higher metallicities. A similar result was found in Ogando et al. (2005), where the low-mass galaxies generally have very flat metallicity gradients, whereas the most massive galaxies show a large spread in Δ[Z/H]. The metallicity of one galaxy in particular decreased as much as 1.0 dex. out to less than one effective radius. Such a large scatter in gradients implies a hybrid formation scenario (Kormendy, 1989; Kobayashi, 2004), where both monolithic collapse and hierarchical clustering contribute as formation processes, with the former producing steep metallicity gradients and the latter tending to destroy them.

Fig.6.1 shows Model Y and O compared to the unperturbed 12 Gyr, $Z_{\odot}$ base model (Model C), for the case when the subpopulation constitutes 3 % in mass, as well as for the 10 % scenario. A contribution of only 3 % can be difficult to discern by eye (but has an important effect on broadband colours, as shown in Chap.5), whereas a 10 %-fraction produces a noticeably tilted SED shape. As it turns out, the highest degree of degeneracy in terms of broadband colour – because with the wavelength range spanned by the MILES library being rather narrow, (*B*-*V*) is really the only one that can be computed – is obtained when the fractions of the subpopulations are of the same size, differing by at most one or two percent. This is also illustrated in Fig.6.2, where the difference in (*B*-*V*) colour is given as a function of the fraction in mass comprised by the subpopulation. The black line gives the colour discrepancy between Model Y and O, given the same amount of contamination, whereas the red line displays how the colour of Model O (old option) evolves compared to the unpolluted Model C. Naturally, the red line shows a steady increase with subpopulation fraction, as the bluer polluter becomes increasingly dominant with respect to the base model, but interestingly, Δ(*B*-*V*) stays very close to zero when comparing Models Y and O, even when the contribution from the minor component reaches 10 % (see also Fig.4.21 for the (*B*-*V*) colour evolution of the MILES SSP models).

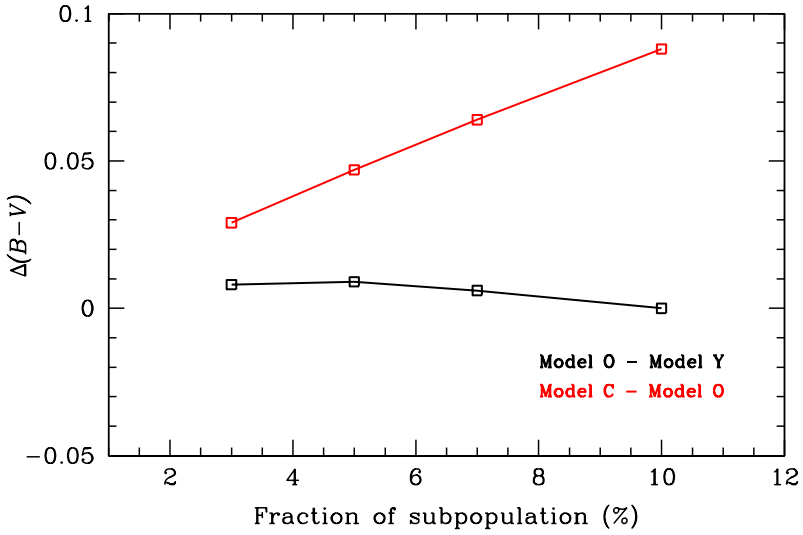

Figure 6.2: Difference in (*B*-*V*) colour as a function of the fraction of the minor component. The black line gives the difference between Models Y and O (given the same subpopulation fraction), and the red line between Models O and C. Models Y and O are clearly degenerate in (*B*-*V*), even when the minor component constitutes up to 10 %.

6.4 Absorption line ratios

Even though Fig.6.1 reveals the degeneracy between Models Y and O on a larger scale, it is not possible to appreciate from this figure alone the behaviour of individual absorption features. In Fig.6.3 we have therefore plotted the normalised flux ratios between the two models (both having a minor component contribution of 10 %), in the sense that values smaller than 1 means a weaker line strength in Model O (old subcomponent). Superimposed as shaded areas are also the central wavelength passbands for the 19 of the original 21 Lick/IDS indices, as defined by Trager et al. (1998) (CN_2 and Mg_2 have been omitted, as they share wavelength range with CN_1 and Mg*b*, respectively). In this way it is possible to check if there are absorption lines that look promising as diagnostic indices, in addition to the already widely used Lick indices.

Certainly, one line in particular stands out from the rest. Ca K, or Ca II λ3933.7, lies just outside the wavelength region covered by the Lick/IDS spectra, and is known to be prominent in cool stars, e.g. the Sun. The difference in Ca K strength appears from a quick glance to be around 20 %, whereas a line such as Hβ at 4861 Å differs by only $\sim$5 %. Further tests also show that, while the majority of absorption line strengths can be made degenerate by changing the relative proportions of subcomponent fraction between the two models (for example, the Hβ ratio spike can be washed out by increasing the contribution from the young, metal-rich population relative to the old, metal-poor one),

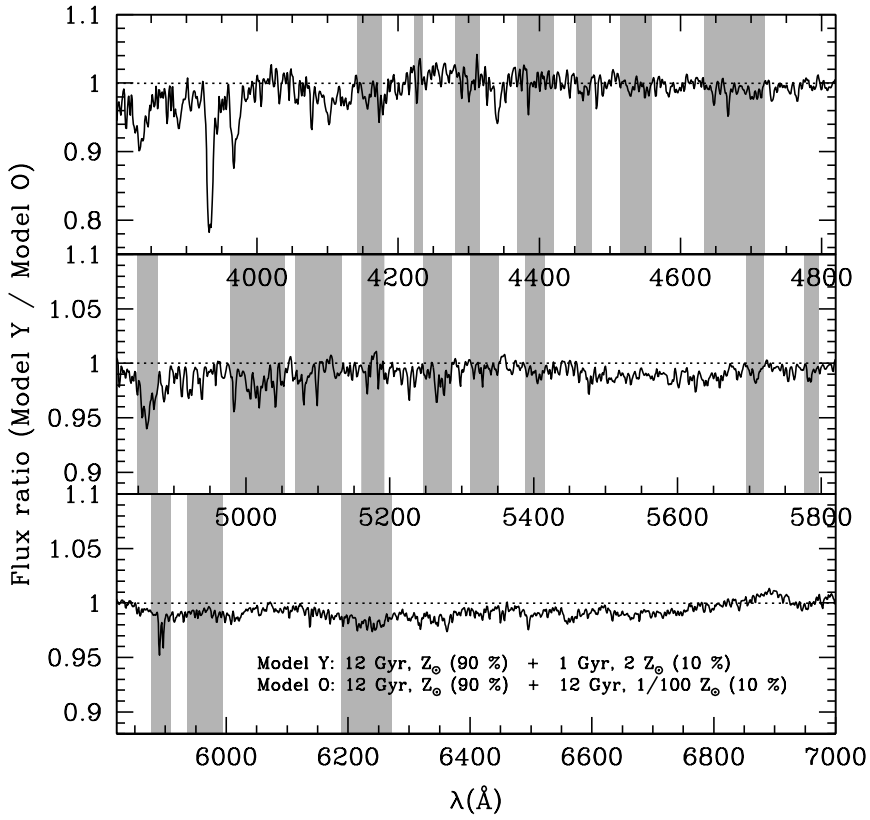

Figure 6.3: Flux ratios between Models Y and O, normalised around 5050 Å for a 10 % minor component. Shaded areas represent the common Lick/IDS index passbands as defined by Trager et al. (1998) (CN_2 and Mg_2 have been omitted, since they overlap with CN_1 and Mg*b*, respectively). Notice the large difference in Ca K strength at 3933.7 Å.

the difference in Ca K will, for all possible combinations considered herein, always be of the order 10-20 % (Model O being weaker). Notice also how the width of several of the Lick/IDS indices (not to mention the pseudo-continua, which are not plotted here) allow for contamination from other lines, something that could be better constrained at higher resolution.

6.5 The potential of a Ca K index

From the previous section it is clear that Ca K has the potential of becoming a valuable aid in any absorption line analysis, and in disentangling age and metallicity effects in particular. In stellar population modelling it has so far been rather neglected in favour of the more commonly used Lick/IDS indices. A few examples of previous work on the

Ca K line in this respect can be found in the literature. Both Rose (1985) and Beers et al. (1990) studied its behaviour in high-resolution spectra, in order to constrain the amount of hot stars in elliptical galaxies, and to use it as a metallicity indicator for Milky Way stars, respectively. Rose (1985) determined that the ratio of Ca K and the combined lines (Ca H + Hϵ) was constant for F, G, and K stars, regardless of metallicity, but experiences a considerable decrease for A and B stars, when the Ca II lines weaken, and Hϵ strengthens. It was also found that this decrease in the index ratio as the effective temperature of the stars increases, seems to be larger for more metal-deficient stars. Beers et al. (1990) used instead synthetic spectra of stars with [Fe/H]< -1.0, and the general trend obtained for their three definitions of the Ca K index was that higher metallicity and lower temperature both give stronger index values, while surface gravity remains relatively unimportant.

6.5.1 Definition of a simplified Ca K index

High-resolution absorption line indices may seem like an untapped potential of spectral analysis, but it is important to remember two things: 1) The narrower the index passband is defined – and this affects also the way one establishes the continuum – the more sensitive it becomes to changes, not only in resolution, but also in stellar parameters (T_{eff}, log(g), [Z/H]). 2) No matter how high the instrumental resolution is, a resolution limit is usually determined by the velocity broadening of a galaxy; the more massive a galaxy is, the lower its effective resolution. The first point can be circumvented by carefully testing the index for variations in velocity dispersion and stellar parameters, something that was partly attempted in Vazdekis & Arimoto (1999). The second point is intrinsic to the galaxies, and can only be solved indirectly, as e.g. in Thomas et al. (2010), where the best-fitting, velocity broadened EPS template for a galaxy spectrum is compared to the same template in its original, higher resolution. The differences in computed absorption line strengths between the broadened and high-resolution template can then be applied to ”unbroaden” the galaxy spectrum.

In this section we will investigate the evolution of a simple Ca K index for stellar populations with age and metallicity. In order to minimise the effect of neighbouring lines entering into the measurement of the desired line, we adopt a narrow wavelength range of 6.2 Å in our definition, which is the average distance between two adjacent peaks in our MILES-based SSP spectra. Similarly, we want to avoid using sidebands to compute a pseudo-continuum (as in e.g. Vazdekis & Arimoto, 1999)), since these are also prone to contamination, and creating a continuum by linking the two ”shoulders” of

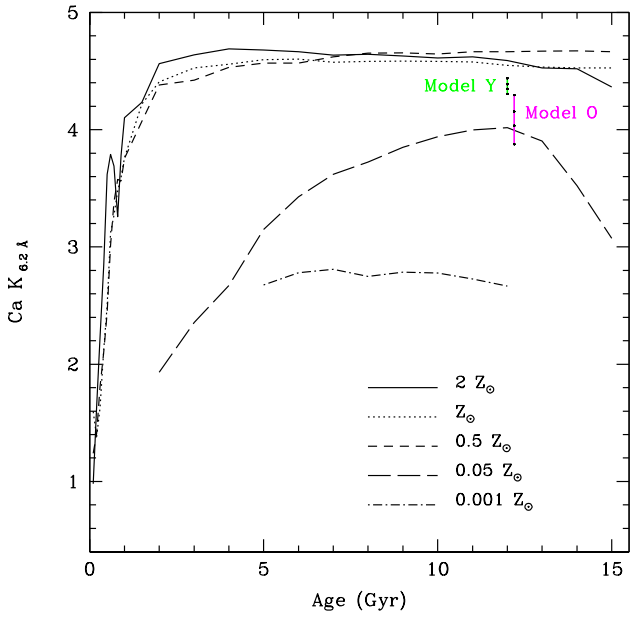

Figure 6.4: Evolution of the Ca K index with age and metallicity, as measured directly on the SEDs of the MILES-based MaStro SSP models with Salpeter IMF in their original resolution. Models Y (green) and O (magenta) with fractions 3, 5, 7, and 10 % of the subpopulation have been included at arbitrary positions on the abscissa (larger fraction gives weaker Ca K).

an absorption line (adopted by Jones & Worthey, 1995)) should be extremely sensitive to changes in both resolution and stellar parameters. Thus, we employ instead the *boosted median continuum* method, introduced by Rogers et al. (2010), which should by more robust against such variations. With this technique, the equivalent width (EW) of a line is computed in a normal fashion,

$$EW = \int_{\lambda_1}^{\lambda_2} \left[1 - \frac{\Phi(\lambda)}{\Phi_C(\lambda)}\right] d\lambda \tag{6.1}$$

where λ_1 and λ_2 define the wavelength limits of the index, $\Phi(\lambda)$ is the flux and $\Phi_C(\lambda)$ is the continuum. The unique feature is the calculation of the latter; the continuum at each pixel is defined as the 90th percentile of all flux values within a 100 Å window around said pixel. Expressed slightly differently, the continuum flux at each pixel will be larger than 90 % of the adjacent flux values within 50 Å to each side of the pixel. For the specific choice of the 90th percentile and a 100 Å window we refer to Rogers et al. (2010).

The evolution of the Ca K index with age and metallicity, as measured directly on the SEDs of the MILES-based MaStro models with Salpeter IMF in their original resolution, is shown in Fig.6.4. In general, the results from previous studies are confirmed, i.e. higher metallicities and cooler average temperatures produce stronger Ca K. At metallicities above half solar the value of Ca K is seen to be roughly constant for ages older than ~ 2 Gyr. This is in accordance with the findings of Rose (1985), in that all stars of spectral type F5 (around 6500 K) or later have approximately constant Ca K regardless of metallicity, because at the transition age of 2 Gyr and [Fe/H] > -0.3 the MS is by far the dominant stellar phase and the MS turnoff temperatures happens to be just above 6500 K. The slightly higher temperatures of the 0.5 $Z_{\odot}$ models compared to the $Z_{\odot}$ and 2 $Z_{\odot}$ cases, also results in a slightly steeper Ca K evolution. More metal-poor models are clearly separated from more metal-rich ones at old ages (which are the only ages that can be modelled at low metallicity with empirical spectra), having much weaker Ca K lines due to their higher temperatures and lower Ca content. The downturn at 12 Gyr for the 0.05 $Z_{\odot}$ models is a consequence of mass loss along the RGB, which has a considerable effect at older ages, thus leading to the production of hotter HB stars. At [Fe/H]$= -2$, Ca K is instead remarkably constant, as the cooler turnoff temperatures with increasing age is counterbalanced by a higher amount of mass loss during the RGB phase and thus a hotter HB. The contribution to the total luminosity at the wavelength of Ca K from each stellar evolutionary phase is given in Fig.6.5

Included in Fig.6.4 at arbitrary positions on the abscissa are also the Ca K values of Models Y and O, for different fractions of the subcomponent; a larger contribution from the subpopulation equates to a weaker Ca K index. As can be seen, Model Y (the young option, green line) has always a stronger Ca K line than Model O (old polluter, magenta line), except when the fraction of the young component in Model Y reaches 10 %, in which case it becomes comparable to Model O with a 3 % metal-poor fraction. In this case there are anyway other discriminants to separate the two models, such as broadband colours.

6.5.2 Robustness against velocity dispersion variations

It is important to remember that Fig.6.4 shows the evolution of our Ca K index at MILES resolution. In reality, measuring absorption line indices on, say, massive ellipticals, is a different matter entirely, since their large velocity dispersions will cause significant broadening of the lines in question. This necessitates a test of how stable our index is against variations in velocity dispersion (effective resolution). Fig.6.6 is basically a

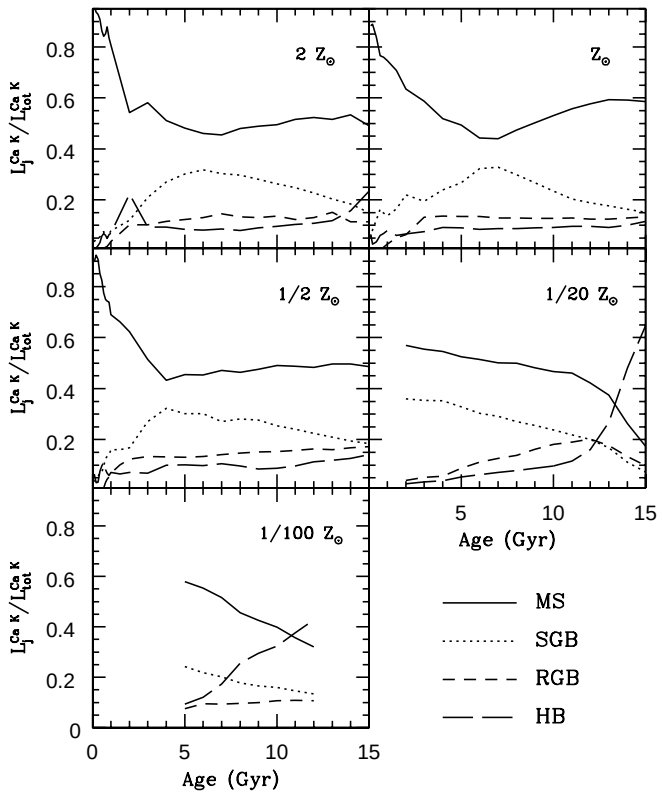

Figure 6.5: Contribution to the total luminosity at the wavelength of Ca K per stellar evolutionary phase. The AGB has been left out as its contribution never exceeds 2 %.

replica of Fig.6.4, with the exception that the resolution of all MaStro models was downgraded to $\sigma = 250$ km/s prior to the index measurements. The scale has been kept the same to enable a straightforward comparison between the two figures. As expected for such a narrow index definition, values will decrease as the features are smoothed out in the transition to coarser resolution. What is striking, however, is how well the relative trends are preserved. Confirming that this is true also for intermediate resolutions (in steps of 50 km/s), and for even more massive galaxies (300 km/s), this suggests that our index is adequately robust over the full spectrum of velocity dispersions, which can be ascribed to the combination of using a high-resolution (narrow wavelength range) index, and the stability of the boosted median continuum method in defining a pseudo-continuum.

Again, the measured Ca K values for Models Y and O, with various fractions of the subcomponent, are placed arbitrarily around 12 Gyr in Fig.6.6. With the decreasing resolution comes also an increasing risk of degeneracies, at least when the fraction of

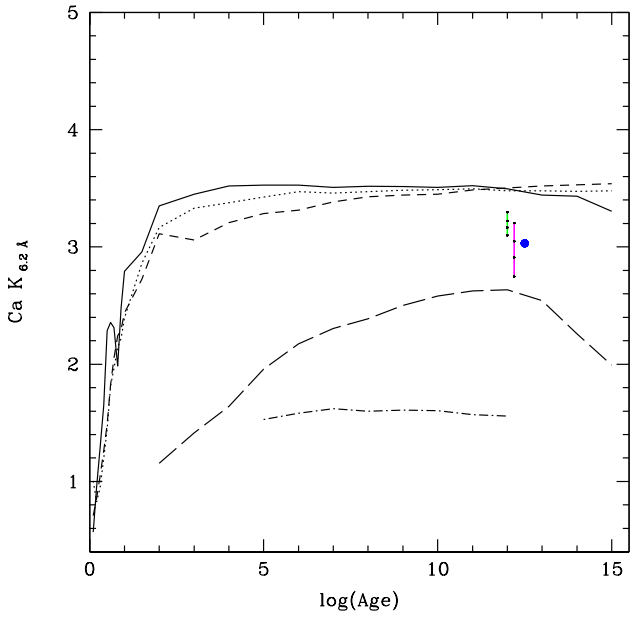

Figure 6.6: Same as Fig.6.4, but measured at a resolution of 250 km/s. The same scale has been used for clarity. The blue dot is the value measured on a stacked spectrum of BOSS LRGs (Daniel Thomas, private communication).

metal-poor stars in Model O (magenta line) is low enough (~ 3 %). In combination with a low S/N ratio in the observed spectrum, a clear picture cannot be obtained from the Ca K line alone.

6.5.3 Application to the SDSS LRGs

The application of the Ca K line to the SDSS LRGs (see Chap.5) seems inevitable, and could settle the dispute whether these old, massive galaxies contain traces of star formation or an old, metal-poor subcomponent. With the index definition proposed here, the solution in Maraston et al. (2009b) – an old major component of solar total metallicity, plus an old, metal-poor minor component amounting to 3 % in mass – would produce a more or less constant value of Ca K over the entire explored redshift range. This is also clearly seen in Fig.6.4, where both the solar metallicity model and the most metal-poor model are completely insensitive to age above ~ 1 Gyr in the former case, and 5 Gyr in the latter (this is an upper limit, since the most metal-poor MaStro-MILES models are not available for any younger ages). Any other solution, involving for example star formation, would result in a strongly varying index with lookback-time, according to the steep evolution of Ca K at young ages, as seen in the same figure. This other solution

would also, of course, still face the problem of reproducing the broadband colours in a satisfying way.

In Fig.6.6 a simpler, snapshot exercise has been performed in the meantime. The blue dot, placed arbitrarily around 12 Gyr, represents the value as measured on a stacked spectrum of LRGs (Daniel Thomas, private communication) from the early *Baryon Oscillation Spectroscopic Survey* (BOSS) data (Schlegel et al., 2007; Eisenstein et al., 2011). As mentioned in the previous section, degeneracies become increasingly larger at lower resolutions, but the LRG value is clearly more compatible with the metal-poor solution, suggesting a minor-component fraction of 5 %, which is in fairly good agreement with our proposed solution of 3 % in (Maraston et al., 2009b). The slightly higher percentage obtained here may be caused by the fact that the MILES spectra used at [Z/H]$= -2.25$ are on average of somewhat higher metallicity than the evolutionary tracks, which is then compensated by a larger fraction. Regarding the young, metal-rich solution, the subcomponent must constitute more than 10 % by mass in order to reach the LRG value. Such a high fraction will undoubtedly leave a trace in the colour evolution to rule it out.

6.5.4 Caveat: Ca abundances in Early-type galaxies and GCs

Calcium belongs to the group of α-elements, and as such, should be enhanced in agreement with other α-elements in stellar populations where formation time-scales were short, e.g. massive ellipticals and globular clusters. However, Thomas et al. (2003a) found that early-type galaxies are actually calcium underabundant, in the sense that [α/Ca]> 0, by typically ~ 0.15 dex. If calcium was, indeed, depleted in early-type galaxies, then lower values of the Ca K index would be measured, especially in the most massive objects, since these are the most metal-rich and the most calcium underabundant. It is important to remember, though, that these galaxies are usually enhanced in [α/Fe] by around 0.2-0.4 dex. (e.g. Thomas et al., 2005), so that [Ca/Fe]> 0 would still hold true and measuring the Ca K index would actually yield *larger* or very similar values compared to the solar-scaled models. At lower metallicities the models are already α-enhanced, and here the calcium underabundance should not be as pronounced as at higher metallicities. We therefore consider it relatively safe to use the SSP models provided here for calcium abundance studies.

Regarding Galactic globular clusters they are generally of low metallicity and exhibit a fair amount of α-enhancement. The exception is of course the bulge and the clusters residing therein, which in some cases display α-enhancement even at high metallicity

(most notably NGC 6528 and NGC 6553, see e.g. Maraston et al. 2003), reminiscent of the situation found in early-type galaxies. Whether the GCs are also deficient in calcium or not has been debated. Thomas et al. (2003b) found by calibrating their models with the GC observations of Puzia et al. (2002) that calcium was enhanced in accordance with other α-elements if a nitrogen-enhanced model was considered, so that [Ca/Fe]=[α/Fe], even for the most metal-rich clusters NGC 6528 and NGC 6553 (this additional nitrogen improved also the match in other poorly constrained indices, while leaving the already well-calibrated indices unaffected). Lee et al. (2009) deduced instead, using the GC compilation of Schiavon et al. (2005), that while Milky Way GCs are enhanced in Mg by about 0.4 dex. the enhancement in Ca is only ~ 0.2 dex., i.e. a similar calcium-underabundance found in early-type galaxies. They also determined that NGC 6528 and NGC 6553 seem to be considerably less α-enhanced compared to their more metal-poor counterparts. Measurements on individual stars by Barbuy et al. (2004) established an [α/Fe]-ratio of about $+0.2$ for these clusters, but other investigations have found different enhancement for different α-elements (e.g. Cohen et al., 1999).

The dependence on metallicity for the Ca K index of MW GCs, colour-coded according to their HB morphology, can be seen in Fig.6.7. As expected the correlation with metallicity is strong, and especially clusters with blue horizontal branch morphology display a fairly tight relation. Towards higher metallicities (and redder HBs) the scatter increases, and the two most metal-rich clusters, NGC 6528 and NGC 6553, deviate significantly from the general trend. The cause of this discrepancy remains to be determined, but it is unlikely to be due to a calcium underabundance, since Cohen et al. (1999) and Carretta et al. (2001) measured [Ca/Fe]$\approx +0.2$ for both clusters, using high-resolution spectroscopy of individual member stars. Other relatively metal-rich bulge clusters, such as NGC 5927 and NGC 6624, do not show any anomalies in their Ca K strengths.

6.6 Discussion

In this chapter we have briefly touched upon an absorption line index that could potentially be a valuable aid in disentangling age and metallicity effects in the spectra of relatively simple composite stellar populations. More specifically, the Ca K index should in most cases be able to successfully distinguish between traces of old, metal-poor or young, metal-rich contamination in old, passively evolving galaxies. Clearly, the metal-poor subpopulation give rise to significantly weaker Ca K lines, even when constituting a smaller fraction of the total mass compared to a young, metal-rich component. With a young enough metal-rich minor component, the two could become degenerate also in

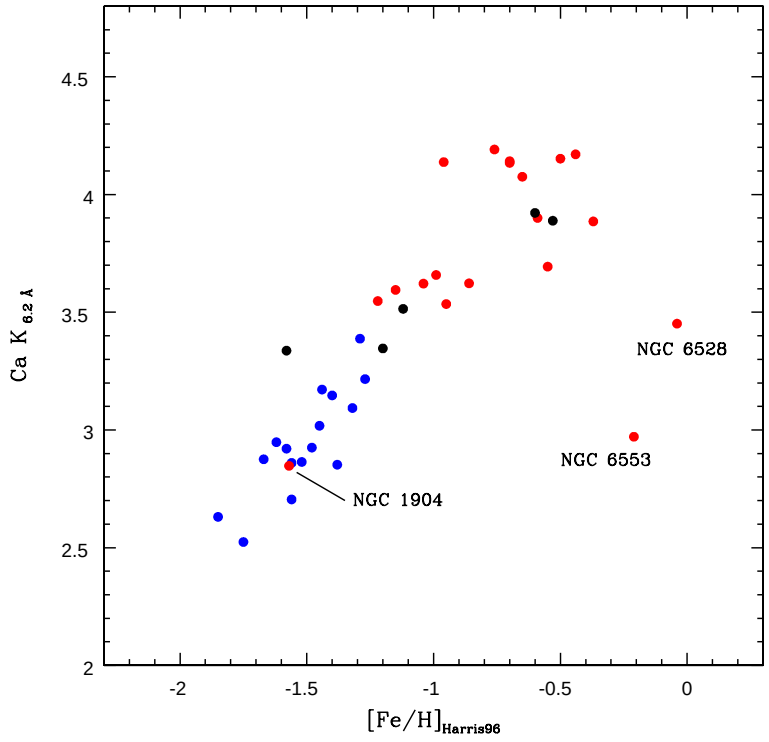

Figure 6.7: Ca K index strengths as a function of metallicity for the Schiavon et al. (2005) sample of MW GCs. Clusters have been colour-coded according to their HB morphology (black being intermediate morphology). Metal-rich bulge clusters NGC 6528 and NGC 6553 have been labelled as they deviate from the general trend, as has NGC 1904, whose HB parameter in Table 1 of Schiavon et al. (2005) appears to have received an extra minus sign. The HB of this cluster is, in reality, blue.

Ca K, but that would simultaneously break a plethora of other degeneracies, e.g. the one in (*B*-*V*) colour. A remark must also be made of the specific metallicities of the subcomponents. We have assumed the young component to be of super-solar metallicity, while a scenario where it is of precisely solar metallicity could also be envisioned. These stars are hotter than their super-solar metallicity counterparts, and could thus reach lower Ca K values, but again this would cause discrepancies in (*B*-*V*) colour (unless the age of the metal-poor component is lowered, which seems highly contradictive, or the age of the young component is raised, in which case the Ca K line would remain unchanged anyway). A very low resolution in connection with a low signal-to-noise does create some degeneracies when applied to individual galaxies, however, and it should be emphasised that the index works better as a complement to other widely used indices, than on its own.

Additionally, the Ca K line is also easily identifiable, and lies in a wavelength region that can be observed from the ground. We have shown that by adopting the boosted median continuum technique for the pseudo-continuum, even a very narrow index is stable against variations in resolution, and can therefore be of use for galaxies in the high-end of the mass range. Further reassurance comes from the comparison with GCs (Fig.5.1), where the Ca K and H lines give very small residuals and seem to be well calibrated.

Yet, much work remains to be done. We have briefly touched upon the deciding role the Ca K line might have on determining the fate of massive ellipticals. This naturally has to be tested. Also, index strengths inferred from EPS models based on fitting functions instead of being measured directly on the model SEDs, should be more reliable, because when constructing fitting functions one has the option of discarding different stars for each index. Rejecting a star that appears miscalibrated in only one index out of many, is a luxury that the SED modeller cannot afford. There simply aren't enough stars in the sky. Therefore, the next obvious step is to create a fitting function for the Ca K index, and put it through extensive testing.

Chapter 7

The Role of the MaStro models in International Collaborations

On the use of MaStro models in large international surveys, and why it's important that spectral libraries in EPS modelling have been constructed for that specific purpose.

7.1 The MaStro models and BOSS...

One of the programs of the newest installment of the huge *Sloan Digital Sky Survey* (SDSS-III, Eisenstein et al., 2011), has the aim of mapping the redshift of around 1.5 million massive galaxies out to $z \sim 0.7$, using the BAO feature associated with large-scale structure in order to accurately measure the distance scale and expansion rate within said redshift limits. Additionally, this particular part of SDSS-III (abbreviated BOSS for the *Baryon Oscillation Spectroscopic Survey*), will gather spectra of about 150000 quasars at redshifts between 2 and 3. The spectrograph commissioned to perform this hefty task covers the rest-frame wavelength range of 3600-10000 Å at a resolution of R~ 2000. The pipeline used for galaxy redshift determinations (in the end having a success rate of over 98 %) naturally required stellar population models of similarly high resolution and wavelength coverage, and the MaStro-MILES and MaStro-MARCS models were well suited for this job (see Bhardwaj et al. 2010 for details on the commissioning of the BOSS spectrographs). MaStro models have also been used in a GANDALF (Sarzi et al. 2006, and Cappellari & Emsellem 2004 for the PPXF routine) analysis of BOSS spectra (Thomas et al. in preparation). Scheduled for next year *Data Release 9* will be the first set of data made available to the public.

7.2 ... and GAMA

Another ambitious undertaking is the *GAlaxy Mass Assembly* survey (Driver et al., 2009), which aims to deliver around 250000 optical galaxy spectra at a resolution of 3-7 Å FWHM, out to a redshift limit of $z \sim 0.4$. Unlike the aforementioned survey, this project will probe fainter magnitudes in order to map all environments, and the optical spectra will be combined with observations from different sources to create a massive, multi-wavelength catalogue of galaxy spectra. MaStro-MILES models in GANDALF have been used on the GAMA spectra to retrieve pure emission and absorption line spectra, to derive properties such as velocity dispersions (both stellar and gaseous) and star formation histories, and to perform line diagnostics (Hopkins et al. in preparation).

7.3 SSP models using SEGUE stars

In the predecessor to SDSS-III (yes, SDSS-II), one of the programs called SEGUE (*Sloan Extension for Galactic Underpinnings and Evolution*, Smith et al., 2004) aimed to unravel the substructures of our own Galaxy in order to gain insights into both the dynamical and evolutionary aspects of the Milky Way. With over 200000 stellar spectra in its database the synergy effects for EPS modelling sounds promising. Using only spectra obtained with the latest selection algorithm (v.4.6) and without any warning flags (this still amounts to over 24000 spectra, compared to ELODIE that can muster ”only” around 1300) we have constructed a SEGUE-based sample intended for EPS modelling. The evolutionary coverage at all metallicities for the entire sample can be seen in Fig.7.1, where 400 Myr and 15 Gyr isochrones from Bertelli et al. (1994) have been superimposed. It is interesting to compare this figure to the corresponding plots in Chap.3, where the stellar libraries were specifically designed to be of use in stellar population modelling. Even though containing 20 times as many stars as e.g. the MILES library, SEGUE is clearly lacking both hot turnoff and lower MS stars, as well as RGB stars, especially at metallicities around solar. At the lowest metallicities the situation is much improved, hinting at the original purpose for this database of probing the outer Galactic structures, but the coolest stars (< 4000 K) are still missing. These gaps in stellar parameter space are in the process of being filled in, but were unfortunately not available during the period of this work.

We have constructed solar metallicity SSP models based on the SEGUE library, in order to test their potential for EPS modelling. The original stellar parameters, necessarily determined through an automated pipeline due to the sheer volume of data in the library

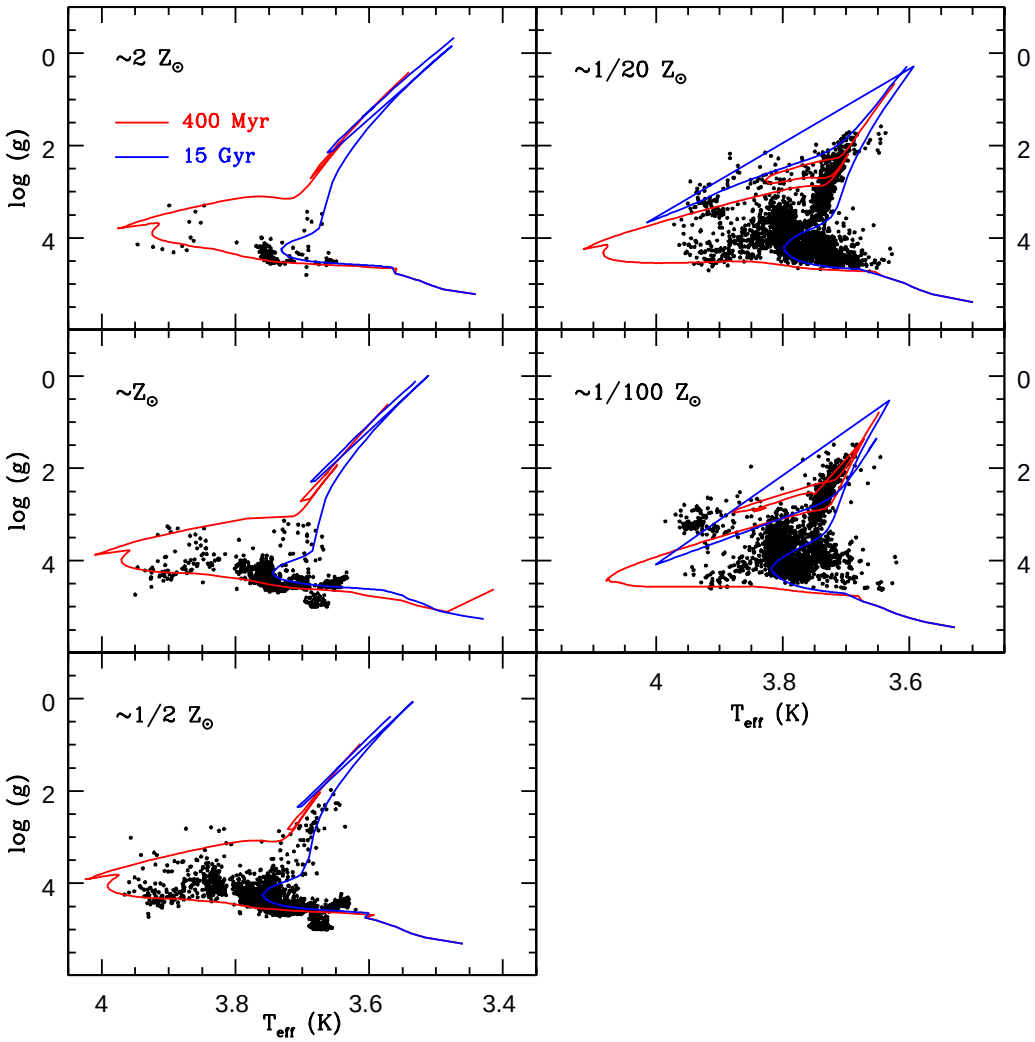

Figure 7.1: Evolutionary coverage of the SEGUE database of stellar spectra. All stars are required to sport no warning flags, and only spectra obtained with the latest selection criteria are shown. Isochrones from Bertelli et al. (1994) are superimposed for reference. This plot should be compared to e.g. Fig.3.4, where the stellar library was purposely designed for stellar population modelling.

(see Lee et al., 2008, for a description of the procedure), were kept during this process, and gaps in the cool regime of stellar parameter space were topped up with Pickles stars (ignoring the effects on the overall resolution). The end result can be seen in Fig.7.2 for the typical case of a 12 Gyr population. It is striking how red the colours displayed by the MaStro-SEGUE models are (for reference, an equally old MaStro-Pickles model is over-plotted) – a behaviour that can be traced to the temperature scale adopted for the SEGUE stars. In Lee et al. (2008) it was shown that the SEGUE parameter pipeline generates temperatures that are overestimated by on average 12 K and 64 K (with a 1-σ scatter of 74 K and 120 K) when compared to the ELODIE and MILES libraries, respectively. However, when restricting the comparison to the temperature range between 4000 K and

5000 K these numbers increase to 243 K and 235 K (average differences) with 91 K and 130 K (standard deviations). Considering the importance of the temperature scale of the RGB for the near-IR flux, as previously shown in this work (see Sec.4.7.3), such a large overestimation of the temperatures will lead to significantly redder colours.

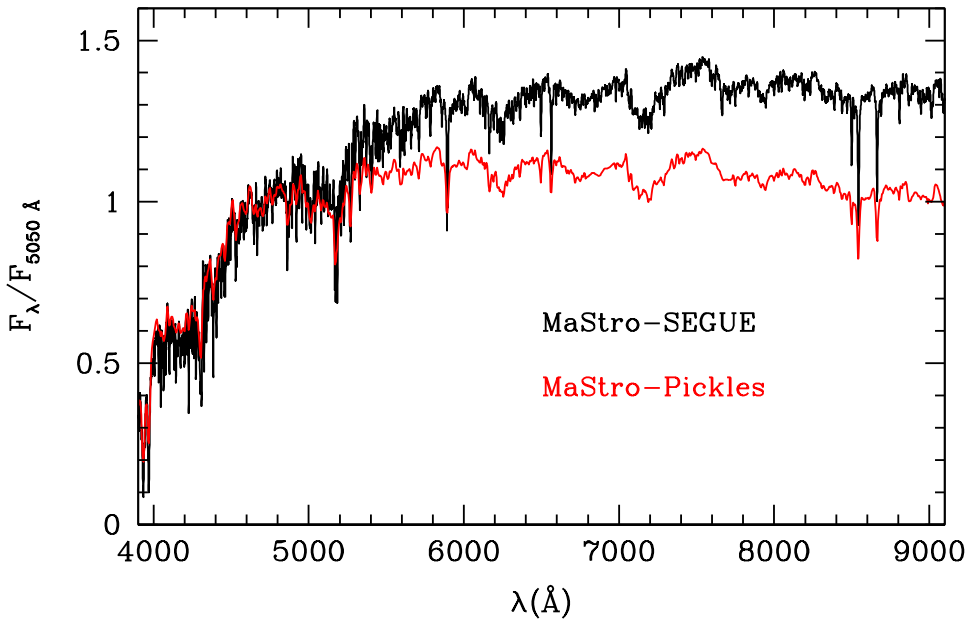

Figure 7.2: Comparison of 12 Gyr, $Z_{\odot}$ MaStro SSPs based on the Pickles and SEGUE libraries (*red* and *black*, respectively). The considerably redder colours of the latter is due to the temperature scale adopted for the SEGUE spectra.

The conclusion to be made from this small exercise is that stellar population modelling benefits from utilising spectral libraries constructed for the specific purpose of stellar population modelling. Not only do such intentions lead to a library that covers the significant evolutionary stages, but the number of spectra are usually small enough to allow for a careful, hands-on calibration of the stellar parameters of each individual spectra (although we are probably getting close to the limit of what is feasible with the current numbers of around 1000 entries). However, by filling in the gaps in stellar parameter space, and possibly recalibrating the temperature scale, the SEGUE library would become an extremely powerful aid in stellar population modelling. SSP models based on these spectra would be entirely in the SDSS photometric and instrumental system, thus minimising systematics in the analysis of SDSS galaxies, which could arise from having observed the stars with a different instrumental setup.

Chapter 8

Summary and Future Directions

The astrophysical applications that require stellar population models are just short of innumerable. By decoding the integrated energy emission of galaxies and star clusters, properties such as ages, metallicities, stellar masses, star formation histories, etc. can be derived. Mapping those parameters in time and space is a key step to unlock the mysteries in galaxy formation and evolution theory as well as in both observational and theoretical cosmology. Technological advancements now permit a vast amount of data to be collected at high resolution and high signal-to-noise over a relatively wide range in both redshift and galaxy mass (e.g. the SDSS and its sequels). Equally high demands must then be put on the corresponding stellar population models in order to avoid loosing precious information, and that is the first goal of this work.

The recent findings of Maraston et al. (2009b) presented evidence that the widely used BaSeL library, which in turn is based on the even more widely used Kurucz model atmospheres, might be somewhat miscalibrated in the optical region of cool stars; the consequences, considering how much work is based on these libraries, are of course significant. Keeping the main ingredients from the M05 models intact, we have therefore explored the impact of a variety of different high-to-intermediate resolution stellar libraries – most of them empirical – on evolutionary population synthesis models, which can be considered the second goal of this work. Previous publications of similar kind have only compared a few libraries at most.

In particular, it is the way in which the empirical spectra have been scaled to absolute flux units and assigned to their respective (T_{eff}, log(g), [Z/H])-bins that have been altered. Other crucial parameters in the code, such as energetics, TP-AGB treatment, and mass loss recipe, remain unchanged, allowing us to isolate the effect from the stars in transforming the stellar evolutionary prescription into observables. We have hereby

shown that whether it be spectral energy distributions or broadband colours, at the same energetics the choice of spectral library matters greatly. This stands in contrast to recent results in the literature (Bruzual & Charlot, 2003; Conroy & Gunn, 2010), albeit they did not explore the variety of stellar compilations utilised herein, and did also not isolate the single effect of the spectral library. That the choice of stellar library is important can certainly be said also for individual absorption lines, although this has not been the main focus here.

The stellar libraries explored herein all have their intrinsic characteristics, which are reflected in the integrated models; the Pickles library consists of standard spectra, covering the UV up to the K-band, which are averages composed of several different observations, but the resolution is fairly low and only solar metallicity models can be constructed from this compilation; STELIB contains spectra of high resolution for a relatively wide wavelength range, but would benefit from more stars at all metallicities in general, and below [Fe/H]$= -1.0$ in particular; MILES provide a homogeneous, high-resolution library with very good evolutionary coverage and adequate wavelength coverage, but their temperature scale differs from those of the other libraries, which generates a lower near-IR flux and therefore also bluer (*B*-*V*) colours; and finally ELODIE, which is comprised of ~ 1400 very high-resolution spectra exhibiting, however, a rather narrow wavelength range, and a clear bias towards solar metallicity.

All MaStro models are available with a UV-extension, through a merging with the high-resolution EPS models of Maraston et al. (2009a), which are based on the theoretical UVBLUE stellar spectra. In addition, we have built purely theoretical models based on the MARCS library that, at very high resolution, range all the way from the UV and far into the IR. The upper limit of 8000 K for stars in this library corresponds to a lower age limit of the stellar population models that is metallicity dependent, but where possible, a merging with these models provide also an IR-extension to the MaStro models. In concordance with M05, the latter are available at three different IMFs (Salpeter, Kroupa and Chabrier), and at two different HB morphologies (blue and intermediate-red).

We have shown how the behaviour of an integrated model can always be traced to the behaviour of individual stellar components. Spectra of the same stars from different libraries have also been compared and found to vary, but in the end, a lack of evidence for a systematic offset in the flux calibration results in most of these differences being smoothed out in the integrated SED. It is instead the intrinsic temperature scale of each library that has the largest impact on the final output. In general, however, a fair level of homogeneity is still achieved between MaStro models. In particular, we can confirm

the findings of Maraston et al. (2009b) that the visual region of models based on empirical spectra display a lower amount of flux (in a normalised sense) with respect to Kurucz-based models. The only exception is perhaps the ELODIE-based models, whose high resolution may have compromised the flux calibration procedure. These results gain support from the theoretical MaStro-MARCS models, which are in good agreement with the empirical-based models, and ensures that the effect did not originate from the complicated procedure of inserting empirical spectra into a population synthesis code, since MARCS spectra are integrated in exactly the same way as the theoretical BaSeL spectra in the original M05 code. Support also comes from comparisons to other EPS models, such as the Vazdekis et al. (2010) and Conroy & Gunn (2010) models, both of which display a similar drop in flux (despite the latter claiming the opposite). The same outcome cannot be verified for the widely used BC03 models; this is most likely due to the specific method used for scaling and inserting the empirical spectra into the synthesis.

In terms of broadband colours the flux drop affects mainly the *V*-band (corresponding approximately to the r'-band in the SDSS system), resulting in bluer (*B*-*V*) colours by a more or less constant offset of $0.05\,mag.$ at old ages. This has led to significant improvements in the modelling of both galaxy and globular cluster colours. The long-standing problem of a low-redshift, opposite mismatch between models and data regarding the $(g'-r')$ and $(r'-i')$ colours of the massive, passively evolving galaxies known as LRGs, was finally resolved with the help of our new models – as was the similarly well-known issue with the (*B*-*V*)-[Z/H] relation of Milky Way GCs, which dates back even further.

In a full SED-fitting procedure the MaStro-MILES models perform mostly well in obtaining the GC parameters as derived from CMD-fitting, even though the confidence intervals are rather large. This is, however, also a testimony to the fact that the age-metallicity degeneracy is perfectly in place also at higher resolutions. Adopting instead absorption line diagnostics we are able to draw two conclusions: i) measuring Lick indices directly on the model SEDs is an adequate method as long as one uses a subsample of indices, the combination of which is little sensitive to abundance ratio effects, but ii) both this approach and SED-fitting are still biased as the element ratio parameter cannot be wholly taken into account. Lick index analysis should preferably be performed using a model with variable abundance ratios, such as the TMJ model (in a separate section we showed that the Lick indices measured on MaStro model SEDs are in good agreement with solar-scaled TMJ values at solar metallicity, and with [α/Fe]-enhanced TMJ values at low metallicity). It is also worth remembering that the CMD-values, to which the

models are compared, are not completely bias-free either. At solar metallicity and composition the composite spectrum of open cluster M67 could be neatly fitted with both STELIB- and MILES-based MaStro models.

MaStro models have already also played a vital role in various multi-continental collaborations, such as the SDSS-III and GAMA, being implemented into external software by other authors and used both for spectrograph calibration, redshift determinations, and galaxy parameter derivations. In addition to this, we showed with a simple exercise involving the SEGUE sample, that population synthesis benefits from spectral libraries compiled with the intention of being used for the specific purpose of stellar population modelling – both from an evolutionary coverage point-of view and from the parameter calibration perspective. However, by filling in the gaps in stellar parameter space, and recalibrating the temperature scale – in particular at low temperatures – the SEGUE library would become a veritable goldmine for population synthesis. Models based on these spectra would also be entirely in the SDSS photometric and instrumental system, thus protecting the analysis of SDSS galaxies from systematics due to having observed the stars with a different instrumental setup.

Finally, with the aid of a higher resolution, and a different approach to absorption line indices by means of the BMC method (Rogers et al., 2010), we have defined a new take on the Ca K index that should be able to discriminate between solutions in simple cases of the age-metallicity degeneracy; more specifically in those scenarios where a major, $Z_{\odot}$ population has been polluted with either a young, metal-rich or an old, metal-poor subcomponent. This is in reality an important case, since there is an ongoing debate about which of these two categories the blue component in massive ellipticals comes from. Also in more complex situations it may be of some enlightening value. Another strength of the index is that the relative behaviour as a function of age is more or less independent of velocity dispersion (resolution). Concerns may be raised, however, due to the fact that the index has so far only been defined and measured on integrated, Milky Way-biased model SEDs, whereas it would be very interesting to see the response when – after a proper fitting function has been constructed – the abundance ratio effects are taken into account.

There can be no doubt that empirical stellar spectra has a place in evolutionary population synthesis. The models presented in this work has led to valuable insights in the modelling of stellar populations, and a few examples of specific astrophysical applications where the improvements were significant have been shown. This does not rule out theoretical spectra from the equation, however. We have additionally shown that

the purely theoretical MARCS library behave in many ways like the empirical libraries regarding broadband colours (the calibration of individual absorption lines in MARCS spectra may not be as well-behaved, but this is left for a future investigation), and in the end this is the library used for filling in missing gaps in the cool regime of stellar parameter space. To further strengthen the cause of theoretical spectra, they can be computed for any arbitrary combination of temperature, gravity, metallicity, abundance ratios, wavelength coverage, resolution etc. With empirical spectra we get what we see (and we often see only in a limited wavelength range), and still have to deal with complicated procedures like flux calibration and temperature scale calibration. Until a complete empirical library is in existence, containing all possible combinations of stellar parameters including α-enhancement at high metallicity (bulge stars), and observed at the full spectral range from the UV into the IR (encompassing at least the K-band), it seems utilising a mixture of empirical and theoretical spectra is the best strategy for now.

8.1 Future Directions

The field of evolutionary population synthesis is as interesting and important now as it ever was. In the key goal of understanding galaxy formation and evolution in a greater cosmological context, EPS models play a vital role. Recent developments over the last decade or so, have greatly improved our knowledge of the galaxies that populate the Universe. From the perspective of EPS modelling these developments have occurred on both the modelling side – with stellar evolutionary calculations now available for very heavy stars, for populations with abundance ratio anomalies, and over previously very uncertain evolutionary phases, such as the TP-AGB (see e.g. Bertelli et al., 2008, 2009; Pietrinferni et al., 2009; Marigo et al., 2008) – and on the observational side – where the amount of galaxy data has increased manyfold thanks to large-scale extragalactic surveys like the SDSS (York et al., 2000), the 2dF Galaxy Redshift Survey (Colless et al., 2001) and the GAMA survey (Driver et al., 2009) to mention only a few.

However, there are still many ingredients of evolutionary population synthesis that can be improved, and much work remains to be done before all areas are perfectly understood, if they ever can be; in other words, the ultimate stellar population model has yet to see daylight. It is my humble hope that this work, where the effect of stellar spectra (i.e. only one of the ingredients) on EPS models has been investigated, will contribute to that end goal. It has been shown, for example, that improvements in many astrophysical applications can generally be obtained by using EPS models based on empirical stellar

spectra instead of theoretical ones. On the other hand, the specific choice of spectral library also matters a great deal, as different empirical libraries do not produce equal results. The future directions regarding the spectral component of the models, which requires either extending an already comprehensive library like MILES with observations at both shorter and longer wavelengths (requiring in turn space-based instruments) and of stars with different element abundance ratios, or improving the theoretical modelling of stellar atmospheres (which is a continuously ongoing activity), has already been discussed to some extent.

It might be pointed out that this work concerns mainly the typical stars that build up normal stellar populations. Many of the uncertainties in EPS modelling are instead associated with some of the more exotic and poorly understood stages of stellar evolution, for which there is a consequently a lack of both theoretical and empirical spectra. These phases, including e.g. TP-AGB, BS, and extreme horizontal branch (EHB) stars, are often short-lived but very luminous, thus contributing substantially to the integrated light of a stellar population during a critical period. This age range can be translated into a redshift range, where galaxies are expected to exhibit more or less light from stars in a given evolutionary phase.

With technological advancements and the exciting prospects of a number of new telescopes comes also an opportunity to rigorously test and improve EPS models. For example, TP-AGB stars completely dominate the near-IR light in populations that are between 0.2 and 2 Gyr old, which are typical galaxy ages at redshift $z \sim$2-3. A proper treatment of TP-AGB stars in EPS models is thus absolutely crucial in order to obtain accurate mass estimates of these high-redshift galaxies. The launch of the *Spitzer Space Telescope* [1] has led to a significant increase in the amount of infrared data, and the upcoming space-based *James Webb Space Telescope*[2] (JWST) as well as the ground-based *European Extremely Large Telescope*[3] will add to that, ensuring that near- and mid-IR astronomy will be a topic of much research over the coming years and a challenge for stellar population models. The JWST will also be able to gather light from a very young Universe, possibly even signals from the first populations of stars (Pop.III stars, see e.g. Schaerer, 2003). Corresponding stellar population models would then also be necessary to interpret the data. For a review of future missions and their connection to stellar population modelling, the interested reader is referred to Brinchmann (2010).

[1] http://www.spitzer.caltech.edu/
[2] http://www.jwst.nasa.gov/
[3] http://www.eso.org/sci/ facilities/eelt/

At redshifts z $\sim$2-3 optical instruments sample the rest-frame UV of young, star-forming galaxies, which is also an area of some uncertainty in EPS models. Empirical spectra of massive O- and B-type stars, which is the dominant source of UV light in young populations, are often heavily attenuated by close-in dust, while stellar evolution theory for these stars and the influence of rotation, mass loss, and binary evolution is not yet completely understood. Similar mechanisms are thought to be responsible also for the horizontal branch morphology. EHBs may for example develop as a result of binary interactions, and since hot HB stars dominate the UV region in old stellar populations (early-type galaxies), it is important for EPS modelling to understand where they come from. Yet another reason why stellar population models in the future should emphasise the UV and near-IR wavelength regions is that they have the potential of effectively breaking the age-metallicity degeneracy, as already mentioned in previous chapters.

Future full-SED stellar population models will most certainly take varying element abundance ratios into account. Whether this can ever be purely empirical in the sense of having full evolutionary coverage at each required combination of abundance ratios is, however, doubtful. There are probably not enough stars at observable distance. At some point the theoretical stellar spectra will most likely also reach a certain level of sophistication, rendering empirical spectra more or less obsolete, as the former are considerably more flexible.

Some consideration of the uncertainties associated with the EPS models will probably also become standard. It is here important to remember that stellar population models are a mixture of several different and complicated ingredients, so that a ”true” picture of the errors is incredibly difficult to obtain. Stellar evolutionary tracks and isochrones (of which there is a plethora of different codes) have their own uncertainties and errors, which the EPS models inherit when adopting them. Similarly, model atmospheres and synthesised stellar spectra are based on calculations and calibrations that carry intrinsic errors and assumptions. Empirical spectra on the other hand are subject to observational errors, both systematic and random, as well as uncertainties in the derivation of surface parameters (T_{eff}, log(g), [Z/H]), and in the accuracy of the flux calibration. Additionally, the question whether the IMF is universal or not will prove crucial, and star clusters used as calibrators, e.g. in the Magellanic Clouds, will benefit from higher precision observations. Therefore, even though EPS models have now reached a certain degree of maturity, many questions remain to be answered, and future developments in the field will be very interesting to follow.

References

Alonso, A., Arribas, S., & Martínez-Roger, C. 1995, Astronomy & Astrophysics, 297, 197

—. 1996, Astronomy & Astrophysics Supplement Series, 117, 227

—. 1999, Astronomy & Astrophysics Supplement Series, 140, 261

Anders, P., Lamers, H. J. G. L. M., & de Grijs, R. 2008, in Astronomical Society of the Pacific Conference Series, Vol. 388, Mass Loss from Stars and the Evolution of Stellar Clusters, ed. A. de Koter, L. J. Smith, & L. B. F. M. Waters, 345

Arnett, D. 1996, Supernovae and nucleosynthesis: An investigation of the history of matter, from the Big Bang to the present (Princeton University Press)

Babel, J. 1995, Astronomy & Astrophysics, 301, 823

Bacon, R., Copin, Y., Monnet, G., Miller, B. W., Allington-Smith, J. R., Bureau, M., Carollo, C. M., Davies, R. L., Emsellem, E., Kuntschner, H., Peletier, R. F., Verolme, E. K., & de Zeeuw, P. T. 2001, Monthly Notices of the Royal Astronomical Society, 326, 23

Barbuy, B., Meléndez, J., Ortolani, S., Zoccali, M., Bica, E., Renzini, A., Hill, V., Momany, Y., Minniti, D., & Rich, M. 2004, Memorie della Societ Astronomica Italiana, 75, 398

Bate, M. R. 2009, Monthly Notices of the Royal Astronomical Society, 397, 232

Bate, M. R., Bonnell, I. A., & Bromm, V. 2003, Monthly Notices of the Royal Astronomical Society, 339, 577

Bedin, L. R., Piotto, G., Anderson, J., Cassisi, S., King, I. R., Momany, Y., & Carraro, G. 2004, The Astrophysical Journal Letters, 605, L125

Beers, T. C., Kage, J. A., Preston, G. W., & Shectman, S. A. 1990, The Astronomical Journal, 100, 849

Beifiori, A., Maraston, C., Thomas, D., & Johansson, J. 2011, Astronomy & Astrophysics, 531, A109+

Bertelli, G., Bressan, A., Chiosi, C., Fagotto, F., & Nasi, E. 1994, Astronomy & Astrophysics Supplement Series, 106, 275

Bertelli, G., Girardi, L., Marigo, P., & Nasi, E. 2008, Astronomy & Astrophysics, 484, 815

Bertelli, G., Nasi, E., Girardi, L., & Marigo, P. 2009, Astronomy & Astrophysics, 508, 355

Bertone, E., Buzzoni, A., Rodríguez-Merino, L. H., & Chávez, M. 2004, Memorie della Societa Astronomica Italiana, 75, 158

Bessell, M. S. 1979, The Publications of the Astronomical Society of the Pacific, 91, 589

Bhardwaj, V., Dawson, K., Anderson, L., Bizyaev, D., Brewington, H., Brown, P., Eisenstein, D. J., Harding, P., Malanushenko, E., Malanushenko, V., Maraston, C., Olmstead, M., Oravetz, D., Pan, K., Roe, N., Schlegel, D. J., Shelden, A., Simmons, A., Snedden, S., & Stromback, G. 2010, in Bulletin of the American Astronomical Society, Vol. 42, American Astronomical Society Meeting Abstracts #215, #471.02–+

Bica, E., & Alloin, D. 1986, Astronomy & Astrophysics, 162, 21

—. 1987, Astronomy & Astrophysics, 186, 49

Blackwell, D. E., & Lynas-Gray, A. E. 1998, Astronomy & Astrophysics Supplement Series, 129, 505

Bono, G., Cassisi, S., Zoccali, M., & Piotto, G. 2001, The Astrophysical Journal Letters, 546, L109

Bressan, A., Chiosi, C., & Fagotto, F. 1994, The Astrophysical Journal Supplement Series, 94, 63

Bressan, A., Granato, G. L., & Silva, L. 1998, Astronomy & Astrophysics, 332, 135

Brewer, J. P., Richer, H. B., & Crabtree, D. R. 1995, The Astronomical Journal, 109, 2480

Brinchmann, J. 2010, in IAU Symposium, Vol. 262, IAU Symposium, ed. G. Bruzual & S. Charlot, 3–12

Brott, I., & Hauschildt, P. H. 2005, in ESA Special Publication, Vol. 576, The Three-Dimensional Universe with Gaia, ed. C. Turon, K. S. O'Flaherty, & M. A. C. Perryman, 565–+

Bruzual, A. G. 1983, The Astrophysical Journal, 273, 105

Bruzual, A. G., & Charlot, S. 1993, The Astrophysical Journal, 405, 538

—. 2003, Monthly Notices of the Royal Astronomical Society, 344, 1000

Buzzoni, A. 1989, The Astrophysical Journal Supplement Series, 71, 817

Cappellari, M., & Emsellem, E. 2004, The Publications of the Astronomical Society of the Pacific, 116, 138

Carney, B. W., Latham, D. W., Laird, J. B., & Aguilar, L. A. 1994, The Astronomical Journal, 107, 2240

Carretta, E., Bragaglia, A., Gratton, R. G., Lucatello, S., Catanzaro, G., Leone, F., Bellazzini, M., Claudi, R., D'Orazi, V., Momany, Y., Ortolani, S., Pancino, E., Piotto, G., Recio-Blanco, A., & Sabbi, E. 2009, Astronomy & Astrophysics, 505, 117

Carretta, E., Cohen, J. G., Gratton, R. G., & Behr, B. B. 2001, The Astronomical Journal, 122, 1469

Carson, D. P., & Nichol, R. C. 2010, Monthly Notices of the Royal Astronomical Society, 408, 213

Cassisi, S., Pietrinferni, A., Salaris, M., Castelli, F., Cordier, D., & Castellani, M. 2006, Memorie della Societa Astronomica Italiana, 77, 71

Cayrel de Strobel, G., Soubiran, C., Friel, E. D., Ralite, N., & Francois, P. 1997, Astronomy & Astrophysics Supplement Series, 124, 299

Cayrel de Strobel, G., Soubiran, C., & Ralite, N. 2001, Astronomy & Astrophysics, 373, 159

Cenarro, A. J., Cardiel, N., Gorgas, J., Peletier, R. F., Vazdekis, A., & Prada, F. 2001, Monthly Notices of the Royal Astronomical Society, 326, 959

Cenarro, A. J., Cardiel, N., Vazdekis, A., & Gorgas, J. 2009, Monthly Notices of the Royal Astronomical Society, 396, 1895

Cenarro, A. J., Peletier, R. F., Sánchez-Blázquez, P., Selam, S. O., Toloba, E., Cardiel, N., Falcón-Barroso, J., Gorgas, J., Jiménez-Vicente, J., & Vazdekis, A. 2007, Monthly Notices of the Royal Astronomical Society, 374, 664

Chaboyer, B. 1995, The Astrophysical Journal Letters, 444, L9

Chaboyer, B., Green, E. M., & Liebert, J. 1999, The Astronomical Journal, 117, 1360

Chabrier, G. 2003, The Publications of the Astronomical Society of the Pacific, 115, 763

Charlot, S., & Bruzual, A. G. 1991, The Astrophysical Journal, 367, 126

Chiosi, C., Bertelli, G., & Bressan, A. 1988, Astronomy & Astrophysics, 196, 84

Coelho, P., Barbuy, B., Meléndez, J., Schiavon, R. P., & Castilho, B. V. 2005, Astronomy & Astrophysics, 443, 735

Coelho, P., Bruzual, A. G., Charlot, S., Weiss, A., Barbuy, B., & Ferguson, J. W. 2007, Monthly Notices of the Royal Astronomical Society, 382, 498

Cohen, J. G., Gratton, R. G., Behr, B. B., & Carretta, E. 1999, The Astrophysical Journal, 523, 739

Colless, M., Dalton, G., Maddox, S., Sutherland, W., Norberg, P., Cole, S., Bland-Hawthorn, J., Bridges, T., Cannon, R., Collins, C., Couch, W., Cross, N., Deeley, K., De Propris, R., Driver, S. P., Efstathiou, G., Ellis, R. S., Frenk, C. S., Glazebrook, K., Jackson, C., Lahav, O., Lewis, I., Lumsden, S., Madgwick, D., Peacock, J. A., Peterson, B. A., Price, I., Seaborne, M., & Taylor, K. 2001, Monthly Notices of the Royal Astronomical Society, 328, 1039

Colucci, J. E., Bernstein, R. A., Cameron, S., McWilliam, A., & Cohen, J. G. 2009, The Astrophysical Journal, 704, 385

Colucci, J. E., Bernstein, R. A., Cameron, S. A., & McWilliam, A. 2011, The Astrophysical Journal, 735, 55

Conroy, C., & Gunn, J. E. 2010, The Astrophysical Journal, 712, 833

Conroy, C., Gunn, J. E., & White, M. 2009, The Astrophysical Journal, 699, 486

Davidge, T. J. 1992, The Astronomical Journal, 103, 1512

De Angeli, F., Piotto, G., Cassisi, S., Busso, G., Recio-Blanco, A., Salaris, M., Aparicio, A., & Rosenberg, A. 2005, The Astronomical Journal, 130, 116

Demarque, P., Woo, J., Kim, Y., & Yi, S. K. 2004, The Astrophysical Journal Supplement Series, 155, 667

di Benedetto, G. P. 1998, Astronomy & Astrophysics, 339, 858

Dotter, A. 2008, The Astrophysical Journal Letters, 687, L21

Dotter, A., Chaboyer, B., Ferguson, J. W., Lee, H., Worthey, G., Jevremović, D., & Baron, E. 2007a, The Astrophysical Journal, 666, 403

Dotter, A., Chaboyer, B., Jevremović, D., Baron, E., Ferguson, J. W., Sarajedini, A., & Anderson, J. 2007b, The Astronomical Journal, 134, 376

Driver, S. P., GAMA Team, Baldry, I. K., Bamford, S., Bland-Hawthorn, J., Bridges, T., Cameron, E., Conselice, C., Couch, W. J., Croom, S., Cross, N. J. G., Driver, S. P., Dunne, L., Eales, S., Edmondson, E., Ellis, S. C., Frenk, C. S., Graham, A. W., Jones, H., Hill, D., Hopkins, A., van Kampen, E., Kuijken, K., Lahav, O., Liske, J., Loveday, J., Nichol, B., Norberg, P., Oliver, S., Parkinson, H., Peacock, J. A., Phillipps, S., Popescu, C. C., Prescott, M., Proctor, R., Sharp, R., Staveley-Smith, L., Sutherland, W., Tuffs, R. J., & Warren, S. 2009, in IAU Symposium, Vol. 254, IAU Symposium, ed. J. Andersen, J. Bland-Hawthorn, & B. Nordström, 469–474

Eisenstein, D. J., Annis, J., Gunn, J. E., Szalay, A. S., Connolly, A. J., Nichol, R. C., Bahcall, N. A., Bernardi, M., Burles, S., Castander, F. J., Fukugita, M., Hogg, D. W., Ivezić, Ž., Knapp, G. R., Lupton, R. H., Narayanan, V., Postman, M., Reichart, D. E., Richmond, M., Schneider, D. P., Schlegel, D. J., Strauss, M. A., SubbaRao, M., Tucker, D. L., Vanden Berk, D., Vogeley, M. S., Weinberg, D. H., & Yanny, B. 2001, The Astronomical Journal, 122, 2267

Eisenstein, D. J., Hogg, D. W., Fukugita, M., Nakamura, O., Bernardi, M., Finkbeiner, D. P., Schlegel, D. J., Brinkmann, J., Connolly, A. J., Csabai, I., Gunn, J. E., Ivezić, Ž., Lamb, D. Q., Loveday, J., Munn, J. A., Nichol, R. C., Schneider, D. P., Strauss, M. A., Szalay, A., & York, D. G. 2003, The Astrophysical Journal, 585, 694

Eisenstein, D. J., Weinberg, D. H., Agol, E., Aihara, H., Allende Prieto, C., Anderson, S. F., Arns, J. A., Aubourg, É., Bailey, S., Balbinot, E., & et al. 2011, The Astronomical Journal, 142, 72

Falcón-Barroso, J., Sánchez-Blázquez, P., Vazdekis, A., Ricciardelli, E., Cardiel, N., Cenarro, A. J., Gorgas, J., & Peletier, R. F. 2011, Astronomy & Astrophysics, 532, A95

Fanelli, M. N., O'Connell, R. W., Burstein, D., & Wu, C. 1992, The Astrophysical Journal Supplement Series, 82, 197

Fanelli, M. N., O'Connell, R. W., Burstein, D., & Wu, C.-C. 1990, The Astrophysical Journal, 364, 272

Fanelli, M. N., O'Connell, R. W., & Thuan, T. X. 1987, The Astrophysical Journal, 321, 768

—. 1988, The Astrophysical Journal, 334, 665

Feltzing, S., Bensby, T., & Lundström, I. 2003, Astronomy & Astrophysics, 397, L1

Ferraro, F. R., Origlia, L., Testa, V., & Maraston, C. 2004, The Astrophysical Journal, 608, 772

Fioc, M., & Rocca-Volmerange, B. 1997, Astronomy & Astrophysics, 326, 950

Fitzpatrick, E. L. 1999, The Publications of the Astronomical Society of the Pacific, 111, 63

Fluks, M. A., Plez, B., The, P. S., de Winter, D., Westerlund, B. E., & Steenman, H. C. 1994, Astronomy & Astrophysics Supplement Series, 105, 311

Forbes, D. A., & Bridges, T. 2010, Monthly Notices of the Royal Astronomical Society, 404, 1203

Gibson, B. K., Loewenstein, M., & Mushotzky, R. F. 1997, Monthly Notices of the Royal Astronomical Society, 290, 623

Gibson, B. K., Madgwick, D. S., Jones, L. A., Da Costa, G. S., & Norris, J. E. 1999, The Astronomical Journal, 118, 1268

Girardi, L., Bressan, A., Bertelli, G., & Chiosi, C. 2000, Astronomy & Astrophysics Supplement Series, 141, 371

Gonzalez, J. J., Faber, S. M., & Worthey, G. 1993, in Bulletin of the American Astronomical Society, Vol. 25, Bulletin of the American Astronomical Society, 1355–+

Guiderdoni, B., & Rocca-Volmerange, B. 1987, Astronomy & Astrophysics, 186, 1

Gustafsson, B., Edvardsson, B., Eriksson, K., Jørgensen, U. G., Nordlund, Å., & Plez, B. 2008, Astronomy & Astrophysics, 486, 951

Harris, W. E. 1996, The Astronomical Journal, 112, 1487

Haxton, W. C. 2008, Publications of the Astronomical Society of Australia, 25, 44

Heavens, A. F., Jimenez, R., & Lahav, O. 2000, Monthly Notices of the Royal Astronomical Society, 317, 965

Heck, A., Egret, D., Jaschek, M., & Jaschek, C. 1984, Astronomy & Astrophysics Supplement Series, 57, 213

Jimenez, R., Bernardi, M., Haiman, Z., Panter, B., & Heavens, A. F. 2007, The Astrophysical Journal, 669, 947

Johansson, J., Thomas, D., & Maraston, C. 2010, ArXiv e-prints

Jones, L. A., & Worthey, G. 1995, The Astrophysical Journal Letters, 446, L31+

Katz, D., Soubiran, C., Cayrel, R., Adda, M., & Cautain, R. 1998, Astronomy & Astrophysics, 338, 151

Kauffmann, G., Heckman, T. M., White, S. D. M., Charlot, S., Tremonti, C., Brinchmann, J., Bruzual, A. G., Peng, E. W., Seibert, M., Bernardi, M., Blanton, M., Brinkmann, J., Castander, F., Csábai, I., Fukugita, M., Ivezic, Z., Munn, J. A., Nichol, R. C., Padmanabhan, N., Thakar, A. R., Weinberg, D. H., & York, D. 2003, Monthly Notices of the Royal Astronomical Society, 341, 33

Kaviraj, S., Rey, S., Rich, R. M., Yoon, S., & Yi, S. K. 2007, Monthly Notices of the Royal Astronomical Society, 381, L74

Kerber, L. O., Santiago, B. X., & Brocato, E. 2007, Astronomy & Astrophysics, 462, 139

Kobayashi, C. 2004, Monthly Notices of the Royal Astronomical Society, 347, 740

Kormendy, J. 1989, The Astrophysical Journal Letters, 342, L63

Kroupa, P. 2001, Monthly Notices of the Royal Astronomical Society, 322, 231

Kurucz, R. L. 1979, The Astrophysical Journal Supplement Series, 40, 1

Lahav, O., Bridle, S. L., Percival, W. J., Peacock, J. A., Efstathiou, G., Baugh, C. M., Bland-Hawthorn, J., Bridges, T., Cannon, R., Cole, S., Colless, M., Collins, C., Couch, W., Dalton, G., de Propris, R., Driver, S. P., Ellis, R. S., Frenk, C. S., Glazebrook, K., Jackson, C., Lewis, I., Lumsden, S., Maddox, S., Madgwick, D. S., Moody, S., Norberg, P., Peterson, B. A., Sutherland, W., & Taylor, K. 2002, Monthly Notices of the Royal Astronomical Society, 333, 961

Lançon, A., Gallagher, III, J. S., Mouhcine, M., Smith, L. J., Ladjal, D., & de Grijs, R. 2008, Astronomy & Astrophysics, 486, 165

Lançon, A., & Mouhcine, M. 2002, Astronomy & Astrophysics, 393, 167

Le Borgne, D., Rocca-Volmerange, B., Prugniel, P., Lançon, A., Fioc, M., & Soubiran, C. 2004, Astronomy & Astrophysics, 425, 881

Le Borgne, J., Bruzual, A. G., Pelló, R., Lançon, A., Rocca-Volmerange, B., Sanahuja, B., Schaerer, D., Soubiran, C., & Vílchez-Gómez, R. 2003, Astronomy & Astrophysics, 402, 433

Lee, H., Worthey, G., & Dotter, A. 2009, The Astronomical Journal, 138, 1442

Lee, Y. S., Beers, T. C., Sivarani, T., Allende Prieto, C., Koesterke, L., Wilhelm, R., Re Fiorentin, P., Bailer-Jones, C. A. L., Norris, J. E., Rockosi, C. M., Yanny, B., Newberg, H. J., Covey, K. R., Zhang, H.-T., & Luo, A.-L. 2008, The Astronomical Journal, 136, 2022

Leitherer, C., & Heckman, T. M. 1995, The Astrophysical Journal Supplement Series, 96, 9

Leitherer, C., Schaerer, D., Goldader, J. D., González Delgado, R. M., Robert, C., Kune, D. F., de Mello, D. F., Devost, D., & Heckman, T. M. 1999, The Astrophysical Journal Supplement Series, 123, 3

Lejeune, T., Cuisinier, F., & Buser, R. 1997, Astronomy & Astrophysics Supplement Series, 125, 229

—. 1998, Astronomy & Astrophysics Supplement Series, 130, 65

Lejeune, T., & Schaerer, D. 2001, Astronomy & Astrophysics, 366, 538

Lotz, J. M., Ferguson, H. C., & Bohlin, R. C. 2000, The Astrophysical Journal, 532, 830

MacArthur, L. A., González, J. J., & Courteau, S. 2009, Monthly Notices of the Royal Astronomical Society, 395, 28

Mannucci, F., Maoz, D., Sharon, K., Botticella, M. T., Della Valle, M., Gal-Yam, A., & Panagia, N. 2008, Monthly Notices of the Royal Astronomical Society, 383, 1121

Maraston, C. 1998, Monthly Notices of the Royal Astronomical Society, 300, 872

—. 2005, Monthly Notices of the Royal Astronomical Society, 362, 799

Maraston, C., Daddi, E., Renzini, A., Cimatti, A., Dickinson, M., Papovich, C., Pasquali, A., & Pirzkal, N. 2006, The Astrophysical Journal, 652, 85

Maraston, C., Greggio, L., Renzini, A., Ortolani, S., Saglia, R. P., Puzia, T. H., & Kissler-Patig, M. 2003, Astronomy & Astrophysics, 400, 823

Maraston, C., Nieves Colmenárez, L., Bender, R., & Thomas, D. 2009a, Astronomy & Astrophysics, 493, 425

Maraston, C., Pforr, J., Renzini, A., Daddi, E., Dickinson, M., Cimatti, A., & Tonini, C. 2010, Monthly Notices of the Royal Astronomical Society, 407, 830

Maraston, C., Stromback, G., Portsmouth, I.-U. o., & Kingdom, U. 2011, ArXiv e-prints

Maraston, C., Strömbäck, G., Thomas, D., Wake, D. A., & Nichol, R. C. 2009b, Monthly Notices of the Royal Astronomical Society, 394, L107

Maraston, C., & Thomas, D. 2000, The Astrophysical Journal, 541, 126

Marigo, P., Girardi, L., Bressan, A., Groenewegen, M. A. T., Silva, L., & Granato, G. L. 2008, Astronomy & Astrophysics, 482, 883

Marín-Franch, A., Aparicio, A., Piotto, G., Rosenberg, A., Chaboyer, B., Sarajedini, A., Siegel, M., Anderson, J., Bedin, L. R., Dotter, A., Hempel, M., King, I., Majewski, S., Milone, A. P., Paust, N., & Reid, I. N. 2009, The Astrophysical Journal, 694, 1498

Martins, L. P., González Delgado, R. M., Leitherer, C., Cerviño, M., & Hauschildt, P. 2005, Monthly Notices of the Royal Astronomical Society, 358, 49

Mehlert, D., Thomas, D., Saglia, R. P., Bender, R., & Wegner, G. 2003, Astronomy & Astrophysics, 407, 423

Mermilliod, J., Mermilliod, M., & Hauck, B. 1997, Astronomy & Astrophysics Supplement Series, 124, 349

Milone, A., Sansom, A. E., & Sánchez-Blázquez, P. 2010, in IAU Symposium, Vol. 262, IAU Symposium, ed. A. G. Bruzual & S. Charlot, 394–395

Milone, A. P., Bedin, L. R., Piotto, G., Anderson, J., King, I. R., Sarajedini, A., Dotter, A., Chaboyer, B., Marín-Franch, A., Majewski, S., Aparicio, A., Hempel, M., Paust, N. E. Q., Reid, I. N., Rosenberg, A., & Siegel, M. 2008, The Astrophysical Journal, 673, 241

Moresco, M., Pozzetti, L., Cimatti, A., Zamorani, G., Mignoli, M., di Cesare, S., Bolzonella, M., Zucca, E., Lilly, S., Kovač, K., Scodeggio, M., Cassata, P., Tasca, L., Vergani, D., Halliday, C., Carollo, M., Contini, T., Kneib, J.-P., Le Févre, O., Mainieri, V., Renzini, A., Bardelli, S., Bongiorno, A., Caputi, K., Coppa, G., Cucciati, O., de la Torre, S., de Ravel, L., Franzetti, P., Garilli, B., Iovino, A., Kampczyk, P., Knobel, C., Lamareille, F., Le Borgne, J.-F., Le Brun, V., Maier, C., Pellò, R., Peng, Y., Perez Montero, E., Ricciardelli, E., Silverman, J. D., Tanaka, M., Tresse, L., Abbas, U., Bottini, D., Cappi, A., Guzzo, L., Koekemoer, A. M., Leauthaud, A., Maccagni, D., Marinoni, C., McCracken, H. J., Memeo, P., Meneux, B., Nair, P., Oesch, P., Porciani, C., Scaramella, R., Scarlata, C., & Scoville, N. 2010, Astronomy & Astrophysics, 524, A67+

Mucciarelli, A., Origlia, L., Ferraro, F. R., Maraston, C., & Testa, V. 2006, The Astrophysical Journal, 646, 939

Munari, U., Sordo, R., Castelli, F., & Zwitter, T. 2005, Astronomy & Astrophysics, 442, 1127

Murphy, T., & Meiksin, A. 2004, Monthly Notices of the Royal Astronomical Society, 351, 1430

Nagashima, M., Lacey, C. G., Okamoto, T., Baugh, C. M., Frenk, C. S., & Cole, S. 2005, Monthly Notices of the Royal Astronomical Society, 363, L31

Norris, J. E., Freeman, K. C., & Mighell, K. J. 1996, The Astrophysical Journal, 462, 241

O'Connell, R. W. 1976, The Astrophysical Journal, 206, 370

—. 1980, The Astrophysical Journal, 236, 430

Ocvirk, P., Pichon, C., Lançon, A., & Thiébaut, E. 2006, Monthly Notices of the Royal Astronomical Society, 365, 74

Ogando, R. L. C., Maia, M. A. G., Chiappini, C., Pellegrini, P. S., Schiavon, R. P., & da Costa, L. N. 2005, The Astrophysical Journal Letters, 632, L61

Olofsson, K. 1989, Astronomy & Astrophysics Supplement Series, 80, 317

Pancino, E., Ferraro, F. R., Bellazzini, M., Piotto, G., & Zoccali, M. 2000, The Astrophysical Journal Letters, 534, L83

Peacock, M. B., Zepf, S. E., Maccarone, T. J., & Kundu, A. 2011, The Astrophysical Journal, 737, 5

Percival, W. J., Reid, B. A., Eisenstein, D. J., Bahcall, N. A., Budavari, T., Frieman, J. A., Fukugita, M., Gunn, J. E., Ivezić, Ž., Knapp, G. R., Kron, R. G., Loveday, J., Lupton, R. H., McKay, T. A., Meiksin, A., Nichol, R. C., Pope, A. C., Schlegel, D. J., Schneider, D. P., Spergel, D. N., Stoughton, C., Strauss, M. A., Szalay, A. S., Tegmark, M., Vogeley, M. S., Weinberg, D. H., York, D. G., & Zehavi, I. 2010, Monthly Notices of the Royal Astronomical Society, 401, 2148

Persson, S. E., Aaronson, M., Cohen, J. G., Frogel, J. A., & Matthews, K. 1983, The Astrophysical Journal, 266, 105

Pessev, P. M., Goudfrooij, P., Puzia, T. H., & Chandar, R. 2008, Monthly Notices of the Royal Astronomical Society, 385, 1535

Pickles, A. J. 1985a, The Astrophysical Journal Supplement Series, 59, 33

—. 1985b, The Astrophysical Journal, 296, 340

—. 1998, The Publications of the Astronomical Society of the Pacific, 110, 863

Pickles, A. J., & van der Kruit, P. C. 1990, Astronomy & Astrophysics Supplement Series, 84, 421

Pickles, A. J., & Visvanathan, N. 1985, The Astrophysical Journal, 294, 134

Pietrinferni, A., Cassisi, S., Salaris, M., Percival, S., & Ferguson, J. W. 2009, The Astrophysical Journal, 697, 275

Piotto, G., Bedin, L. R., Anderson, J., King, I. R., Cassisi, S., Milone, A. P., Villanova, S., Pietrinferni, A., & Renzini, A. 2007, The Astrophysical Journal Letters, 661, L53

Piotto, G., King, I. R., Djorgovski, S. G., Sosin, C., Zoccali, M., Saviane, I., De Angeli, F., Riello, M., Recio-Blanco, A., Rich, R. M., Meylan, G., & Renzini, A. 2002, Astronomy & Astrophysics, 391, 945

Pipino, A., Devriendt, J. E. G., Thomas, D., Silk, J., & Kaviraj, S. 2009, Astronomy & Astrophysics, 505, 1075

Poole, V., Worthey, G., Lee, H., & Serven, J. 2010, The Astronomical Journal, 139, 809

Prugniel, P., & Soubiran, C. 2001, Astronomy & Astrophysics, 369, 1048

Prugniel, P., Soubiran, C., Koleva, M., & Le Borgne, D. 2007, ArXiv Astrophysics e-prints

Puzia, T. H., Saglia, R. P., Kissler-Patig, M., Maraston, C., Greggio, L., Renzini, A., & Ortolani, S. 2002, Astronomy & Astrophysics, 395, 45

Ravindranath, S., Giavalisco, M., Ferguson, H. C., Conselice, C., Katz, N., Weinberg, M., Lotz, J., Dickinson, M., Fall, S. M., Mobasher, B., & Papovich, C. 2006, The Astrophysical Journal, 652, 963

Reichardt, C., Jimenez, R., & Heavens, A. F. 2001, Monthly Notices of the Royal Astronomical Society, 327, 849

Reimers, D. 1977, Astronomy & Astrophysics, 61, 217

Renzini, A., & Buzzoni, A. 1986, in Astrophysics and Space Science Library, Vol. 122, Spectral Evolution of Galaxies, ed. C. Chiosi & A. Renzini, 195–231

Renzini, A., & Voli, M. 1981, Astronomy & Astrophysics, 94, 175

Riffel, R., Pastoriza, M. G., Rodríguez-Ardila, A., & Bonatto, C. 2009, Monthly Notices of the Royal Astronomical Society, 400, 273

Rodríguez-Merino, L. H., Chavez, M., Bertone, E., & Buzzoni, A. 2005, The Astrophysical Journal, 626, 411

Rogers, B., Ferreras, I., Peletier, R., & Silk, J. 2010, Monthly Notices of the Royal Astronomical Society, 402, 447

Rose, J. A. 1985, The Astronomical Journal, 90, 1927

Salaris, M., & Cassisi, S. 1996, Astronomy & Astrophysics, 305, 858

Salasnich, B., Girardi, L., Weiss, A., & Chiosi, C. 2000, Astronomy & Astrophysics, 361, 1023

Salpeter, E. E. 1955, The Astrophysical Journal, 121, 161

Sánchez-Blázquez, P., Peletier, R. F., Jiménez-Vicente, J., Cardiel, N., Cenarro, A. J., Falcón-Barroso, J., Gorgas, J., Selam, S., & Vazdekis, A. 2006, Monthly Notices of the Royal Astronomical Society, 371, 703

Sandberg Lacy, C. H., Torres, G., Claret, A., Charbonneau, D., O'Donovan, F. T., & Mandushev, G. 2010, The Astronomical Journal, 139, 2347

Sarzi, M., Falcón-Barroso, J., Davies, R. L., Bacon, R., Bureau, M., Cappellari, M., de Zeeuw, P. T., Emsellem, E., Fathi, K., Krajnović, D., Kuntschner, H., McDermid, R. M., & Peletier, R. F. 2006, Monthly Notices of the Royal Astronomical Society, 366, 1151

Schaerer, D. 2003, Astronomy & Astrophysics, 397, 527

Schaller, G., Schaerer, D., Meynet, G., & Maeder, A. 1992, Astronomy & Astrophysics Supplement Series, 96, 269

Schiavon, R. P., Caldwell, N., & Rose, J. A. 2004, The Astronomical Journal, 127, 1513

Schiavon, R. P., Rose, J. A., Courteau, S., & MacArthur, L. A. 2005, The Astrophysical Journal Supplement Series, 160, 163

Schlegel, D. J., Blanton, M., Eisenstein, D., Gillespie, B., Gunn, J., Harding, P., McDonald, P., Nichol, R., Padmanabhan, N., Percival, W., Richards, G., Rockosi, C., Roe, N., Ross, N., Schneider, D., Strauss, M., Weinberg, D., & White, M. 2007, in Bulletin of the American Astronomical Society, Vol. 38, American Astronomical Society Meeting Abstracts, 132.29–+

Smith, J. A., McGehee, P. M., Tucker, D. L., Beers, T., Rockosi, C. M., Yanny, B., Allam, S. S., Stoughton, C., Neilsen, Jr., E. H., Rider, C. J., Moore, D. C., Rodgers, C. T., Cantrell, K. A., Knapp, G., & SDSS. 2004, in Bulletin of the American Astronomical Society, Vol. 36, American Astronomical Society Meeting Abstracts, 1453–+

Thevenin, F. 1998, VizieR Online Data Catalog, 3193, 0

Thomas, D., Maraston, C., & Bender, R. 2003a, Monthly Notices of the Royal Astronomical Society, 343, 279

—. 2003b, Monthly Notices of the Royal Astronomical Society, 339, 897

Thomas, D., Maraston, C., Bender, R., & Mendes de Oliveira, C. 2005, The Astrophysical Journal, 621, 673

Thomas, D., Maraston, C., & Johansson, J. 2011, Monthly Notices of the Royal Astronomical Society, 412, 2183

Thomas, D., Maraston, C., & Korn, A. 2004, Monthly Notices of the Royal Astronomical Society, 351, L19

Thomas, D., Maraston, C., Schawinski, K., Sarzi, M., & Silk, J. 2010, Monthly Notices of the Royal Astronomical Society, 404, 1775

Tinsley, B. M. 1972, Astronomy & Astrophysics, 20, 383

—. 1978, The Astrophysical Journal, 222, 14

Tinsley, B. M., & Gunn, J. E. 1976, The Astrophysical Journal, 203, 52

Tojeiro, R., Heavens, A. F., Jimenez, R., & Panter, B. 2007, Monthly Notices of the Royal Astronomical Society, 381, 1252

Tojeiro, R., Wilkins, S., Heavens, A. F., Panter, B., & Jimenez, R. 2009, The Astrophysical Journal Supplement Series, 185, 1

Trager, S. C., Faber, S. M., Worthey, G., & González, J. J. 2000, The Astronomical Journal, 119, 1645

Trager, S. C., & Somerville, R. S. 2009, Monthly Notices of the Royal Astronomical Society, 395, 608

Trager, S. C., Worthey, G., Faber, S. M., Burstein, D., & Gonzalez, J. J. 1998, The Astrophysical Journal Supplement Series, 116, 1

Tripicco, M. J., & Bell, R. A. 1995, The Astronomical Journal, 110, 3035

Valdes, F., Gupta, R., Rose, J. A., Singh, H. P., & Bell, D. J. 2004, The Astrophysical Journal Supplement Series, 152, 251

van den Bergh, S., Cohen, J. G., Hogg, D. W., & Blandford, R. 2000, The Astronomical Journal, 120, 2190

Vazdekis, A. 1999, The Astrophysical Journal, 513, 224

Vazdekis, A., & Arimoto, N. 1999, The Astrophysical Journal, 525, 144

Vazdekis, A., Cenarro, A. J., Gorgas, J., Cardiel, N., & Peletier, R. F. 2003, Monthly Notices of the Royal Astronomical Society, 340, 1317

Vazdekis, A., Sánchez-Blázquez, P., Falcón-Barroso, J., Cenarro, A. J., Beasley, M. A., Cardiel, N., Gorgas, J., & Peletier, R. F. 2010, Monthly Notices of the Royal Astronomical Society, 404, 1639

Wake, D. A., Nichol, R. C., Eisenstein, D. J., Loveday, J., Edge, A. C., Cannon, R., Smail, I., Schneider, D. P., Scranton, R., Carson, D., Ross, N. P., Brunner, R. J., Colless, M., Couch, W. J., Croom, S. M., Driver, S. P., da Ângela, J., Jester, S., de Propris, R., Drinkwater, M. J., Bland-Hawthorn, J., Pimbblet, K. A., Roseboom, I. G., Shanks, T., Sharp, R. G., & Brinkmann, J. 2006, Monthly Notices of the Royal Astronomical Society, 372, 537

Walcher, C. J., Coelho, P., Gallazzi, A., & Charlot, S. 2009, Monthly Notices of the Royal Astronomical Society, 398, L44

Weiss, A., & Ferguson, J. W. 2009, Astronomy & Astrophysics, 508, 1343

Worthey, G. 1994, The Astrophysical Journal Supplement Series, 95, 107

Worthey, G., Faber, S. M., & Gonzalez, J. J. 1992, The Astrophysical Journal, 398, 69

Worthey, G., Faber, S. M., Gonzalez, J. J., & Burstein, D. 1994, The Astrophysical Journal Supplement Series, 94, 687

Worthey, G., & Ottaviani, D. L. 1997, The Astrophysical Journal Supplement Series, 111, 377

York, D. G., Adelman, J., Anderson, Jr., J. E., Anderson, S. F., Annis, J., Bahcall, N. A., Bakken, J. A., Barkhouser, R., Bastian, S., Berman, E., Boroski, W. N., Bracker, S., Briegel, C., Briggs, J. W., Brinkmann, J., Brunner, R., Burles, S., Carey, L., Carr, M. A., Castander, F. J., Chen, B., Colestock, P. L., Connolly, A. J., Crocker, J. H., Csabai, I., Czarapata, P. C., Davis, J. E., Doi, M., Dombeck, T., Eisenstein, D., Ellman, N., Elms, B. R., Evans, M. L., Fan, X., Federwitz, G. R., Fiscelli, L., Friedman, S., Frieman, J. A., Fukugita, M., Gillespie, B., Gunn, J. E., Gurbani, V. K., de Haas, E., Haldeman, M., Harris, F. H., Hayes, J., Heckman, T. M., Hennessy, G. S., Hindsley, R. B., Holm, S., Holmgren, D. J., Huang, C., Hull, C., Husby, D., Ichikawa, S., Ichikawa, T., Ivezić, Ž., Kent, S., Kim, R. S. J., Kinney, E., Klaene, M., Kleinman, A. N., Kleinman, S., Knapp, G. R., Korienek, J., Kron, R. G., Kunszt, P. Z., Lamb, D. Q., Lee, B., Leger, R. F., Limmongkol, S., Lindenmeyer, C., Long, D. C., Loomis, C., Loveday, J., Lucinio, R., Lupton, R. H., MacKinnon, B., Mannery, E. J., Mantsch, P. M., Margon, B., McGehee, P., McKay, T. A., Meiksin, A., Merelli, A., Monet, D. G., Munn, J. A., Narayanan, V. K., Nash, T., Neilsen, E., Neswold, R., Newberg, H. J., Nichol, R. C., Nicinski, T., Nonino, M., Okada, N., Okamura, S., Ostriker, J. P., Owen, R., Pauls, A. G., Peoples, J., Peterson, R. L., Petravick, D., Pier, J. R., Pope, A., Pordes, R., Prosapio, A., Rechenmacher, R., Quinn, T. R., Richards, G. T., Richmond, M. W., Rivetta, C. H., Rockosi, C. M., Ruthmansdorfer, K., Sandford, D., Schlegel, D. J., Schneider, D. P., Sekiguchi, M., Sergey, G., Shimasaku, K., Siegmund, W. A., Smee, S., Smith, J. A., Snedden, S., Stone, R., Stoughton, C., Strauss, M. A., Stubbs, C., SubbaRao, M., Szalay, A. S., Szapudi, I., Szokoly, G. P., Thakar, A. R., Tremonti, C., Tucker, D. L., Uomoto, A., Vanden Berk, D., Vogeley, M. S., Waddell, P., Wang, S., Watanabe, M., Weinberg, D. H., Yanny, B., & Yasuda, N. 2000, The Astronomical Journal, 120, 1579

Zinn, R., & West, M. J. 1984, The Astrophysical Journal Supplement Series, 55, 45